

THE ROLE OF INTERLEUKIN-6 IN HEALTH AND
DISEASE OF RETINAL GANGLION CELLS

By

Franklin D. Echevarria

Dissertation

Submitted to the Faculty of the
Graduate School of Vanderbilt University
in partial fulfillment of the requirements

for the degree of

DOCTOR OF PHILOSOPHY

in

Neuroscience

June 30, 2017

Nashville, Tennessee

Approved:

Rebecca M. Sappington, Ph.D.

David J. Calkins, Ph.D.

Alissa M. Weaver, M.D., Ph.D.

Fiona E. Harrison, Ph.D.

Christine L. Konradi, Ph.D.

Copyright © 2017 by Franklin D. Echevarria
All Rights Reserved

I dedicate this doctoral thesis to my parents- Barbara and Franklin, my brothers- Dennis and

Kenny, my fiancée Mary, Jack the cat, and June the dingo.

Thank you all from the bottom of my heart for your support!

ACKNOWLEDGEMENTS

First and foremost, I would like to send my deepest gratitude to my advisor Dr. Rebecca Sappington. Looking back on my graduate school experience, her guidance and mentorship have been amazing and I have gained a tremendous amount of knowledge as a scientist under her supervision. As her first graduate student, I'm sure that I did not come with a set of instructions. Despite some hiccups, she never gave up on me and I'm forever grateful for her invested time and energy into my development as both a scientist and a person. Along with Dr. Sappington, I received excellent guidance from my thesis committee. I am thankful for Dr. David Calkins, who served as the chair of my thesis committee. Outside of my committee meetings, he also served as a second advisor and made sure I was performing at my highest potential. I'm also grateful for Drs. Fiona Harrison and Christine Konradi, for whom I benefitted from their expertise in neurodegeneration and the CNS. Finally, I'm thankful for Dr. Alissa Weaver who served as my "non-neuroscience" committee member. Her tough questions allowed me to think outside the box regarding my research project and helped me grow as a scientist.

Completing a thesis project becomes more enjoyable when you are placed in an excellent working environment. I was very fortunate to have an amazing team around me courtesy of Dr. Sappington. First, I would like to thank Master Cathryn Formichella for being an excellent lab manager by: making sure supplies I requested were ordered promptly, helping me countless times with my experiments, and allowing me to help her with crossword puzzles. Second, I am forever grateful to the former post-docs in the lab, including Dr. Heather Cathcart and Dr. D'Anne Duncan for assisting with my development early in my graduate training and starting me off on the right track. Third, I would like to thank the other graduate student in the lab- Rachel Fischer for always willing to help me with experiments and discuss any questions.

Fourth, I would like to thank the incredibly wonderful high school and undergraduate students that I've had the chance to mentor including Abigail Waterson, Michelle Won, Caroline Walker, Emma Kingsbury, Michael Dublin, Brandy Sweet, and Veronica Hamilton. I thank them for all their hard work in obtaining and analyzing data relating to my thesis project. Finally, I would like to thank all of the other members of the Sappington Lab, past and present, including Rachel Roberson, Sarah Franklin, William McLaughlin, Stephen Davis, Noah Vasilakes, Hannah Mallaro, Simone Abella, Sean Lee, Payton Russom, Amanda Rehorn, Jimbo Dickerson, Steven Patalano, Abigail Roux, Marisol Rodriguez, Priya Sankaran, Daanish Chawala, and Jeremy Hatcher for providing a great working environment.

I was fortunate to conduct my research in an open lab space, allowing me to collaborate freely with the adjoining labs. I'm thankful to Dr. Calkins for allowing me to utilize his wonderful research staff and graduate students to assist with various components of my project. Specifically, I would like to thank Dr. Wendi Lambert and Brian Carlson for their help with microbead injections and Dr. Michael Risner, Dr. Silvia Pasini and Melissa Cooper for their help in preparing for my oral defense. I would also like to thank former graduate student Dr. Nick Ward for always willing to help me navigate the neuroscience graduate program and assisting with my preparation for my qualifying exam and navigating copyright clearances for my written thesis document. I'm also thankful to the lab personnel of Dr. Tonia Rex, Dr. Rachel Kuchtey and Dr. John Kuchtey including Dr. Courtney Bricker-Anthony, Dr. Wesley Bond, Dr. Ana Maria De Lucas, Dr. Jon Backstrom, Jessica Hines-Beard and Dr. Ralph Hazlewood for always being available and willing to answer questions and give their opinions regarding my experiments and papers.

My research was made possible by a number of funding sources. I first want to thank Drs. Roger Chalkley and Linda Sealy for supporting me during my 1st two years at Vanderbilt University through the Initiative to Maximize Student Diversity grant (IMSD; R25 GM 62459-9). I also want to thank Drs. Chalkley and Sealy as well as Dr. Christina Keeton-Williams for always being there when I needed advice in both science and graduate student life. Along with the IMSD, my work was also supported by various grants obtained by Dr. Sappington including those from the National Eye Institute (R01EY020496), the Vanderbilt Vision Research Center (VVRC; P30EY08126) and Research to Prevent Blindness, Inc. I also want to thank Dr. Doug McMahon and Dr. Bruce Carter, both who served as directors of the Neuroscience Graduate Program during my tenure as a graduate student, and Dr. Mark Wallace, former director of the Vanderbilt Brain Institute (VBI) for their exhaustive efforts in building quality neuroscientists.

My research was also heavily aided by many individuals and core facilities outside of the ophthalmology department including Sean Schaffer of the Cell Imaging Shared Resource (CISR), Jared LeBoeuf of the Vanderbilt Core Lab for Clinical and Translational Research, Suzan Vaughan of the Hormone Assay Core, and Mariesol Rodriguez and Dr. Purnima Ghose of the Vision Research Center Histology Core. I would also like to thank the tireless work of the many administrative assistants from the VVRC, VBI and the Vanderbilt Eye Institute (VEI) that have helped me along the way including Vanessa Alderson (VEI), Jill Brott (VVRC), Sara Hamawandi (VEI) Susan Kelton (VEI), Roz Johnson (VBI), Beth Sims (VBI), and Mary Michael-Woolman (VBI). Finally, I would like to thank Joselyn Taylor and James Thomas for their pleasant conversations and making sure our laboratory was clean and ready for the next day's work.

I would not have gotten into Vanderbilt Neuroscience Program had it not been for the amazing individuals who prepared me for the rigors of graduate school. I first want to thank my first grade teacher Mrs. Rita Ennis for introducing me to the wonders of science at a young age. I'm also extremely grateful for my undergraduate advisors Dr. Matthew Ellinwood, Dr. Mike Muszynski, Dr. Maureen Hahn and Dr. Hugh Fentress for instilling me with the basic tools of a scientist. I'm also thankful for my post-baccalaureate advisor Dr. Rocio Rivera for teaching me that a mediocre work ethic will give you mediocre results in both life and science. Finally, I want to thank my grandfather Dr. Juan Gonzalez for not only providing me with the genetic material of a successful scientist, but for continually reminding me that science is beautiful.

Finally, I want to thank my family for supporting me throughout my studies. Knowing I had them in my corner made this journey that much easier. I also want to acknowledge the many friends I made during my time in Nashville. Thank you all for the laughs, the support and the love.

TABLE OF CONTENTS

	Page
DEDICATION.....	iii
ACKNOWLEDGEMENTS	iv
LIST OF FIGURES	xii
1. INTRODUCTION.....	1
Inflammation in the central nervous system	1
The optic projection as a model system.....	5
Anatomy of the optic projection.....	5
The optic projection as a model of the CNS	9
Glaucoma: Neurodegeneration of the optic nerve	11
Clinical manifestations of glaucoma	11
Glaucoma: Age-related sensitivity to ocular hypertension	13
Progression of glaucoma in the optic projection.....	17
Animal Models of glaucoma	18
Deficits in axon transport	21
RGC Dysfunction	24
Axon degeneration.....	25
Synapse elimination and dendritic pruning	27
Vision Loss	29
The Final Step: RGC Apoptosis.....	30
Neuroinflammation and a role for IL-6 in RGC survival.....	32
The complement system	33
TLR activation.....	34
Cytokine release	35
IL-6 as a potential target in glaucoma	36
Interleukin-6 impacts CNS function.....	36
IL-6 family of cytokines.....	36
IL-6 signal transduction.....	37
IL-6: Classical vs Trans-signaling.....	38
Expression and regulation of IL-6 in the CNS	39
IL-6 in CNS degeneration: friend or foe?.....	41
Specific Aims of Dissertation.....	44
Aim 1. Establish the expression profile for IL-6 machinery in response to glaucoma-related stressors.....	44
Aim 2. Determine whether IL-6 influences RGC degeneration caused by ocular hypertension	44
Aim 3. Identify structural and functional outcomes of constitutive IL-6 signaling in the naïve optic projection	45

2. ELEVATED PRESENCE OF THE SOLUBLE IL-6Rα IN RESPONSE TO GLAUCOMA RELATED- STRESSORS.....	46
Introduction.....	46
Material and Methods	49
Animals.....	49
IOP measurements.....	49
Tissue preparation	49
Lipopolysaccharide (LPS) stimulation.....	50
Gp130 and soluble IL-6R α quantification.....	50
Neural transport tracing.....	51
Immunohistochemistry	51
Co-localization analysis.....	52
Statistical analysis	53
Results.....	54
Glaucoma-related stressors promote sIL-6R α production.....	54
sIL-6R α increases in response to acute inflammatory stress in the retina.....	54
sIL-6R α is most strongly associated with RGC soma in glaucomatous retina	58
sIL-6R α localization is related to RGC integrity.....	60
Gp130 is not a reliable predictor of RGC integrity	64
Discussion	67
3. IL-6 DEFICIENCY IMPEDES RETINAL GANGLION CELL AXONOPATHY AND GLAUCOMA RELATED- VISION LOSS	71
Introduction.....	71
Material and Methods	73
Animals.....	73
Induction of ocular hypertension using the microbead occlusion model.....	73
IOP measurements.....	74
Immunohistochemistry	75
Quantification of glial coverage	75
Anterograde axon measurements	76
Quantification of axon density and optic nerve area	78
Psychophysical visual testing.....	78
Corneal imaging using spectral domain optical coherence tomography and quantification of corneal injury area.....	79
Statistical analysis	79
Results.....	81
IL-6 deficiency does not affect microbead-induced elevations in IOP	81
<i>Il-6</i> ^{-/-} mice exhibit deficits in corneal wound healing	82
IL-6 deficiency does not prevent IOP-induced deficits in anterograde axon transport.....	84
IL-6 deficiency preserves optic nerve structure following IOP elevation.....	86
IL-6 deficiency preserves visual acuity following IOP elevation	88
IL-6 deficiency enlarges the microglia population in retina	90
Discussion	93

4. IL-6 CONTRIBUTES TO THE DEVELOPMENT OF AXONS IN THE OPTIC PROJECTION	99
Introduction.....	99
Materials and Methods.....	102
Animals.....	102
Tissue preparation	102
Immunohistochemistry	102
Fluorescent <i>in-situ</i> hybridization.....	103
Anterograde axon transport measurements	103
Spectral domain optical coherence tomography (SD-OCT) and quantification of retinal layer thickness	104
Quantification of brain width	105
FVEPs.....	105
Psychophysical visual testing using optometry.....	106
Quantification of RGC somas and axons	106
Quantification of axon diameter and g-ratio	106
Immunoblotting	107
Statistical Analysis	107
Results.....	108
IL-6 is constitutively expressed by RGCs during post-natal development and in the mature retina.....	108
IL-6 deficiency alters retinal layer thickness without impacting gross morphology or structure.....	110
IL-6 deficiency alters the cortical response to light stimuli	112
IL-6 deficiency impedes anterograde axon transport	114
IL-6 deficiency increases RGC axon diameter.....	120
IL-6 deficiency alters microtubule arrangement in RGC axons.....	124
Acute exposure to IL-6 influences tubulin arrangement and fast axon transport.....	129
Discussion	132
5. SUMMARY	136
Purpose of studies	136
Aim 1: Outcomes and Future Directions	136
Establishing the expression profile for IL-6 machinery in response to glaucoma-related stressors	137
Aim 1: Future Directions	138
Aim 2: Outcomes and Future Directions	140
Determining whether IL-6 influences RGC degeneration caused by ocular hypertension.....	140
Aim 2: Future Directions	141
Aim 3: Outcomes and Future Directions	146
Identifying structural and functional outcomes of constitutive IL-6 signaling in the naive optic projection.....	146
Aim 3: Future Directions	147

Potential mechanism behind outcomes of IL-6 signaling in RGC health and disease148
Conclusions.....152
REFERENCES.....154

LIST OF FIGURES

Figure	Page
1.1 Proposed timeline of RGC degeneration in glaucoma.....	4
1.2 Retinal cell types and circuitry	6
1.3 Eye specific and topographic maps of RGC connections in the mouse brain	8
1.4 Formation and progression of optic disc cupping in glaucoma	12
1.5 Visual loss in human glaucoma patients	13
1.6 Aqueous humor dynamics in the eye	16
1.7 Critical steps in RGC degeneration in glaucoma.....	19
1.8 IL-6 signals in a classical and trans fashion.....	40
2.1 Glaucoma related stressors affect gp130 and IL-6R α isoform expression	55
2.2 sIL-6R α production increases in the retina in response to LPS	57
2.3 Glaucoma-related sIL-6R α is associated with RGCs	59
2.4 Age-dependent IOP elevation is associated with decreased CTB uptake and intra-retinal transport by RGCs.....	61
2.5 sIL-6R α is primarily associated with RGCs exhibiting poor CTB uptake and transport	63
2.6 No significant relationship between gp130 expression and CTB uptake of RGCs	65
3.1 Induction of ocular hypertension by microbead induced occlusion of aqueous humor outflow.....	74
3.2 RGC to SC CTB transport measurements and resulting retinotopic map	77
3.3 IL-6 deficiency does not affect magnitude and duration of microbead induced ocular hypertension.....	81
3.4 <i>Il-6</i> ^{-/-} mice present with defects in corneal wound healing following microbead/saline injection	83
3.5 IL-6 deficiency does not affect CTB transport deficits caused by elevated IOP	85

3.6 IL-6 ablation mitigates axonopathy caused by IOP elevation	87
3.7 <i>Il-6</i> ^{-/-} mice are resistant to IOP-induced deficits in visual acuity	89
3.8 IL-6 deficiency affects microglial coverage regardless of IOP	91
4.1 RGCs express <i>Il-6</i> mRNA throughout post-natal development	109
4.2 IL-6 deficiency does not affect retinal morphology	111
4.3 <i>Il-6</i> ^{-/-} mice present with an impaired cortical response to light	113
4.4 <i>Il-6</i> ^{-/-} mice present with deficiencies in anterograde transport	115
4.5 Transport deficits not due to impairments in RGC soma of <i>Il-6</i> ^{-/-} mice.....	117
4.6 Axon transport deficits are due to a delay in axon transport in <i>Il-6</i> ^{-/-} mice.....	119
4.7 <i>Il-6</i> ^{-/-} mice have fewer RGC axons	121
4.8 <i>Il-6</i> ^{-/-} mice have larger axons	123
4.9 <i>Il-6</i> ^{-/-} mice contain disorganized microtubules in retina.....	125
4.10 Cytoskeletal abnormalities in <i>Il-6</i> ^{-/-} mice are restricted to microtubules.....	126
4.11 Microtubule abnormalities also occur in hippocampus of <i>Il-6</i> ^{-/-} mice.....	127
4.12 Transport latencies in <i>Il-6</i> ^{-/-} mice improve with recombinant IL-6	130
5.1 IL-6 deficiency influences glaucoma-related changes in gene expression of neuroinflammatory, cell health and gp130 modulators	143
5.2 Glaucoma-related stressors elevate expression of IL-6 family members in a stressor dependent manner.	145
5.3 Proposed mechanism behind outcomes of IL-6 signaling in RGC health and disease.....	151
5.4 Integration of results with proposed timeline of glaucomatous RGC degeneration.....	153

CHAPTER 1

INTRODUCTION¹

Inflammation in the central nervous system

Inflammation is a component of the immune response that is characterized by edema, pain and increased blood flow and is defined by activation and recruitment of peripheral immune cells and the release of cellular signaling molecules known as cytokines (Medzhitov, 2008). It is typically initiated in response to injury, autoimmune activation or infiltration of infectious agents and enables the body to neutralize harmful stimuli, remove necrotic cells and repair damaged tissue (Medzhitov, 2008). Inflammation is normally an acute process, with built-in feedback mechanisms in place to reduce production of pro-inflammatory cytokines that maintain its activation (Medzhitov, 2008). Consequently, disruption of these feedback mechanisms can lead to a state of chronic inflammation, an event that is characterized by consistently elevated levels of inflammatory cytokines and implicated in cancers, Crohn's disease, inflammatory bowel disease and rheumatoid arthritis (Rubin et al., 2012, Straub and Schradin, 2016).

While inflammation is well-characterized in the periphery, less is known regarding how it is initiated and regulated in the central nervous system (CNS). The CNS consists of the retina, brain and spinal cord and is formed primarily of post-mitotic neurons and glia. For better part of the last century, it was commonly accepted that the CNS was "immune privileged" due to: 1) the presence of the blood-brain-barrier (BBB), which separates the CNS from the peripheral blood

¹ Portions of this chapter were published as Echevarria FD (2014) Interleukin-6 signaling in the central nervous system: Pointing the finger at trans-signaling in neuroinflammatory-mediated neurodegeneration. VRN 6.

supply and 2) the lack of dendritic cells, which targets T-cells to invading pathogens (Carson et al., 2006). This suggested that the CNS did not respond to cytokines released during peripheral inflammation and did not initiate any type of inflammatory response. While now known to be grossly exaggerated, this definition of immune privilege **had** merit. Studies revealed that injection of pathogens into the CNS parenchyma resulted in little to no inflammatory response compared to peripheral skin injection and tissue grafts to survive longer when placed within the CNS parenchyma than when placed underneath the skin (Medawar, 1948, Perry et al., 1997). This definition was also conducive to the construction of the CNS, which makes it more sensitive to responses associated with inflammation. The retina, brain and spinal cord are encased in spaces with little structural flexibility (eye, skull and vertebrate column respectively) and therefore cannot tolerate infiltration of peripheral immune cells and increased pressure associated with the influx of fluid seen with edema (Carson et al., 2006). Finally, inflammatory mediators released by peripheral immune cells have the potential to be neurotoxic and lead to cell death, which is problematic in a cell population that cannot readily regenerate (Hendriks et al., 2005).

Over the last 30 years however, research in neuro-immunology led to a paradigm shift, effectively describing that not only can the CNS respond to cytokines released during peripheral inflammation, but that the CNS is capable of releasing cytokines as well (Carson et al., 2006). This process was coined “neuroinflammation” and is implicated not only in protecting the CNS from infection and injury, but in the development and maintenance of neuronal networks as well (Deverman and Patterson, 2009, Xanthos and Sandkuhler, 2014). Neuroinflammation is primarily characterized by cytokine release from neurons and glia as well as changes in glial morphology (Frank-Cannon et al., 2009, Xanthos and Sandkuhler, 2014). Unlike peripheral inflammation, neuroinflammation generally lacks peripheral immune cell recruitment, vascular

changes, and edema (Ransohoff and Brown, 2012). To compensate, glia (e.g astrocytes, microglia, and retina-specific Müller glia) serve as the resident immune cells and deal with invading pathogens and diseased cells directly (Ransohoff and Brown, 2012). Similar to peripheral inflammation, the process of cytokine release in neuroinflammation is tightly regulated. While acute induction is essential for CNS development, maintenance and protection (Deverman and Patterson, 2009, Xanthos and Sandkuhler, 2014), failure to properly down-regulate cytokine release long after the initial insult can lead to a state of chronic neuroinflammation (Lucas et al., 2006). In this state, the integrity of the blood-CNS-barrier becomes compromised, peripheral immune cells infiltrate the CNS and prolonged elevations in neurotoxic agents (e.g. reactive oxygen/nitrogen species, glutamate) lead to neuronal cell death (Lucas et al., 2006). Indeed, chronic neuroinflammation is associated with many age-related neurodegenerative diseases including Alzheimer's disease, Parkinson's disease, Huntington's disease, multiple sclerosis and glaucoma (Soto and Howell, 2014, Deleidi et al., 2015, Williams et al., 2017).

Elucidating how specific cytokines are involved in these neurodegenerative diseases as well as CNS development and homeostasis is important for: 1) development of new therapies towards neurodegenerative disease and 2) expanding our knowledge on how the CNS functions and responds to stress. This thesis elucidates the impact of constitutive and disease-related Interleukin-6 (IL-6) signaling on structure and function of the optic projection. Glaucoma is an age-related neurodegenerative disease of retinal ganglion cells (RGCs) and their axons, which make up the optic nerve. Like other neurodegenerative diseases, degeneration of RGCs in glaucoma follow a specific timeline, where functional deficits precede structural degeneration and the RGC axon degenerates prior to the RGC soma (Figure 1.1). Using a number of

functional and histological assessments in multiple glaucoma animal models, we can elucidate not only if IL-6 signaling contributes to degeneration in glaucoma, but where among the proposed timeline does IL-6 signaling contribute to degeneration in glaucoma.

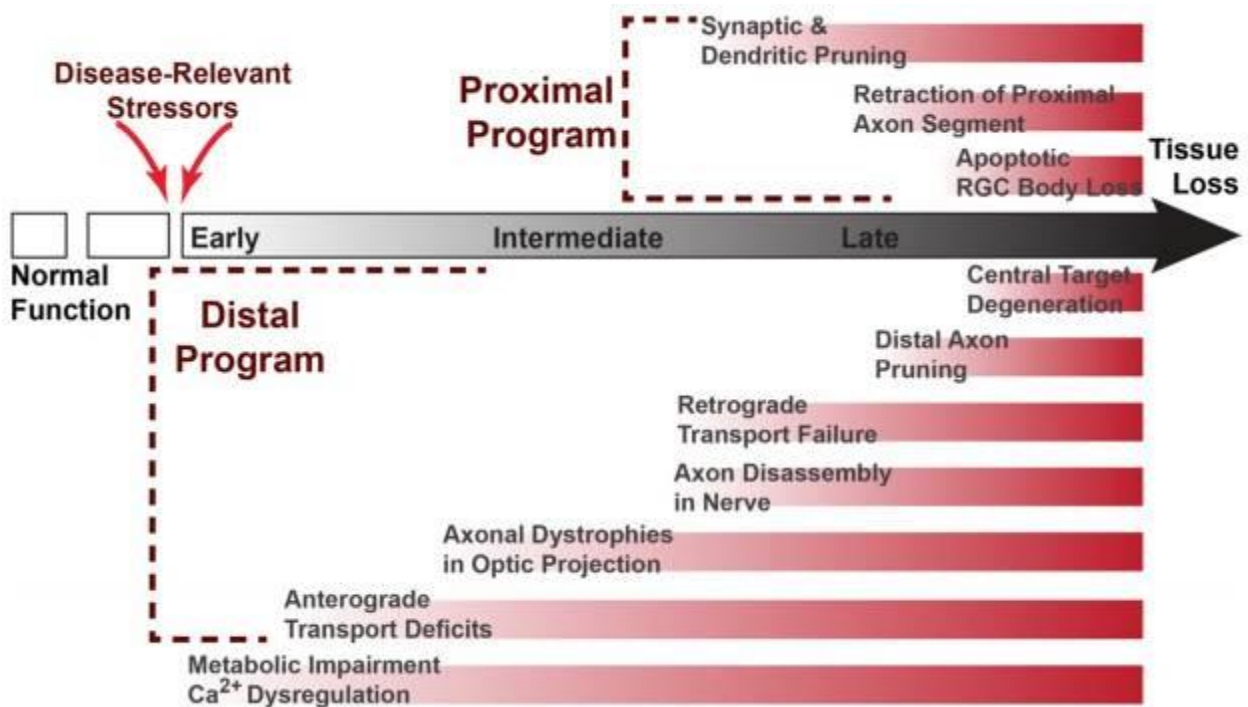


Figure 1.1. Proposed timeline of RGC degeneration in glaucoma. Disease relevant stressors such as Ca²⁺ dysregulation and metabolic impairment within RGCs, lead to dysfunction in the distal portion of the RGC axon including disruption of anterograde axonal transport and the formation of axon dystrophies. Later in progression the distal axon begins to degenerate followed by proximal degeneration of dendrites within the RGC soma. In the late stage of the disease, proximal degeneration of the RGC axon occurs followed by apoptosis of the RGC soma, leading to irreversible tissue loss.

Figure from (Calkins, 2012) and used in accordance with Copyright Clearance Center's RightsLink service.

The optic projection as a model system

Studying the effects of cytokines in the CNS can be difficult in an *in vivo* setting, especially for neuroscientists studying neuronal populations within the brain and spinal cord. This is primarily due to the skull and vertebral column, components of the skeletal anatomy evolved to protect the brain and spinal cord respectively. While indeed protective, these bony structures limit accessibility to neuronal populations within the brain and spinal cord. Fortunately however, the retina and optic nerve, collectively known as the optic projection, allows neuroscientists to bypass these limitations and study a neuronal population that shares numerous similarities to those found in the brain and spinal cord (London et al., 2013).

Anatomy of the optic projection

During embryonic development, the retina forms as a protuberance of the diencephalon and as a result is considered part of the CNS (Heavner and Pevny, 2012). The retina is a multi-layered neural tissue located at the posterior portion of the eye. It consists of five major classes of neurons- rod/cone photoreceptors, horizontal cells, bipolar cells, amacrine cells and ganglion cells (Heavner and Pevny, 2012) (Figure 1.2). When light hits the retina, photons activate the rod and cone photoreceptors, which propagate a graded glutamatergic signal to bipolar cells, which in turn releases glutamate onto retinal ganglion cells (RGCs). RGCs are the primary output neuron, transforming the graded signal into an action potential. The glutamatergic signal between these three neurons is refined by inhibitory neurotransmission (i.e. GABAergic, glycinergic, etc.) from horizontal and amacrine cell interneurons. Horizontal cells, which are GABAergic, refine the signal between photoreceptors and bipolar cells, while amacrine cells refine the signal between bipolar cells and RGCs. Amacrine cells are either GABAergic or glycinergic with

subpopulations of GABA-ergic amacrine cells that are also dopaminergic and cholinergic (Wassle, 2004).

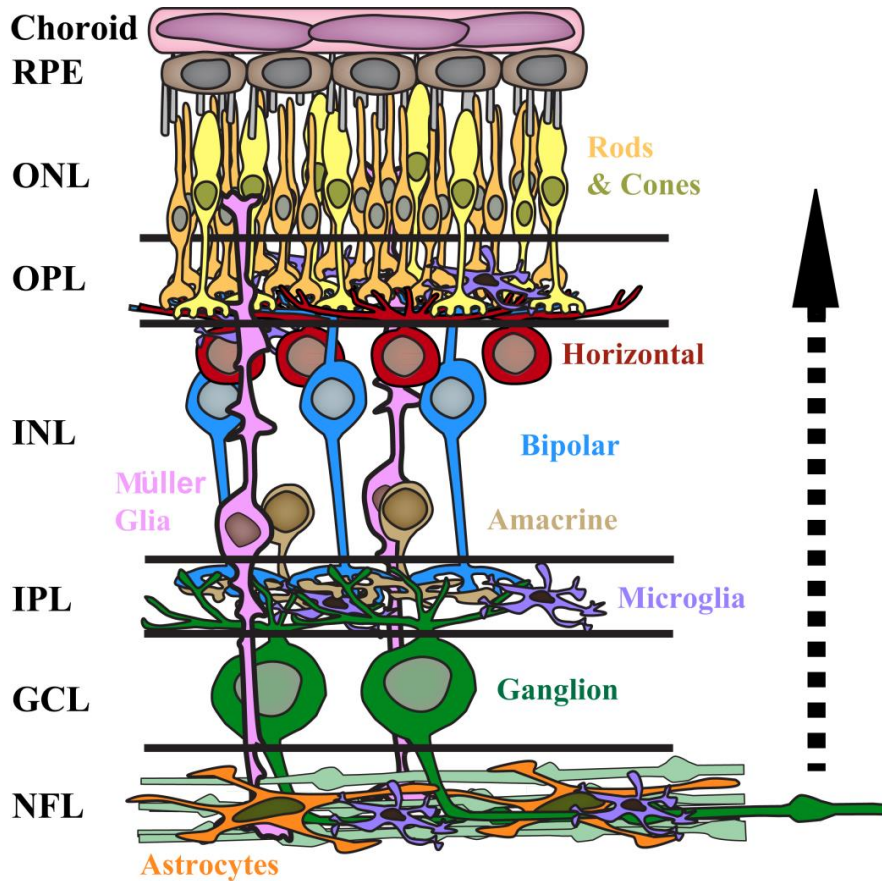


Figure 1.2. Retinal cell types and circuitry. In order to activate the light sensitive photoreceptors (rods & cones) in the outer nuclear layer (ONL), light must transverse the entire retina (direction of arrow). Transmission of the graded visual signal occurs in a top-down fashion. Activated photoreceptors send information through excitatory processes in the outer plexiform layer (OPL) to the bipolar cells in the inner nuclear layer (INL). The signal is then sent through excitatory processes in the inner plexiform layer (IPL) to the retinal ganglion cell (RGC) bodies in the ganglion cell layer (GCL). Prior to reaching the bipolar cells and RGCs, the activity of the signal is modulated by horizontal cells and amacrine cells in the OPL and IPL respectively. RGCs transform this graded signal into an action potential and send it along their axons in the nerve fiber layer. Axons exit the eye at the optic disc where they are myelinated and form the optic nerve. Glial cells (astrocytes, Müller Cells and microglia) also reside in the retina and work to maintain proper health and function within the retina.

Figure modified from (Calkins, 2012) with permission from DJ Calkins and used in accordance with Copyright Clearance Center's RightsLink service.

From their cell bodies, RGCs send action potentials along their axons, which collectively exit through the optic disc at the back of the eye and form the optic nerve. Axons within the optic nerve synapse at one of several structures within the brain, which are responsible for interpreting different aspects of visual input and optimizing the quantity and quality of visual input (Figure 1.3). The percentage of axons synapsing at each target varies with each mammalian species. In primates, including humans, the majority (~85%) of RGC axons project to the lateral geniculate nucleus (LGN) of the thalamus (Bunt et al., 1975, Perry et al., 1984), a structure responsible for processing details associated with vision including contrast, color, movement and depth perception (Livingstone and Hubel, 1988). The LGN then sends this information to the primary visual cortex from which it proceeds to higher cortical areas along dorsal and ventral streams. In rodents, it is thought that only about 25% of RGC axons project to the LGN (Dreher et al., 1985). However, approximately 80% of the RGCs that innervate the LGN also innervate the SC (Ellis et al., 2016). The remaining RGC axons send information to structures that optimize that quantity and quality of visual input. In humans 10% of RGC axons project to the superior colliculus (SC), while approximately 88% of rodent RGCs project to the SC (Dreher et al., 1985, Ellis et al., 2016). The SC helps coordinate rapid eye movements (i.e. saccades) that assist in collecting as much information from our visual field as possible (Kalesnykas and Sparks, 1996, Moschovakis, 1996). Additional and smaller RGC projections to the pre-tectum and suprachiasmatic nucleus (SCN) are involved in regulating pupillary eye reflexes and circadian rhythm respectively (Chen et al., 2011b).

Along with neurons, glial cells also populate the optic projection. In the retina, astrocytes and Müller cells maintain proper neuronal signaling by siphoning extraneous potassium (K^+), calcium (Ca^{2+}) and glutamate from the extracellular space (Vecino et al., 2016) (Figure 1.2).

Together with endothelial cells, astrocytes and Müller cells wrap their processes around the retinal vasculature to form the protective blood-retinal barrier (Vecino et al., 2016). At the optic nerve head, astrocytes converge on the unmyelinated RGC axons to form the glia lamina, which

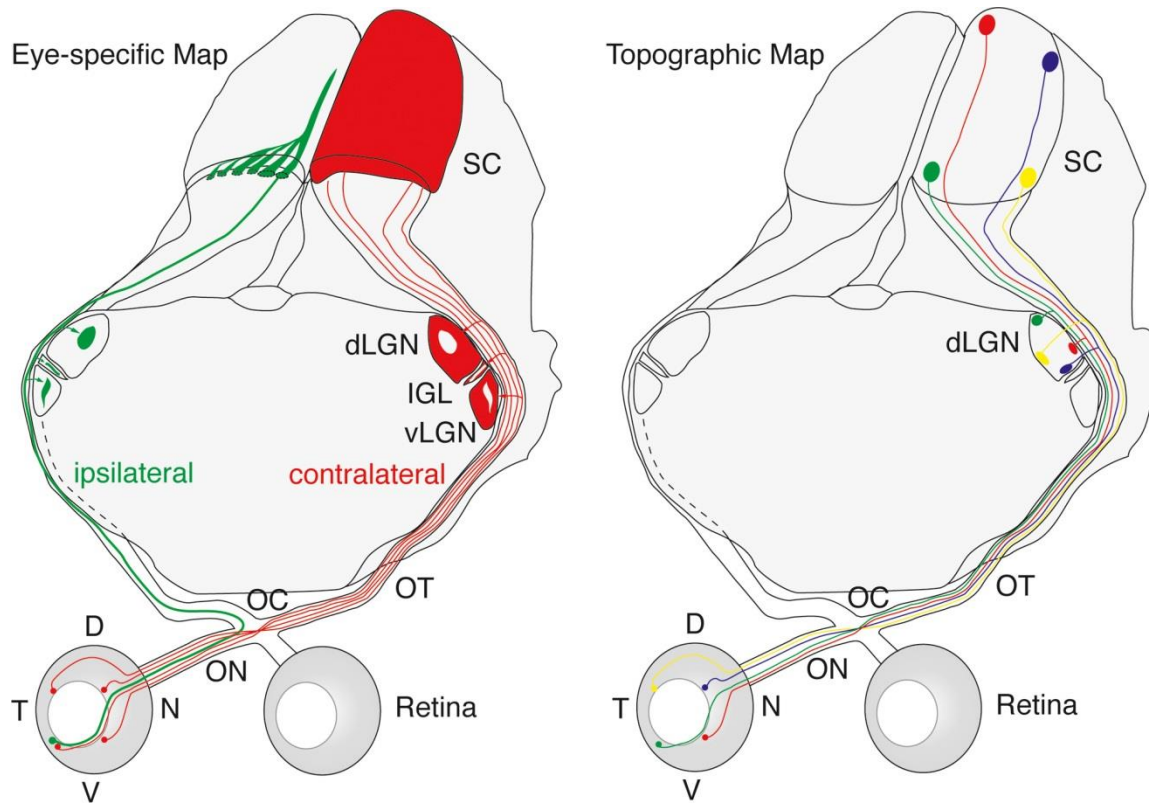


Figure 1.3. Eye specific and topographic maps of RGC connections in the mouse brain. **(Left)** Upon entering the brain, RGCs project primarily to contralateral (red) visual processing areas including the lateral geniculate nucleus (LGN) and the superior colliculus (SC). A small population of RGCs also makes ipsilateral connections to these structures (green). **(Right)** RGCs project to the LGN and SC in a topographic manner in that RGCs from quadrant of the retina (e.g dorsal quadrant, blue) all project to the same area (blue region) in the LGN and SC.

Figure from (Assali et al., 2014) and used in accordance with Copyright Clearance Center’s RightsLink service.

provides structural support and insulation (Sun et al., 2009). In primates, this is accompanied by a porous scaffold of extracellular matrix called the lamina cribosa (Vecino et al., 2016). Exiting the lamina, RGC axons enter the retrolaminar transition zone, where the axons are myelinated by oligodendrocytes for saltatory conduction just prior to exiting the globe (Vecino et al., 2016).

Microglia, similar to the rest of the CNS, serves as the resident macrophage in the retina, optic nerve head and myelinated optic nerve, surveying for and phagocytosing biological material that could be pathogenic (Vecino et al., 2016).

The optic projection as a model of the CNS

Two primary advantages that allow the optic projection to serve as an exceptional model for studying the CNS are the similarities RGCs have to other CNS populations, the highly conserved nature of retinal structure and its increased accessibility (London et al., 2013). While physically separate from the brain and spinal cord, RGCs are highly comparable to projection neurons found elsewhere in the CNS. RGCs display classic morphological components of neurons, including a cell body, dendrites and an axon. The axon, while unmyelinated in the retina, is myelinated by oligodendrocytes as it exits the globe. Unlike other structures in the CNS, retinal architecture is highly conserved within and even between species (Hoon et al., 2014). In all vertebrates, the retina is composed of three cellular layers and two synaptic layers containing five major neuronal classes (Hoon et al., 2014). While the total number of cells within each neuronal class varies greatly between species, variation decreases with increasing genetic similarity. For example, while significant variation of retinal cell number still exists between different inbred strains of mice, the variability within each inbred strain is extremely minimal (Williams et al., 1996, Williams and Moody, 2003, Keeley et al., 2014). For some species and elements of the circuit, we even know the approximate number of synapses between cell types (Chen and Chiao, 2014, Behrens et al., 2016). This increases our ability to detect neuron loss due to injury/disease and thus, characterize earlier and more modest pathology.

In terms of accessibility, the absence of bony structures coupled with a transparent window (i.e. cornea) at the anterior portion of the eye allows for unparalleled access to a neuronal population *in vivo* (London et al., 2013). This is even more so when using rodents to study the optic projection, as the proximal portion of the optic nerve is accessible without invasive surgery. These characteristics enable neuroscientists to not only visualize and track retinal pathology in real time, but introduce injury and/or potential therapeutic agents directly to RGCs with minimal effort or extraneous injury (London et al., 2013).

Comparable to other CNS neurons, mechanical injury to RGC axons within the optic nerve leads to gliosis, active transport deficits, structural degeneration, and lastly, apoptosis of the cell body (Crish and Calkins, 2011, Calkins, 2012). Similar to other CNS axons, optic nerve axon regeneration is limited due to factors that inhibit neurite outgrowth (London et al., 2013). RGC degeneration is also manifested in many brain diseases including Parkinson's disease and Alzheimer's disease (London et al., 2013), further corroborating the strong link between the retina and the brain. In Parkinson's disease (PD), patients suffer from motor dysfunction due to a deficiency in dopamine (Archibald et al., 2009). As the retina utilizes dopamine to encode differences in contrast, many patients with PD also experience defects in retinal function and thinning of the retina (Inzelberg et al., 2004, Moschos et al., 2011). In patients with Alzheimer's disease (AD), accumulation of amyloid-B and phosphorylated tau in the brain are associated with areas of neuron degeneration (Wenk, 2003). Similar accumulations are seen in the retina of both AD patients and mouse models of AD (Guo et al., 2010a, Chiu et al., 2012, Sivak, 2013). Interestingly, the accumulation of amyloid- β is also prevalent in the optic neuropathy glaucoma (Sivak, 2013), suggesting a link between AD and glaucoma. Indeed, a number of studies report a higher prevalence of glaucoma in patients affected by AD (Cesareo et al., 2015).

Glaucoma: Neurodegeneration of the optic nerve

Glaucoma is a collection of degenerative optic neuropathies that results in continuous vision loss caused by progressive degeneration of RGCs (Calkins, 2012). It is the number one cause of *irreversible* blindness and the second leading cause of blindness worldwide, with 60 million people affected worldwide in 2010 (Quigley and Broman, 2006). While genetics and race can influence the chances of developing glaucoma, age and sensitivity to intraocular pressure (IOP) are the two primary risk factors (Calkins, 2012). Similar to other neurodegenerative diseases, there is no therapy available that completely halts or reverses neuronal degeneration in glaucoma. Current treatments, which aim to lower IOP, only slow down RGC degeneration and subsequent vision loss (Calkins, 2012).

Clinical manifestations of glaucoma

Degeneration of RGCs in glaucoma leads to both functional and structural manifestations that are utilized by clinicians for diagnosis and monitoring disease progression. Progressive loss of RGC axons leads to increased "cupping" or excavation of the optic disc, a phenomenon that causes the center of the optic disc, known as the optic cup, to enlarge in comparison to the optic disc (Quigley, 1985, Kalesnykas and Sparks, 1996, Moschovakis, 1996) (Figure 1.4). Loss of RGC axons also leads to thinning of the retinal layer where RGC axons reside, known as the retinal nerve-fiber layer (NFL) (Hood and Kardon, 2007) (Figure 1.2). Using funduscopy and optical coherence tomography (OCT), clinicians can monitor nerve cupping and RNFL thinning respectively during routine eye exams. To assess vision loss, clinicians commonly utilize perimetry, an exam that involves the patient fixing their gaze at a specific point while a light flashes at different locations in the patient's visual field (Yaquib, 2012).

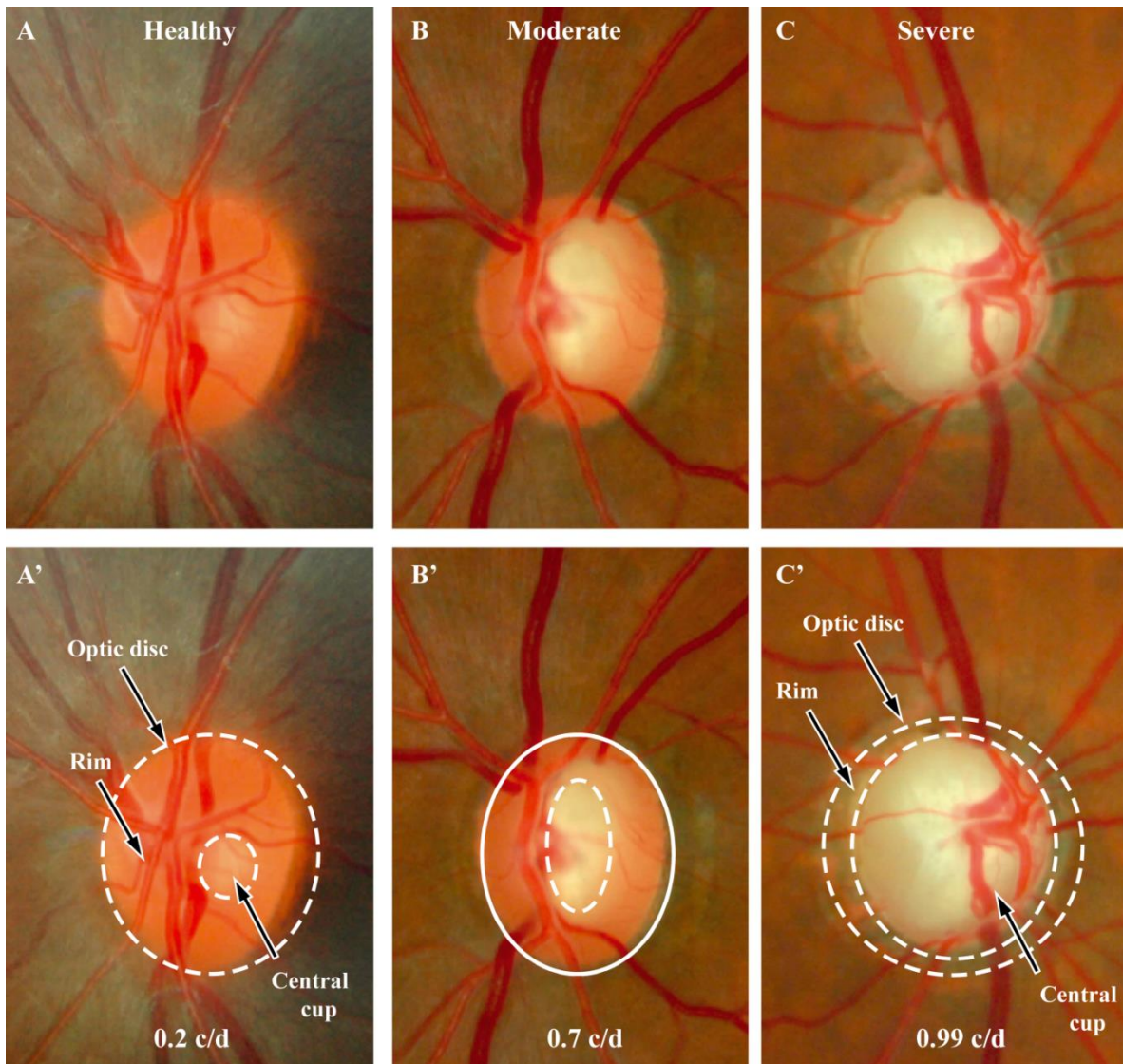


Figure 1.4. Formation and progression of optic disc cupping in glaucoma. The optic disc is where RGC axons collect to exit the eye and to form the optic nerve. **(A, A')** A fundus image of a healthy optic disc. The slightly cupped shape indicative of the central cup (inner circle, **A'**) is the location where RGC axons come together to exit the eye. Notice the large rim (area between optic disc and central cup), which is indicative of a small optic cup-to-disc (c/d) ratio (0.2 c/d in **A'**). This measurement is used by clinicians to diagnose and track glaucoma. **(B, B')** As glaucoma progresses and axons are lost, the central cup gets larger and the cup-to-disc ratio increases (0.7 c/d in **B'**). **(C, C')** In individuals with severe glaucoma, the central cup represents almost all of the optic disc area (0.99 c/s in **C'**).

Figure modified from (Bourne, 2012) and used in accordance with the Creative Commons Attribution-Non Commercial 4.0 International License.

Areas in the visual field where light flashes are not perceived constitute areas of visual deficits known as scotomas (Figure 1.5). Scotomas generally begin at the periphery of the temporal portion of the retina before progressing through either the superior or inferior poles and terminating at the nasal end of the retina (Levin, 2001, Yaqub, 2012) (Figure 1.5). This translates into a perceived loss of peripheral vision, which is affected before central vision. In a large number of patients, scotoma formation goes unnoticed until well formed (Health Quality, 2006), stressing the importance of yearly eye exams to catch structural pathology early.

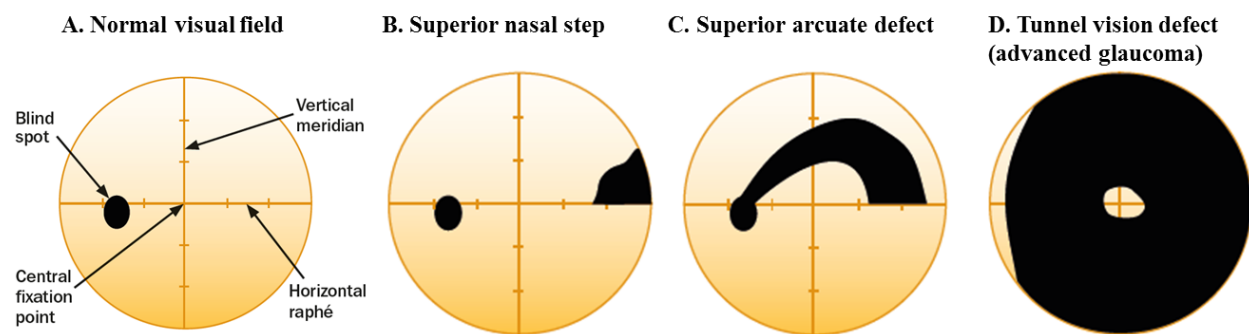


Figure 1.5. Visual loss in human glaucoma patients. **(A-D)** Representations of visual field maps collected using standard perimetry from glaucoma patients with varying degrees of vision loss. Each map is from a patient's left eye. Dark areas correspond to areas of decreased visual sensitivity. **(A)** Map of an individual with no apparent visual field deficits, except for the natural blind spot present in all individuals caused by the optic nerve head. **(B-C)** Glaucoma typically affects peripheral vision first as noted by scotomas in the periphery of the visual field that progress to an arcuate defect. **(D)** Map from a late stage patient shows the individual only retains their central vision.

Figure from (Broadway et al., 2013) and used in accordance with the Creative Commons Attribution-Non Commercial 4.0 International License.

Glaucoma: Age-related sensitivity to ocular hypertension

It has long been theorized that the primary insult to RGCs in glaucoma occurs at the optic nerve head (ONH), where RGC axons come together to form the optic nerve (Calkins, 2012). A current hypothesis describes the ONH and the surrounding scleral tissue as a biomechanical

structure, comprised of elastic connective tissue and glial cells that protect RGC axons from the stress and strain caused by normal eye movements and IOP (Burgoyne et al., 2005). In the clinic, glaucoma is typically split into three subtypes: open angle glaucoma (OAG), closed angle glaucoma (CAG), and normotensive glaucoma (NTG) (Shields, 2008, Hollands et al., 2013, Weinreb et al., 2014). While all result in the aforementioned clinical profile, the mechanism responsible is different among all three.

In OAG and CAG, consistent IOP elevation or ocular hypertension (> 21 mm/Hg) is the major causative factor, thus the importance of recording IOP measurements during routine eye exams (Quigley, 1993, Nongpiur et al., 2011). IOP is the fluid pressure within the anterior chamber of the eye and is determined by the net outcome of aqueous humor production and drainage (Weinreb et al., 2014). Aqueous humor is produced by the ciliary body, where it flows towards the angle formed by the cornea and iris (i.e. iridocorneal angle), and drains into the bloodstream through the trabecular meshwork (Figure 1.6). Normal IOP in humans ranges from 10-20 mmHg; however, recent data in non-human primates suggests that IOP constantly fluctuates, with overall changes of 15-40mmHg occurring from second to second (Downs et al., 2011, Downs, 2015a). During ocular hypertension, the dynamics of aqueous humor drainage become disrupted, leading to a buildup of aqueous humor in the anterior chamber. In CAG, disrupted outflow is caused by a occlusion or collapse of the iridocorneal angle, preventing aqueous humor from accessing the trabecular meshwork (Nongpiur et al., 2011). CAG is generally asymptomatic; however, a small percentage of patients experience large increases in IOP (> 30 mmHg), causing intense ocular pain, nausea and intermittent blurring (Salmon, 1999). In OAG, IOP elevation is not attributable to physical obstruction drainage canals, rather it is associated with altered fluid dynamics of various etiologies (Freddo and Gong, 2009). This often

gradual increase in IOP elevation typically goes un-noticed in patients (Quigley, 1993). In both OAG and CAG, the resulting IOP elevation is transduced from the anterior portion of the eye to the ONH. This culmination of IOP mediated stress is thought to alter the biomechanical properties of the ONH, leading to compression of the un-myelinated axons at the ONH and initiation of glaucoma specific RGC degeneration (Calkins, 2012).

While IOP elevation is a risk factor for glaucoma, some individuals with ocular hypertension do not develop glaucoma. Conversely, a significant portion of glaucoma patients develop normotensive glaucoma, a form of the disease that forms and progresses without ocular hypertension (Heijl et al., 2002, Iester et al., 2012). However, NTG patients still benefit from therapies designed to lower IOP. These two observations suggest that defining glaucoma as a disease caused by IOP elevation is an oversimplification. Like other neurodegenerative diseases, the risk of developing glaucoma increases with age, with individuals over the age of 55 being seven times more likely to become affected (Crish and Calkins, 2011). Throughout aging, the sclera and ONH lose elasticity and become increasingly rigid, mainly due to increased collagen deposition in the extracellular matrix (ECM) by astrocytes and astrocyte hypertrophy in the ONH (Albon et al., 1995, Downs, 2015b). It is hypothesized that these changes prevent the sclera and ONH from efficiently absorbing the mechanical stress and strain caused by normal IOP fluctuations, leaving RGC axons more sensitive and vulnerable to damage (Burgoyne et al., 2005, Downs, 2015b). This suggests that glaucoma is not due to IOP elevations *per se*, but is rather due to changes in sensitivity to IOP (Calkins, 2012).

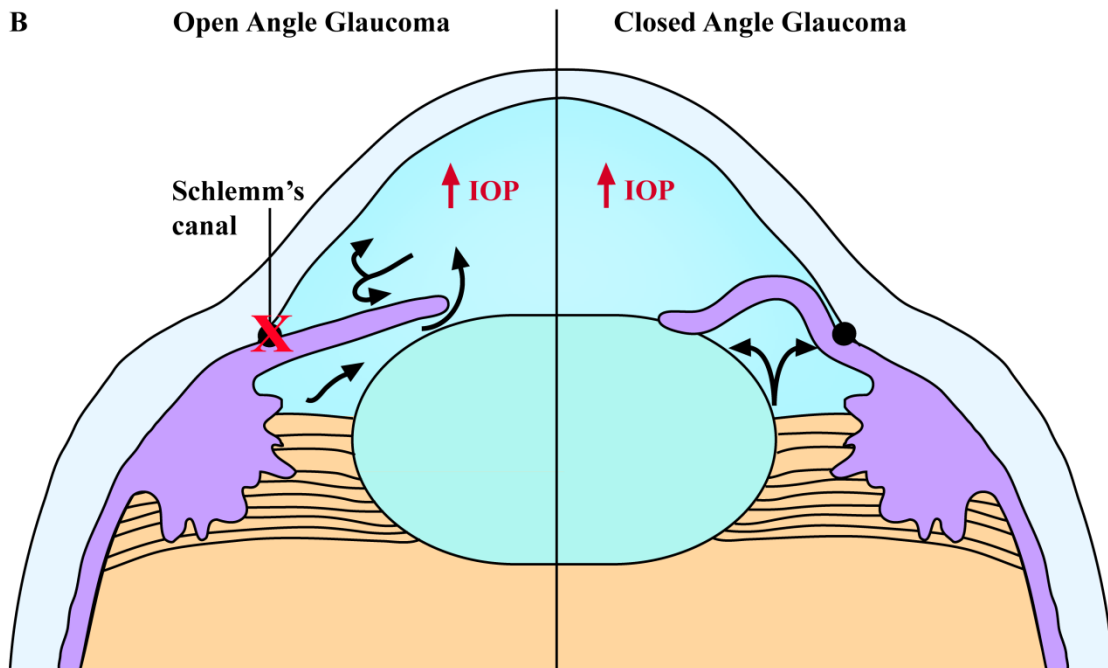
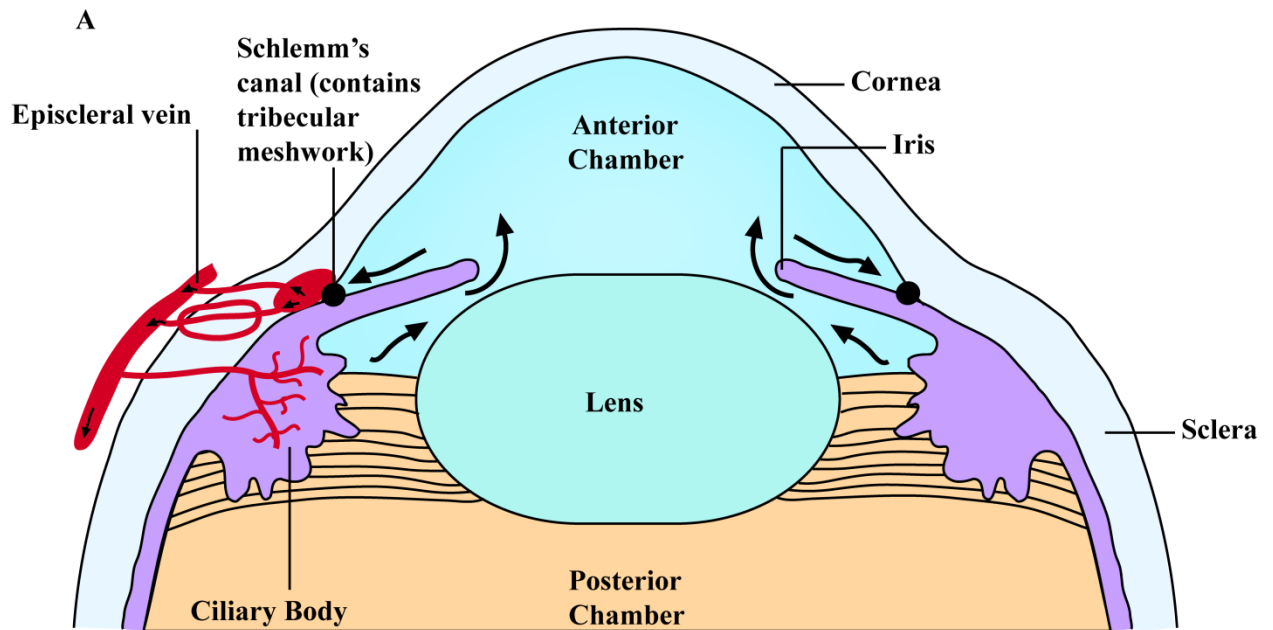


Figure 1.6. Aqueous humor dynamics in the eye. **(A)** Aqueous humor is constantly produced by the ciliary body in order to nourish and moisten the avascular tissues in the eye. Aqueous humor flows towards the anterior portion of the eye where it subsequently drains through the trabecular meshwork in Schlemm's canal and into the episcleral vein. The net outcome between aqueous humor production and drainage determines the intraocular pressure (IOP) of the eye. **(B)** In open angle glaucoma (OAG) (left), aqueous humor drainage through Schlemm's canal is compromised due to an obstruction or degeneration of the trabecular meshwork. In closed angle glaucoma (CAG) (right), the iris collapses, preventing aqueous humor from reaching Schlemm's canal. In both situations, IOP becomes elevated.

Figure adapted from (Weinreb et al., 2016) and used in accordance with Copyright Clearance Center's RightsLink service.

Progression of glaucoma in the optic projection

RGC degeneration in glaucoma occurs along a specific temporal sequence of events that is similar to that observed in other neurodegenerative conditions, including Alzheimer's Disease, Parkinson's Disease and ALS (Crish and Calkins, 2011). Glaucoma is nicknamed the "silent thief of sight", as the disease is generally asymptomatic in nature until vision loss is noticed. Unfortunately, the onset of vision loss coincides with significant disease progression (Calkins, 2012). However, evidence suggests that functional deficits (e.g. axon transport, electrical activity) of RGCs precede structural degeneration, while the RGC soma persists well after the axon has degenerated (Figure 1.7). This suggests a potential window for future therapies in not only rescuing functional deficits before RGCs degenerate, but regenerating axons in RGCs that have lost them. In order to develop such therapies, an understanding of the events that lead to RGC loss is needed. While our understanding is still incomplete, studies using animal models of glaucoma have shed light on these events leading up to RGC loss.

Animal Models of Glaucoma

Animal models have and continue to provide invaluable insight into the manifestation, progression and treatment of RGC degeneration in glaucoma. While it is known that ocular hypertension does not automatically equate to glaucoma in humans, the majority of glaucoma models incorporate naturally-occurring or induced IOP elevation to reproduce the clinical features of the disease. Two such models that have been utilized historically and compose a significant portion of my thesis studies include the inducible microbead occlusion model of glaucoma (Sappington et al., 2010) and the DBA/2J mouse model of inherited glaucoma (John et al., 1998, Anderson et al., 2002, Libby et al., 2005a).

Artificial induction of IOP elevation has historically and continues to be utilized to model glaucomatous pathology across mammalian models (Johnson and Tomarev, 2010, Bouhenni et al., 2012). While artificial induction can only model short term exposure (typically < 8 weeks) to elevated IOP, they allow scientists to test the impact of age and genetics on glaucomatous pathology. Generally, all models elevate IOP by preventing aqueous humor drainage. While some models impede drainage by occlusion of the trabecular meshwork (Levkovitch-Verbin et al., 2002, Sappington et al., 2010, Ito et al., 2016), others impede aqueous humor drainage into the surrounding vasculature (Garcia-Valenzuela et al., 1995, Morrison et al., 1997, WoldeMussie et al., 2001). While studies show that all these models result in some form of glaucomatous pathology, the microbead occlusion model has become the method of choice for modeling glaucoma (Sappington et al., 2010, Della Santina et al., 2013, Ward et al., 2014, Bond et al., 2016, Ito et al., 2016). In this model, a single injection of microbeads leads to a robust 20-35% elevation in IOP that is sustained for at least 4 weeks and is reproducible across cohorts (Sappington et al., 2010). Unlike other methods that induce 50-100% increases in IOP, ocular

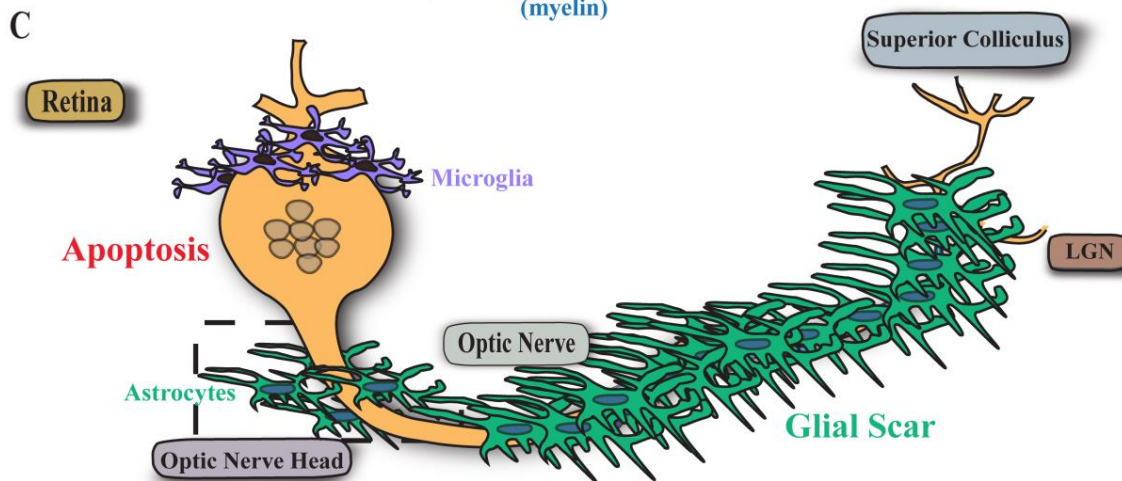
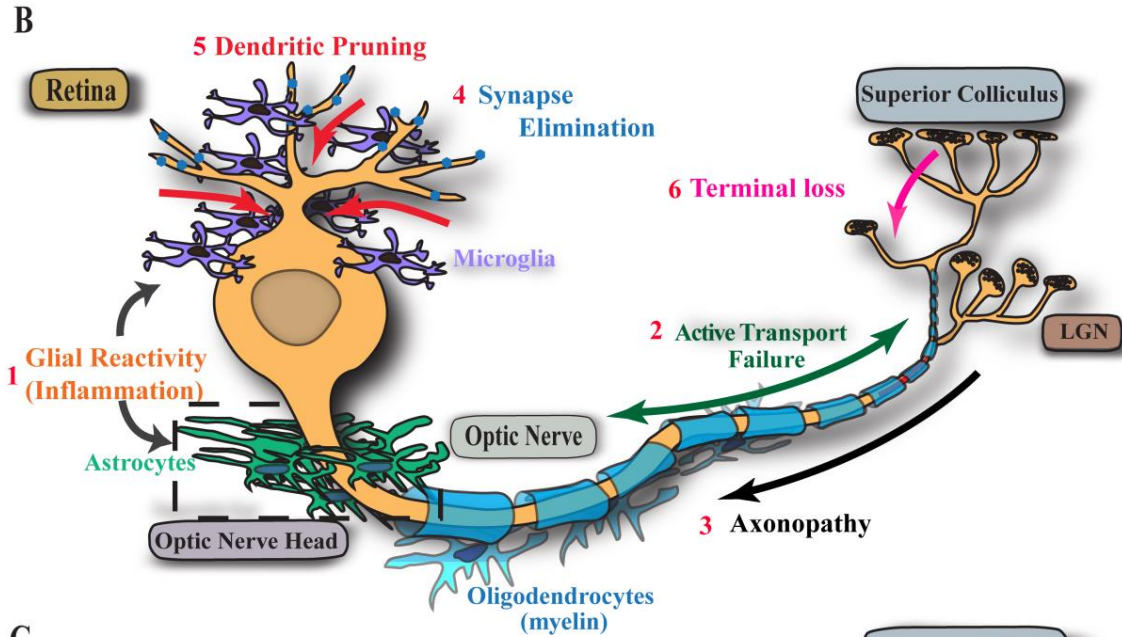
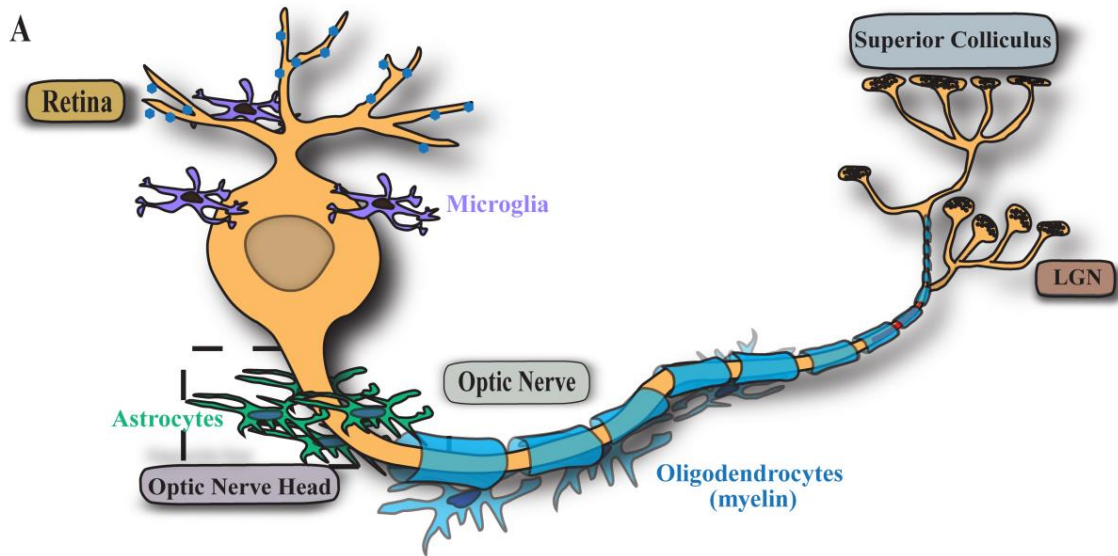


Figure 1.7. Critical steps in RGC degeneration in glaucoma. **(A)** A representative healthy RGC in the optic projection. **(B)** Upon a disease relevant stressor (e.g. age, elevated IOP) RGC axons in the optic nerve head become stressed, leading to glial reactivity of astrocytes within the optic nerve head (1). The chronic stress at the optic nerve head leads to a series of events within the RGC projection including axon transport failure (2), distal to proximal axonopathy (3), synapse elimination on dendrites due to microglia (4) followed by dendritic retraction (5) and distal terminal loss. **(C)** The cumulative impact of this stress initiates apoptosis within the RGC soma. At this point the axon has significantly degenerated and is replaced by a glial scar in the optic nerve.

Figure adapted from (Calkins and Horner, 2012) with permission from DJ Calkins and used in accordance with Copyright Clearance Center's RightsLink service.

hypertension in the microbead model better represents IOP elevation seen in patients with moderate OAG, thus providing a more physiological representation of the primary disease type. Additionally, the amount of surgical injury induced by the microbead occlusion model is minimal compared to other models, as measured by the lack of ocular ischemia and neovascularization (Goldblum and Mittag, 2002, Pang and Clark, 2007).

While the microbead occlusion model is valuable when testing how glaucomatous degeneration is affected by specific genes or age, its acute nature prevents us from modeling the temporal progression of the disease in response to age related increases in IOP that are seen in a large number of OAG and CAG patients. For these studies, the DBA/2J inbred mouse line is more appropriate. The DBA/2J mouse is one of the oldest inbred mouse strains and contains mutations in the *Gpnmb* and *Tyrp1* genes (Anderson et al., 2002). These mutations lead to iris pigment dispersion and iris stromal atrophy respectively, causing iris pigment to detach from the iris and clog the trabecular meshwork, obstructing aqueous outflow (John et al., 1998, Chang et al., 1999). This again more closely models CAG and more specifically, exfoliation glaucoma, which is caused by iris pigment dispersion in humans (Ritch, 2002). While some DBA/2J mice experience ocular hypertension at 3 months of age, the majority of DBA/2J mice present with

IOP elevation by 5-6 months of age (Inman et al., 2006). Despite the advantage the DBA/2J mouse has in more closely representing the human condition, the degree of variability in IOP elevation (2.5mmHg-8mmHg), onset of IOP elevation (3-6 months of age), and degree of pathology can confound interpretation of data when using this model to test potential therapies (Inman et al., 2006, Calkins, 2012).

Deficits in Axon Transport

Subsequent to the initial insult at the optic nerve head, the earliest sign of glaucomatous pathology in the optic project are deficits in axon transport (Crish et al., 2010) (Figure 1.7). Axon transport is the process in which neurons transport cargo, such as organelles, lipids, proteins and synaptic vesicles from their soma towards synaptic terminals (anterograde transport) or from synaptic terminals to their soma (retrograde transport). Cargo is transported along microtubule roadways composed of the cytoskeletal protein tubulin by specialized motor proteins known as kinesin and dynein, which utilize ATP for anterograde and retrograde transport respectively (Maday et al., 2014). Like in other neurons, proper axon transport is vital to multiple aspects of RGC function, including delivery of neurotransmitters for signaling, supplying neurotrophic factors for cell survival and redistributing mitochondria to meet energy requirements (DiStefano et al., 1992, Calkins, 2012, Saxton and Hollenbeck, 2012).

The temporal progression of axon transport deficiencies in glaucoma are best characterized in studies using the DBA/2J mouse. In analyzing anterograde axon transport, Crish and colleagues (Crish et al., 2010) injected the anterograde tracer CTB into the vitreal space and measured its localization in RGC projection sites in the brain. Deficits in the SC occurred as early as 3 months of age, with near complete loss of CTB label by 12 months. Additionally,

deficits were sectorial in nature, starting close to the periphery and moving towards the optic disc. Despite loss of CTB signal in the SC, CTB signal still appeared in more proximal projections (LGN) and in RGC soma, suggesting that anterograde transport failure progresses in a distal to proximal fashion. Separate studies evaluating retrograde transport by injecting the neural tracer fluorogold (FG) into the SC and quantifying the number of RGCs with FG uptake, did not observe deficits in FG+ RGCs until 6-8 months of age (Buckingham et al., 2008). This coupled with the observation that almost complete ablation of FG+ RGCs isn't seen until about 13-15 months of age, argues that anterograde transport is lost before retrograde transport (Buckingham et al., 2008). Dengler-Criss and colleagues (Dengler-Criss et al., 2014) corroborated this hypothesis by measuring anterograde and retrograde transport in the same cohort of DBA/2J mice. While the authors did not compare age of transport deficit onset, they reported that anterograde transport deficits were significantly larger than retrograde deficits in DBA/2J mice between 9-12 months of age.

An obvious suggestion to axon transport loss in the DBA/2J mouse would be axon degeneration. However, examination of DBA/2J mice at 10-12 months of age with significant transport deficits revealed substantial preservation of RGCs, axons and RGC synaptic terminals in the SC (Criss et al., 2010). In other neurodegenerative disorders, axon transport blockade is associated with disruptions in cytoskeletal organization, suggesting that components mediating transport within the axon might be compromised in glaucoma (Chevalier-Larsen and Holzbaur, 2006). Indeed, reports in the DBA/2J mouse point to modifications in cytoskeleton related proteins (i.e. neurofilaments, microtubules) as the primary cause of axon transport deficits (Dengler-Criss et al., 2014, Wilson et al., 2016). While microtubules provide the substrate in which motor proteins use to transport cargo, neurofilaments are transported along the axon to

help stabilize microtubule structure (Maday et al., 2014). In DBA/2J mice, studies show neurofilament pathology, including accumulation and phosphorylation, occurs prior to axon loss (Howell et al., 2007b, Soto et al., 2008, Wilson et al., 2016). Studies in other neurodegenerative disorders show excessive phosphorylation slows down its kinesin mediated transport down the axon, causing it to accumulate and impede transport of other cargo. In later stages of pathology (10-12 months), significant degeneration of neurofilaments and microtubules occur (Wilson et al., 2016). This loss of microtubules may also be due to the initial aggregation of neurofilaments as excessive phosphorylation impairs its affinity for microtubules, causing microtubules to become disorganized and aggregate (Wang et al., 2012).

Deficits in axon transport are also present in models of acute ocular hypertension. However, progression occurs much more rapidly. In models where IOP is elevated 100-1000% above normal, failure of anterograde transport occurs within hours. In one of the first reports characterizing axon transport following IOP elevation in non-human primates, Quigley and colleagues (Quigley and Anderson, 1976) show that anterograde transport deficiencies start only after two hours of inducing ocular hypertension, with full failure occurring after 8 hours. Additionally, reversing IOP back to physiological levels for 4 hours following ocular hypertension significantly mitigated axon transport failure, suggesting that short term deficits can be rescued. In rodents subjected to the microbead model, multiple studies report a 40-50% deficit in anterograde transport only after 4-6 weeks of moderate IOP elevation in mice (Ward et al., 2014, Bond et al., 2016), while another study shows similar deficits in rats after only 2 weeks of similar IOP elevation (Crish et al., 2010). Similar to anterograde transport, loss of retrograde transport also occurs quickly in induced glaucoma models. In a follow up to Quigley and Anderson's study, Minckler and colleagues (Minckler et al., 1977) reported that 12 hours of

100% IOP elevation in non-human primates is sufficient to obstruct retrograde transport. In rodent studies, 8 weeks of IOP elevation via microbead injection led to a ~45% reduction in FG+ RGC density (Chen et al., 2011a), while 100% IOP elevations for 1 week led to over a 70% decrease in FG+ RGC density (Salinas-Navarro et al., 2009).

RGC dysfunction

Subsequent to deficits in axon transport, RGC dysfunction becomes prominent in glaucoma (Porciatti, 2015). The majority of these abnormalities are centered on RGC responses to light based stimuli, which can eventually lead to scotoma formation and vision loss. In both patients and animal models, RGC dysfunction can be measured using electrophysiological recording techniques such as electroretinography (ERG) and visual evoked potentials (VEP). These techniques measure the electrical response, portrayed as a waveform, of the RGC soma and cortical RGC inputs respectively, using either a series of flashing lights (FERG/FVEP) or a patterned stimulus (PERG/PVEP). RGC dysfunction in the ERG and VEP waveforms is usually reported as a muted waveform response, with significant deficits in the amplitude and latency of characteristic waveform components (Porciatti, 2015).

In the clinic, abnormalities to both the PERG and VEP waveforms are noted prior to vision loss and structural degeneration (Parisi et al., 2006, Banitt et al., 2013, Jafarzadehpour et al., 2013). Specifically with PERG, one study reporting a timeline of 8 years between PERG abnormalities and thinning of the RNFL layer (Banitt et al., 2013). Similar findings in the DBA/2J mouse show that degeneration of the PERG waveform occurs early, with one study showing PERG defects 2-4 months prior to significant axon degeneration and RNFL thinning (Howell et al., 2007a, Saleh et al., 2007, Baltan et al., 2010, Domenici et al., 2014). In inducible

models, PERG/PVEP dysfunction also occurs prior to structural defects (Marx et al., 1988, Holcombe et al., 2008, Alsarraf et al., 2014). Corroborating the ERG/VEP waveform deficits, multi-electrode or single cell recordings of RGCs following 2-4 weeks of acute ocular hypertension show alterations in spontaneous rate and light induced activity (Della Santina et al., 2013, Ward et al., 2014). Equivalent to deficits in axon transport, PERG/VEP changes may be reversible prior to vision loss as various studies show treatment with IOP lowering therapies or various neuroprotective agents can prevent and reverse PERG/VEP deficits in both patients and DBA/2J mice (Sehi et al., 2010, Sullivan et al., 2011, Domenici et al., 2014, Porciatti, 2015, Feng et al., 2016).

Axon degeneration

Subsequent to functional deficits and degradation of the axon cytoskeleton, degeneration of the axon structure starts to transpire (Figure 1.7). Axon degeneration in most glaucoma studies is characterized by loss of axon density or total number of axons within the nerve (Calkins, 2012). Similar to deficits in the SC, axon loss in glaucoma is sectorial, with patches of degenerating axons clustered together (Schlamp et al., 2006, Soto et al., 2011). Following axon degeneration, astrocyte processes fill in the gap and create a glial scar which helps maintain the volume of the optic nerve and the integrity of the remaining axons (Calkins, 2012, Lye-Barthel et al., 2013).

In DBA/2J studies, loss of axons is reported to occur as early as 10 months, with some studies not noting significant axon degeneration until 13 months. It appears as if axon degeneration is more sensitive to IOP elevation than age, as several studies in the DBA/2J mouse show axon loss is associated to the degree of IOP elevation (Libby et al., 2005a, Inman et al.,

2006). The impact of IOP elevation is also prevalent in inducible models. Multiple microbead studies in rodents show significant axon degeneration (20%-25%) following 4-6 weeks of moderate IOP elevation (Sappington et al., 2010, Ward et al., 2014, Bond et al., 2016), while models that incorporate larger IOP elevations report between 30%-50% axon degeneration (Lambert et al., 2011, Kitaoka et al., 2013). Similar to the DBA/2J mouse, a meta-analysis of inducible glaucoma studies show that axon degeneration increases linearly with increasing IOP, further corroborating the impact of IOP in axon degeneration (Calkins, 2012).

The two primary mechanisms in which axon degeneration occurs in the CNS are “dying back” and Wallerian degeneration. Depending on the model used to recapitulate the disease, reports indicate both mechanisms may be relevant to the pathology of glaucoma (Calkins, 2012). The ‘dying back’ phenomenon corresponds to distal to proximal degeneration, where axon degeneration begins at the most distal end and slowly (weeks to months) progresses towards the cell body. In the DBA/2J mouse, studies show that estrogen related receptor beta (ERR β) signal in the SC, a marker of RGC input terminals, persists well after axon transport is compromised (Crish et al., 2010). Loss of ERR β signal is not seen until 13-15 months, when multiple studies show significant axonopathy (Crish et al., 2010). Additionally, analysis of degenerating axons along the optic nerve shows that distal segments present with significantly more degeneration than proximal segments, indicative of distal to proximal progression (Schlamp et al., 2006, Crish et al., 2010).

Following large (>100%) acute IOP elevations, studies in rodents and monkeys show structural pathology of the optic nerve soon after induced IOP elevation, including axonal swelling and protein accumulation, suggesting early axonopathy occurs at the ONH (Kompass et al., 2008, Joos et al., 2010, Chidlow et al., 2011). In one study the author’s show increased axon

loss in proximal portions of the optic nerve relative to distal portions after 2 weeks of 100% IOP elevation before evening out at 4 weeks (Beirowski et al., 2008). This is indicative of Wallerian degeneration, a form of pathology seen in models of axotomy in which degeneration begins at the distal portion of the injury and progresses rapidly in a proximal to distal manner (Calkins, 2012). Therefore, it is possible that intense IOP elevation commonly seen in inducible with large IOP elevation models leads to an “axotomy like” injury at the ONH, leading to a Wallerian degeneration profile (Crish and Calkins, 2011).

Regardless of mechanism of axon degeneration, it is evident from both DBA/2J and inducible models that axon degeneration precedes loss of the ganglion cell soma (Calkins, 2012). In their comprehensive study, Buckingham and colleagues did not note significant decreases in structural RGC density until 18-21 months of age in the DBA/2J mouse (Buckingham et al., 2008). Additionally, in the aforementioned meta-analysis of inducible glaucoma models, ganglion cell loss is 2-3X less than axon loss across all IOP exposures (Calkins, 2012). Finally, comparison of electrical responses from both RGC soma (PERG) and input terminals (VEP) in two year old DBA/2J mice shows complete degradation of the signal from RGC axon inputs, whereas RGC soma responses are diminished, but present (Heiduschka et al., 2010a).

Synapse elimination and dendritic pruning.

In the CNS, dendrites are branched projections of a neuron that receive electrochemical information from axons of efferent neurons via synapses. In the retina, RGC dendrite synapses connect with axons of their input bipolar and amacrine cells. In glaucoma and other neurodegenerative diseases, elimination of synapses and subsequent dendritic pruning precede neuronal cell loss (Calkins, 2012) (Figure 1.7). A current hypothesis suggests that synapse

elimination in glaucoma is driven by the complement cascade, a mechanism of the neuro-immune system that targets cellular material for phagocytosis and removal. In the DBA/2J mouse, several studies show that PSD-95, a marker of synapses, is reduced in RGC dendrites at 10-11 months of age (Stevens et al., 2007, Berry et al., 2015). In one study, this down-regulation of PSD-95 was accompanied by an upregulation of C1q, a complement protein that targets synapses for elimination by microglia (Stevens et al., 2007). This hypothesis was corroborated by a more recent study showing that genetic or pharmaceutical inhibition of C1q prevents early synapse and dendrite degeneration in both the DBA/2J and microbead models of glaucoma (Williams et al., 2016). Additionally, the loss of synapses may be related to deficiencies in neurotrophic factors associated with deficits in axon transport.

Following synapse elimination, dendrites undergo degeneration resulting in a loss of complexity and coverage of their dendritic branches. This is evident in the DBA/2J, where dendritic remodeling and shrinkage are prevalent in 11-12 month old mice (Jakobs et al., 2005, Berry et al., 2015). In various inducible models involving mice, cats, monkeys or rats, elevation of IOP led to decreases in dendritic field radius, total dendritic length and number of dendritic branches (Weber et al., 1998, Shou et al., 2003, Berry et al., 2015). Additionally, these studies suggest that certain types of RGCs are more susceptible to damage. In the primate study, parasol RGCs display greater dendritic loss than midget RGCs, while alpha RGCs display greater dendritic loss than beta RGCs in the cat (Weber et al., 1998, Shou et al., 2003). Regardless of species, it appears as if dendritic changes occur prior to soma shrinkage and axon pathology, suggesting that RGC dendrites are affected sooner than other parts of the RGC.

Recent studies using the microbead model provides further insight into the progression of dendritic degeneration and the more susceptible RGC types (Feng et al., 2013, El-Danaf and

Huberman, 2015). In one study, groups of mice with different fluorescently tagged RGCs underwent 7 days of IOP elevation (El-Danaf and Huberman, 2015). The authors reported that unlike populations of RGCs that stratify their dendrites in the ON sub-lamina of the IPL, those that stratify dendrites in the OFF sub-lamina undergo significant reductions in dendritic length and dendritic field area. The susceptibility of OFF-type RGCs to elevated IOP was corroborated by Della Santa and colleagues (Della Santina et al., 2013), who showed functional deficits of specific OFF-type RGCs prior to dendritic degeneration, suggesting that changes in RGC activity are not necessarily due to structural changes.

Vision loss

Aside from RGC death, vision loss is thought to be one of the final stages of glaucoma. In a meta-analysis looking at RGC density in the retina and corresponding deficits in the visual field from patients as measured by perimetry, only 25-35% of RGCs are lost in areas of the retina that contained visual field deficits (Harwerth and Quigley, 2006, Medeiros et al., 2013). These results suggest that vision loss occurs prior to RGC soma loss. While measuring visual field loss using perimetry is appropriate in a clinical setting, it is not very feasible in animal models, especially rodents. To measure vision loss in rodents, researchers commonly use the optokinetic reflex test, a paradigm involving the rodent's natural optokinetic reflex (Thomas et al., 2004, Douglas et al., 2005). While the test is unable to correlate visual defects to specific areas of the retina, it is able to measure the animal's overall visual acuity and contrast sensitivity thresholds. While not commonly used in the clinic, studies have reported deficits in the optokinetic response in glaucoma patients (Tong et al., 2002).

Glaucoma- related vision loss is present in both inducible glaucoma models and the DBA/2J mouse. In one study using the microbead model in mice, visual acuity threshold decreases almost 50% throughout the 30 day period of IOP elevation, with Brn3a+ RGC density also decreasing about 50% (Della Santina et al., 2013). Interestingly, another microbead study didn't see 50% decreases in visual acuity until after 6 months of elevated IOP (Feng et al., 2016). At a similar time point as presented in the former study, the latter study only saw 25% decreases in visual acuity. In the DBA/2J mouse, one study shows reductions of 30 and 200% decreases in visual acuity and contrast sensitivity thresholds respectively between 6 week old and 8 month old mice (Burroughs et al., 2011). Another study shows a similar 30% reduction in visual acuity threshold at 8 months, which progresses to 60% at 14 months of age. In the latter study, this corresponded to a 30% and 75% decrease in Brn3a+ RGC density (Rangarajan et al., 2011). While the majority of these studies show comparable decreases between visual acuity and Brn3a+ RGC density correspond with decreases in visual acuity, Brn3a+ labeling of RGCs in glaucoma is controversial. Several studies show that Brn3a is down-regulated in intact RGCs compromised by induced IOP elevation (Guo et al., 2009, Guo et al., 2010b), suggesting loss of Brn3a signal is more indicative of RGC dysfunction than loss.

The Final Step: RGC Apoptosis

Following the degeneration of axon transport, RGC function, dendritic structure and axon structure, RGC cell bodies succumb to these multitudes of stressors and become the last component of the RGC to degenerate (Figure 1.7). In the DBA/2J mouse significant loss of RGCs, as measured in one study using a disease independent marker, doesn't occur until around 18 months of age (Buckingham et al., 2008). Even in acute inducible models where loss of RGCs

occur within a week of IOP elevation, studies reporting both RGCs and axon counts show significantly less RGC loss compared to axon loss (Calkins, 2012). Consistent with other deficits in glaucoma, RGC loss is sectorial, with RGC loss occurring in clusters (Calkins, 2012).

Ample evidence from both human and animal tissue suggests that the mechanism behind RGC death in glaucoma is “programmed cell death” or apoptosis (Qu et al., 2010, Crish and Calkins, 2011). Unlike necrosis, a form of cell death that results from cellular injury such as lysis, apoptosis does not lead to expulsion of intracellular contents, which can damage surrounding cells. Instead, apoptosis is a tightly regulated and controlled process that condenses and breaks up organelles and DNA within the plasma membrane (Qu et al., 2010). Like all mammalian cells, apoptosis can be initiated via two pathways: the extrinsic pathway and the intrinsic pathway, with evidence showing relevancy of both pathways in glaucoma (Qu et al., 2010, Nickells, 2012).

The extrinsic pathway, also known as the death receptor pathway, involves extracellular signals (i.e. Fas ligand; FasL and tumor necrosis factor alpha; TNF α) that bind to cell surface receptors (i.e. Fas, TNFR) on the plasma membrane. Binding of these signals to their receptors on the cell surface leads to activation of “initiator” caspase 8, which is responsible for initiating apoptosis. Activated caspase 8 then activates “effector” caspases 3, 6, and 7 which are responsible for degradation of cellular components. Indeed, several studies show that FasL, Fas, TNF α , TNFR and caspases -8 and -3 are involved in certain inducible glaucoma models (McKinnon et al., 2002, Huang et al., 2005, Kim and Park, 2005, Ju et al., 2006, Nakazawa et al., 2006, Levkovitch-Verbin et al., 2007, Qu et al., 2010). An upregulation of these factors is also found in the iris and ciliary body of the DBA/2J mouse (Zhou et al., 2005); however, the upregulation is most likely due to apoptosis of pigmented cells of the iris that detach and occlude

the trabecular meshwork. Interestingly, no reports could be found characterizing an upregulation of these factors in the glaucomatous retina of the DBA/2J mouse.

While the extrinsic pathway is facilitated on external signals, the intrinsic pathway is catalyzed by internal signals, specifically those that come from mitochondria (Qu et al., 2010). Specifically, cellular stress leads to mitochondria dysfunction, prompting members of the pro-apoptotic family Bcl-2 (i.e. Bax, Bid, Bad) to release cytochrome c. In the healthy mitochondria, cytochrome c is involved in the electron transport chain, which produces energy for the cell in the form of ATP. Once released into the cell, cytochrome c binds to the apoptotic protease activating factor -1 (APAF-1), ATP and pro-caspase-9 to form the apoptosome. Once the apoptosome is formed, pro-caspase-9 is cleaved into caspase-9, serving as an initiator to activate the effector caspase-3. Similar to the intrinsic pathway, components of the extrinsic pathway are also upregulated in glaucoma, including cytochrome c, members of the Bcl-2 family and caspase -9 (Qu et al., 2010). However, the relevancy of the extrinsic pathway is highlighted by studies in Bax deficient mice, where RGCs are spared from apoptosis in the DBA/2J model of glaucoma (Libby et al., 2005b).

Neuroinflammation and a role for IL-6 in RGC survival

A number of mechanisms are suggested for facilitating RGC pathology in glaucoma including neurotrophin deprivation, oxidative stress, Ca²⁺ dysregulation and neuroinflammatory processes (Qu et al., 2010). Within the last decade however, the role of neuroinflammation has been extensively studied due to observations of increased glial reactivity at multiple “stages” in glaucomatous degeneration of RGCs (Soto and Howell, 2014) (Figure 1.7). While the exact neuroinflammatory signaling mechanisms behind specific events in glaucoma are not yet known,

gene and protein expression profiles of ONH and retinal samples from glaucoma patients and animal models provide insight into the inflammatory processes occurring during early stages of the disease. Elucidating mechanisms of early neuroinflammation are important, as it provides information on potential mechanisms that occur prior to significant degeneration. Targeting these mechanisms may lead to potential therapies not involved with lowering IOP. Based on these studies, early neuroinflammatory pathways involve the complement cascade, Toll like receptor (TLR) signaling, and cytokine release (Williams et al., 2017).

The complement system

The complement system is a component of the immune system that assists in targeting microbes or damaged cells for removal by cell lysis and subsequent phagocytosis. The complement system is composed of three pathways: classical, lectin and alternative (Williams et al., 2017). In the classical pathway, damaged cells upregulate or are tagged by the C1 complex. This leads to activation of other complement proteins (i.e. C3, C5, C9), which are responsible for the formation of the membrane attack complex (MAC), a structure that promotes cell lysis/apoptosis. In glaucoma, studies suggest that different outcomes in glaucoma are attributed to specific components of the classical pathway (Stasi et al., 2006, Steele et al., 2006, Stevens et al., 2007, Howell et al., 2011, Panagis et al., 2011, Howell et al., 2013). For example in DBA/2J mice, up-regulation of C1q occurs in response to IOP elevation and co-localizes with PSD-95 synapses in the dendrites of RGCs in the IPL (Stevens et al., 2007). As mentioned previously, these changes are followed by synapse elimination, dendritic pruning, and RGC dysfunction. Genetic or pharmaceutical inhibition of C1 ameliorates dendritic changes and subsequent degeneration in both DBA/2J and inducible models (Howell et al., 2011, Williams et al., 2016).

Despite the reported role of C1 in DBA/2J glaucoma, the overall impact of the classical complement system was unknown until just recently. The DBA/2J inbred strain is naturally deficient in C5, a necessary component in MAC formation. To determine its effect on DBA/2J specific glaucoma, Howell and colleagues (Howell et al., 2013) backcrossed a functional C5 gene from the C57Bl/6J mouse into the DBA/2J mouse. Interestingly, while significantly more DBA/2J^{C5; B6} display severe axon pathology 6 weeks earlier than WT DBA/2J mice, no difference in pathology is noted by 12 months of age. This suggests that the presence of C5 is sufficient to promote axonopathy early in disease, but it is not necessary.

TLR Activation

TLRs are a group of pattern recognition receptors that recognize surface proteins found on pathogens (Yu et al., 2010). Currently, 13 types of TLRs (11 in humans) have been characterized, with each one recognizing a different ligand. Aside from pathogen recognition, TLR2 and TLR4 can recognize host specific ligands, specifically signals implicated in stress (Yu et al., 2010). In glaucoma, these include upregulation of heat shock proteins or changes in ECM composition (Sakai et al., 2003, Luo et al., 2010). Upon recognition of its specific ligand, TLRs activate signaling cascades that lead to the release of neuroinflammatory factors such as cytokines. In the retina, TLRs are typically found on glial cells in the retina, although some studies suggest some neuronal populations express them as well (Luo et al., 2010, Xu and Wang, 2016). In respect to glaucoma, multiple types of TLRs are upregulated (Luo et al., 2010). Additionally, TLR gene polymorphisms, specifically TLR4, are associated with both normotensive and open angle glaucoma in three separate populations (Shibuya et al., 2008, Takano et al., 2012, Navarro-Partida et al., 2017). While the specific phenotypes of these

mutations are not yet known, it is plausible to suggest that they exacerbate neuroinflammatory mechanisms in some way. Indeed, studies using genetic or pharmaceutical inhibition of TLR4 in models of optic nerve crush or retinal ischemia/reperfusion, show decreases in glial reactivity and cytokine production, while at the same time inhibiting RGC loss (Dvorianchikova et al., 2010, Morzaev et al., 2015, Nakano et al., 2017).

Cytokine Release

While complement proteins and toll like receptors assist retinal cells in *recognizing* whether neighboring cells are compromised, the subsequent release of cytokines from glial cells facilitates survival or apoptosis of stressed RGCs. One of the more studied cytokines in glaucoma is TNF α . Along with a number of studies reporting roles for TNF α in the vitreous, retina and optic nerve of glaucoma patients and animal models (Yuan and Neufeld, 2000, Nakazawa et al., 2006, Tezel, 2008, Yang et al., 2011, Cueva Vargas et al., 2015), a number of *TNF α* gene polymorphisms are associated with increased chances of developing glaucoma (Lin et al., 2003a, Mossbock et al., 2006, Bozkurt et al., 2012, Xin et al., 2013). As a known initiator of the extrinsic pathway of apoptosis, it is not surprising to suggest that TNF α is directly responsible for RGC pathology in glaucoma. In fact, several studies in various glaucoma models show that genetic or pharmaceutical inhibition of TNF α signaling is neuroprotective to RGCs (Nakazawa et al., 2006, Cueva Vargas et al., 2015). In addition to promoting apoptosis, there is evidence to suggest that TNF α mediates cell survival by activating the transcription factor NF κ B (Tezel, 2008). Upon activation, NF κ B initiates transcription of other cytokines (i.e. IL-6) that are capable of initiating signaling cascades that prevent apoptosis (Sappington and Calkins, 2006, Sappington et al., 2006).

IL-6 as a potential target in glaucoma

In the optic projection, recent studies from us and others show involvement of the cytokine IL-6 in facilitating RGC survival in response to various stressors. In the healthy retina, IL-6 is constitutively released (Sims et al., 2012). However in response to elevated IOP, IL-6 levels increase in the retina and optic nerve head (Sappington et al., 2006, Cvenkel et al., 2010, Johnson et al., 2011, Chidlow et al., 2012). *In vitro*, elevated hydrostatic pressure leads to IL-6 release from microglia, which when supplied to RGCs, protects them from pressure induced apoptosis (Sappington et al., 2006). IL-6 also facilitates axon regeneration and in some instances prevents degeneration of RGCs in response to optic nerve crush (Leibinger et al., 2013, Leibinger et al., 2016). However, it is unclear whether IL-6 impacts RGC axonopathy similarly in response to a more subtle chronic injury *in vivo* as seen in glaucoma.

Interleukin-6 impacts CNS function

The IL-6 family of cytokines

IL-6 is the founding member of the glycoprotein-130 (gp130) family of cytokines, which also includes IL-11, IL-27, IL-31, ciliary neurotrophic factor (CNTF), leukemia inhibitory factor (LIF), cardiotrophin-1 (CT-1), cardiotrophin-2 (CT-2) and cardiotrophin-like cytokine factor-1 (CLCF-1) (Erta et al., 2012). This family is named for their common use of gp130, with the exception of IL-31, to initiate signal transduction (Mousa and Bakhiet, 2013). While functional redundancy between the members of the gp130 family exists, gene KO studies in mice of specific gp130 ligands and receptors provide evidence of individual roles within the body, including specific roles in the CNS (Mousa and Bakhiet, 2013)..

First characterized as a factor in T-cell activation, B-cell maturation, and the acute-phase response in the mid 1980's, IL-6 has since earned a pleiotropic reputation with roles in lipid metabolism, insulin resistance, hematopoiesis, osteogenesis and myogenesis (Franchimont et al., 2005, Hoene et al., 2013, Hunter and Jones, 2015). However, soon after its initial characterization, separate studies published in 1988 and 1989 implicated IL-6 as neurotrophic factor, capable of promoting a neuronal phenotype in neuroblast precursors and extending survival of mature neurons *in vitro* (Satoh et al., 1988, Hama et al., 1989). Since then, a plethora of *in vitro* and *in vivo* reports have corroborated these initial observations while also providing evidence for a role in exacerbating neurodegeneration (Erta et al., 2012).

IL-6 signal transduction

IL-6 signaling is mediated by IL-6 binding to its alpha receptor (IL-6R α) followed by recruitment and binding to the signal transduction receptor gp130. While there is controversy over the number of IL-6 and IL-6R α involved in the signaling complex, it is accepted that two copies of gp130 are required for IL-6 dependent gp130 signal transduction (Grotzinger et al., 1999). Gp130 signal transduction occurs in the cytoplasmic tail of gp130 (Heinrich et al., 1998). Near the plasma membrane, two proline rich regions known as box motifs recruit and bind tyrosine kinases including JAK1 and JAK2 (Heinrich et al., 1998). Prior to IL-6 mediated gp130 dimerization, JAKs reside in an inactive state on the gp130 box motifs. In response to gp130 dimerization, the JAKs on each gp130 unit are brought into close proximity, causing a mutual phosphorylation event between them (Heinrich et al., 1998). The phosphorylated JAKs are then capable of phosphorylating a number of more distal tyrosine residues on gp130 (Heinrich et al., 1998). Interestingly, each residue phosphorylated corresponds to different signaling cascades.

For example, phosphorylation of the tyrosine at position 767 (Y767) or 814 (Y814) leads to STAT3 phosphorylation, while phosphorylation of Y905 or Y915 leads to STAT1 phosphorylation (Heinrich et al., 1998). Activation of the MAPK/ERK and Akt/mTOR pathway appears to be mediated by phosphorylation of Y759 (Heinrich et al., 1998). Phosphorylation of STAT1/3, ERK and mTOR influences gene expression associated with proliferation, cell survival or production of neuroinflammatory mediators (Erta et al., 2012).

To regulate IL-6/gp130 signaling, the cell has multiple regulatory mechanisms in place. For example, the phosphatase SHP2 acts on phosphorylated JAKs to prevent subsequent activation of distal tyrosine residues (Heinrich et al., 1998). In the nucleus, the protein inhibitor of activated STAT (PIAS) protein attaches itself to phosphorylated STATs, inhibiting STAT mediated transcription (Heinrich et al., 1998). One of the more recently characterized mechanisms involves STAT mediated transcription of suppression of cytokine signaling-1 and -3 (SOCS-1,-3) genes. Following translation, SOCS-1 and SOCS-3 act not only on phosphorylated JAK to prevent subsequent gp130 and STAT1/3 phosphorylation, but also on naïve JAK to prevent their initial phosphorylation (Heinrich et al., 1998).

IL-6: Classical vs Trans-signaling

The pleotropic nature of IL-6 signaling is facilitated through two pathways: classical and trans-signaling (Scheller et al., 2011a) (Figure 1.8). Classical signaling involves a membrane bound IL-6R α (mIL-6R α), while trans-signaling incorporates a soluble form of the IL-6R α (sIL-6R α) (Scheller et al., 2011a). In humans, synthesis of sIL-6R α occurs by alternative splicing of IL-6R α mRNA or cleavage of mIL-6R α by metalloproteases (i.e. ADAM10, ADAM17), while mice only produce sIL-6R α by proteolytic cleavage (Scheller et al., 2011a). While the

consequences of the pathways are not well understood, the current literature suggests different roles for classical and trans-signaling (Hunter and Jones, 2015). In the naïve state, it is believed classical signaling is dominant due to minute levels of IL-6 (1-5pg/ml) and sIL-6R α (25-35 ng/pg) in the plasma (Hunter and Jones, 2015). Classical signaling is also associated with more homeostatic functions including glucose metabolism, T-cell differentiation, regeneration of intestinal epithelial cells, and hematopoiesis (Hunter and Jones, 2015). However, in response to a local injury, the increase in sIL-6R α and shift towards IL-6 trans-signaling acts as an “alarmin”, recruiting neutrophils and peripheral macrophages to the injury site to prevent infection and promote healing (Hunter and Jones, 2015).

Expression and regulation of IL-6 in the CNS

Following the discovery that IL-6 is capable of acting as a neurotrophic factor, questions were asked regarding where IL-6 and its receptors were expressed in the CNS. Various *in vitro* studies indicate that neurons and glial cells are able to express IL-6, IL-6R α , and gp130 to some degree (Tada et al., 1994, Marz et al., 1998, Lee et al., 2002, Erta et al., 2012). In contrast, endothelial cells of the CNS vasculature only express IL-6 and gp130 (Reyes et al., 1999, Chalaris et al., 2007). *In vivo*, IL-6, IL-6R α , and gp130 are expressed in the retina, striatum, hippocampus, hypothalamus, cortex, cerebellum and dorsal root ganglia (Schobitz et al., 1992, Yan et al., 1992, Gadiant and Otten, 1993, Schobitz et al., 1993, Gadiant and Otten, 1994a, b, 1995, Vallieres and Rivest, 1997, Chidlow et al., 2012, Sims et al., 2012). Similar to the periphery, gp130 expression is higher compared to IL-6 and IL-6R α in the CNS (Vallieres and Rivest, 1997).

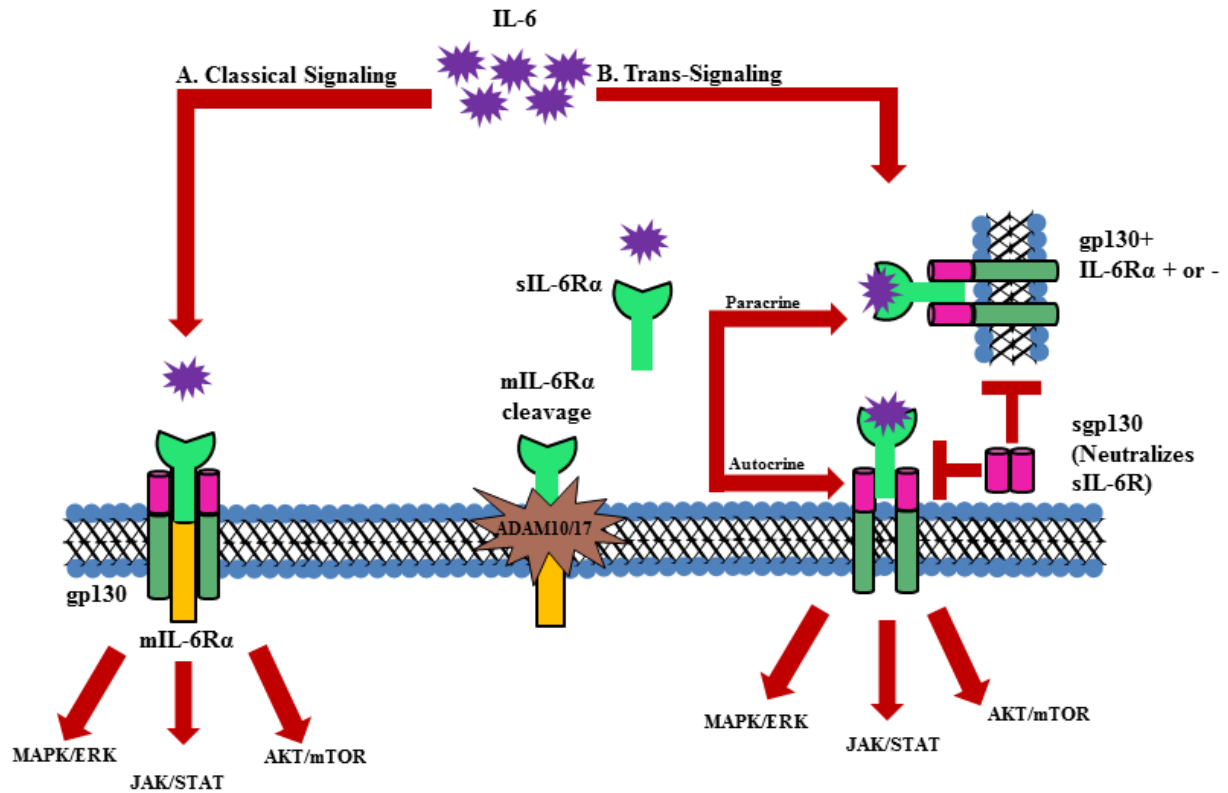


Figure 1.8. IL-6 signals in a classical and trans fashion. (A) In classical signaling, IL-6 binds to a membrane bound IL-6R α (mIL-6R α) followed by two copies of gp130. From there, multiple signaling pathways can be initiated including JAK/STAT, MAPK/ERK and Akt/mTOR. (B) In trans-signaling, the matrix metalloproteases ADAM10 and ADAM17 cleave mIL-6R α to form sIL-6R α . Unlike other soluble receptors, sIL-6R α serves as an agonist by binding IL-6 in the extracellular space followed by binding to gp130 on the cell surface. This allowed sIL-6R α to confer IL-6 sensitivity to cells that do not express mIL-6R α . In humans, but not mice, a soluble form of gp130 also exists, which serves to inhibit trans-signaling.

Figure adapted from (Erta et al., 2012) and used in accordance with the Creative Commons Attribution-Non Commercial 4.0 International License.

Infection, injury and even basal activity are capable of influencing IL-6 expression in the CNS. *In vitro*, application of the bacterial endotoxin lipopolysaccharide (LPS) or pro-inflammatory cytokines IL-1 β and TNF- α induce *Il-6* mRNA expression in glial cells (Sawada et al., 1992, Lee et al., 1993, Sebire et al., 1993) and neurons (Sebire et al., 1993). Up-regulated production of IL-6 from glia is also seen *in vivo* after peripheral injection of LPS in mice (Beurel

and Jope, 2009). In animal models of CNS trauma, IL-6 elevation is seen after seizure (Lehtimaki et al., 2003), acute IOP elevations (Sanchez et al., 2003, Johnson et al., 2011, Chidlow et al., 2012), optic nerve crush (Chidlow et al., 2012, Leibinger et al., 2013), brain ischemia (Hagberg et al., 1996, Loddick et al., 1998, Clark et al., 1999, Ali et al., 2000), closed head injury (Shohami et al., 1994) and peripheral nerve injury (Arruda et al., 1998). In the clinic, IL-6 elevation in both serum and CSF is also seen in people who have experienced traumatic brain injuries (Shohami et al., 1994, Kossmann et al., 1995, Kossmann et al., 1996, Bell et al., 1997, Arruda et al., 1998, Hans et al., 1999a, Hans et al., 1999b, Woiciechowsky et al., 2002, Winter et al., 2004). Interestingly, even acute physiological stressors are capable of influencing IL-6 expression. For example, application of NMDA or depolarization of the plasma membrane induces IL-6 expression (Sallmann et al., 2000), suggesting that basic neuronal activity can induce IL-6 release. In addition, mechanical stressors such as elevations in pressure can also induce IL-6 expression in both glia and neurons (Sappington and Calkins, 2006, Sappington et al., 2006, Crish et al., 2010).

IL-6 in neurodegeneration: friend or foe?

Previously, it was mentioned that chronic neuroinflammation is associated with neurodegenerative disease. Indeed, increased levels of IL-6 are reported in Alzheimer's (Blum-Degen et al., 1995), Parkinson's (Mogi et al., 1996), multiple sclerosis (Maimone et al., 1997), Huntington's (Dalrymple et al., 2007) and glaucoma (Chen et al., 1999, Takai et al., 2012, Huang et al., 2014, Du et al., 2016). However, whether IL-6 released in chronic neuroinflammation is beneficial or detrimental to neuronal survival is a topic of controversy. In basal conditions, exogenous IL-6 is capable of improving cell viability and promoting cell

differentiation (Sato et al., 1988, Hama et al., 1989). When coupled with a specific stressor, pre-treatment with IL-6 prevents apoptosis in neural cells exposed to NMDA (Toulmond et al., 1992, Yamada and Hatanaka, 1994, Peng et al., 2005), elevated hydrostatic pressure (Sappington et al., 2006), increased intracellular calcium (Umegaki et al., 1996), and certain toxins (Spittau et al., 2012) (Leibinger et al., 2013), suggesting that IL-6 is neuroprotective. This is further corroborated in some *in vivo* models of CNS injury. In response to focal brain injury, GFAP-IL-6 mice present with mitigated neuronal apoptosis at the injury site and quicker healing time compared to WT mice (Penkowa et al., 2003). In contrast, *Il-6*^{-/-} mice show a worsened CNS pathology after mechanical brain injury (Penkowa et al., 1999, Penkowa et al., 2000, Penkowa et al., 2001), optic nerve crush (Leibinger et al., 2013), brain ischemia (Clark et al., 2000), and dorsal column crush (Cafferty et al., 2004).

Conversely, other evidence suggests that IL-6 is neurotoxic. Previously, it was mentioned that over-expression of IL-6 leads to significant changes in CNS development that lead to functional deficits. In addition to that, over expression of IL-6 leads to progressive neurodegeneration of the cerebellum by 3 months of age in GFAP-IL-6 mice (Campbell et al., 1993). In addition, IL-6 deficient mice are resistant to EAE mediated axon degeneration and demyelination as well as glutamate toxicity and age related degeneration in forebrain GABA-ergic interneurons (Samoilova et al., 1998, Dugan et al., 2009).

Recent observations suggest that classical and trans-signaling mediate the respective neuroprotective and neurotoxic outcomes associated with IL-6 signaling. In the CNS, GFAP-IL-6 mice genetically modified to produce sgp130 are protected from the pathological phenotypes caused by IL-6 over expression (Campbell et al., 2014). Additionally, intra-cerebroventricular injection of sgp130 protects senescent mice from LPS mediated deficits in learning and memory,

social behavior and locomotion (Burton et al., 2011, Burton and Johnson, 2012, Burton et al., 2013). These results are not surprising as IL-6 trans-signaling is implicated in the pathology of various diseases in the periphery including Crohn's disease, inflammatory bowel disease and rheumatoid arthritis (Scheller et al., 2011a, Hunter and Jones, 2015). Blocking trans-signaling using sgp130 improves disease outcome in certain mouse models of these diseases and a clinical trial for sgp130 in inflammatory bowel disease is currently in development (Scheller et al., 2011a, Hunter and Jones, 2015). While therapies targeting both classical and trans-signaling are already in use in human patients, the homeostatic functions of classical signaling suggests an advantage in only targeting trans-signaling (Scheller et al., 2011a, Hunter and Jones, 2015). This is especially true in the CNS, where classical signaling may have roles in hippocampal neurogenesis and other yet-characterized processes (Bowen et al., 2011).

Specific Aims of Dissertation

The *objective* of this thesis project is to characterize the role of IL-6 (interleukin-6) in RGCs during conditions of homeostasis and glaucoma related disease. Our *central hypothesis* is that IL-6 activity has opposing roles in the healthy and glaucomatous RGC projection. Specifically, IL-6 promotes IOP-related RGC degeneration, but is necessary for proper development and function of a healthy RGC projection. This hypothesis is based on: 1) previous studies showing elevation of IL-6 in response to ocular hypertension and other chronic stressors, 2) reduced CNS degeneration in response to mitigation or ablation of IL-6 signaling, and 3) *in vivo* studies in *Il-6*^{-/-} mice showing structural and functional deficits in the central and peripheral nervous systems. To test our central hypothesis, we have developed these specific aims:

Aim 1: Establish the expression profile for IL-6 machinery in response to glaucoma-related stressors. The production of the soluble IL-6R α isoform and subsequent trans-signaling is a hallmark of many neurodegenerative diseases. *Our working hypothesis that IL-6R α shifts from a membrane to a soluble isoform in response to glaucoma related stressors.* In young (4mo) and aged (8mo) DBA/2J and C57 retina, we will: **(1)** determine protein concentration of gp130, **(2)** determine the population of (m) or soluble (s) IL-6R α . In DBA/2J retina we will also **(3)** measure the relationship between IL-6R α isoform and RGC health.

Aim 2: Determine whether IL-6 influences RGC degeneration caused by ocular hypertension. Elevated levels of IL-6 are present in neurodegenerative disease, including glaucoma. *Our working hypothesis is that IL-6 promotes RGC degeneration caused by ocular hypertension.* We will examine whether genetic ablation of IL-6 protects against RGC

degeneration associated with microbead- induced ocular hypertension. We will assess RGC degeneration by: **(1)** measuring anterograde axon transport from RGCs to the superior colliculus, **(2)** quantifying changes in axon survival and **(3)** measuring deficits in threshold visual acuity. Within the retina we will also **(4)** quantify changes in microglia and astrocyte glia populations.

Aim 3: Identify the outcomes of constitutive IL-6 signaling in the naïve optic projection.

IL-6 deficiency leads to structural and functional deficits in the central and peripheral nervous systems. *Our working hypothesis is that constitutive IL-6 signaling is necessary for proper development and function of the optic projection.* In naïve WT and *Il-6*^{-/-} mice we will: **(1)** assess the laminar structure of the retina **(2)** assess the cortical response to a light induced stimulus, **(3)** assess axon transport latency from RGCs to the superior colliculus, **(4)** quantify size and degree of myelination in axons of the optic nerve structure in the myelinated optic nerve, and **(5)** assess cytoskeletal morphology of RGC axons in the retina.

CHAPTER 2

ELEVATED PRESENCE OF THE SOLUBLE IL-6R α IN RESPONSE TO GLAUCOMA RELATED- STRESSORS²

Introduction

A common theme surrounding the majority of neurodegenerative diseases is age, with the average age of onset for PD, AD, ALS, and glaucoma occurring after the age of 50 (Blumberg et al., 2015, Boland and Platt, 2015). One hypothesis for the correlation between age and neurodegenerative disease involves age related chronic inflammation (Deleidi et al., 2015). As we age, the culmination of genetic and environmental stressors on our immune system causes 1) an increased production of inflammatory cytokines and 2) a decrease in our ability to terminate an inflammatory response (Franceschi et al., 2000, Licastro et al., 2005, Deleidi et al., 2015). In the CNS, this imbalance between pro-inflammatory and anti-inflammatory mechanisms results in a state of chronic neuroinflammation. Not surprisingly, chronic neuroinflammation is a common component of age-related neurodegenerative disease including AD, PD, HD, MS and glaucoma (Soto and Howell, 2014, Deleidi et al., 2015, Williams et al., 2017). The pro-inflammatory cytokine IL-6 is upregulated in chronic neuroinflammation and is associated with neurodegenerative disease, including RGC degeneration in glaucoma (Chen et al., 1999, Ghanem et al., 2011, Erta et al., 2012, Sims et al., 2012). In the retina, IL-6 is constitutively expressed by RGCs and glia (Sims et al., 2012). However, elevated pressure, a risk factor for glaucoma can

² Portions of this chapter were published as: Echevarria et al., (2013) Stressor-dependent Alterations in Glycoprotein 130: Implications for Glial Cell Reactivity, Cytokine Signaling and Ganglion Cell Health in Glaucoma. *J Clin Exp Ophthalmol* 4.

elevate IL-6 release from RGCs and glia (Sappington et al., 2006, Cvenkel et al., 2010, Johnson et al., 2011, Chidlow et al., 2012, Sims et al., 2012). Interestingly, the impact of IL-6 signaling in respect to retinal neurodegeneration is variable. While we have presented evidence that IL-6 protects RGCs from pressure induced apoptosis *in vitro* (Sappington et al., 2006), other studies suggest that inflammatory responses producing elevated IL-6 exacerbate pathological conditions that can impact RGC survival such as experimental autoimmune encephalomyelitis and retinal ischemia and reperfusion injury (Fisher et al., 2001, Horstmann et al., 2013).

IL-6 signaling is mediated by IL-6 binding to its alpha receptor (IL-6R α) followed by binding to the signal transduction receptor gp130 on the cell surface (Scheller et al., 2011a). Two types of IL-6 signaling exist and correspond to a specific IL-6R α isoform. In its membrane-bound isoform (mIL-6R α), IL-6R α mediates classical IL-6 signaling, while its soluble isoform (sIL-6R α) mediates trans-signaling (Scheller et al., 2011a). Unlike some soluble receptors that serve as antagonists to their specific ligand, sIL-6R α acts as an agonist. This is accomplished by sIL-6R α binding to IL-6 in the periphery, followed by associating with and activating gp130 on the cell surface (Scheller et al., 2011a). Regardless of IL-6R α isoform however, the IL-6/IL-6R α /gp130 complex initiates signaling through similar signal transduction pathways, including JAK/STAT, MAPK/ERK and AKT/mTOR (Rose-John, 2013). A soluble form of gp130 (sgp130) is also characterized in humans, but not mice (Scheller et al., 2011a). Unlike sIL-6R α , sgp130 only serves as an antagonist, selectively binding the IL-6/sIL-6R α complex. As it has no inhibitory effect on the IL-6/mIL-6R α , it is believed that sgp130 is produced to specifically regulate IL-6 trans-signaling (Scheller et al., 2011a). While the full complement of cellular responses induced by both classical and trans-signaling are not yet known, classical signaling is thought to be involved with homeostatic processes, while trans-signaling is implicated in a

variety of chronic inflammatory diseases in the periphery including inflammatory bowel disease, rheumatoid arthritis and Crohn's disease (Scheller et al., 2011a, Hunter and Jones, 2015).

Recent studies also show a role for trans-signaling in CNS degeneration/ dysfunction following chronic stressors (Burton et al., 2011, Burton and Johnson, 2012, Burton et al., 2013, Campbell et al., 2014). However, trans-signaling or the presence of the soluble receptor has not been associated to a specific neurodegenerative disease. Previous work in the lab indicates that expression and localization of IL-6 and IL-6R α become more spatially variable in response to age and elevated IOP, two primary risk factors in glaucoma (Sims et al., 2012). However, it is not known whether these stressors include alterations in IL-6R α receptor isoform or gp130, both of which can influence IL-6 mediated signaling. In this chapter, we tested how age and IOP elevation affects expression and localization of mIL-6R α , sIL-6R α and gp130 using the DBA/2J mouse model of glaucoma. DBA/2J mice are relevant to human forms of glaucoma as they develop IOP elevation and subsequent RGC pathology in an age dependent manner (Chang et al., 1999, Anderson et al., 2002, Inman et al., 2006). We then correlated glaucoma related changes in IL-6R α isoform and gp130 expression to RGC integrity. Together, these results suggest that a shift from IL-6 classical to trans-signaling could be a pathological component of glaucoma.

Materials and Methods

Animals

4 month and 8 month male DBA/2J mice, age matched C57Bl/6J (C57) mice, and 4 month male and female B6;129SF2/J mice were obtained from Jackson Laboratories (Bar Harbor, Maine). Mice were housed in accordance with the National Institutes of Health guidelines. All study procedures conformed to the ARVO Statement for the Use of Animals in Ophthalmic and Vision Research and were approved by the Institutional Animal Care and Use Committee of Vanderbilt University Medical Center. Animals were maintained on a 12-hour light/12-hour-dark cycle and were given unrestricted access to food and water.

IOP measurements

We obtained IOP measurements from all DBA/2J mice a minimum of once per month beginning at 3 months of age. IOP for each eye was calculated as the mean of 5-10 measurements and evaluated at least monthly using a tonometer (TonoLab; Reichert, Depew, NY), as previously described (Inman et al., 2006, Sappington and Calkins, 2008, Crish et al., 2010). The average IOP for DBA/2J mice used all studies was 15.2 ± 1.48 mmHg and 18.4 ± 2.30 mmHg for 4 month and 8 month old mice, respectively. The average IOP for DBA/2J mice was 15.2 ± 1.48 mmHg and 18.4 ± 2.30 mmHg for 4 month and 8 month old mice, respectively.

Tissue preparation

For fresh tissue analyses, mice were sacrificed via cervical dislocation followed by decapitation. Eyes were enucleated, flash frozen on dry ice and stored at -80°C until use. For fixed tissue analyses, For histological assays, mice were euthanized with an overdose of

pentobarbital and perfused trans-cardially with 100ml of 1X PBS (Sigma Aldrich, St. Louis, MO) followed by 100ml of 4% paraformaldehyde (PFA; Electron Microscopy Sciences, Hatfield, PA). Whole eyes were enucleated and post-fixed in 4% PFA for at least 24 hours at 4°C. Whole eyes and whole retina were prepared for cryo-sectioning and whole mount immunohistochemistry, respectively, as previously described (Echevarria et al., 2013, Echevarria et al., 2016)

Lipopolysaccharide (LPS) stimulation

For fixed tissue experiments, B6;129SF2/J mice (n = 5) received intravitreal injection of 2µl of 5µg/ul LPS (LPS; Cat# L4391-1MG, Sigma) in the right eye, while the left eye served as an internal control and received an equal volume injection of saline. For fresh tissue experiments, B6;129SF2/J mice received 2µl of 5mg/µl LPS in the right eye and an equal volume injection of saline in the left eye (n=15) or no experimental manipulation (n = 10). All mice were sacrificed and tissue collected 6 hours post LPS/saline injection.

Gp130 and soluble IL-6R α quantification

To quantify gp130 and sIL-6R α in retinal lysates, soluble and trans-membrane protein fractions were isolated and analyzed using the Milliplex™ Map Mouse Soluble Cytokine Receptor Magnetic Bead Panel immunoassay kit (cat# MSCRMAG-42K; Millipore). Soluble and membrane fractions were separated from retinal lysates (5 retinas/ sample), using the ProteoExtract® Trans-membrane Protein Extraction Kit (cat# 71772-3; Millipore) according to manufacturer's instructions. Quality controls and standards were run concurrently with experimental samples. Each control, standard and sample was run in duplicate. Total protein

concentrations were determined using a BCA Protein assay (cat# 23227; Thermo-Fisher). Value reported for gp130 was recorded from the transmembrane fraction, as soluble gp130 is not expressed in mice. For sIL-6R α , the value reported in the data is the concentration of IL-6R α (pg IL-6R α /ml/ μ g total protein) measured in the soluble fraction of a sample as a percentage of the total IL-6R α concentration (soluble + membrane fraction).

Neural transport tracing

For neural tracing studies, mice received an intravitreal injection of CTB (2 μ l; 10 μ g/ μ l) conjugated to Alexa Fluor-594 (cat# C-22842; Life Technologies) 48 hours prior to sacrifice, as previously described (Echevarria et al., 2013, Formichella et al., 2014). CTB labeling in fixed, whole mounted retina was imaged with an inverted confocal microscope (Olympus FV-1000; Center Valley, PA) through the Vanderbilt University Medical Center Cell Imaging Shared Resource Core. Three dimensional z-stack images of the retina were acquired using a digital camera and image analysis software (FV-100 ASW; Olympus). For each retina, at least 5 pseudo-random images were acquired in mid central/mid-peripheral areas at 60x magnification through the ganglion cell and nerve fiber layers. CTB intensity in whole mounted retina was measured using Image J software (National Institute of Health). Intensity is reported in arbitrary units and is the average intensity found within the entire image.

Immunohistochemistry

Immunolabeling of whole eye cryosections was performed, as previously described (Echevarria et al., 2016). Sections were co-labeled with primary antibodies against epitopes in the cytoplasmic domain (rabbit anti-IL-6R α /M20; 1:50; cat# SC660; Santa Cruz) and

extracellular domains (rat anti-IL-6R α /CD126; 1:300; cat# MAB18301; R&D Systems) of IL-6R α . Primary antibody binding was detected by fluorophore-conjugated secondary antibodies: anti-rabbit Dylight 488 (1:200; cat# 711-486-152; Jackson ImmunoResearch) and anti-rat rhodamine red-x (1:200; cat# 712-296-150; Jackson ImmunoResearch). Sections were imaged using a Nikon Ti Eclipse microscope (Nikon Instruments Inc.) equipped with FITC/TRITC/Cy5 filters for epifluorescence. Fluorescent images at 20x magnification were captured using a CoolSNAP HQ² black and white camera (Roper Scientific). Whole-mount immunohistochemistry was performed as previously described (Sims et al., 2012, Echevarria et al., 2013, Echevarria et al., 2016). Whole retinas were labeled with the primary antibodies described above or gp130 (rat anti-gp130 (1:12.5; cat# MAB4681; R&D Systems) and the following secondary antibodies: anti-rabbit Dylight 647 (1:200, cat# 711-605-152; Jackson ImmunoResearch) and anti-rat Alexa Fluor 488 (1:200, cat# 712-545-150; Jackson ImmunoResearch). Quantification of gp130 intensity was done as described in neural tracing studies.

Co-localization analysis

Co-localization between antibodies recognizing the cytoplasmic (M20) and extracellular domains (CD126) of IL-6R α was quantified by observer grading. A co-localization grading between 1 and 4 was assigned to each confocal micrograph by an observer blind to experimental cohorts. A score of 1 was assigned to images with the least co-localization of immunolabeling and a score of 4 was assigned to images with the most co-localization (Figure 2.2). Scores of 2 and 3 were assigned to images with more/less co-localization than images scored with 1 and 4, respectively.

Statistical analysis:

Statistical analysis was conducted with SigmaPlot Version 11.1 (Systat Software Inc, San Jose, CA). For comparison of two populations of data passing normality and equal variance criteria, a student's t-test was performed. For data sets which failed normality and equal variance criteria, a Mann-Whitney RANK Sum Test was used. Data sets that passed normality and equal variance criteria were represented as bar graphs or point plots. Data sets that did not pass normality and equal variance criteria were represented as box plots. For all, p -values < 0.05 were considered statistically significant.

Results

Glaucoma-related stressors promote sIL-6R α production.

Both age and elevated IOP are risk factors for glaucoma (Crish and Calkins, 2011). To determine whether these stressors alter gp130 and IL-6R α demographics in retina, we examined aging alone in C57Bl/6J (C57) mice and aging plus elevated IOP using the DBA/2J mouse. We first examined protein levels of IL-6R α isoforms in soluble and trans-membrane fractions of protein lysates from retina of young (4mo) and aging (8mo) C57 and DBA/2J mice. We found that the sIL-6R α isoform accounted for approximately 47% of total IL-6R α (IL-6R α soluble fraction + IL-6R α membrane fraction) in aging C57 retina, compared to 5% in young retina ($p < 0.001$; Figure 2.1A). In aging DBA/2J mice with elevated IOP, sIL-6R α accounted for nearly 25% of total IL-6R α in retina, compared to 8% in young DBA/2J mice with normal IOP ($p = 0.023$; Figure 2.1B). For gp130 protein, no protein was detected in soluble fractions. In membrane fractions, gp130 protein levels were significantly elevated by 33% in aging C57 retina compared to young retina ($p < 0.05$; Figure 2.1C). Although not statistically significant, there is also a trend towards decreased gp130 protein expression in aging DBA/2J retina, as compared to young C57 retina ($p = 0.06$; Figure 2.1D).

sIL-6R α increases in response to acute inflammatory stress in the retina.

Examining the potential relevance of IL-6 trans-signaling to glaucoma presented a key technical hurdle. The most widely studied models of glaucoma are rodent models. In rodents, sIL-6R α is produced by proteolytic cleavage that frees the extracellular domain from existing mIL-6R α (Garbers et al., 2011, Scheller et al., 2011b). As such, the two isoforms differ only by the presence or absence of the intracellular domain. While this hurdle can be rather easily

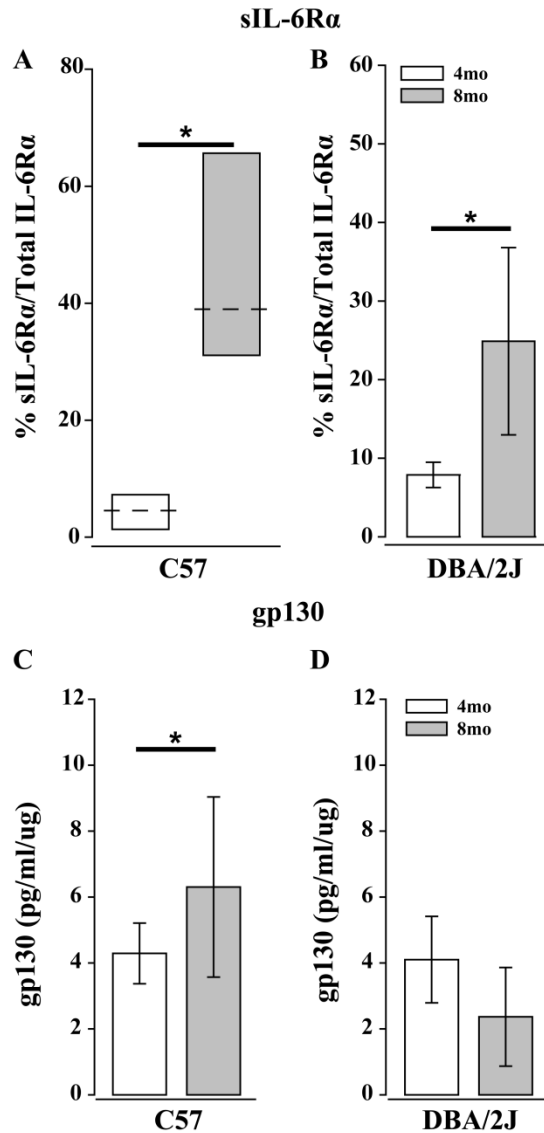


Figure 2.1 Glaucoma related stressors affect gp130 and IL-6R α isoform expression (**A,B**) Graphical representation of percentage of sIL-6R α (IL-6R α in soluble fractions) compared to total IL-6R α (IL-6R α in soluble and membrane fractions) from retina protein lysates from young (4 month; white) and aging (8mo; gray) C57 (**A**) and DBA/2J (**B**) mice. Age leads to significant increases in percent sIL-6R α in both C57 ($p < 0.001$, Mann-Whitney RANK Sum Test) and DBA ($p < 0.023$, student's t-test). Dashed lines in box plot indicate median value. Error bars in bar graph indicate standard deviation. (**C,D**) Bar graphs of retinal gp130 protein concentration (pg gp130/ml/ μ g total protein) in membrane fractions of young (4mo; white) and aging (8mo; gray) C57 (**C**) and DBA/2J (**D**) mice. Normal aging leads to a significant increase in retinal gp130 in C57 ($p < 0.05$, student's t-test), while aging coupled with IOP elevation leads to a trend towards a decrease in retinal gp130 in DBA/2J. ($p = 0.06$, student's t-test). * = $p < 0.05$. Error bars in bar graphs indicate standard deviation.

Parts of this figure are taken from (Echevarria et al., 2013) and used in accordance with the Creative Commons Attribution-Non Commercial 4.0 International License.

addressed in biochemical assays, our previous work indicates spatial regulation of IL-6 signaling is highly relevant in glaucoma. To differentiate sIL-6R α and mL-6R α in fixed tissue, we devised a co-immunolabeling strategy with antibodies against the C-terminal (M20; intracellular) and N-terminal (CD126; extracellular) portions of IL-6R α . Utilizing different secondary antibodies to label the M20 (green) and CD126 (red) antibodies respectively, mL-6R α (yellow) can be differentiated from sIL-6R α (red) (Figure 2.2A).

To validate our IL-6R α isoform outcomes in retina, we first examined sIL-6R α and mL-6R α expression and localization in response to gram-negative endotoxin lipopolysaccharide (LPS), a well-described inducer of IL-6 trans-signaling (de Vos et al., 1994, Mo and Streilein, 2001, Rosenbaum et al., 2011). In one group of young (4mo) mice, we injected 10 μ g (2 μ l) of LPS into the vitreal cavity of the right eye, while injecting an equal amount of diluent (saline) in the left eye. Another group served as controls and received no injection. Six hours after injection, we separated membrane and soluble protein fractions from all samples and probed for IL-6R α , using a high-throughput ELISA. In naïve and saline retinas, the sIL-6R α isoform accounted for approximately 13.1% and 16.7% of all retinal IL-6R α , respectively ($p > 0.05$; Figure 2.2B). In LPS-treated retina, sIL-6R α concentrations increased significantly to account for nearly 25.2% of all IL-6R α ($p = 0.014$; Figure 2.2B). To determine localization patterns for sIL-6R α and mL-6R α , we co-immunolabeled whole eye sections from LPS- and saline-injected mice with antibodies against the extracellular and intracellular segments of IL-6R α , as described above (Figure 2.2C). Retina from saline-injected mice exhibited strong immunolabeling with both antibodies, particularly in the outer (OPL) and inner plexiform (IPL) layers, the ganglion cell layer (GCL) and the nerve fiber layer (NFL; Figure 2.2C). Signal from the two antibodies strongly co-localized in these layers (Figure 2.2C). However, labeling intensity for the

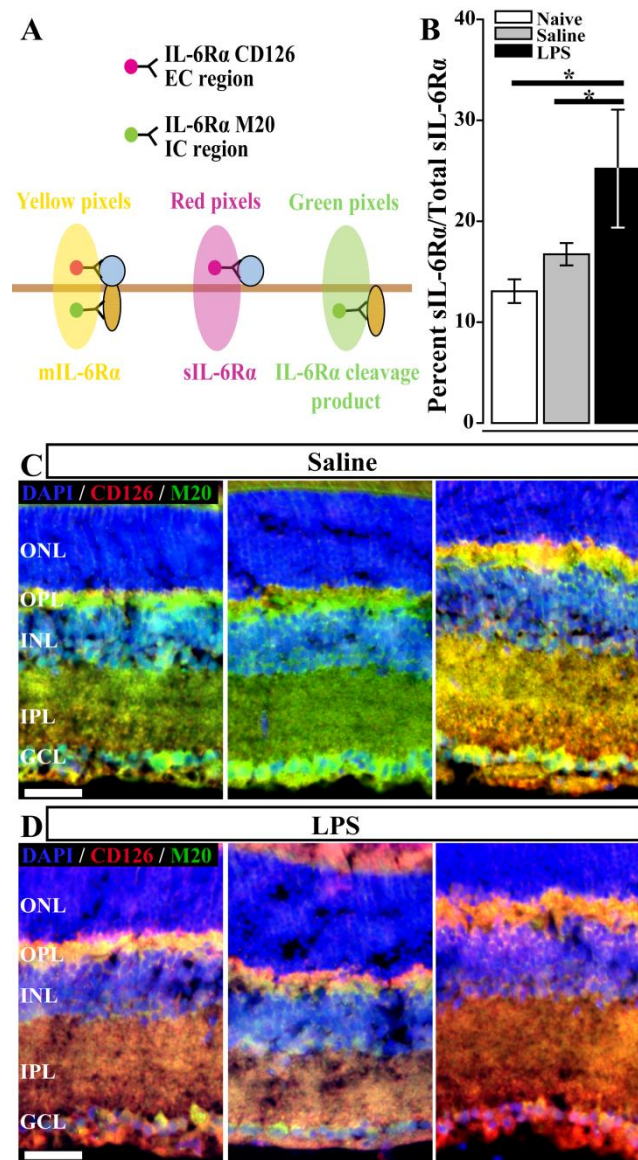


Figure 2.2. sIL-6R α production increases in the retina in response to LPS. **(A)** Schematic of dual-immunolabeling technique to differentiate sIL-6R α and mIL-6R α *in situ*. Tissue is immunolabeled with two anti-IL-6R α antibodies. One antibody recognizes an epitope in the extracellular domain of the IL-6R α protein (CD126; red), while the second antibody recognizes an epitope in the intracellular domain (M20; green). Co-localization of the antibodies (yellow) identifies intact mIL-6R α . Separation of red and green labeling identifies sIL-6R α and the cleaved intracellular domain, respectively. **(B)** Graphical representation of percentage of sIL-6R α compared to total IL-6R α (membrane + soluble fractions) detected in the soluble fraction of retina protein lysates from naïve retina (white) or 6 hours after intravitreal injection of 10 μ g LPS (black) or saline (gray). Error bars indicate standard deviation. $*=p<0.05$. **(C-D)** Representative images (20X) of retina 6 hours post saline **(C)** or 10 μ g LPS **(D)** injection co-immunolabeled with CD126 (red) and M20 (green) antibodies against IL-6R α . Retina from saline-injected mice exhibits strong co-localization of CD126 and M20 antibodies (yellow; mIL-6R α) within the GCL and INL layers. LPS injection leads to a robust increase in CD126 signal (red; sIL-6R α) in cell

membranes of RGCs in the GCL layer as well as decreased co-localization (yellow) of CD126 with M20 (green) labeling. Scale bar represents 20 μ M and is applicable to all images. ONL: outer nuclear layer, OPL: outer plexiform layer, INL: inner nuclear layer, IPL: inner plexiform layer, GCL: ganglion cell layer, NFL: nerve fiber layer.

intracellular (M20) segment tended to be higher than that of the extracellular (CD126) segment, particularly in RGC somas (Figure 2.2C). In contrast, retina from LPS-injected mice exhibited a marked increase in the intensity of CD126 labeling with far fewer instances of M20-CD126 co-localization (Figure 2.2D). Thus, our immunohistochemical data corresponded well with our traditional biochemical assays for detection of sIL-6R α and mIL-6R α .

sIL-6R α is most strongly associated with RGC soma in glaucomatous retina.

To determine the spatial attributes of sIL-6R α production in glaucoma, we examined localization of sIL-6R α and mIL-6R α in young and aging DBA/2J mice, which represents both aging- and IOP-related stressors. Using the dual-labeling technique described in Figure 2.2A, we examined localization of IL-6R α isoforms in the GCL and NFL of whole-mounted retina. We quantified the degree of co-localization (yellow signal) between the red (CD126) and green (M20) signals of the two isoforms on a 4 point scale, with 4 representing near complete co-localization and 1 representing near complete separation (Figure 2.3A). Although there were varying degrees of localization across retinal images from both young and aging DBA/2J (Figure 2.3A), the majority of images from young DBA/2J retina presented with co-localization of M20 and CD126, especially in RGC soma (Figure 2.3A; left). In contrast, the majority of images from aging DBA/2J retina exhibited clear separation of C-terminal and N-terminal IL-6R α labeling that both associated with RGCs (Figure 2.3A; right). Quantification of co-localization by grading confirmed extracellular and intracellular domains of IL-6R α were co-localized more frequently in young DBA/2J retina than in aging DBA/2J retina ($p=0.022$; Figure 2.3B).

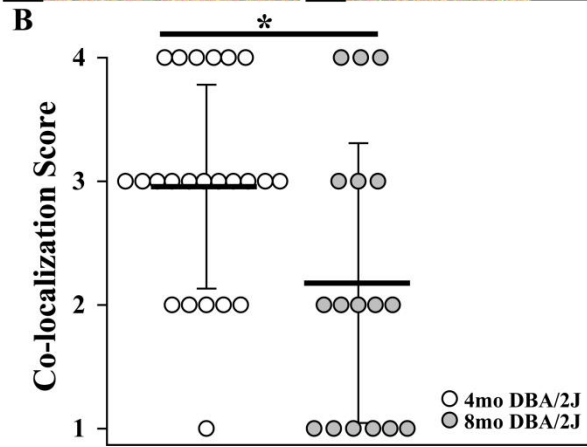
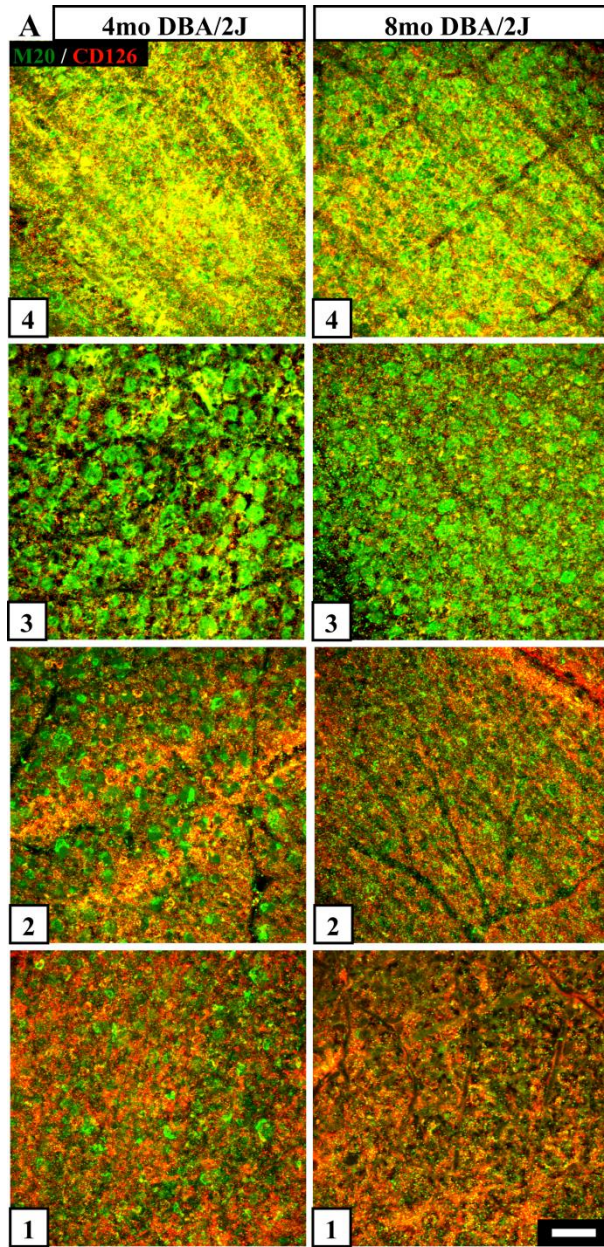


Figure 2.3. Glaucoma-related sIL-6R α is associated with RGCs. **(A)** Confocal micrographs (60X) images of the GCL and NFL in whole mount retina from young (4mo; left) and aging (8 mo; right) DBA/2J mice co-immunolabeled with CD126 (red) and M20 (green) antibodies against IL-6R α . Score of 1 represents little co-localization (red and green separation), while a score of 4 indicates greatest co-localization (yellow). Scale bar represents 20 μ M and is applicable to all images. **(B)** Point plot depicting co-localization grading for individual images of whole mount retina from 4mo (white) and 8mo (gray) DBA/2J mice. There is a significant decrease in co-localization score in 8mo DBA/2J compared to 4mo DBA/2J ($p < 0.05$, student's t-test). The mean co-localization score is indicated by the black bar. Error bars represent standard deviation. * = $p < 0.05$.

sIL-6R α localization is related to RGC integrity

One component of glaucomatous pathology in the DBA/2J mouse is decreased uptake and intra-retinal transport of the active uptake, active transport neural tracer CTB by RGCs (Crish et al., 2010, Formichella et al., 2014). To measure RGC integrity, we delivered CTB to young and aging DBA/2J mice via intravitreal injection and imaged whole-mounted retina 3 days later. As a control for normal aging, we also delivered CTB to age matched C57 mice. We quantified CTB uptake and intra-retinal transport by quantifying CTB fluorescent intensity in images controlled for eccentricity. In retina from young C57, aging C57 and young DBA/2J mice, CTB was robustly detected across the retina, with expected variances in CTB intensity related to eccentricity (Figure 2.4A-C). In contrast, retina from aging DBA/2J mice exhibited varying degrees of uptake and intra-retinal transport in areas of equivalent eccentricity (Figure 2.4D). Furthermore, consistent with previous findings, CTB labeling in the soma persisted longer than that in the unmyelinated segment of RGC axons (Figure 2.4D) (Crish et al., 2010). Quantification of mean CTB labeling within each image revealed that CTB intensity did not differ between young and aging C57 mice ($p > 0.05$; Figure 2.4E). However, CTB labeling intensity was 55% lower in aging DBA/2J retina than in young DBA retina ($p < 0.001$; Figure 2.4E)

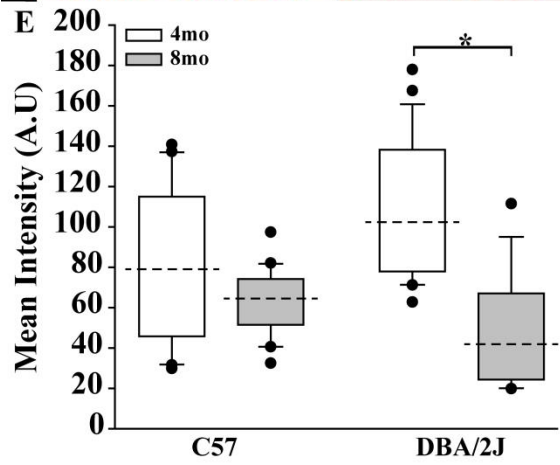
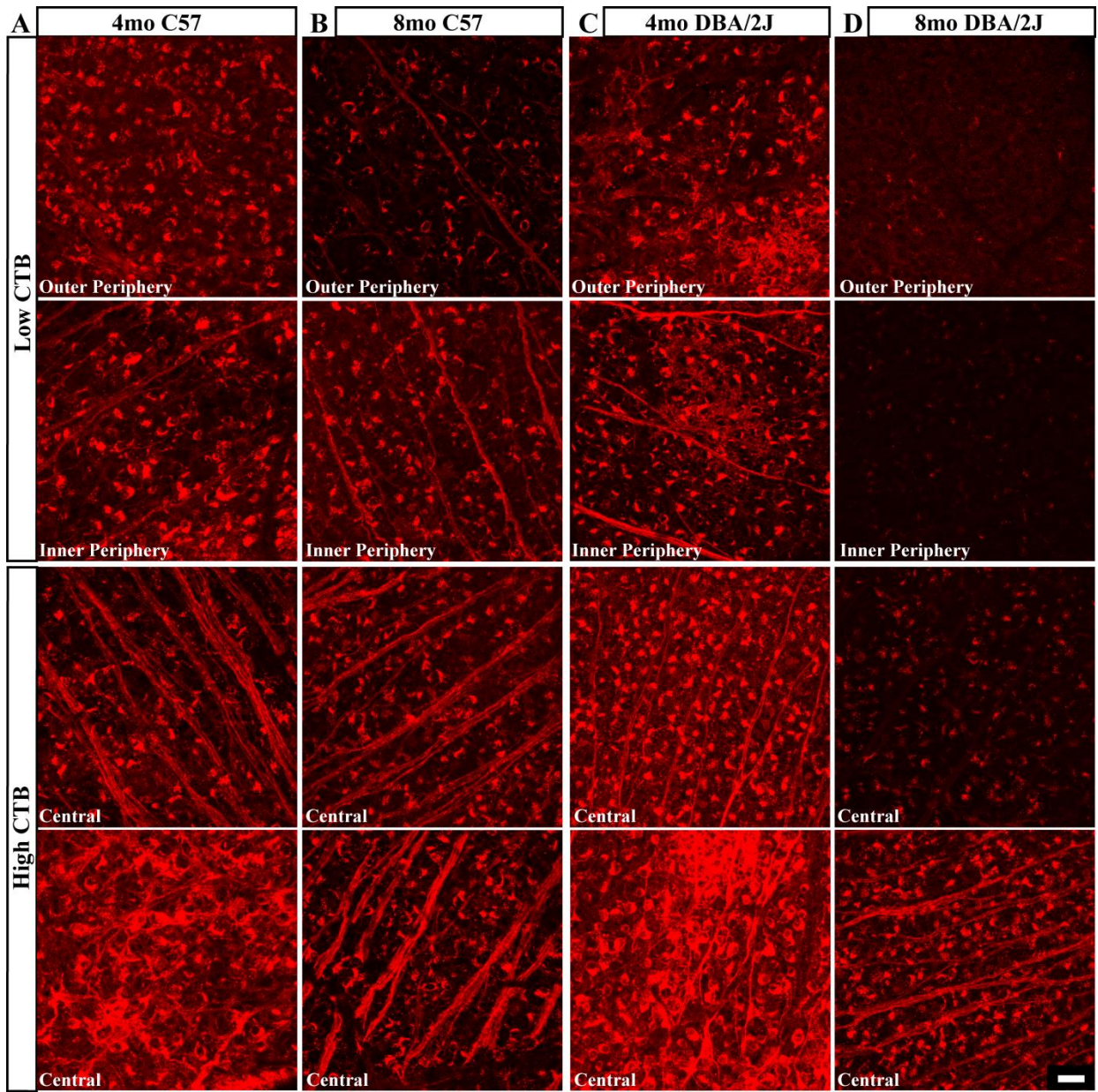


Figure 2.4. Age-dependent IOP elevation is associated with decreased CTB uptake and intra-retinal transport by RGCs. (A-D) Representative confocal micrographs (60X) of CTB labeling (red) in whole-mount retina from young (4mo) C57 (A), aging (8mo) C57 (B), young DBA/2J (C) and aging DBA/2J (D) mice. In accordance with eccentricity-dependent RGC soma and axon density, CTB intensity is higher in central regions of young C57, aging C57, and young DBA retina than peripheral regions (A-C). Aging DBA/2J retina exhibit decreased CTB intensity in both central and peripheral regions of the retina (D). Scale bar represents 20 μ M and is applicable to all images. (E) Graphical representation of mean CTB intensity across all retinal areas in young (4mo; white) and aging (8mo; gray) C57 and DBA/2J retina shows a significant decrease in CTB uptake in aging DBA ($p<0.001$, Mann-Whitey RANK Sum Test), but not aging C57 ($p=0.093$, Mann-Whitey RANK Sum Test), when compared to young DBA/2J and young C57, respectively. Dashed line indicates median value. * = $p<0.001$.

To determine whether spatial variations in sIL-6R α corresponded to spatial differences in RGC integrity, we examined spatial coincidence of sIL-6R α localization and degree of CTB labeling intensity in the ganglion cell/nerve fiber layer of whole-mounted retina from young and aging DBA/2J mice. In young DBA/2J mice, images from central retina, and thus higher CTB intensity, tended to display higher co-localization scores for M20 and CD126 (Figure 2.5A). Correspondingly, images from peripheral retina, and thus lower CTB intensity, represented the lowest co-localization scores in this group (Figure 2.5A). As reported above, co-localization of M20 and CD126 was generally less appreciable in aging DBA/2J retina than in young DBA retina (Figure 2.5B). Within this shifted range of co-localization scores, images with low M20 and CD126 co-localization scores corresponded to lower CTB intensity and vice versa, regardless of eccentricity (Figure 2.5C). This was confirmed by Pearson correlation analysis, which indicated no significant relationship between the M20-CD126 co-localization score and CTB labeling intensity in young DBA/2J mice ($R^2=0.406$, $p=0.07$; Figure 2.5C), but a significant and positive correlation in aging DBA/2J mice ($R^2=0.668$, $p<0.01$; Figure 2.5C).

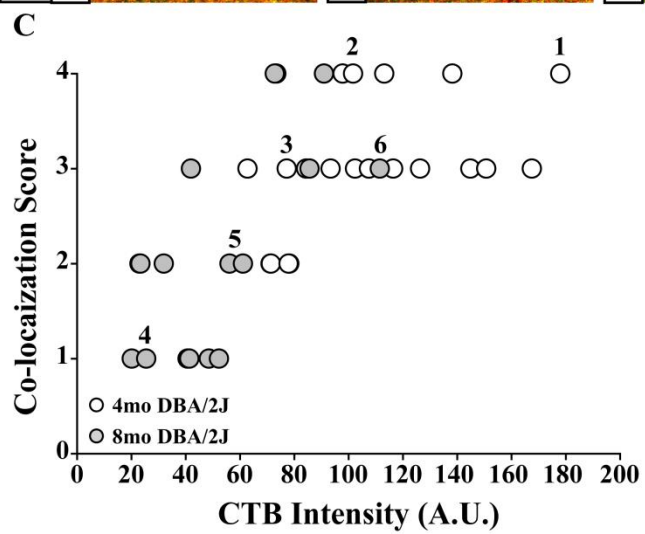
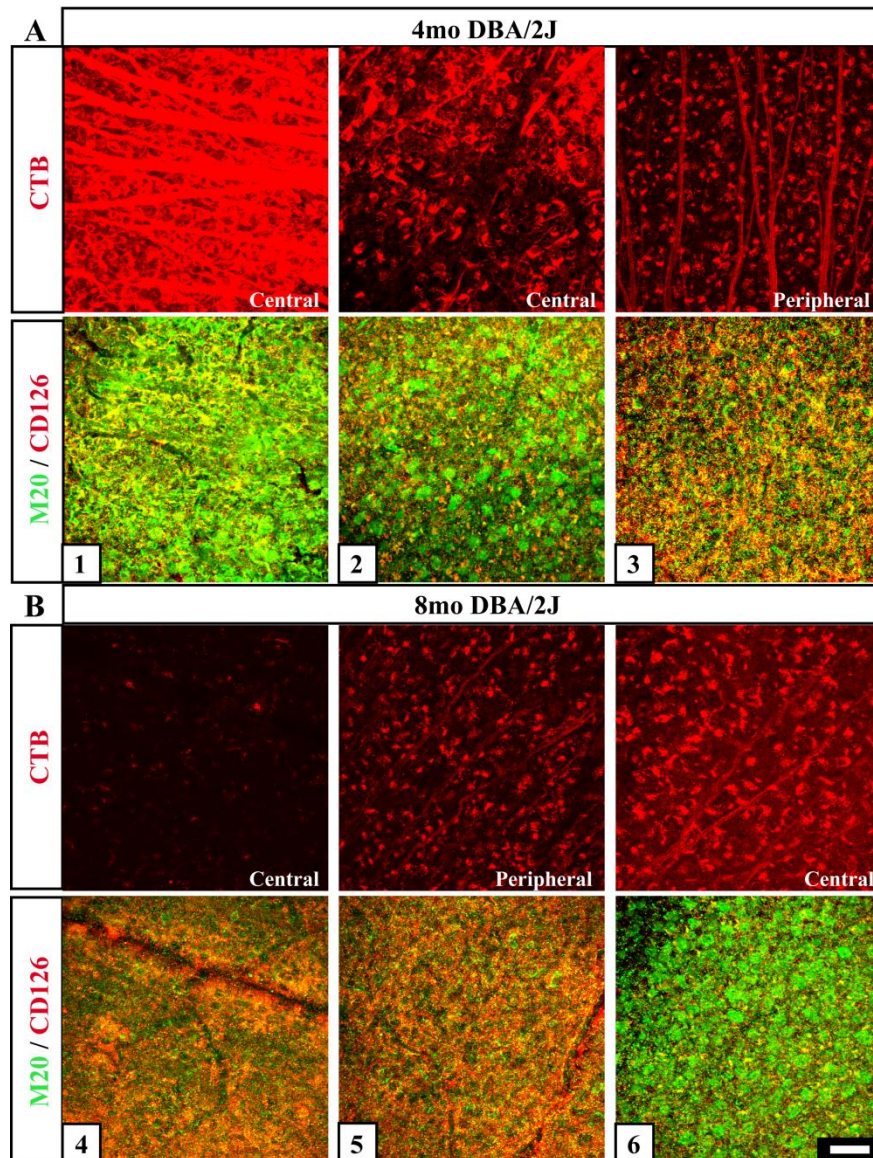


Figure 2.5. sIL-6R α is primarily associated with RGCs exhibiting poor CTB uptake and transport. **(A,B)** Representative confocal micrographs (60X) of CTB labeling (top; red) and CD126 (red) and M20 (green) co-immunolabeling (bottom) in whole-mount retina from young (4mo) **(A)** and aging (8mo) **(B)** DBA/2J mice. Co-localization of CD126 and M20 immunolabeling is greatest in areas with robust CTB labeling for both young and aging DBA/2J retina. This effect is eccentricity-dependent in young mice **(A)**, but eccentricity-independent in aging DBA/2J mice **(B)**. Scale bar represents 20 μ M and is applicable to all images. **(C)** Scatter plot depicting CD126/M20 co-localization grading as a function of CTB labeling intensity in each image of whole-mount retina from young (4mo; white) and aging (8mo; gray) DBA/2J mice. Numbers next to data points correspond to the representative images in **(A,B)**. Pearson correlation analysis indicated no significant relationship between the M20-CD126 co-localization score and CTB labeling intensity in young DBA/2J mice ($R^2=0.406$, $p=0.07$), but a significant and positive correlation in aging DBA/2J mice ($R^2=0.668$, $p<0.01$).

Gp130 expression is not a reliable predictor of RGC integrity

While increased production of sIL-6R α can influence the impact of IL-6 signaling, both sIL-6R α and mIL-6R α require gp130 to initiate an IL-6 dependent signaling cascade (Scheller et al., 2011a). Therefore, significant changes in gp130 protein expression within RGCs could influence the effect of increased sIL-6R α localization to RGCs. To address this caveat, we measured gp130 fluorescent signal and CTB signal from the ganglion cell and nerve fiber layers of whole-mount retina in another cohort of young and aging DBA/2J mice. Similar to our biochemical data from whole retina (Figure 2.1B), there was no age-dependent difference in gp130 fluorescent intensity within the GCL/NFL layer of the DBA/2J retina (Figure 2.6A). In respect to CTB intensity within RGCs, the average CTB intensity was significantly decreased in the aging DBA/2J ($p<0.05$; Figure 2.6A), putting it in line with our CTB intensity measurements from the IL-6R α cohort (Figure 2.4E). To determine if differences in gp130 intensity spatially corresponded with changes in CTB intensity, we plotted CTB intensity measurements as a function of gp130 intensity measurements from both young and aging DBA/2J retina. Interestingly, we observed a slight negative relationship between gp130 intensity and CTB intensity in young DBA/2J mice, where areas containing higher CTB intensity presented with

relatively lower gp130 intensity. However, Pearson correlation analysis indicated no significant relationship between gp130 and CTB intensity ($R^2=-0.265$, $p=0.143$; Figure 2.6C). In aging DBA/2J mice, no observed or calculated relationship was present ($R^2=-0.0525$, $p=0.803$; Figure 2.6D).

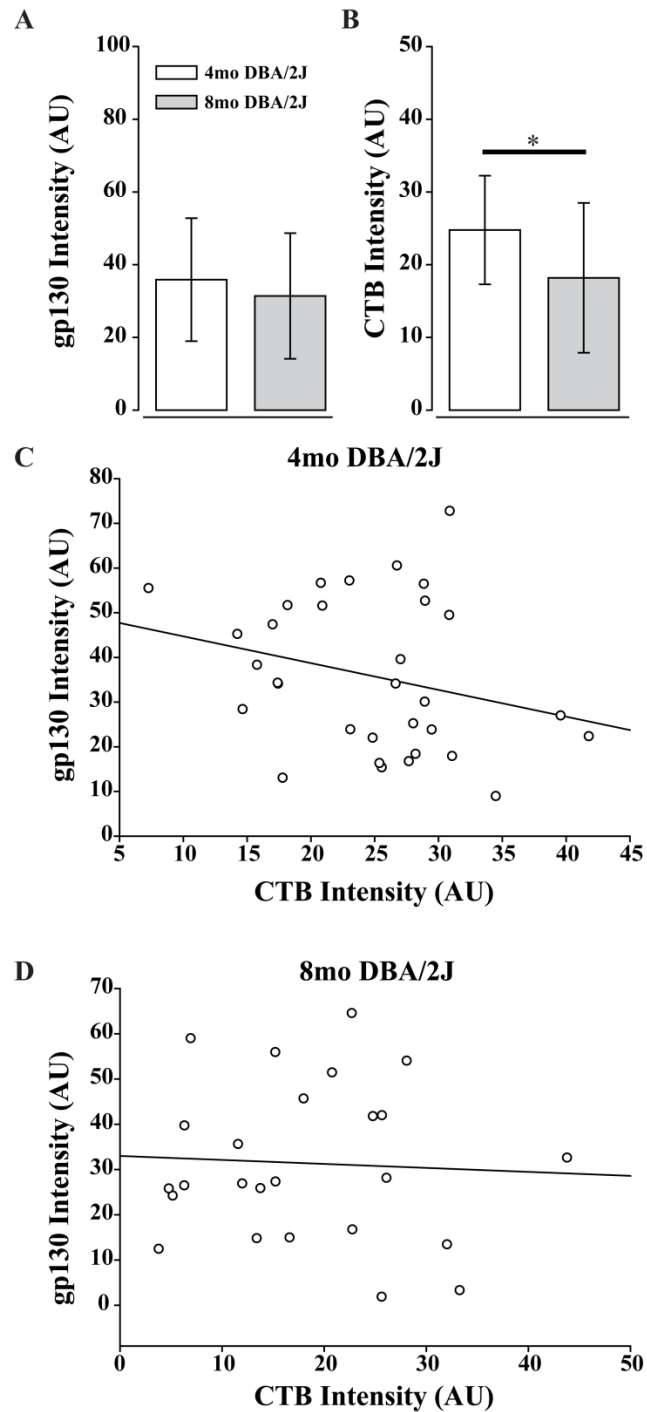


Figure 2.6. No significant relationship between gp130 expression and CTB uptake of RGCs. **(A-B)** Quantification of fluorescent intensity of gp130 signal **(A)** and CTB uptake **(B)** in the ganglion cell and nerve fiber layers of mid central to mid peripheral regions of whole-mounted retina from young (4mo; white) and aging (8mo; DBA/2J) DBA/2J mice. No significant difference in gp130 intensity was noted between age groups ($p=0.330$, student's t-test; **A**). Similar to the IL-6R α cohort, this cohort of 8mo DBA/2J showed significantly less CTB intensity within RGCs ($p<0.05$; student's t-test; **B**). **(C-D)** Scatter plots depicting gp130 labeling intensity as a function of CTB labeling intensity in each image of whole-mount retina from young (4mo; **C**) and aging (8mo; **D**) DBA/2J mice. Pearson correlation analysis indicated no significant relationship between gp130 intensity and CTB labeling intensity in 4mo DBA/2J mice ($R^2=-0.265$, $p=0.143$) or 8mo DBA/2J mice ($R^2=-0.0525$, $p=0.803$). $*=p<0.05$.

Parts of this figure are adapted from (Echevarria et al., 2013) and used in accordance with the Creative Commons Attribution-Non Commercial 4.0 International License.

Discussion

Chronic neuroinflammation is a recognized component of age-related neurodegenerative disease, including glaucoma (Soto and Howell, 2014, Deleidi et al., 2015, Williams et al., 2017). Previous studies show that the cytokine IL-6 is elevated in response to glaucoma related stressors (Sappington et al., 2006, Cvenkel et al., 2010, Johnson et al., 2011, Chidlow et al., 2012, Sims et al., 2012). In other areas of the CNS, IL-6 mediated activation of gp130 via its soluble isoform is associated with neurodegeneration (Burton et al., 2011, Burton and Johnson, 2012, Burton et al., 2013, Campbell et al., 2014). We previously reported that spatial variability of IL-6 and IL-6R α in the retina increases in response to glaucoma-related stressors (Sims et al., 2012). Here, we follow up on that study by measuring changes in gp130 protein concentration and IL-6R α isoform demographics induced by aging and IOP. Overall, we provide evidence that the shift in IL-6R α isoform towards increased sIL-6R α may be relevant for declining RGC integrity in glaucomatous retina.

Our biochemical analysis of gp130 revealed that normal aging (C57 mice) led to significant increases of retinal gp130, while aging coupled with IOP elevation (DBA/2J mice) trended towards a decrease (Figure 2.1). The latter finding is in contrast with another study in the retina, showing increased gp130 protein levels up to 48 hours following NMDA exposure (Inomata et al., 2003). This raises the possibility that gp130-mediated signaling is induced early following acute injury, but is downregulated with chronic insults, such as IOP-induced glaucoma. As gp130 is required for IL-6 mediated signaling, changes in gp130 availability can influence the magnitude of a cell's response to IL-6. In regards to IL-6R α , elevated sIL-6R α production occurred with normal aging (aging C57 mice) and aging plus elevated IOP (aging DBA/2J mice) (Figure 2.1). This demonstrates that aging alone is sufficient to shift IL-6R α

demographics towards the sIL-6R α isoform and that this age-related shift remains with the introduction of elevated IOP. A shift in the sIL-6R α isoform indicates a reciprocal shift away from mIL-6R α -mediated classical signaling and towards sIL-6R α -mediated trans-signaling. As such, these data suggest that glaucoma-related stressors promote IL-6 signaling through the trans-signaling mechanism.

RGCs are the principal cell types that undergo degeneration in glaucoma. In delineating how induction of IL-6 trans-signaling may relate to RGC degeneration in glaucoma, two factors are of particular importance: when and where. These two factors are important with respect to both RGC degeneration and IL-6 signaling. IL-6, IL-6R α and gp130 are constitutively expressed by RGCs (Sims et al., 2012) (Figure 2.1) and thus, are sensitive to IL-6 mediated signaling. We previously reported that glaucoma-induced changes in IL-6 signaling are not uniform across the retina, but instead occur in smaller micro-domains such that, a glaucomatous retina contains areas of both enhanced and reduced IL-6 signaling (Sims et al., 2012). Similarly, indicators of RGC degeneration also exhibit spatial patterning, where pockets of dysfunction and degeneration are evident in a single subject (Crish et al., 2010, Lambert et al., 2011, Formichella et al., 2014, Ward et al., 2014). The temporal pattern is also relevant for RGC degeneration which progresses from functional deficits to structural degeneration over time (Buckingham et al., 2008, Crish et al., 2010, Calkins and Horner, 2012)

Although our data cannot address all of the “when” and “where” components empirically, we can draw some reasonable conclusions that speak to these factors. Using a dual-labeling histological approach, we examined the spatial localization of sIL-6R α relative to mIL-6R α and correlated the localization pattern with uptake and intra-retinal transport of the neural tracer CTB. First, we validated our dual-labeling approach with LPS, which is well-known to induce

sIL-6R α production and IL-6 trans-signaling (de Vos et al., 1994, Mo and Streilein, 2001, Rosenbaum et al., 2011) (Figure 2.2). Consistent with our biochemical data, we found that mIL-6R α , as identified by co-localization of our antibodies targeting the C- and N-terminals of IL-6R α , was predominant and distributed rather uniformly in retina from young (4mo) DBA/2J mice (Figure 2.3). In contrast, retina from aging (8mo) DBA/2J mice exhibited an overall decrease in co-localization between the two antibodies and numerous regions with clear separation of labeling, indicating the presence of sIL-6R α . Again, this corresponded well with our biochemical data (Figure 2.3). Upon examination of spatially-coincident CTB tracing, we found that areas of aging DBA/2J retina with low CTB intensity contained primarily the sIL-6R α isoform. Likewise, areas with higher CTB intensity contained a mix of sIL-6R α and mIL-6R α . This positive correlation between mIL-6R α (co-localization) and RGC integrity, as measured by CTB uptake and intra-retinal transport, was highly significant (Figure 2.5).

Throughout CNS and the periphery, it is believed that gp130 protein concentration is higher than that of IL-6R α (Zhao et al., 2008, Erta et al., 2012, Hsu et al., 2015). This suggests that the release of sIL-6R α increases the propensity for IL-6 signaling events to occur in domains where IL-6 is released. That being said, the amount of available gp130 at any given time is the final indicator of how IL-6 signaling impacts the system. Similar to our measurements in whole retina, our measurements within the area where RGCs reside suggest no changes in gp130 protein content in response to age-related increases in IOP (Figure 2.6). Additionally, unlike sIL-6R α localization data, decreases in CTB intensity did not correlate to gp130 intensity (Figure 2.6). This suggests that: 1) changes in gp130 are not reliable indicators of RGC integrity in the DBA/2J mouse and 2) sensitivity to IL-6 signaling in the DBA/2J model of glaucoma is facilitated by sIL-6R α production and not by gp130.

In the context of the known progression of CTB transport deficits in DBA/2J mice (Crish et al., 2010, Formichella et al., 2014, Bond et al., 2016), we can infer a temporal relationship between induction of IL-6 trans-signaling and progression of RGC degeneration. The highest values for CTB labeling represented detectable signal in both the RGC soma and the unmyelinated segment of the RGC axon. The lowest values for CTB labeling represented detectable signal only in the soma (Figures 2.4 and 2.5). Based on these data, we propose that the shift from IL-6 classical signaling to IL-6 trans-signaling is likely to occur near the mid-point in disease progression, well after the onset of functional deficits (i.e. axon transport) in RGC axons, but prior to structural degeneration of the RGC axon.

CHAPTER 3

IL-6 DEFICIENCY ATTENUATES RGC AXONOPATHY AND GLAUCOMA RELATED- VISION LOSS³

Introduction

IL-6 signaling is associated with a variety of CNS pathologies including RGC degeneration in glaucoma (Chen et al., 1999, Ghanem et al., 2011, Erta et al., 2012, Sims et al., 2012). In the previous chapter, we showed that the soluble isoform of IL-6R α , a marker of pathogenic IL-6 trans-signaling, is upregulated in RGCs compromised by glaucoma related stressors (Chapter 2). While this provides additional evidence of the association between IL-6 signaling and glaucoma, it does not elaborate on the direct contribution of IL-6 signaling to RGC pathology. Elsewhere in the CNS, its classification as either protective or destructive to neuronal populations continues to be highly contested. In support of the idea that IL-6 signaling is protective, pre-treatment of various neurons with IL-6 *in vitro* prevents apoptosis in neural cells exposed to a number of physiological stressors (Yamada and Hatanaka, 1994, Pavelko et al., 2003, Sappington et al., 2006, Spittau et al., 2012, Fang et al., 2013, Perigolo-Vicente et al., 2013, Chucair-Elliott et al., 2014). *In vivo* however, the effect of IL-6 on neuronal health is variable, as studies suggest that IL-6 signaling promotes both viability and dysfunction (Campbell et al., 1993, Bluthe et al., 2000, Fisher et al., 2001, Sparkman et al., 2006, Mukaino et al., 2010, Burton et al., 2011, Burton and Johnson, 2012, Burton et al., 2013)

³ Portions of this chapter were published as: Echevarria et al., (2017) Interleukin-6 Deficiency Attenuates Retinal Ganglion Cell Axonopathy and Glaucoma-related Vision Loss. *Front. Neuro.* 11:318

depending on the model of CNS injury. In the optic projection, IL-6 protein is upregulated near retinal ganglion cells (RGCs) and their axons in rodent models of glaucoma (Sappington and Calkins, 2008, Chidlow et al., 2012, Sims et al., 2012, Wilson et al., 2015). Like elsewhere in the CNS, the role of IL-6 in RGC axonopathy is unclear. Application of recombinant IL-6 to RGCs *in vitro* prevents pressure-induced apoptosis (Sappington et al., 2006). *In vivo*, while IL-6 appears to protect RGCs and enhance axon regeneration following optic nerve crush in some studies (Leibinger et al., 2013, Leibinger et al., 2016), other studies indicate that IL-6 deficiency protects against RGC loss in response to glutamate excitotoxicity and optic nerve crush (Fisher et al., 2001).

While there are advantages to using glaucoma model systems that involve a more acute, severe injury such as elevated hydrostatic pressure *in vitro* or optic nerve crush *in vivo*, they don't accurately model the modest, chronic stress that is consistent with IOP elevation in human glaucoma. To better elucidate the impact of IL-6 signaling on RGC axonopathy in response to ocular hypertension, we comprehensively examined and compared optic nerve morphology, visual acuity, active axonal transport and retinal glial reactivity in IL-6 deficient (*Il-6^{-/-}*) and wildtype (WT) mice following 8 weeks of ocular hypertension using the microbead occlusion model of glaucoma (Sappington et al., 2010). Together, our data indicates that IL-6 deficiency prevents glaucoma-induced deficits in visual function and optic nerve structure without improvement in axon transport or reduction in microglia reactivity. This suggests that IL-6 may play a specific role in the progression of RGC axonopathy from functional deficits to structural degeneration.

Materials and Methods

Animals

7-9 month old male and female *Il-6*^{-/-} mice (B6;129S2-*IL6*^{tm1kopf}/J) and respective genomic controls (B6;129SF2/J) were used for all experiments. *Il-6*^{-/-} mice contain a neomycin selection cassette in exon 2 of the *Il-6* gene preventing transcription of the mRNA product (Kopf et al., 1994). Founder mice were obtained from Jackson Laboratories (Bar Harbor, ME) and experimental mice were bred and genotyped in-house using the following primers provided by Jackson Labs: 5'-TTC-CAT-CCA-GTT-GCC-TTC-TTG-G-3', 5'-TTC-TCA-TTT-CCA-CGA-TTT-CCC-AG-3' and 5'-CCG-GAG-AAC-CTG-CGT-GCA-ATC-C-3'. Mice were housed in accordance with NIH guidelines and maintained on a 12hr light/dark cycle with *ad libitum* access to standard mouse chow and water. This study was carried out in accordance with the ARVO statement for the use of animals in ophthalmic and vision research and was approved by the IACUC of Vanderbilt University Medical Center.

Induction of ocular hypertension using the microbead occlusion model

Acute IOP elevation was induced in WT and *Il-6*^{-/-} mice using the microbead occlusion model, as previously described (Sappington et al., 2010) (Figure 3.1). For anterograde axonal transport, axon density measurements and retinal gliosis, a cohort of 5-6 mice from both genotypes received a unilateral injection of 1.5µl (1×10^6 microbeads/mL) of 15µm polystyrene beads conjugated to an Alexa Fluor 488 chromophore. The contralateral eye served as a surgical control and was injected with an equal volume of saline. For experiments looking at visual acuity and corneal thickness, 7-11 mice from both genotypes received bilateral injections of 1.5µl microbeads and a separate cohort of mice served as controls and received bilateral injections of

an equivalent volume of saline. All mice received two microbead/saline injections 4 weeks apart to raise IOP for a total of 8 weeks. Following IOP elevation, mice were euthanized and perfused as previously described (Chapter 2). Eye and brain tissue were stored in 4% PFA at 4°C until use.

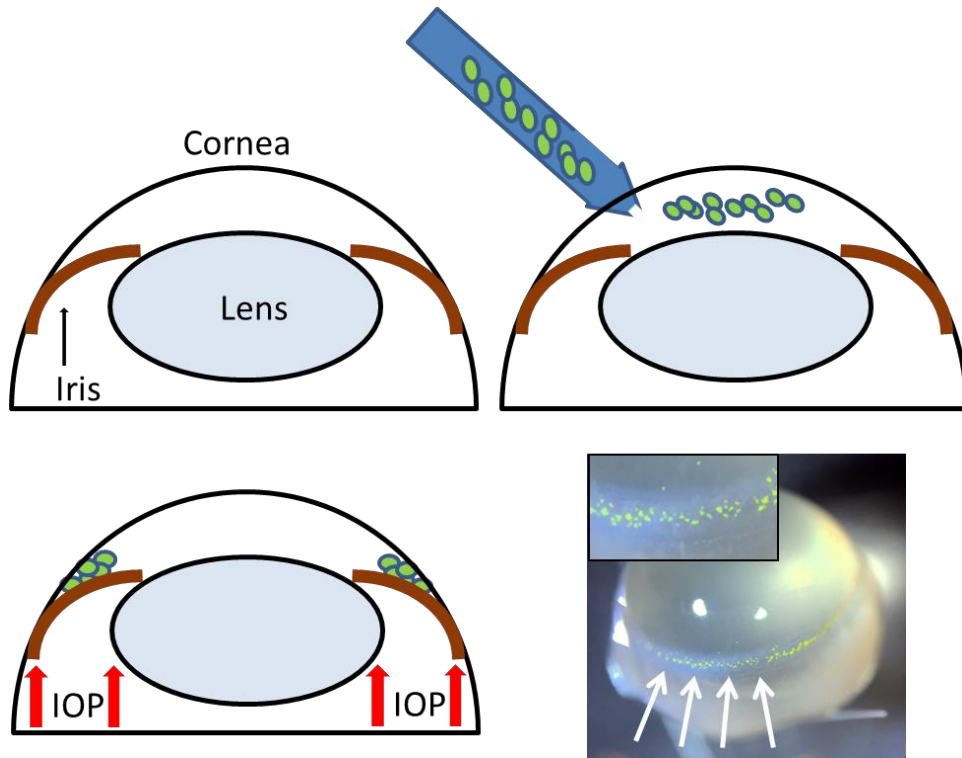


Figure 3.1. Induction of ocular hypertension by microbead induced occlusion of aqueous humor outflow. 15 μ m polystyrene microbeads are injected into the anterior chamber with a glass pipette (top right). Over a period of 24 hours, the beads settle and accumulate at the iridocorneal angle (bottom), blocking aqueous humor from draining through the trabecular meshwork in Schlemm’s canal.

IOP measurements

IOP was measured in awake, behaving mice, using a Tonolab rebound tonometer (TonoLab; Reichert, Depew, NY), as previously described (Echevarria et al., 2013; Formichella et al., 2014; Echevarria et al., 2016). Prior to initial injection, mean baseline IOP for each mouse was calculated from approximately 60 individual readings taken over a period of 6 days (10

measurements/day) within a two week timeline. Following microbead or saline injections, weekly IOP was determined as the mean of 20-30 measurements, taken over 2-3 days (10 measurements/day) each week for a total of 8 weeks. IOP measurements were taken at the same time of day to remove any effect of circadian rhythm on IOP measurements. To avoid corneal irritation and discomfort, 0.5% proparacaine anesthetic drops (Akorn Inc, Lake Forest, IL) and lubricating eye drops were applied to each eye before and after IOP measurements were taken respectively.

Immunohistochemistry

Fixed whole-mounted retinas were bisected and processed for either astrocyte or microglia labeling as previously described (Sappington et al., 2009, Crish et al., 2010, Echevarria et al., 2013, Echevarria et al., 2016). We used primary antibodies against glial fibrillary acidic protein (GFAP, 1:500; Cat# Z033429-2; DAKO) to label astrocytes and ionized calcium-binding adapter molecule-1 (Iba-1, 1:250; Cat# 019-19741; WAKO) to label microglia. Secondary antibodies were used at a concentration of 1:200 and consisted of donkey α -rabbit attached to a Rhodamine Red-X fluorophore (Cat# 711-295-152; Jackson Immuno Labs).

Quantification of glial coverage

GFAP or Iba1 labeling in fixed, whole-mount retina were imaged at 60X using an inverted confocal microscope (Olympus FV-1000; Center Valley, PA) through the Vanderbilt University Medical Center Cell Imaging Shared Resource Core. 7-9 pseudo-random z-stack images in the mid central/mid-peripheral areas through the ganglion cell (GCL) and nerve fiber layers (NFL) of the retina were acquired using a digital camera and image analysis software (FV-

100 ASW; Olympus). GFAP and Iba1 percent area was calculated using NIS elements AR software (Nikon Instruments, Melville, NY). The area (mm^2) of the image containing above background signal intensity of Iba1 or GFAP was calculated and reported as a percentage of the total area of the image. Total area of each image and background signal threshold was equal among all images. Microglia cell density was calculated by counting the number of Iba1 positive cell soma and dividing the counts by the area of the image.

Anterograde axon transport measurements

Anterograde axonal transport capabilities of RGCs were assessed with cholera toxin beta-subunit (CTB) conjugated to a 488 fluorophore. Briefly, mice were given a 1.5-2 μl intravitreal injection of CTB (10 $\mu\text{g}/\mu\text{l}$ in sterile ddH₂O; Cat# C-34775, Life Technologies) using a 33 gauge needle attached to a Hamilton syringe under 2.5% isoflurane anesthesia. Five days after CTB injection, mice were euthanized with pentobarbital and perfused trans-cardially with 100ml of 1X PBS (Sigma Aldrich, St. Louis, MO) followed by 100ml of 4% paraformaldehyde (PFA; Electron Microscopy Sciences, Hatfield, PA). To quantify axon transport, whole brains were cryopreserved in 30% sucrose for 24-48 hours at 4°C. Using a sliding microtome, 50 μm sections were obtained through the superior colliculus (SC). CTB signal in these sections was imaged *en montage* at 10X, using a Nikon Eclipse Ti inverted microscope (Nikon Instruments, Melville, NY). Anterograde axonal transport was quantified as previously described (Crish et al., 2010) (Figure 3.2). Briefly, the SC from each image was outlined and CTB signal above background was divided by total pixel area to determine the volume of SC with CTB labeling. This value was used to create a colorimetric 2D retinotopic map of CTB transport ranging from 0% (blue) and

100% (red). Intact transport was defined as percent area with CTB signal $\geq 70\%$ density (red/yellow).

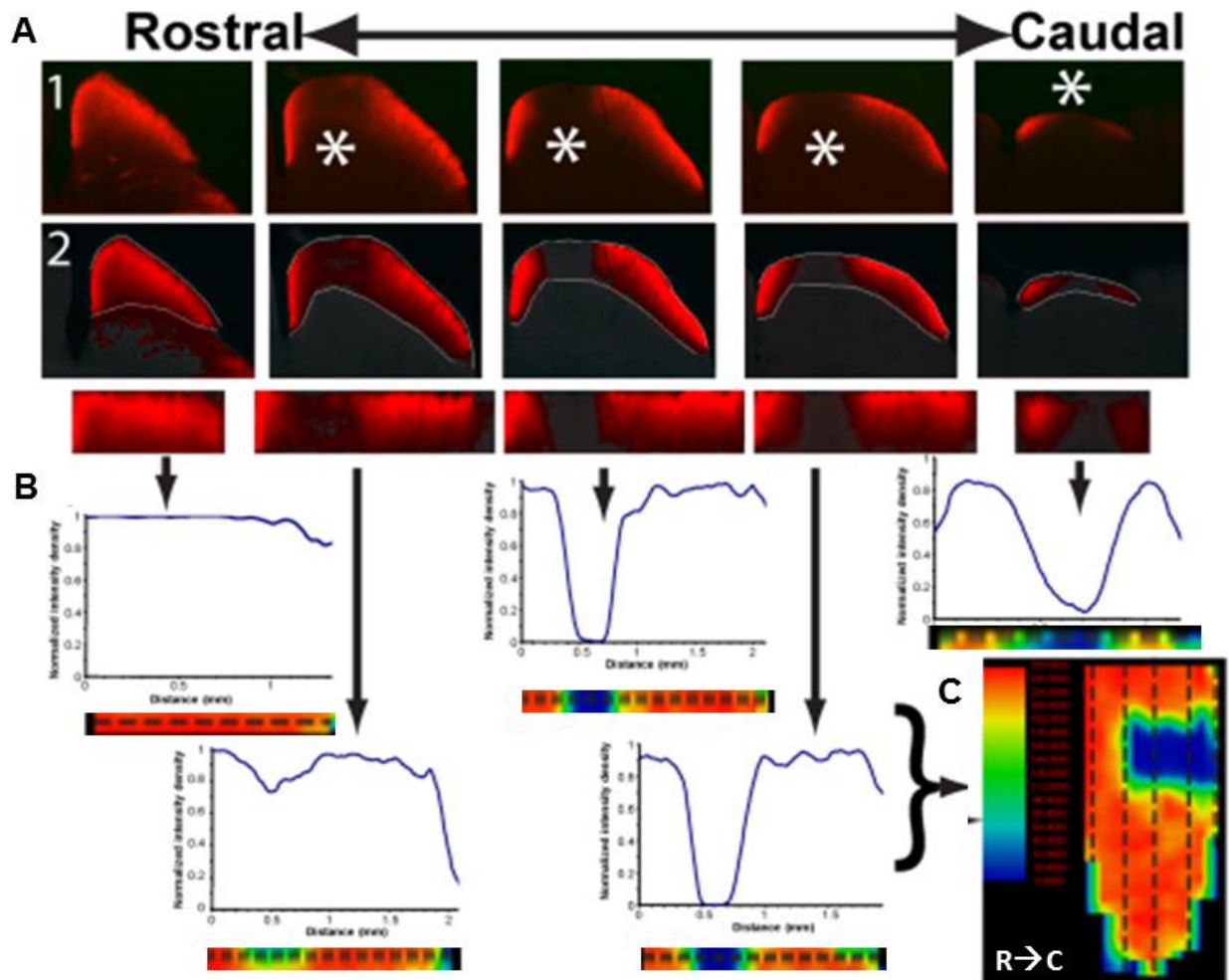


Figure 3.2. RGC to SC CTB transport measurements and resulting retinotopic map. (A) Images of serial brain sections through the SC with CTB signal (red) are arranged in a rostral to caudal fashion (A1). Images are run through a custom macro where the SC is traced manually (A2). (B) The macro then calculates the average pixel intensity along each row of pixels (graphs). These measurements are then run through a second macro where each row is converted into a colometric label (below graphs in B) and then lined up rostral to caudal to reconstruct the retinotopic map of CTB transport in the SC. Intensity measurements 70% above background are represented as warmer colors (red/yellow) and indicate intact transport. Anything below 70% is represented as cooler colors (green/blue) and indicates transport deficits.

Image graciously provided by DJ Calkins and modified with his permission to fit the needs of this thesis.

Quantification of axon density and optic nerve area

Axon density was measured in semi-thin sections of optic nerve, as previously described (Sappington et al., 2010, Ward et al., 2014). Briefly, optic nerves were post fixed at least 48 hours in 2.5% glutaraldehyde and embedded in epon. Semi-thin (700nm) cross-sections of optic nerve near the chiasm were stained with 1% p-Phenylenediamine (PPD) and 1% toluidine blue to highlight myelin and glia, respectively. Optic nerve cross-sections were imaged *en montage* at 100X magnification on an upright Olympus Provis AX (Olympus, Melville, NY) microscope. To calculate axon density, a 50x50 μ m grid mask was placed on the montaged image using NIS elements AR software and the number of axons was manually counted by a blind-observer in 8-10 squares of the grid. Each square counted was equal in area (0.0025 mm²). To measure nerve area, the circumference of the entire nerve was traced in montaged images of optic nerve cross-sections. Nerve area was calculated as the area (mm²) within this outline, using NIS elements software.

Psychophysical visual testing

The optokinetic response is a naturally occurring reflex that serves as a functional tool for quantitative analyses of visual system function in mice (Douglas et al., 2005). Briefly, each mouse was placed on a platform surrounded by four LCD computer monitors. A sinusoidal grating of alternating white and black bars rotating in either a clock-wise or counter clock-wise fashion was projected on the monitors. Mice able to perceive the moving stimulus produced a reflexive movement of the head in the direction of the stimulus. The visual acuity of each mouse was measured by changing the spatial frequency of the black and white bars. The visual acuity threshold was determined as the highest spatial frequency for which reflexive tracking was

noted. The presence of the reflexive head movement was recorded by an observer using a camera mounted above the mouse. Mice were tested for baseline visual acuity threshold 1-2 weeks before microbead/saline injection and 4 and 8 weeks post-initial microbead/saline injection.

Corneal imaging using Spectral Domain Optical Coherence Tomography (SD-OCT) and quantification of corneal thickness

Mice were anesthetized with a ketamine/xylazine cocktail (80 µg/5 µg/gram of mouse), pupils were dilated with 0.5% Tropicamide and eyes lubricated with tear drops. Live volumetric scans of the cornea were obtained using SD-OCT running the Bioptogen ultra-high resolution spectral domain OCT system with cornea bore (Bioptogen, Morrisville, NC). Quantification of injury area was done using Image J software (National Institute of Health).

Statistical analysis

Statistical analysis was conducted with SigmaPlot Version 11.1 (Systat Software Inc, San Jose, CA). For baseline and delta baseline IOP comparisons between WT and *Il-6*^{-/-}, a Mann-Whitney Rank Sum test and a One-Way ANOVA with Holm-Sidak post-hoc correction was done respectively. For post injection IOP comparisons, a One-Way ANOVA on RANKS with Dunn's post hoc correction was done. For corneal wound area measurements, a two-tailed t-test was done between WT and *Il-6*^{-/-} mice at each time point. Differences in visual acuity throughout the 8 week experimental time course were assessed with a One-Way Repeated Measures ANOVA between baseline visual acuity, acuity at 4 weeks post initial injection and 8 weeks post initial injection within each experimental group. Differences between all

experimental groups at each time point were assessed with a One-Way ANOVA with Holm-Sidak post-hoc correction. Differences in percent baseline visual acuity at 8 weeks between all experimental groups were assessed with a One-Way ANOVA on RANKS with Dunn's post hoc correction. All other comparisons were made with a One-Way ANOVA on RANKS with Dunn's post hoc correction (percent glia coverage, microglia cell density) or a One-Way ANOVA with Holm-Sidak post-hoc correction (SC transport, axon density/nerve area). For all, p -values less than 0.05 were considered statistically significant.

Results

IL-6 deficiency does not affect microbead-induced elevations in IOP

To examine the impact of IL-6 deficiency on the progression of IOP-induced RGC neurodegeneration, we utilized the microbead occlusion model (Sappington et al., 2010) of glaucoma to elevate IOP for a total of 8 weeks in WT and *Il-6*^{-/-} mice. Baseline IOP was slightly lower (4%) in *Il-6*^{-/-} mice, compared to WT mice ($p < 0.01$; Figure 3.3A; left). Microbead

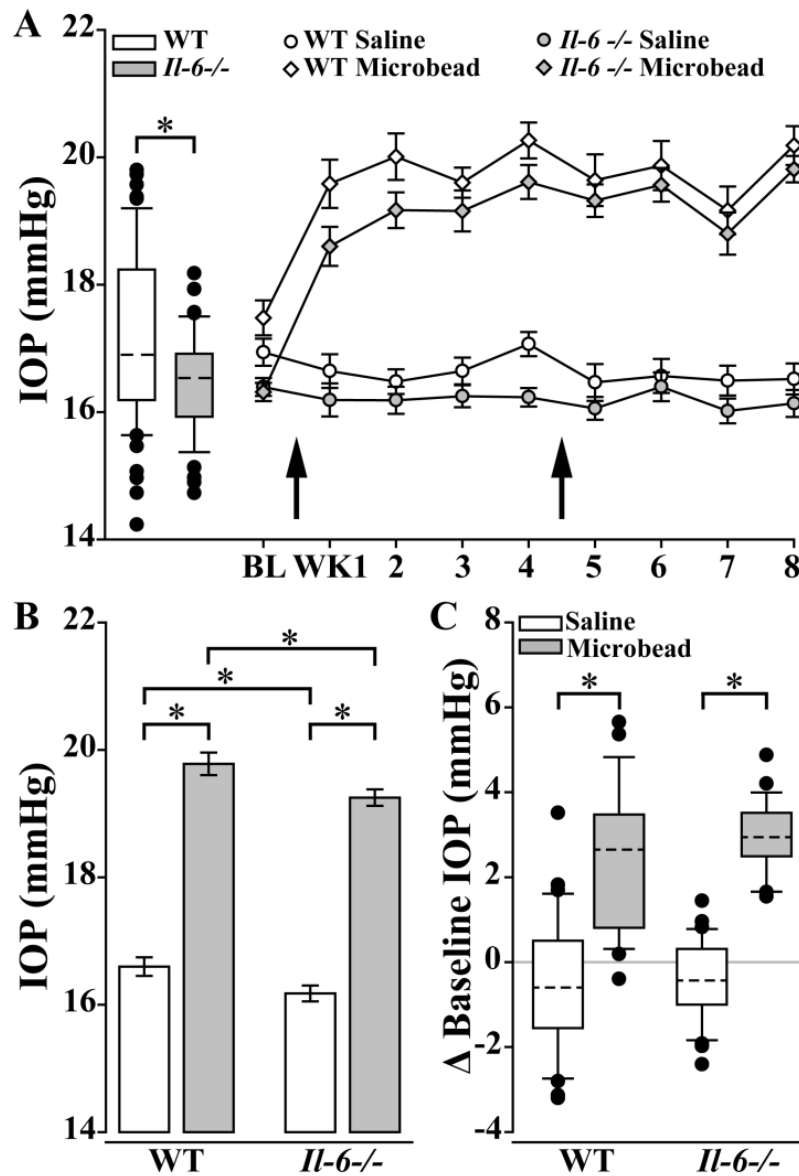


Figure 3.3. IL-6 deficiency does not affect magnitude and duration of microbead induced ocular hypertension. **(A; left)** Boxplot of baseline (BL) IOP of WT (white) and *Il-6*^{-/-} (gray) mice from all experimental cohorts prior to microbead/saline injection. Baseline IOP of *Il-6*^{-/-} mice is decreased by 4% compared to baseline IOP of WT mice. **(A; right)** Line plot (mean \pm SEM) showing baseline and weekly post saline (circle) or microbead (diamond) IOP in WT (white) or *Il-6*^{-/-} (gray) eyes. Arrows indicate time of saline/microbead injections. Throughout the 8 week experiment, microbead injected eyes from both WT and *Il-6*^{-/-} show a 15-20% increase in IOP compared to baseline measurements and saline injected eyes. **(B)** Bar graph of average IOPs (mean \pm SEM) taken post initial microbead (gray) or saline (white) injection in WT and *Il-6*^{-/-} mice. A significant IOP increase in microbead- injected eyes versus saline- injected eyes is seen in both genotypes. A genotype specific IOP reduction is seen in both saline- and microbead- injected *Il-6*^{-/-} mice. **(C)** Boxplot showing magnitude of IOP difference in saline (white) and microbead (gray) injected WT and *Il-6*^{-/-} mice compared to baseline measurements. A significant elevation in IOP is present in microbead- injected eyes compared to saline- injected eyes in both genotypes. However, no genotype specific differences in IOP seen. $\ast=p<0.05$. $n=26-34$ eyes/genotype/condition. Dashed lines in box plot indicate median value.

Figure from (Echevarria et al., 2017) and used in accordance with the Creative Commons Attribution-Non Commercial 4.0 International License.

injection increased IOP by 15-20%, as compared to saline-injected controls for both genotypes (WT; $p<0.001$, *Il-6*^{-/-}; $p<0.001$, Figure 3.3A; right and Figure 3.3B). In accordance with baseline IOP measurements, the mean IOP (mmHg) for both saline- ($p<0.05$) and microbead-injected ($p<0.05$) was lower in *Il-6*^{-/-} mice than their WT counterparts (Figure 3.3B). However, with respect to baseline IOP, the magnitude of IOP elevation was similar (~ 2.5 mmHg) in microbead-injected WT and *Il-6*^{-/-} mice ($p>0.05$, Figure 3.3C).

***Il-6*^{-/-} mice exhibit deficits in corneal wound healing**

Previous studies indicate *Il-6*^{-/-} mice exhibit deficits in wound healing (Lin et al., 2003b, McFarland-Mancini et al., 2010). As the microbead/saline injections require puncturing of the cornea, we used spectral-domain optical coherence tomography (SD-OCT) imaging to monitor corneal healing throughout the 8 week experiment. Two weeks following intra-cameral injection of saline or microbeads in WT eyes, SD-OCT imaging revealed complete healing of the

epithelial layer and near complete healing of the stroma and endothelial layers at the injection site (Figure 3.4A). In *Il-6*^{-/-} mice, the corneal wound appeared to heal at the epithelial surface, but the wound remained in the stroma and endothelial layers even at 8 weeks post injection (Figure 3.4B). Quantification of corneal injury revealed that the corneal wound was 2-fold larger in *Il-6*^{-/-} mice than in WT mice throughout the 8 week experiment ($p < 0.05$; Figure 3.4C).

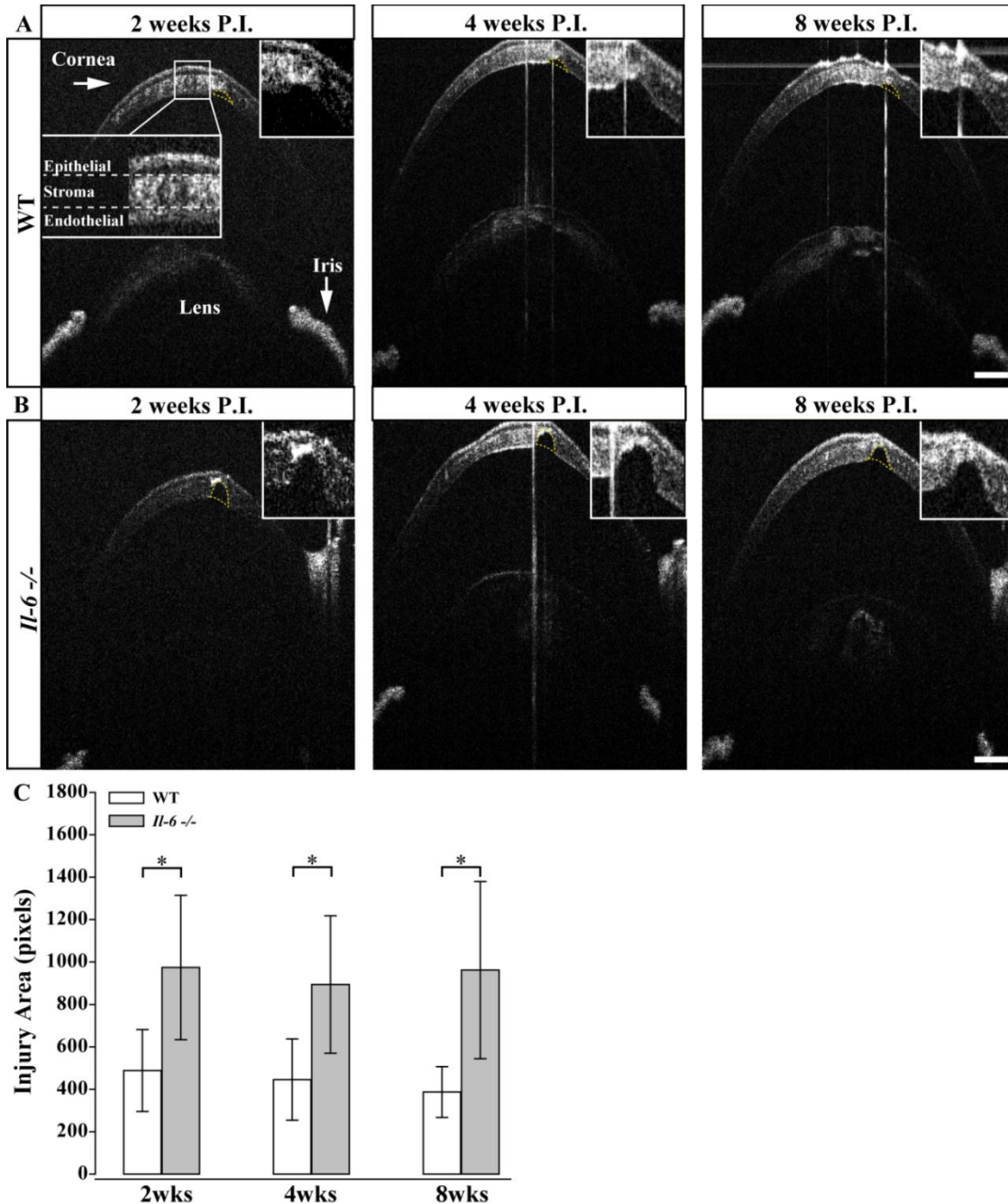


Figure 3.4. *Il-6*^{-/-} mice present with defects in corneal wound healing following microbead/saline injection. **(A)** Representative images of corneal wounds at 2, 4 and 8 weeks post initial injection in WT mice. Insert **(A; far left)** outlines layers of the cornea. 2 weeks after corneal puncture due to saline or microbead delivery, WT mice left display small gaps in the corneal stroma and endothelium (yellow dotted lines). The size of the injury persists after 4 (middle) and 8 (right) weeks after injury. **(B)** Representative images of corneal wounds at 2, 4 and 8 weeks post injection in *Il-6*^{-/-} mice. *Il-6*^{-/-} mice however, present with significantly larger gaps 2 weeks (left) in the corneal stroma after puncture that also persists at 4 (middle) and 8 (right) weeks after injury. **(C)** Bar graph showing quantification of corneal injury area (mean \pm STDEV). *Il-6*^{-/-} mice have significantly larger corneal injuries at all time points. $\ast=p<0.05$. n=9 eyes/genotype/group. Scale bars= 100 μ m for all images.

Figure from (Echevarria et al., 2017) and used in accordance with the Creative Commons Attribution-Non Commercial 4.0 International License.

IL-6 deficiency does not prevent IOP-induced deficits in anterograde axon transport

Previous reports indicate that functional deficits in anterograde axon transport along the optic projection precede structural degeneration of RGC axons in glaucoma (Crish et al., 2010, Crish et al., 2013). To measure and compare active anterograde transport in RGC axons, we injected the active uptake, active transport tracer cholera toxin beta subunit (CTB) into the vitreous of *Il-6*^{-/-} and WT mice 8 weeks after the initial microbead or saline injection. We measured anterograde transport of CTB from RGC soma in the retina to RGC terminals in the superior colliculus (SC) by quantifying CTB labeling in serial sections of SC and generating 2D reconstructions of CTB labeling in the SC. In WT mice, 8 weeks of elevated IOP led to a ~50% decrease in CTB transport to the SC, as compared to saline-injected mice ($p<0.001$, Figure 3.5C; left). Interestingly, in *Il-6*^{-/-} mice, IOP elevation also resulted in a ~50% decrease in CTB transport ($p<0.001$, Figure 3.5C; right). Similar to previously published studies (Crish et al., 2010, Lambert et al., 2011, Ward et al., 2014), these deficits occurred in a sectoral manner, extending from the periphery towards the optic disc in WT and *Il-6*^{-/-} mice (Figure 3.5A-B). No

differences in axon transport were noted between genotype in saline-injected animals ($p>0.05$, Figure 3.5C).

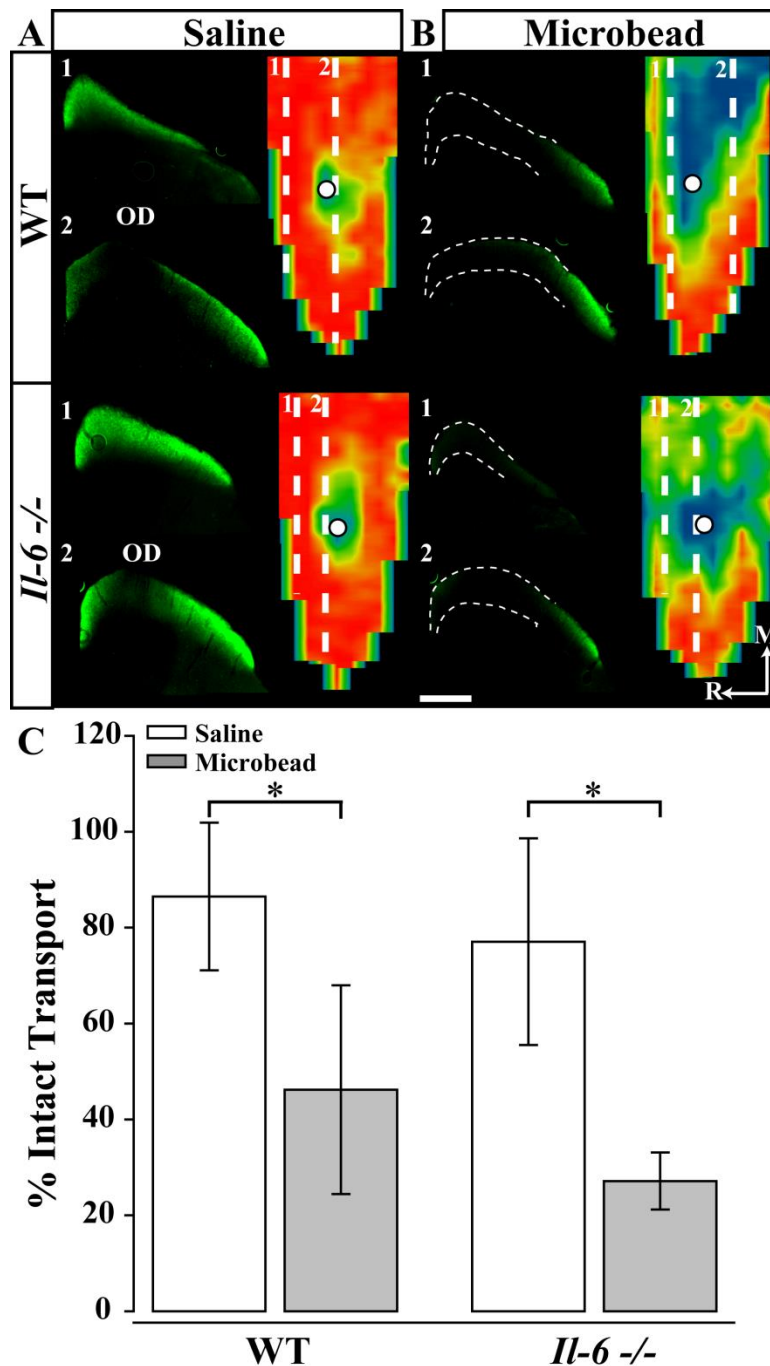


Figure 3.5. IL-6 deficiency does not affect CTB transport deficits caused by elevated IOP. (A-B) Representative coronal sections through the superior colliculus (SC) and respective retinotopic heat maps after 5 days of CTB transport in WT (A) and (B) *Il-6*^{-/-} mice. Outlines in coronal sections indicate areas of transport deficits. Dashed lines in map indicate position of coronal

section. Density of the CTB signal for heat maps range from 0% (blue) to 50% (green) to 70% (yellow) to 100% (red). Numbered, dashed lines in retinotopic maps indicate the location of respective coronal section and white circles indicate position of the optic disk (OD). Medial (M) and rostral (R) orientations are indicated. (C) Bar graph showing average percent intact transport (mean \pm STDEV, $\geq 70\%$ density of CTB signal; red/yellow areas) from SC following saline (white) or microbead (gray) injection in WT (left) and *Il-6*^{-/-} (right) mice. SC from both microbead- injected WT and *Il-6*^{-/-} mice show a ~50% deficit in intact axon transport compared to saline- injected mice. $\ast = p < 0.05$. n=5-6 SC/genotype/condition. Scale bars= 500 μ m for all images.

Figure from (Echevarria et al., 2017) and used in accordance with the Creative Commons Attribution-Non Commercial 4.0 International License.

IL-6 deficiency preserves optic nerve structure following IOP elevation

In glaucoma, degeneration of the optic nerve starts at the distal end of the optic nerve and progresses in a distal to proximal fashion (Crish et al., 2010). Therefore, we focused our examination of optic nerve axons to the distal half of the optic nerve closest to the chiasm.

Unlike the distal optic nerve of saline-injected WT mice (Figure 3.6A; top), the distal optic nerve of microbead-injected WT mice presented with signs of structural pathology, including increased glial infiltration and degenerating axon profiles (Figure 3.6A; bottom). This was accompanied by a slight enlargement in nerve area (Figure 3.6C; left) and a 15% decrease in myelinated axon density, as compared to saline-injected mice ($p < 0.05$, Figure 3.6; left). In contrast, while distal optic nerves from microbead-injected *Il-6*^{-/-} mice presented with some gliosis, no change in degenerating axon profiles were noted (Figure 3.6B). Similarly, there were no measurable changes either in nerve area (Figure 3.6D; right) or myelinated axon density ($p > 0.05$, Figure 3.6C; right), as compared to saline-injected *Il-6*^{-/-} mice. However, independent of IOP, optic nerves from *Il-6*^{-/-} mice contained approximately ~15% fewer RGC axons than those from WT mice ($p < 0.05$, Figure 3.6C).

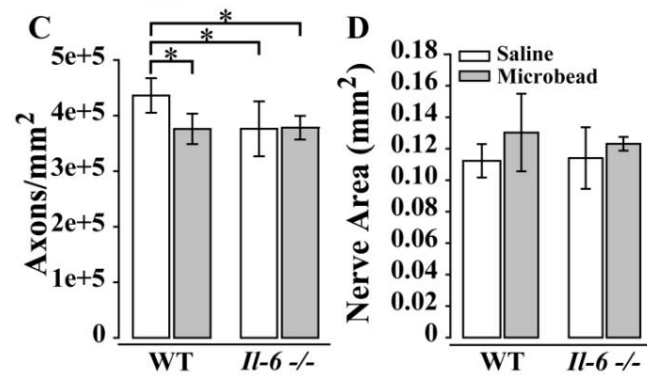
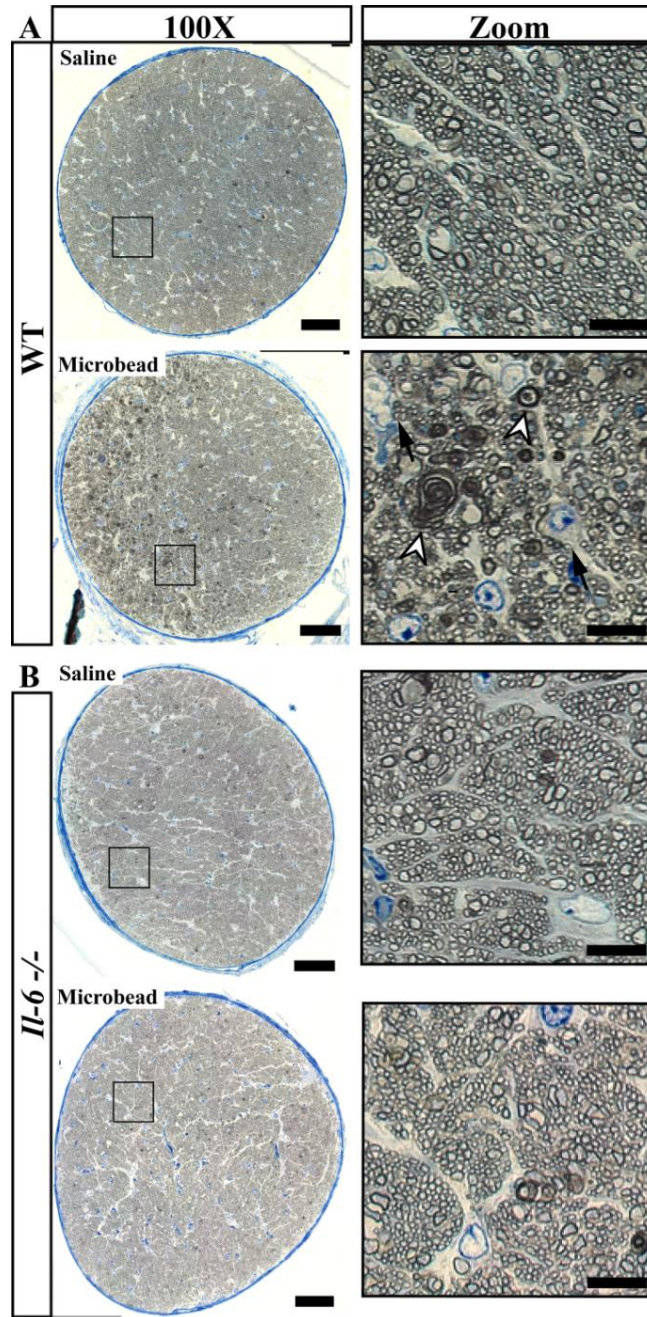


Figure 3.6. IL-6 ablation mitigates axonopathy caused by IOP elevation. **(A-B)** Representative 100X montaged optic nerve cross sections from WT **(A)** and *Il-6*^{-/-} **(B)** optic nerves following saline (top) or microbead (bottom) injection. Black box in montaged image (left) corresponds to location of zoomed images highlighting axon and glia (right). IOP elevation results in increased glial infiltration (black arrows) and degenerative axon profiles (white arrow heads) in optic nerves from microbead injected WT, but not *Il-6*^{-/-} mice. **(C)** Bar graph of average (mean \pm STDEV) myelinated axon density measurements in WT and *Il-6*^{-/-} mice following saline (white) or microbead (gray) injection. Saline- injected *Il-6*^{-/-} mice show a genotype specific decrease in myelinated axon density compared to saline- injected WT mice. However, microbead- injected WT eyes show a significant 15% decrease in myelinated axon density compared to saline- injected WT eyes, while no difference is seen between microbead- and saline- injected *Il-6*^{-/-} eyes. **(D)** Bar graph of average nerve area (mean \pm STDEV) among groups shows no significant difference. $*=p<0.05$. n=40-50 density measurements/genotype/group. Scale bars= 50 μ m for 100X montaged optic nerves and 10 μ m for zoomed images.

Figure from (Echevarria et al., 2017) and used in accordance with the Creative Commons Attribution-Non Commercial 4.0 International License.

IL-6 deficiency preserves visual acuity following IOP elevation

Loss of vision in glaucoma is irreversible and is caused by degeneration of RGC axons (Calkins, 2012). To determine whether the axon degeneration seen in our cohort was sufficient to induce deficits in visual acuity threshold, we performed bilateral injections of microbeads in one cohort of WT and *Il-6*^{-/-} mice. A second cohort received bilateral injections of saline. We measured visual acuity by optometry every four weeks for the duration of the experiment. Over the course of 8 weeks, microbead-injected WT mice exhibited significant depreciation of visual acuity at each time point compared to baseline, resulting in an overall 22% decrease in visual acuity ($p<0.001$ for all, Figure 3.7A; gray). However, in saline-injected WT mice, visual acuity did not significantly differ from baseline at either time point ($p>0.05$, Figure 3.7A; white). Comparison of visual acuity between saline- and microbead-injected WT mice revealed a significant ~15% decrease in both raw visual acuity ($p<0.05$, Figure 3.7C) and percent baseline visual acuity ($p<0.05$, Figure 3.7D). In *Il-6*^{-/-} mice, visual acuity dropped 8% with either saline ($p<0.01$) or microbeads ($p<0.05$), as compared to baseline acuity (Figure 3.7B). However, this

initial reduction in visual acuity did not differ between saline- and microbead-injected *Il-6*^{-/-} mice ($p>0.05$, Figure 3.7C,D) and remained unchanged between 4 and 8 weeks for both groups (saline: $p>0.05$; microbead: $p>0.05$; Figure 3.7B). That this slight decrease in visual acuity was noted in both saline- and microbead-injected *Il-6*^{-/-} mice and remained stable for the 8 week experiments suggest that it is likely due to the observed deficits in corneal wound healing (Figure 3.4). No difference in visual acuity was noted between WT and *Il-6*^{-/-} mice at any time point ($p>0.05$, Figure 3.7C).

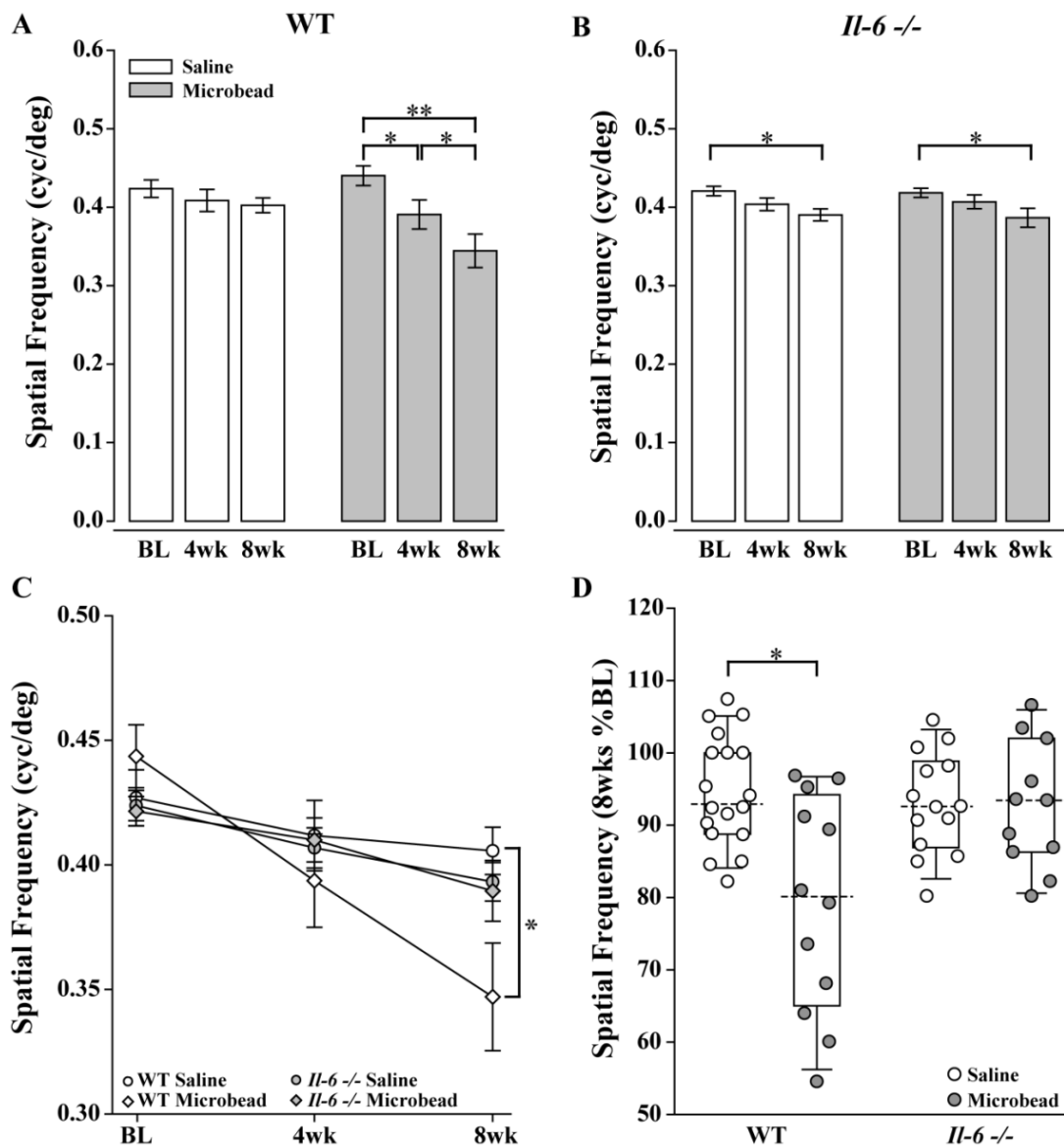


Figure 3.7. *Il-6*^{-/-} mice are resistant to IOP-induced deficits in visual acuity. **(A)** Bar graph showing average visual acuity threshold (mean \pm SEM) of WT mice at baseline (BL) and 4 and 8 weeks post initial saline (white) or microbead (gray) injection. WT mice injected with microbeads show a significant decrease in visual acuity at both 4 weeks and 8 weeks post-injection compared to baseline. **(B)** Bar graph showing average visual acuity threshold (mean \pm SEM) of *Il-6*^{-/-} mice at baseline and 4 and 8 weeks post initial saline (white) or microbead (gray) injection. *Il-6*^{-/-} mice injected with either saline or microbeads show a significant decrease in visual acuity at 8 weeks compared to baseline. **(C)** Line graph comparing visual acuity of WT saline (white circle), WT microbead (white diamond), *Il-6*^{-/-} saline (gray circle) and *Il-6*^{-/-} microbead (gray diamond) at each time point. Visual acuity decreases significantly in microbead-injected WT mice compared to saline-injected WT mice. Visual acuity does not differ between saline- and microbead- injected *Il-6*^{-/-} or between genotypes. **(D)** Boxplot of the percentage visual acuity remaining at 8 weeks compared to baseline measurements for WT and *Il-6*^{-/-}. WT mice injected with microbeads show a significant decrease in the remaining visual acuity when compared to the saline- injected WT mice. *Il-6*^{-/-} mice injected with microbeads show no difference in the remaining visual acuity when compared to the saline injected *Il-6*^{-/-} cohort. *= $p < 0.05$, **= $p < 0.001$. n=13-17/group. Dashed lines in boxplot indicate median value of data set.

Figure from (Echevarria et al., 2017) and used in accordance with the Creative Commons Attribution-Non Commercial 4.0 International License.

IL-6 deficiency enlarges the microglia population in retina

Recent studies suggest that changes in glial reactivity in the retina occur in response to IOP elevation in both genomic and inducible models of glaucoma (Martin et al., 2003, Sappington and Calkins, 2006, Inman and Horner, 2007, Bosco et al., 2008, Johnson and Morrison, 2009, Johnson et al., 2011, Echevarria et al., 2013, Lye-Barthel et al., 2013, Formichella et al., 2014, Hines-Beard et al., 2016). To determine whether IL-6 plays a role in glial reactivity associated with RGC axonopathy, we performed a morphological analysis of astrocyte and microglia reactivity in retina. We visualized astrocytes and microglia in whole-mount retina from saline- and microbead- injected WT and *Il-6*^{-/-} mice with immunolabeling against the astrocyte- specific label glial fibrillary acidic protein (GFAP) and the microglia- specific marker ionized calcium binding adaptor molecule (Iba-1). We quantified percent area coverage of GFAP⁺ astrocytes and Iba-1⁺ microglia. Our previous work indicates that percent

area coverage is a highly reliable measure of reactivity that accounts for both increases in density and hypertrophy, two hallmarks of gliosis (Formichella et al., 2014). GFAP immunolabeling revealed no gross genotype- or IOP-dependent changes in astrocytic morphology (Figure 3.8A). This was confirmed by quantification of percent area coverage, which indicated no significant difference in the retinal area covered by GFAP+ astrocytes with respect to either IOP or genotype ($p>0.05$ for all; Figure 3.8C). In contrast, Iba-1 immunolabeling revealed qualitative changes in microglia

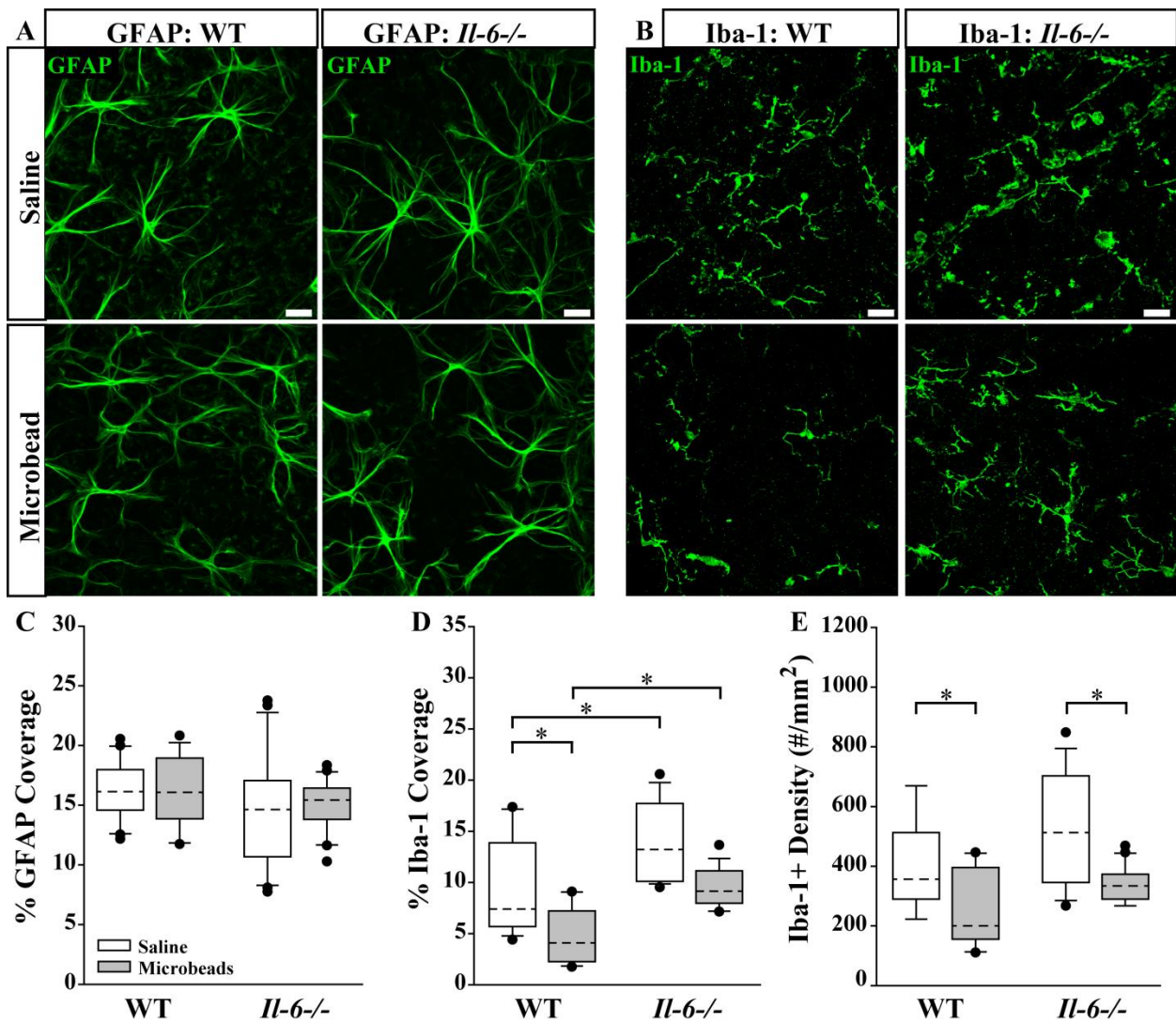


Figure 3.8. IL-6 deficiency affects microglial coverage regardless of IOP. (A-B) Representative 60X confocal images depicting GFAP+ astrocyte (green; A) and Iba1+ microglia (green; B)

labeling in whole mount retina of microbead- and saline- injected WT and *Il-6*^{-/-} eyes. **(C)** Boxplot of percent coverage of GFAP+ astrocytes in saline (white) and microbead (gray) injected WT (left) and *Il-6*^{-/-} (right) eyes. No genotype or IOP dependent changes were calculated. **(D)** Boxplot of percent coverage of Iba1+ microglia in saline- (white) and microbead- (gray) injected WT (left) and *Il-6*^{-/-} (right) eyes. While an IL-6 dependent increase in percent coverage of microglia is seen in both saline and microbead- injected eyes, only an IOP dependent decrease is seen in microbead- injected WT eyes. **(E)** Boxplot of Iba1+ microglia cell density (counts/mm²) in saline- (white) and microbead- (gray) injected WT (left) and *Il-6*^{-/-} (right) eyes. IOP dependent decreases in microglia counts are evident in microbead- injected eyes are evident in both WT and *Il-6*^{-/-} eyes. *= $p < 0.05$. n=6-8 images/eye/condition/genotype. Scale bars= 30 μ m for all images. Dashed lines in boxplot indicate median value of data set.

Figure from (Echevarria et al., 2017) and used in accordance with the Creative Commons Attribution-Non Commercial 4.0 International License..

that appeared to relate to both genotype and IOP (Figure 3.8B). Quantification of percent area coverage revealed that Iba-1+ microglia covered 32% more area in retina from saline-injected *Il-6*^{-/-} mice versus WT mice ($p < 0.05$; Figure 3.8D). Microbead-induced IOP elevation decreased the percent area covered by Iba-1+ microglia by 45% in WT retina ($p < 0.05$) as compared to saline-injected controls (Figure 3.8D). Although the mean percent area covered was 30% lower in microbead- injected *Il-6*^{-/-} mice, this did not reach statistical significance ($p > 0.05$, Figure 3.8D). Comparing genotypes, more retinal area remained covered by microglia in microbead injected *Il-6*^{-/-} mice than in WT mice ($p < 0.05$, Figure 3.8E). Based on qualitative assessment, IOP-induced changes in percent area coverage appeared to arise from changes in microglia density (Figure 3.8B). To quantitatively test this observation, we measured the density of Iba-1+ microglia across all experimental groups. We found that microbead-induced IOP elevation decreased the density of microglia by 37% in WT retina ($p < 0.05$) and by 36% in *Il-6*^{-/-} mice ($p < 0.05$), as compared to saline-injected controls (Figure 3.8E). There was no significant difference in microglial density between WT and *Il-6*^{-/-} mice regardless of treatment ($p > 0.05$; Figure 3.8E).

Discussion

IL-6 is broadly associated with neurodegeneration across the CNS. However, the impact of IL-6 signaling on neurodegeneration is controversial, with studies reporting both beneficial and detrimental effects (Erta et al., 2012, Campbell et al., 2014). The present work investigated the relevance of IL-6 signaling to RGC axonopathy following microbead-induced ocular hypertension. By comparing functional and structural outcomes of IOP elevation on RGC axonopathy in *Il-6*^{-/-} and WT mice, we were able to link IL-6 signaling with specific events in RGC axonopathy. These studies delineate a role for IL-6 in the progression from functional deficits to structural degeneration within the axonopathy continuum. Secondly, our data also indicated a role for IL-6 in corneal wound healing and potentially IOP regulation.

Glaucoma is associated with elevated IOP and current therapies, directed towards lowering IOP, delay pathology (Calkins, 2012). Not surprisingly, animal models of glaucoma are generally characterized by elevated IOP and subsequent degeneration of RGCs (Johnson and Tomarev, 2010, Bouhenni et al., 2012). Our data indicates that IL-6 deficiency modestly, but significantly, decreases baseline IOP by ~4% compared to WT (Figure 3.1). This differential in baseline IOP was maintained following IOP elevation via microbead injection, such that the relative magnitude in IOP elevation was equivalent between the genotypes (Figure 3.1). There is some indication that modulation of IL-6 signaling accompanies IOP elevations in human patients, including both primary open angle and angle closure glaucoma (Takai et al., 2012, Engel et al., 2014, Huang et al., 2014, Du et al., 2016). However, in a recent study of porcine anterior segment, IL-6 did not appear to alter outflow facility that determines IOP (Birke et al., 2011). Our data suggest that, at least in mice, IL-6 signaling may impact the IOP “set-point”.

However, it is unclear whether this results from direct modulation of aqueous humor dynamics or from IL-6 signaling during development of the anterior chamber.

The microbead occlusion model is an inducible model of glaucoma that elevates IOP by intracameral injection of microbeads (Figure 3.1) (Sappington et al., 2010). This intracameral injection requires a small diameter (approx. 100 μ m) puncture in the cornea. OCT imaging revealed that IL-6 deficiency prevented stitching and filling of the stromal and endothelial layers of the cornea, which was visible in WT mice within 2 weeks of puncture (Figure 3.2).

Interestingly, the epithelial layer of the cornea in *Il-6*^{-/-} mice was indistinguishable from WT mice (Figure 3.3). This suggests that IL-6 signaling plays a prominent role in healing of stromal and endothelial, but not epithelial, layers of cornea. That a deficit in corneal wound healing was noted in our studies is not surprising, as IL-6 is strongly associated with wound healing and tissue regeneration in other systems (Blindenbacher et al., 2003, Lin et al., 2003b, Tiberio et al., 2008, McFarland-Mancini et al., 2010).

One of the earliest characteristics of RGC degeneration in glaucoma are deficits in active, anterograde transport that occurs prior to structural degeneration of the axon and loss of vision. (Crish et al., 2010, Crish et al., 2013). Consistent with previously published studies (Sappington et al., 2010, Lambert et al., 2011, Ward et al., 2014, Bond et al., 2016), microbead-induced IOP elevation in WT mice resulted in a 50% decrease in anterograde transport of CTB to the SC (Figure 3.3). Interestingly, *Il-6*^{-/-} mice exhibited a similar decrease in anterograde transport (Figure 3.3). However in respect to axon degeneration and subsequent vision loss, IL-6 deficiency preserved both the structure of RGC axons and visual acuity following 8 weeks of elevated IOP (Figure 3.4 and 3.5). Consistent with previous findings (Sappington et al., 2010, Lambert et al., 2011, Ward et al., 2014, Bond et al., 2016), microbead-induced IOP elevation in

WT mice resulted in significant loss of RGC axons in the optic nerve and the presence of degeneration profiles and macrogliosis (Figure 3.4). This was accompanied by a significant and IOP-dependent decrease in visual acuity (Figure 3.5), which is also consistent with previous findings (Della Santina et al., 2013). Aside from a genotype-specific decrease in myelinated axon density (approx. 15%), we did not see any gross structural abnormalities of the optic nerve following IOP elevation in *Il-6*^{-/-} (Figure 3.4). This lack of structural degeneration was supported by no change in visual acuity following IOP elevation, as compared to saline control (Figure 3.5). However, it should be noted that, while baseline visual acuity did not differ between WT and *Il-6*^{-/-} mice, visual acuity decreased modestly, but significantly (8%), following both saline and microbead injection (Figure 3.5). That this decrease was noted following both types of injection and did not change over time, it is highly likely that visual acuity was negatively impacted by the observed deficits in corneal wound healing (Figure 3.2). Together, these data delineate a temporal window in which IL-6 signaling contributes to RGC axonopathy. Specifically, this temporal window begins after the onset of axon transport deficits and prior to the onset of structural degeneration and decreased visual function. More generally, our data suggest that axon transport deficits and structural degeneration of axons occurs via, at least partially, independent mechanisms.

Our analysis of gliosis in the GCL and NFL revealed a strong association between microglia, IOP and IL-6, but no association with astrocyte reactivity. This is contrary to studies of astrocyte reactivity in other models, where both retinal astrocyte hypertrophy and hypotrophy are associated with elevated IOP. Notably, most of these studies were conducted in either chronic models (Inman and Horner, 2007, Formichella et al., 2014) or inducible models with much higher IOP elevation (Wang et al., 2000, Gallego et al., 2012). Differences in the duration and

magnitude of IOP elevation, as well as severity of RGC pathology, could account for our contradictory findings. With respect to microglia, IL-6 deficiency increased the percent area of the GCL/NFL that was covered by microglia, as compared to WT (Figure 3.6). Elevated IOP decreased the percent area of the GCL/NFL that was covered by microglia in both WT and *Il-6*^{-/-} mice (Figure 3.6). However, more retinal area remained covered by microglia in microbead-injected *Il-6*^{-/-} than in WT mice (Figure 3.6). IOP-related reductions in area covered were, at least partially, due to a decrease in the density of microglia in the GCL/NFL for both genotypes (Figure 3.6). Based on previous literature, changes in microglia density likely arise from migration of microglia to other retinal layers, particularly in outer retina (Rojas et al., 2014). In contrast, the genotype-dependent increase in microglia coverage is not largely attributable to changes in density, as the trend towards increased microglia density failed to reach statistical significance. This suggests that increased size and ramification of microglia is likely to contribute to the larger representation of microglia in retina of *Il-6*^{-/-} mice. That IOP-induced changes in microglia were similar in *Il-6*^{-/-} mice and WT suggests that IL-6 does not play a causal role in microglia migration or temporal onset of microglia reactivity in this model. Furthermore, in combination with our optic nerve and visual function data, expansion of the microglia population noted in the GCL/NFL of *Il-6*^{-/-} retina did not negatively impact progression of axonopathy.

Overall, these findings support a detrimental role for IL-6 in RGC axonopathy, particularly with respect to structural degeneration and subsequent visual dysfunction. Prior to degeneration, stressed myelinated axons undergo repeated myelination (Crish et al., 2010, Joos et al., 2010) leading to the presence of degenerative profiles. We noted fewer degenerating profiles in microbead-injected *Il-6*^{-/-} mice than WT mice and preservation of RGC myelinated axon

density in comparison to their respective saline- injected controls. The apparent reduction in degenerating profiles may result from the absence of repeated myelination. In the experimental autoimmune encephalomyelitis (EAE) model of multiple sclerosis, IL-6 deficiency protects against myelin degradation. Multiple studies report that myelin degeneration in the spinal cord seen in WT mice affected with EAE is absent in *Il-6*^{-/-} mice, a result thought to be due to lack of infiltrating T-cells (Eugster et al., 1998, Mendel et al., 1998, Okuda et al., 1998, Samoiloova et al., 1998). In the cuprizone model of de-myelination, blocking IL-6 signaling pharmacologically improved re-myelination following injection (Makinodan et al., 2016). These studies indicate that the reduction in degenerating profiles we noted could arise from IL-6 mediated effects on myelin, particularly myelin repair. Further studies of axon sub-structure are needed to elucidate the impact of IL-6 deficiency on myelin formation.

As discussed previously, our results showing IL-6 deficiency is protective aligns with some IL-6 literature, but not others. Indeed, studies that describe a neuroprotective role for IL-6 and other IL-6 family members arise primarily from *in vitro* models and the optic nerve crush model. *In vitro* models utilize RGCs harvested from mechanically dissociated retina following transection of the optic nerve and the optic nerve crush model utilizes forceps to directly and mechanically injure the optic nerve. In these model systems, IL-6 and several of its family members promote regeneration and/or preservation of RGC axons (Mendonca Torres and de Araujo, 2001, Schuettauf et al., 2005, Sappington et al., 2006, Chidlow et al., 2012, Leibinger et al., 2013, Perigolo-Vicente et al., 2013, Pernet et al., 2013, Ogai et al., 2014, Perigolo-Vicente et al., 2014, Xia et al., 2014, Leibinger et al., 2016). Additionally, studies that suggest a neuro-destructive role for IL-6 tend to utilize models in which RGC axons remain intact and RGC degeneration is secondary to a diffuse stressor, like demyelination, retinal detachment and

ischemia (Fisher et al., 2001, Dvorianchikova et al., 2010, Horstmann et al., 2013, Fischer et al., 2015). Our microbead occlusion model aligns more with the latter form of injury, as RGC axons remain structurally-intact and IOP elevation is a diffuse stressor.

In conclusion, our findings indicate that two defining features of RGC axonopathy - axon transport deficits and structural degeneration of axons - likely occur via independent mechanisms. That the functional and structural components of RGC axonopathy could be mechanistically separated has tremendous implications for therapeutic targeting. Our data indicate that IL-6 is part of a mechanism that specifically leads to structural degeneration of axons. Furthermore, its absence is sufficient to prevent both structural degeneration of the optic nerve and vision loss. Together, our findings support the proposition that functional deficits in axon transport represent a therapeutic window for RGC axonopathy and identify IL-6 signaling as a strong target for such a therapeutic.

CHAPTER 4

IL-6 CONTRIBUTES TO THE DEVELOPMENT OF AXONS IN THE OPTIC PROJECTION

Introduction

The subject of cytokine signaling in the CNS is primarily focused on its impact in neuronal health during chronic neuroinflammation. However, there is increasing evidence that cytokine signaling, especially gp130 signaling, is associated with development and maintenance of the central and peripheral nervous systems (Mousa and Bakhiet, 2013). While functional redundancy between the members of the gp130 family exists, gene ablation studies in mice of specific gp130 ligands and receptors provide evidence of individual roles within the nervous systems. For example, LIF is responsible for astrocyte differentiation from progenitors during CNS development (Bauer et al., 2007), while evidence points to CNTF and LIF facilitating Müller cell and photoreceptor development in the retina (Rhee and Yang, 2010). In neurons, genetic ablation of OSM leads to deficiencies in certain populations of nociceptive neurons (Morikawa et al., 2004), while deficiency of CT-1 or its receptors leads to a decrease in motor neuron survival in the brain stem and spinal cord during embryonic development (Oppenheim et al., 2001).

In regards to IL-6, *Il-6*^{-/-} mice show deficits in temperature sensitivity, pain response thresholds and sensory compound action potential (Xu et al., 1997, Murphy et al., 1999, Zhong et al., 1999), suggesting a role for IL-6 in responding to noxious stimuli. Indeed, other studies show that IL-6/gp130 activation sensitizes nociceptors to noxious stimuli by upregulating various members of the mechanosensitive transient receptor potential (TRP) channel family

(Andratsch et al., 2009, Malsch et al., 2014). In the CNS, a number of studies point to a role for IL-6 in hippocampal mediated learning and memory. For example, gene expression of hippocampal IL-6 increases following tasks that are known to induce long-term potentiation in the hippocampus, a form of synaptic plasticity that is instrumental to learning and memory (Gruol et al., 2014). Indeed, *Il-6*^{-/-} mice present with decreases in the neural progenitor cell population in the sub-ventricular zone, dentate gyrus and posterior peri-ventricle of the hippocampus (Bowen et al., 2011), as well as present with significant learning and memory deficits (Baier et al., 2009). Aside from the hippocampus, *Il-6*^{-/-} mice also show altered sleep rhythms, hyperactivity, and behaviors associated with decreased depression, increased anxiety and aggression (Alleva et al., 1998, Armario et al., 1998, Butterweck et al., 2003, Morrow and Opp, 2005, Chourbaji et al., 2006, Kong et al., 2015). In humans, roles for IL-6 signaling not directly associated with injury or pathogen mediated disease involve sleep regulation and development of several psychiatric diseases. In regards to sleep, plasma levels of IL-6 in humans exhibit a circadian rhythm with levels highest at night (Agorastos et al., 2014). Similar to rodents, IL-6 appears to specifically regulate the rapid eye movement (REM) stage of sleep (Spath-Schwalbe et al., 1998, Hogan et al., 2003). In regards to psychiatric disease, individuals with depression have elevated levels of IL-6 in their plasma (Hodes et al., 2016). In mice, IL-6 activity is thought to contribute to depressive behavior by upregulating the serotonin transporter, leading to decreased serotonin in the synaptic space (Kong et al., 2015). Elevated levels of IL-6 are also seen in people with schizophrenia and autism (Wei et al., 2012). One hypothesis for the development of these disorders is due to exposure to IL-6 *in utero* caused by maternal infection (Smith et al., 2007, Khan et al., 2014). Overall, these studies suggest that IL-6 signaling mediates development of the CNS.

In the optic projection, *in vitro* studies show a direct relationship between IL-6 application and increased neurite out growth from RGCs (Chidlow et al., 2012, Leibinger et al., 2013). *In vivo*, IL-6 deficiency inhibits axon regrowth following optic nerve crush, while intravitreal application of IL-6 improves axon regrowth, suggesting that IL-6 facilitates optic nerve axon growth in response to injury (Leibinger et al., 2013). However, it is unknown whether similar IL-6 development is involved in the development and maintenance of the mature optic projection. To ascertain the role of constitutive IL-6 signaling in the mature optic projection we compared gross retinal structure, RGC mediated cortical light responses, axon transport, and axon morphology in both the unmyelinated and myelinated optic nerve between WT and *Il-6*^{-/-} mice. Overall, our data points to a role for constitutive IL-6 signaling in the development of axons in the optic projection neurons by influencing organization of microtubules. This data along with previously published studies, have broad implications for the understanding of constitutive functions of cytokines in the CNS and the development of cytokine-based therapies.

Materials and Methods

Animals

Neonatal (P3, P7, P21) or adult (2-3mo) male and female *Il-6*^{-/-} mice (B6.129S2-*IL6*^{tm1kopf/J}) and respective genomic controls (B6129SF2/J) were used for all experiments. For experiments utilizing neonates, day of birth was designated P0. Mice were housed in accordance with NIH guidelines and maintained on a 12hr light/dark cycle with *ad libitum* access to standard mouse chow and water. All experiments complied with the ARVO statement for the use of animals in ophthalmic and vision research and were approved by the IACUC of Vanderbilt University Medical Center.

Tissue preparation

For histological assays, mice were euthanized and perfused as previously described (Chapter 2 material and methods). Eyes, optic nerve and brain were processed as previously described (Crish et al., 2010). For assays requiring fresh tissue, mice were sacrificed by cervical dislocation followed by decapitation. Eyes were enucleated and snap frozen on dry ice and stored at -80°C until use.

Immunohistochemistry

Labeling of whole-mount retinas, retinal cryosections, optic projections and floating brain sections were done as previously described (Sappington et al., 2009, Crish et al., 2010, Echevarria et al., 2013, Echevarria et al., 2016). We used primary antibodies against Brn3a (1:50; Cat# sc-31984; Santa Cruz) to visualize RGCs, β -Tubulin III (TUJ1, 1:500; Cat#845501; BioLegend), SMI-31 (1:1000; cat# SMI-31R; Covance) and Phalloidin (actin, 1:50; Cat# P1951;

Sigma) to visualize RGCs and their axons or neurons in the brain, ERR β (1:500; Cat# E0156; Sigma) to label RGC synaptic terminals in the SC, Cav-1 (1:250; cat# sc-894; Santa Cruz) to highlight Cav-1 localization in the retina and Tau (1:50; cat# sc-1995; Santa Cruz) to highlight microtubule associated proteins in axons. Secondary antibodies, if applicable, were used at a concentration of 1:200 and consisted of donkey α -host species of primary- 488, Rhodamine Red or 647(Jackson ImmunoResearch).

Fluorescent *In-situ* hybridization

Generation of IL-6 probes and FISH in whole mount retina were done as previously described (Crish et al., 2013). Probes were made against a nucleotide sequence encompassing exons 2-5 of *Il-6* (nucleotides 107-651 of [NCBI Ref Seq: NM_031168.2]). The transcript inserted into the pGEM-T Easy Vector (Promega, Madison WI) was generated by PCR using primers to IL-6 (forward 5'-ATCCAGTTGCCTTCTTGGGACTGA-3' and reverse 5'TGGCTAAGGACCAAGACCATCCAA-3').

Anterograde axon transport measurements

Anterograde axonal transport capabilities of RGCs were assessed with CTB and WGA conjugated to a fluorophore, both established markers for active uptake and transport in the optic projection (Crish et al., 2010, Lambert et al., 2011, Fernandez et al., 2012, Wong and Brown, 2012, Echevarria et al., 2013, Formichella et al., 2014, Ward et al., 2014). Briefly, mice were given a 1.5-2 μ l intravitreal injection of CTB (10ug/ μ l in sterile PBS; Life Technologies) or WGA (20ug/ μ l in sterile PBS; Life Technologies) using a 33 gauge needle attached to a Hamilton syringe under 2.5% isoflurane anesthesia. 3 days after CTB/WGA injection, mice were

sacrificed by transcardial perfusion as described above. Quantification of CTB/WGA signal in the SC and construction of retinotopic maps was done as previously described (See Chapter 2). Creation and quantification of 2D retinotopic map of ERR β staining within the SC was done in a similar fashion. For experiments studying delayed CTB or WGA transport, mice were sacrificed 5 days after CTB/WGA injection. To confirm uniform CTB/WGA exposure to RGCs, a subset of whole-mount retinas were imaged *en montage* at 20X using confocal microscopy. For tracing experiments involving recombinant IL-6, mice were given intravitreal injections of either 500ng (250ng/ μ l in 0.1% BSA; R&D Systems) of recombinant murine IL-6 or 2ul of 0.1% BSA 24 hours before CTB injection.

Spectral Domain Optical Coherence Tomography (SD-OCT) and quantification of retinal layer thickness

Live volumetric scans of the retina (1.4mm x 1.4mm x 1.637mm) were obtained using SD-OCT (Envisu R22 UHR, Bioptogen, Morrisville, NC) as described elsewhere (Ferguson et al., 2014). Each volumetric scan was obtained with the optic nerve head (ONH) at the center and consists of 100 axial slices (B-scans) through the retina. Thickness of the total retina and individual retinal layers were measured manually using InVivoVue Diver Software (Ver 2.0, Bioptogen, Morrisville, NC). Measurements were obtained by placing a 5x5 ROI marker grid on the volumetric image, with the center ROI marker corresponding to the optic nerve head. ROI markers were equally spaced from each other (0.23mm). At each ROI marker, individual retinal layers (GCL/NFL, IPL, INL, OPL, ONL, IS/OS and RPE) as well as total retinal thickness (GCL/NFL-RPE) were measured. No measurements were obtained from ROI markers located at the optic nerve head or any ROI marker where layers could not be easily measured.

Quantification of brain width

Brain width from brain sections located 0.145mm rostral of Bregma and 1.995mm caudal of Bregma were imaged *en montage* at 5X using a Nikon Eclipse Ti inverted microscope (Melville, NY). Width was measured at widest points using NIS-Elements AR software. Bregma locations were determined by matching sections measured to most represented section located in the Allen Reference Mouse Atlas (Dong, 2008).

FVEPs

Prior to testing, mice were dark adapted overnight for a period of at least 12 hours. Following dark adaptation, mice were anesthetized with an IP injection of a ketamine/xylazine cocktail (80/5 $\mu\text{g}/\text{gram}$ of mouse) and pupils were dilated using 0.5% Tropicamide. Mice were placed in a Ganzfeld dome (Diagnosys, Lowell, MA) containing a heated stage to maintain body temperature at 37°C. Platinum needle electrodes (Grass Technologies, West Warwick, RI) were placed over the right and left cortex about 2mm lateral of lambda and GenTeal lubricating eye drops were applied to prevent drying. Within the ganzfeld dome, photopic stimulation at luminance levels of 0.01 $\text{cd}\cdot\text{sec}/\text{m}^2$ were emitted at a frequency of 1 Hz with an inner sweep delay of 500 msec, followed by stimulation at luminance levels of 1.0 and 5.0 $\text{cd}\cdot\text{sec}/\text{m}^2$ at equal frequency. Waveform from each luminance level of each animal was a result of 200 sweeps. Waveforms presented (Figure 1) are an average of waveforms from each animal in the cohort. Similar to other publications (Sullivan et al., 2011, Bond et al., 2016), N1 is designated as the first major depolarization event following the stimulus, while the P1 was designated as the first major hyper polarization event following the N1 depolarization event. N1 and P1 amplitude

measurements were taken from the N1 trough and P1 peak. Respective time at which the N1 trough and P1 peak occurred, were designated as N1 and P1 latency.

Psychophysical visual testing

Baseline visual acuity threshold was determined as previously described (See Chapter 2 material and methods).

Quantification of RGC somas/axons

For RGC density, 5-7 pseudo-random z-stack images were taken throughout the mid – peripheral/mid-central retina at 60X using an Olympus confocal microscope. TUJ1/SMI31 dual positive RGCs were counted from each image and divided by the area of the counting field (0.101mm^2) to get RGC density. Approximate total number of myelinated axons from each nerve was calculated using the average myelinated axon density multiplied by the area of each nerve. Myelinated axon density was measured as previously described (See Chapter 2).

Quantification of axon diameter and gRatio.

Total axon diameter (myelin sheath + axon) and inner axon diameter (axon only) was measured from 100X montaged images of optic nerve sections using NIS-Elements AR (See Figure 4.8A). Myelin thickness was calculated using the following formula: (Total Axon Diameter – Inner Axon Diameter / 2). gRatio was calculated using the following formula: (Inner Axon Diameter/Total Axon Diameter).

Immunoblotting.

Single retinas and western blot processing was done as previously described (Echevarria et al., 2016). Probing of Cav-1 and β -actin was accomplished using anti-rabbit Cav-1 (1:250; cat# sc-894; Santa Cruz) and anti-mouse β -actin (1:1000; cat# AM4302; Ambion). Secondary antibodies utilized were donkey anti-mouse IRDye 680RD (1:1000; Cat# 925-68072; Li-Cor) and donkey anti-rabbit IRDye 800CW (1:1000; Cat# 925-32213; Li-Cor). Cav-1 and β -actin bands were detected using the Odyssey Infrared Imaging System (Li-Cor; Lincoln, NE). Cav-1 bands were subjected to densitometry analysis (Odyssey Application Software V3.0; Li-Cor) and normalized to β -actin. All samples used for densitometry analysis were run on the same gel and transferred to the same nitrocellulose membrane.

Statistical Analysis

Statistical analysis was done using SigmaPlot (version 11.1 SYSTAT). For two independent data sets that passed normality and equal variance tests, statistical significance was determined using a two-sided t-test. Mann-Whitney Rank Sum Tests were used for data sets that did not meet normality and/or equal variance requirements. *p* values less than 0.05 were considered statistically significant. Number of measurements and specific *p*-values are indicated in results or figure legends.

Results

IL-6 is constitutively expressed by RGCs during post-natal development and in mature retina.

We previously published that IL-6 protein is constitutively present in the adult mouse retina (Sims et al., 2012) (Chapter 2). Here, we examined retinal *Il-6* mRNA expression throughout postnatal development to determine possible cell types responsible for IL-6 release. Using in situ hybridization, we examined expression and localization of *Il-6* mRNA from retinal cryosections of mice from postnatal day (PD) 3 to 21. Starting at PD3, we detected robust *in situ* anti-sense signal in the developing ganglion cell layer (GCL) with some weaker labeling near the inner margin of the neuroblast layer (NBL; Figure 4.1A). By PD7, *Il-6* labeling in the GCL increased in intensity and compaction. Labeling previously associated with the inner margin of the NBL transitioned to a band of higher intensity labeling in the inner margin of the now developed inner nuclear layer (INL; Figure 4.1B). By PD21, *Il-6* labeling in the GCL increased further in intensity and appeared to fill the soma of neurons in this layer (Figure 4.1B). Labeling of the INL noted at PD7 dissipated and a novel band of labeling was noted in the outer margin of the outer plexiform layer (OPL; Figure 4.1C). No significant signal from the sense probe was noted at any of these time points.

Based on mRNA localization patterns, constitutive *Il-6* mRNA expression appears to be most consistently and robustly associated with soma in the GCL, suggesting that RGCs are constitutively producing IL-6. In 3 month old mice, we examined localization of *IL-6* mRNA in wholemount retina co-immunolabeled with the RGC-specific marker β -Tubulin (TUJ1). To confirm specificity of our probes, we examined expression and localization in WT and *Il-6*^{-/-} mice. Anti-sense labeling for *Il-6* mRNA localized to TUJ1⁺ positive RGCs in WT (Figure

4.1D; left). Anti-sense labeling for *Il-6* mRNA was not detected in *Il-6*^{-/-} mice (Figure 4.1D; right). Similarly *Il-6* mRNA labeling was not detected following incubation with the sense probe in either genotype (Figure 4.1E).

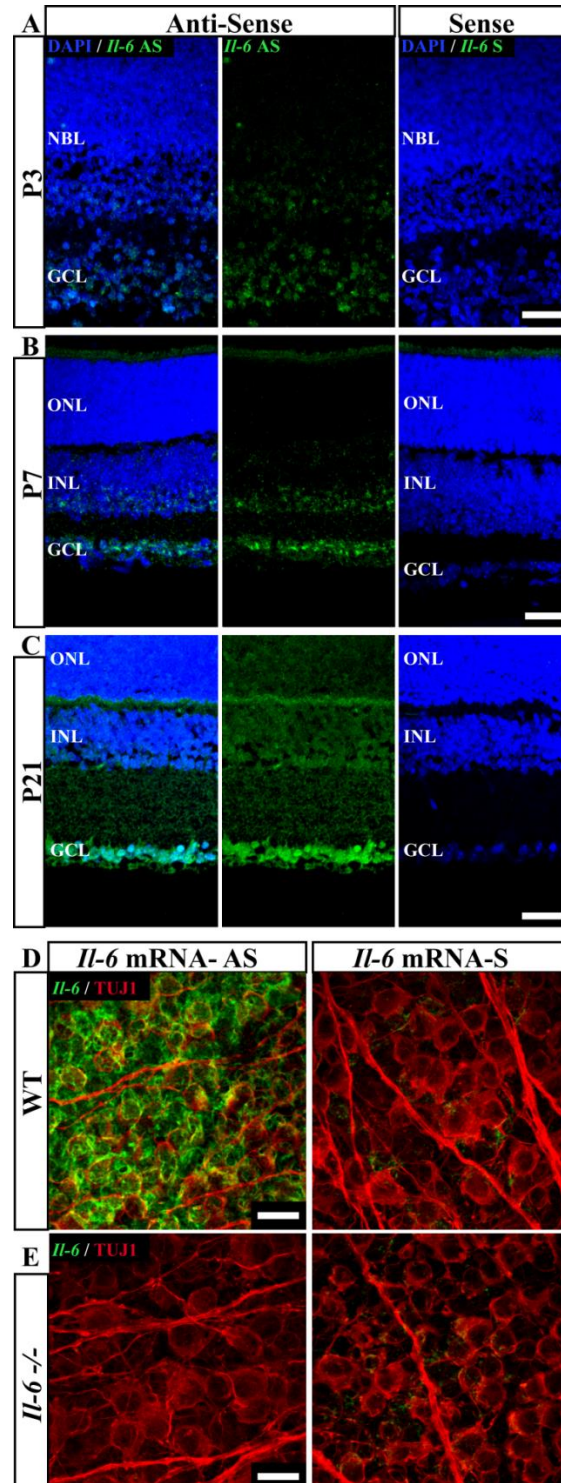


Figure 4.1. RGCs express *Il-6* mRNA throughout post-natal development. (A-C) Representative 40X confocal images of retinal cryo-sections displaying *Il-6* mRNA expression (green) from cells in ganglion cell layer (RGCs) at post-natal day (PD) 3 (A), PD7 (B) and PD21 (C). Cryo-sections incubated with anti-sense probe towards *Il-6* mRNA (left) and control sense probe (right). Scale bars for (A-C) = 30 μ m. (NBL= neuroblast layer, ONL= outer nuclear layer, INL= inner nuclear layer, GCL= ganglion cell layer). (D-E) Representative 100X confocal image of retinal whole mount from adult (3mo) WT (D) and *Il-6*^{-/-} mice (E) incubated with an anti-sense (AS; left) or sense probe (S; right) towards *Il-6* mRNA (right). Signal from AS probe (green) is found within β -Tubulin (TUJ1) positive RGCs (D, red; arrow heads) in WT mice (D). No signal was present in retinas from *Il-6*^{-/-} mice (E; right) or during incubation with sense probe (D,E; left). Scale bars= (D,E); 20 μ m.

IL-6 deficiency alters retinal layer thickness without impacting gross morphology or structure.

To determine the role of constitutive IL-6 signaling in retina, we first examined overall retina morphology and structure in WT and *Il-6*^{-/-} mice, using spectral-domain optical coherence tomography (SD-OCT). We obtained sagittal cross-sections throughout the entire retina and measured thickness of individual layers and the entire retina. The gross laminar structure of the retina and position and size of the optic nerve head were unremarkable in *Il-6*^{-/-} mice, compared to WT mice (Figure 4.2A,B). However, quantification of total retinal thickness in SD-OCT scans revealed a slight, yet significant 2% reduction in *Il-6*^{-/-} mice versus WT mice ($p < 0.001$, Figure 4.2C). Quantification of layer thicknesses revealed that the reduction of total retina thickness was attributable to thinning of the outer plexiform layer (OPL), outer nuclear layer (ONL) and retinal pigment epithelium (RPE; $p < 0.001$, Figure 4.2C). However, thinning of these layers was offset by a significant increase in thickness of the inner nuclear layer (INL; $p < 0.001$; Figure 4.2C).

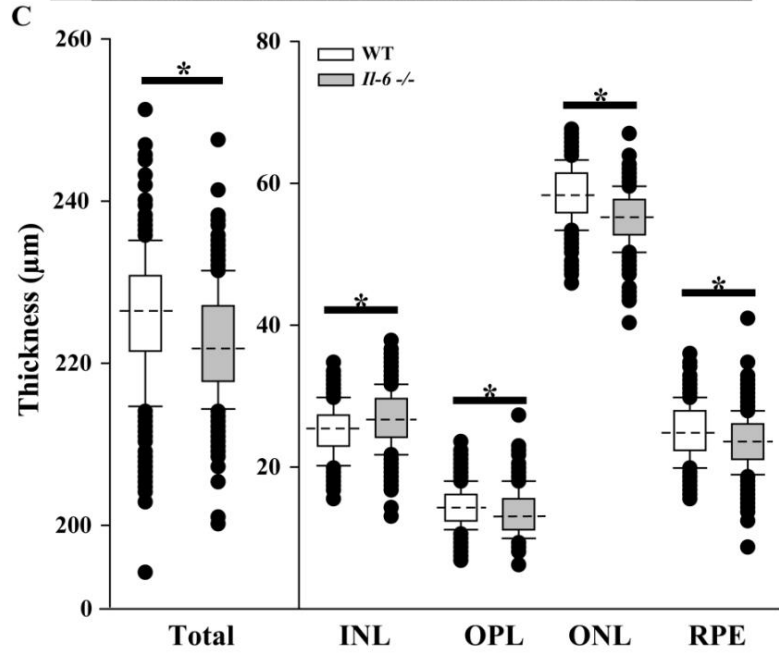
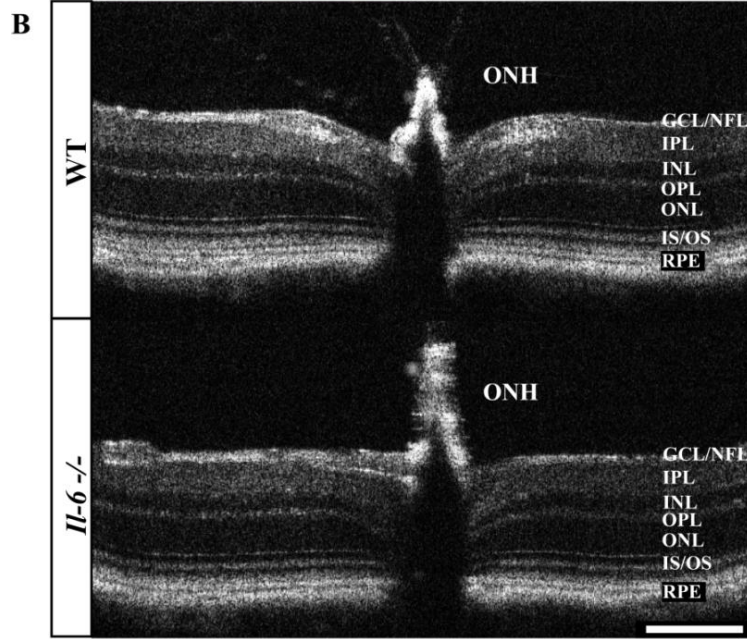
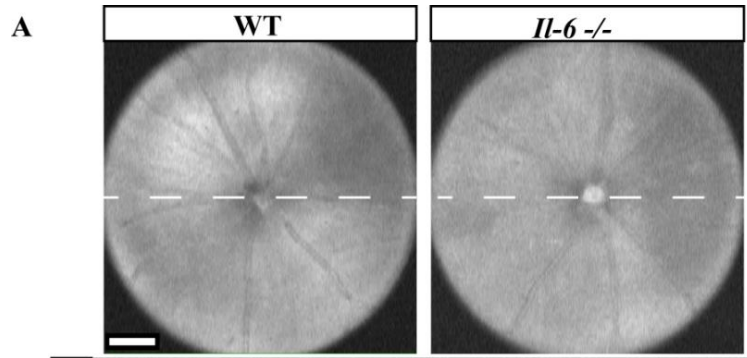


Figure 4.2. IL-6 deficiency does not affect retinal morphology. **(A-B)** Representative images of retinal volumetric scan **(A)** and retinal cross-sections **(B)** obtained by SD-OCT outlying retinal layer morphology in WT and *Il-6*^{-/-} mice (n=25 measurements/retina, 16 retina/genotype). Scale bars= **(A,B)**; 200 μ m. Dashed lines in **(A)** correspond to location of retinal cross sections in **(B)**. **(C)** Box plot of retinal layers (INL, OPL, ONL, RPE) that were significantly different result in a small, yet significant, 2% reduction in total retinal thickness in *Il-6*^{-/-} mice ($p < 0.001$; Mann-Whitney Rank Sum Test). $*=p < 0.001$. Dashed lines in boxplots indicate median value. GCL/NFL; ganglion cell layer/nerve-fiber layer, IPL; inner plexiform layer, INL; inner nuclear layer, OPL; outer plexiform layer, ONL; outer nuclear layer, IS/OS; inner segment/outer segment of the photoreceptors, RPE; retinal pigment epithelium, ONH; optic nerve head.

IL-6 Deficiency Alters the Cortical Response to Light Stimuli

Examination of visual function with flash visual-evoked potentials (FVEP) and optometry revealed that modest changes in retinal morphology noted in *Il-6*^{-/-} mice were accompanied by significant alterations to the N1 depolarization event of FVEP waveform (Figure 4.3B,C). At light intensities of 1.0 (Figure 4.3B) and 5.0 cd.s/m² (Figure 4.3C), the N1 depolarization event of *Il-6*^{-/-} mice was ~20% larger ($p=0.042$ and $p=0.041$; *left*) and ~4-5% delayed ($p=0.03$ and $p=0.024$; *middle*) compared to WT mice. No significant difference in amplitude ($p=0.804$; *left*) and latency ($p=0.337$; *middle*) was noted in the N1 depolarization event at low light intensity (0.01 cd.s/m², Figure 4.3A). Interestingly, there was no change in amplitude or latency of the P1 hyperpolarization event at any light intensity ($p > 0.05$ for all, Figure 4.3A-C; *right*). However, it is important to note that while P1 amplitudes and latencies were unremarkable, *Il-6*^{-/-} waveforms failed to reach baseline WT levels at light intensities of 1.0 and 5.0 cd.s/m² (Figure 4.3B,C). Despite altered F-VEP waveforms, *Il-6*^{-/-} mice exhibited normal visual acuity, as measured by optometry ($p=0.496$, Figure 4.3D).

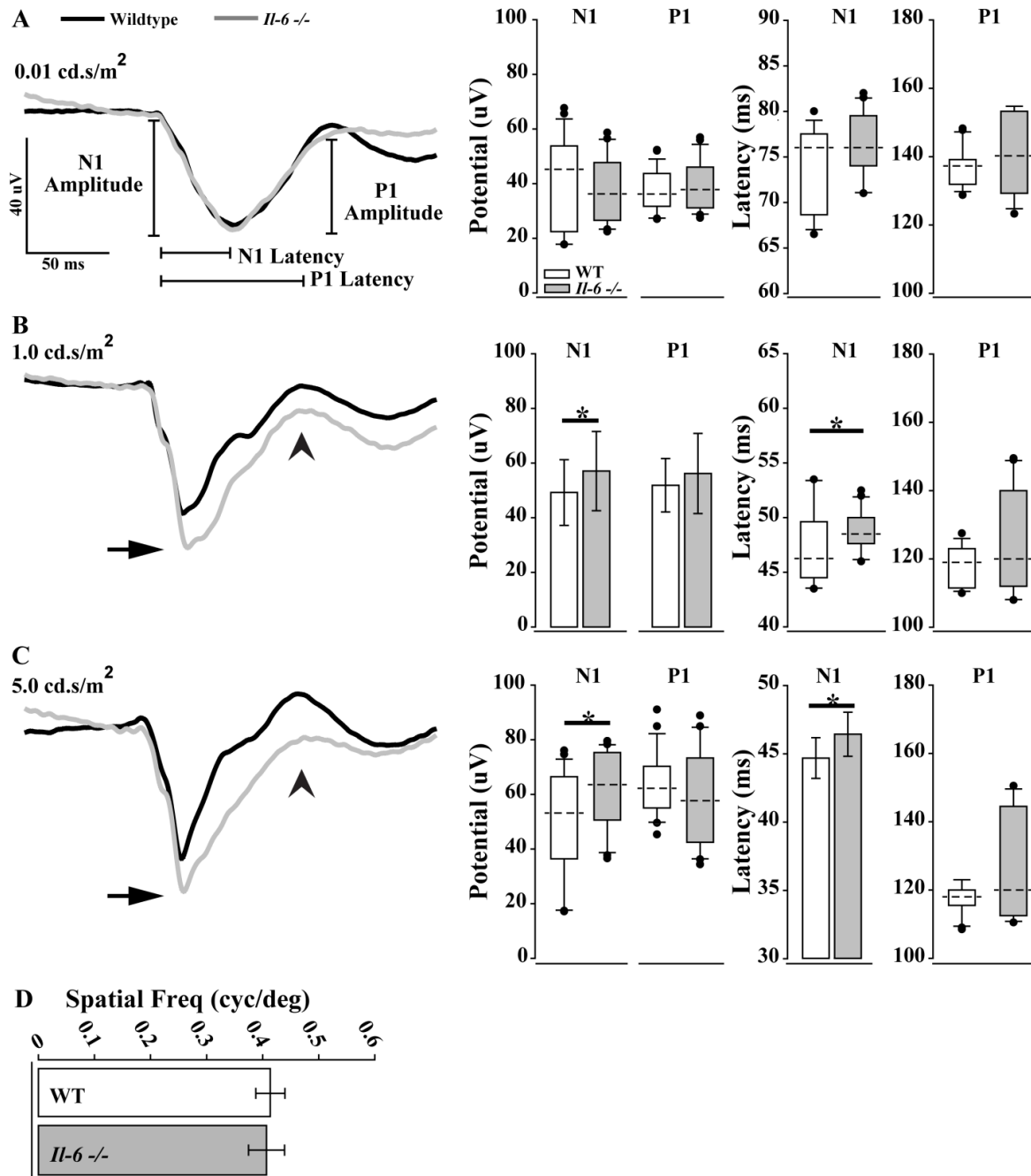


Figure 4.3. *Il-6*^{-/-} mice present with an impaired cortical response to light. (A-C) Flash Visual Evoked Potential (FVEP) responses at light intensities 0.01 (A), 1.0 (B) and 5.0 cd.s/m² (C) in WT and *Il-6*^{-/-} mice (n=12-15 animals/genotype). Waveform (left) and calculated amplitude and latency of waveform components (N1, P1; right) are present for each light intensity. (A) Following a 0.1 cd.s/m² light pulse, no significant differences in N1 or P1 amplitude (N1; $p=0.804$, P1; $p=0.680$, Mann-Whitney Rank Sum Test) or latency (N1; $p=0.337$, P1; $p=0.286$, Mann-Whitney Rank Sum Test) are present. (B) Following a 1.0 cd.s/m² light pulse, a larger and delayed depolarization (N1; arrow) event occurs in *Il-6*^{-/-}, but not WT mice. Additionally, unlike WT mice, the repolarization event (arrow head; P1) does not reach baseline. Quantification of

N1 and P1 amplitude and latency at 1.0 cd.s/m², shows a significant difference in amplitude ($p=0.042$, two-tailed t-test) and latency ($p=0.03$, Mann-Whitney Rank Sum Test). No significant difference at 1.0 cd.s/m² noted for P1 amplitude ($p=0.450$, two-tailed t-test) or latency ($p=0.299$, Mann-Whitney Rank Sum Test). **(C)** At 5.0 cd.s/m², a similar waveform pattern occurs in *Il-6*^{-/-} mice. Quantification of N1 and P1 components show a significant decrease in the N1 amplitude ($p=0.041$, Mann-Whitney Rank Sum Test) and latency ($p=0.024$, two tailed t-test). No significant difference was noted in the P1 amplitude ($p=0.776$, Mann-Whitney Rank Sum Test) or latency ($p=0.091$, Mann-Whitney Rank Sum Test). **(D)** Psycho-visual assessment of visual acuity using the optokinetic reflex test, showed no significant difference in visual acuity between WT and *Il-6*^{-/-} mice ($p=0.496$, two-tailed t-test, (n=8-10 mice/genotype)). $*=p<0.05$. Dashed lines in boxplots indicate median value. Error bars on bar graphs indicate standard deviation.

IL-6 Deficiency Impedes Anterograde Axon Transport

FVEP abnormalities suggest that IL-6 deficiency alters function of the optic projection. In mice, 70-80% of RGC axons in the optic nerve project to the superior colliculus (SC) (Dreher et al., 1985). To determine whether altered FVEP waveforms arose from changes in the physical connectivity of the retina to the superior colliculus, we performed neural tracing in *Il-6*^{-/-} and WT mice, using cholera toxin beta subunit (CTB). CTB is routinely used to trace the RGC projection as well as to measure fast axonal transport (Crish et al., 2010, Abbott et al., 2013, Ward et al., 2014). In WT mice, CTB labeled the majority of the SC 3 days after intravitreal CTB injection (median = 98.131%; Figure 4.4A,C). Interestingly, there was significant variability in the degree of CTB transport noted in *Il-6*^{-/-}, which ranged from almost full transport to only 40% (Figure 4.4B,C). In all cases of transport deficiency, areas of low transport in the SC corresponded to the area surrounding the optic disc representation and spread outward towards the periphery (Figure 4.4B). As a whole, CTB transport to the SC was diminished by ~10% in *Il-6*^{-/-} mice (median = 87.000%), as compared to WT mice ($p=0.014$; Figure 4.4C). Examination of earlier terminations in the optic tract revealed similar deficiencies in CTB transport, suggesting impairment throughout the RGC projection (Figure 4.4C). This impairment

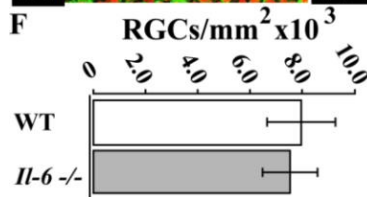
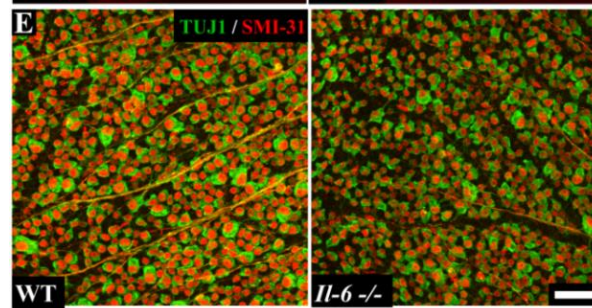
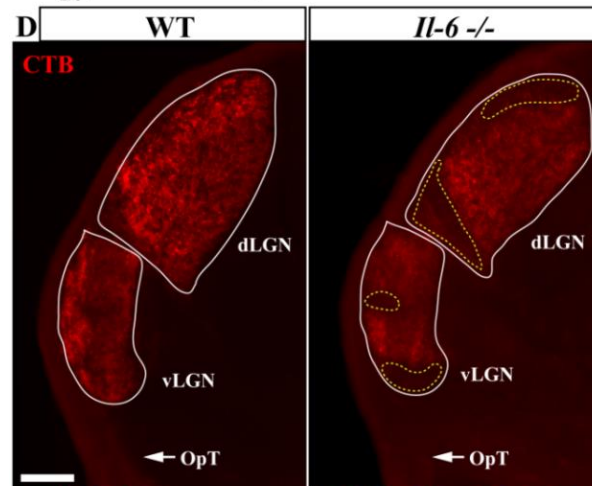
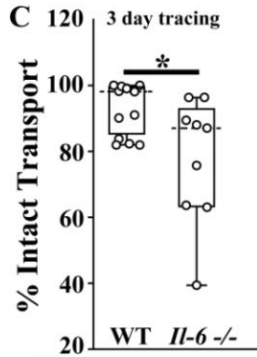
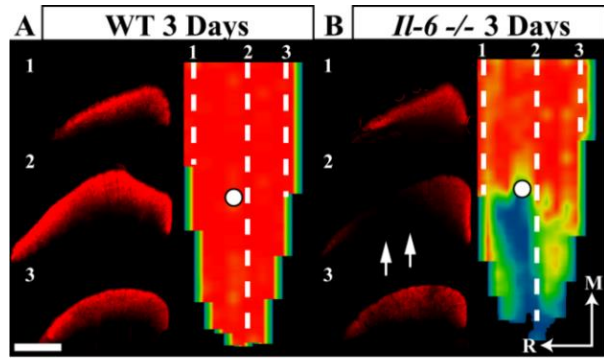


Figure 4.4. *Il-6*^{-/-} mice present with deficiencies in anterograde transport. **(A-B)** Representative coronal sections through the superior colliculus (SC) and respective retinotopic heat maps after 3 days of CTB transport in WT **(A)** and *Il-6*^{-/-} mice **(B)**. Arrows in coronal sections indicate areas of transport deficits. Density of the CTB signal for the heat maps range from 0% (blue) to 50% (green) to 70% (yellow) to 100% (red). Numbered dashed lines in retinotopic maps indicate the location of respective coronal section and white circles indicate position of the optic disk (OD). Medial (M) and rostral (R) orientations are indicated. Scale bars= 500 μ m for all images. **(C)** Quantification of intact transport (\leq 70% Density). *Il-6*^{-/-} mice show a significant reduction of intact transport 3 days after CTB injection when compared to WT mice ($p=0.014$, Mann-Whitney RANK Sum test, $n=9-12$ SC/genotype). **(D)** Anterograde axon transport is also delayed in more rostral areas of the optic projection (dLGN, vLGN) in *Il-6*^{-/-} mice (right) compared to WT mice (left). **(E)** Representative 40X images of dual labeled TUJ1/SMI-31 positive RGCs from mid-central/mid-peripheral retina in WT (left) and *Il-6*^{-/-} (right) mice. **(F)** Quantification of RGC density showed no significant difference between WT and *Il-6*^{-/-} mice ($p=0.284$, two-tailed t-test, $n=5-7$ images/retina, 3 retina/genotype). * $=p<0.05$. Dashed lines in boxplots indicate median value.

was not due to a decreased number of RGCs in the retina. Immunolabeling with beta-tubulin (TUJ1) and neurofilament (SMI-31) confirmed that the distribution RGC soma appeared unremarkable and there was no significant difference in the density of RGCs between *Il-6*^{-/-} and WT mice ($p=0.284$, Figure 4.4D).

To further ascertain the source of transport impairment, we first examined whether the transport impairment reflected a decrease in successful RGC termination in the SC. We examined the spatial distribution and density of $ERR\beta^+$ RGC terminals in the SC and found that, even in areas of CTB deficiency, *Il-6*^{-/-} mice exhibited full innervation of the SC that was comparable to WT mice (Figure 4.5A,B). Next, we determined whether transport impairment was due to abnormalities at the site of uptake in the retina. We examined the distribution and uptake of CTB in RGC soma (Figure 4.5C,D) and assessed the expression profile of caveolin-1 (Cav-1; Figure 4.5D,E), an uptake mediator of CTB. In the retina, CTB uptake and localization to RGC soma was comparable between WT and *Il-6*^{-/-} mice. Additionally, Cav-1 also localized comparably to RGCs in both genotypes, with densitometric quantification of Cav-1 protein

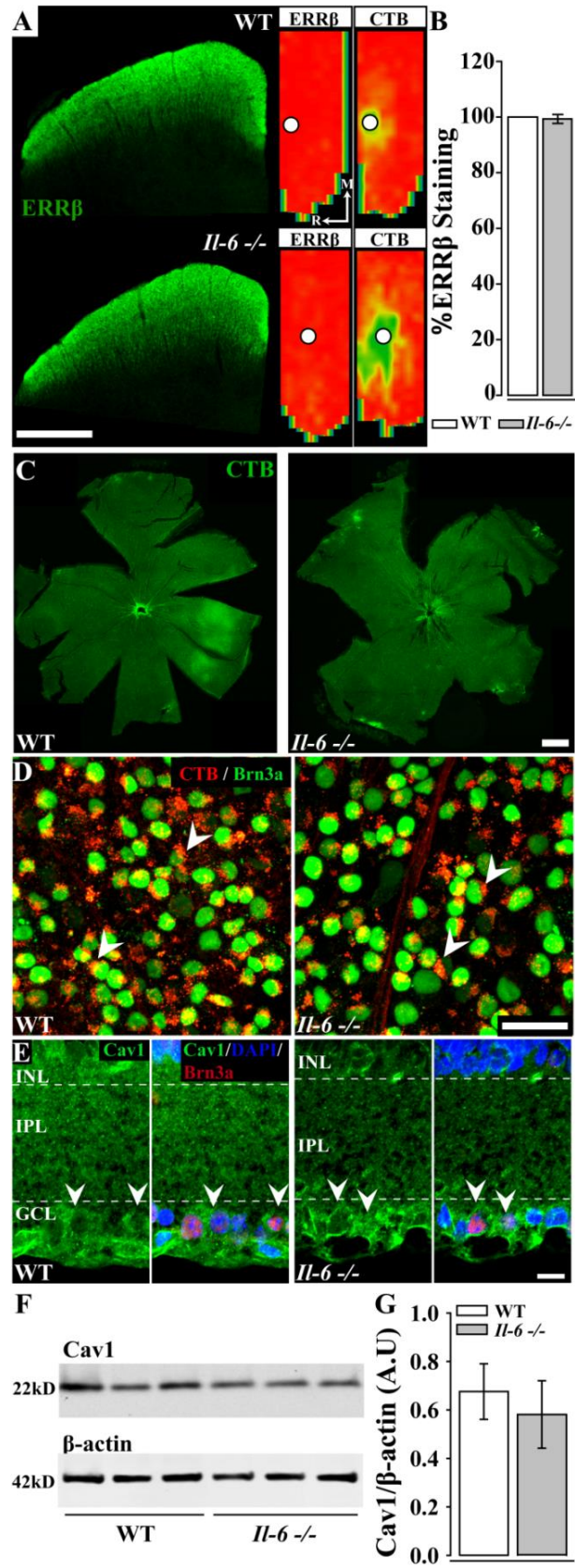


Figure 4.5. Transport deficits not due to impairments in RGC soma of *Il-6*^{-/-} mice. **(A-B)** Representative images of ERRβ localization in the SC **(A)** and quantification of ERRβ signal density **(B)** suggests no alteration in the structure of RGC post-synaptic inputs to the SC between WT and *Il-6*^{-/-} mice. Scale bars= 500μm. **(C)** Representative 10X montaged micrographs of WT (left) and *Il-6*^{-/-} (right) retinas exposed to CTB (green) shows no difference in CTB uptake. Scale bar= 500μm. **(D)** Representative 100X micrographs of retinas exposed to CTB show similar uptake of tracer by Brn3a⁺ (green) RGCs (white arrow heads) in WT (left) and *Il-6*^{-/-} mice (right). Scale bars= 50μm. **(E)** Localization of CTB uptake protein caveolin-1 (Cav-1) to Brn3a⁺ RGC cell bodies (red; arrowheads) in WT and *Il-6*^{-/-} mice. Scale bars= 20μm. **(F-G)** Western blot **(F)** and densitometric quantification of Cav-1 normalized to β-actin **(G)** shows no significant difference between WT (white) and *Il-6*^{-/-} (gray) mice ($p=0.416$, two-tailed t-test, $n=3$ retina/group). Error bars indicate standard deviation.

revealing no significant difference between WT and *Il-6*^{-/-} retina ($p=0.416$, Figure 4.5G).

Finally, we examined whether impairments in CTB transport reflected a decrease in the actual rate of transport. We extended the latency of CTB tracing from 3 days to 5 days. After 5 days, CTB labeling in the SC of *Il-6*^{-/-} mice was comparable to that of WT mice (median= 98.945%, $p=0.671$, Figure 4.6A,B). We confirmed this apparent reduction in the rate of axon transport, using another neural tracer wheat germ agglutinin (WGA). With a tracing latency of 3 days, *Il-6*^{-/-} mice again showed variable (20-90%), yet overall significant, deficiencies in WGA transport compared to WT mice (median values, WT; 94.709% intact transport, 3 Day *Il-6*^{-/-}; 81.381%, $p=0.004$, Figure 4.6C,D,F). As in our CTB transport studies, increasing the tracing latency for WGA to 5 days resolved WGA tracing deficiencies in the SC of *Il-6*^{-/-} mice (median values, WT; 94.709% intact transport, 5 Day *Il-6*^{-/-} 91.589%, $p=0.202$, Figure 4.6C,E,F).

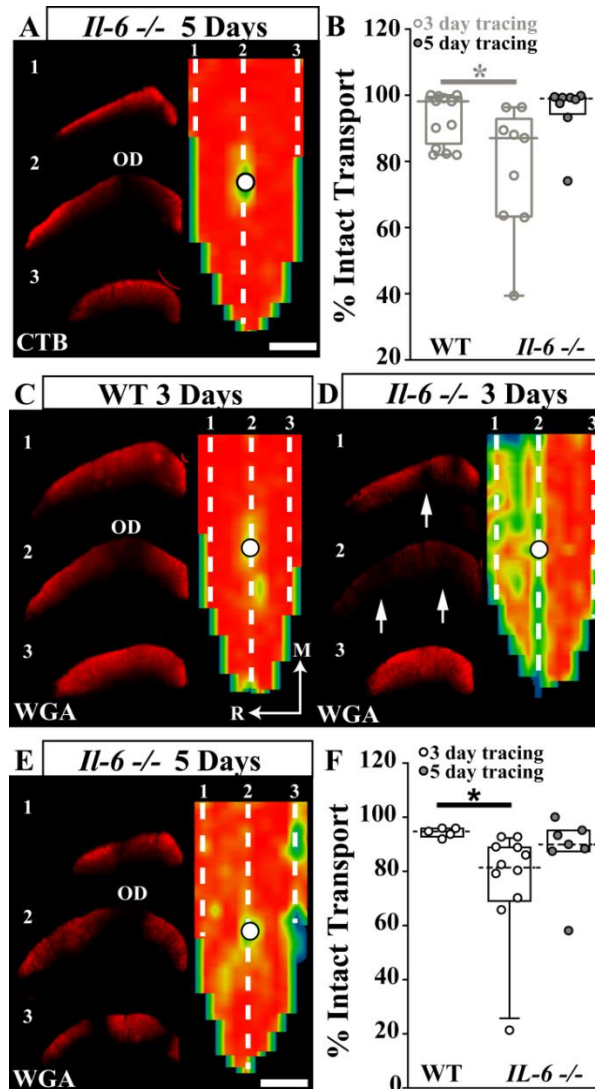


Figure 4.6. Axon transport deficits are due to a delay in axon transport in *Il-6*^{-/-} mice. (A) Representative coronal sections through the SC and respective retinotopic heat maps after 5 days of CTB transport in *Il-6*^{-/-} mice. OD= optic disk. Scale bar= 500 μ m. (B) Quantification of intact transport reveals similar amounts of intact transport 5 days after CTB injection in *Il-6*^{-/-} mice compared to WT mice ($p=0.671$, Mann-Whitney RANK SUM test, $n=8-12$ SC/genotype). Dashed lines in boxplots indicate median value. (C-E) Transport delays not restricted to CTB. Representative coronal sections through the SC and respective retinotopic heat maps after 3 days of WGA transport in WT mice (C) and 3 days (D) and 5 days (E) of WGA transport in *Il-6*^{-/-} mice. Arrows in coronal sections indicate areas of transport deficits. Scale bars= 500 μ m. (F) Quantification of intact transport ($\leq 70\%$ Density) following 3 (white) or 5 (gray) days of WGA injection. Similar significant transport delays in *Il-6*^{-/-} mice are evident after 3 days of WGA transport when compared to WT mice ($p=0.004$, Mann-Whitney RANK Sum test, $n=5-11$ SC/genotype), but similar amounts of intact transport 5 days after WGA injection ($p=0.202$, Mann-Whitney RANK Sum test, $n=5-7$ SC/genotype). $*=p<0.05$. Dashed line in boxplot indicates median value.

IL-6 Deficiency Increases RGC Axon Diameter

Our data thus far suggests that IL-6-related changes in the rate of axon transport are likely localized to the RGC axon. To examine the impact of IL-6 deficiency on RGC axons specifically, we first examined the structural integrity of the optic nerve. Upon dissection, we noted that the optic nerve of *Il-6*^{-/-} mice appeared thinner than that of WT mice, specifically in the proximal portion of the optic nerve (Fig. 4.7A). Measurement of nerve length from the eye to optic chiasm revealed no difference between the two genotypes ($p=0.409$, Figure 4.7B). However, quantification of total nerve area in cross sections of optic nerve revealed that the proximal segment (closer to the globe) was 20% smaller in *Il-6*^{-/-} mice than that is WT mice ($p<0.001$, Figure 4.7C-E; left). The distal segment of the nerve however, did not differ between the two genotypes ($p=0.066$, Figure 4.7C-E; right). Quantification of optic nerve axon number revealed that *Il-6*^{-/-} optic nerves contained ~20% fewer RGC axons in both proximal ($p=0.020$) and distal ($p=0.002$) sections, when compared to WT optic nerves (Figure 4.7F). In the proximal segment of the nerve, this IL-6-related decrease in the number of RGC axons corresponds well to the smaller overall size of the nerve (Figure 4.7E; left). However, the size of the distal segment of the nerve in *Il-6*^{-/-} did not differ from that of WT mice, suggesting that space in the distal nerve is being filled in some other way. As examination of macroglia revealed no obvious differences between genotypes (Figure 4.7C,D; right), we next looked at axon morphology, axon diameter, myelin thickness and g-ratio in cross-sections of the distal optic nerve.

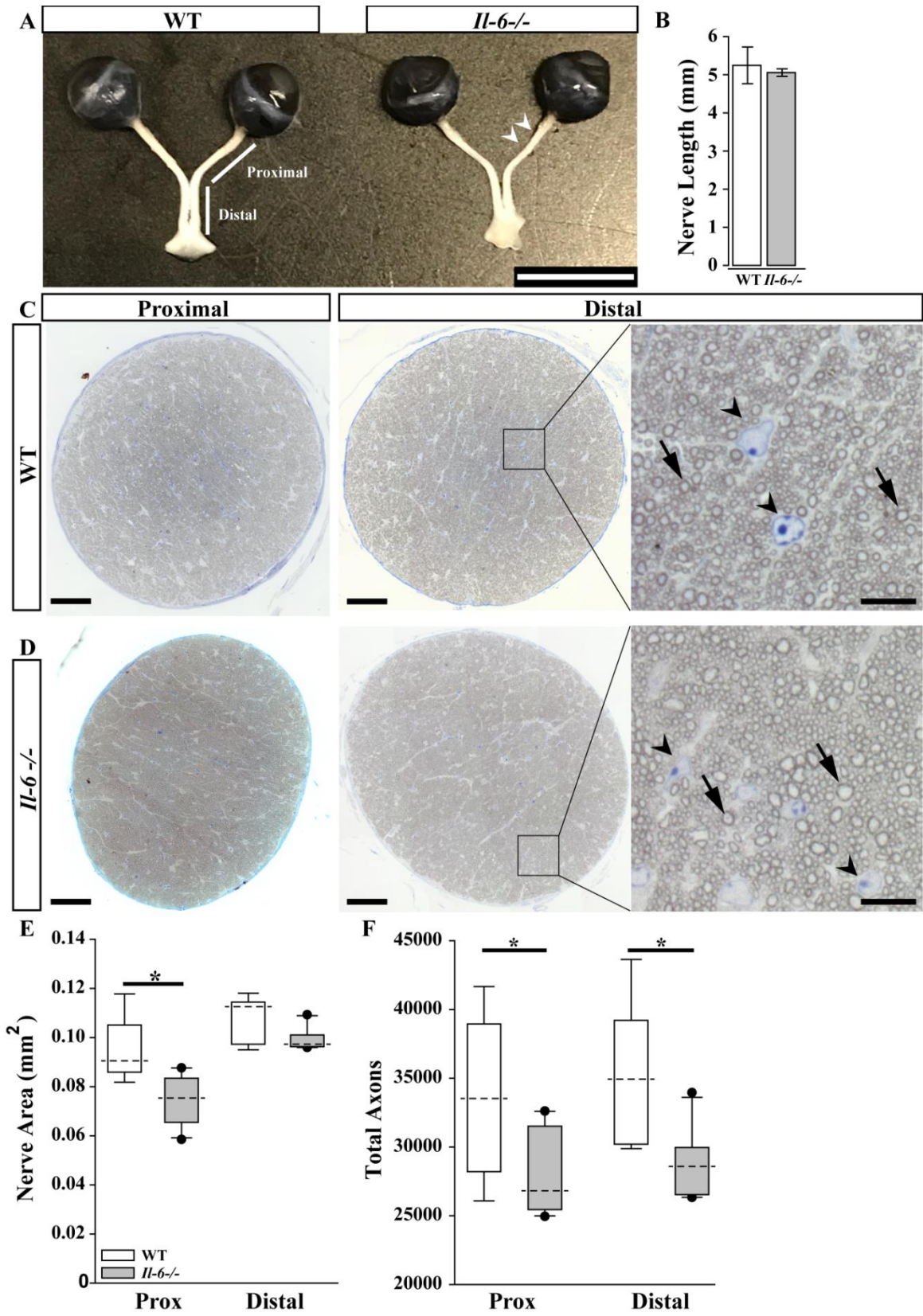


Figure 4.7. *Il-6*^{-/-} mice have fewer RGC axons. **(A)** Representative optic nerves from WT (left) and *Il-6*^{-/-} (right) mice show no gross defects besides a slight thinning in the proximal portion (arrow heads) of the optic nerve in *Il-6*^{-/-} mice. Scale bar= 5mm. **(B)** Quantification of optic nerve length reveals no significant difference between genotypes ($p=0.409$, two tailed t-test, $n=5-8$ nerves/genotype). Error bars indicate standard deviation. **(C-D)** Representative 10X montaged images of proximal (left) and distal (right) optic nerve sections from WT **(C)** and *Il-6*^{-/-} **(D)** mice. Scale bar= 50 μ m. Proximal and distal designation noted in A. Boxed regions were enlarged to highlight individual glial (arrow heads) and axon (arrows) morphology. Scale bars= 10 μ m. **(E)** Quantification of optic nerve cross-section area shows a significant decrease in proximal ($p<0.001$, Mann-Whitney Rank Sum test), but not distal ($p=0.066$, Mann-Whitney Rank Sum test) portions of optic nerve in *Il-6*^{-/-} mice compared to WT mice ($n=9-10$ nerves/genotype). **(F)** Quantification of total axons reveals *Il-6*^{-/-} mice have fewer axons in both the proximal ($p=0.020$, Mann-Whitney Rank Sum test) and distal ($p=0.002$, Mann-Whitney Rank Sum test) portions of the optic nerve compared to WT ($n=9-10$ nerves/genotype). $*=p<0.05$. Dashed line in boxplots indicates median value.

RGC axons in *Il-6*^{-/-} optic nerve had a larger overall diameter (Dt) compared to WT optic nerve ($p<0.001$, Figure 4.8A,B). This increase in size was due to both a significant increase in inner axonal diameter (Di) ($p<0.001$, Figure 4.8A,C) and myelin thickness ($p<0.001$, Figure 4.8A,D). The corresponding increases in inner axon diameter and myelin thickness maintained a g-ratio (Di/Dt) of 0.627 μ m in *Il-6*^{-/-} optic nerve, which did not differ from that measured in WT optic nerve (0.621 μ m, $p=0.356$, Figure 4.8A,E). That the extent of myelination did not differ between the two genotypes was further confirmed by plotting total axon diameter against inner axon diameter (Figure 4.8E). The scatter plot revealed the *Il-6*^{-/-} axon population is shifted to the right of the WT population. However, the slopes (g-ratio) of the two populations are similar (Figure 4.8E).

A

Dt: Total Axon Diam
Di: Inner Axon Diam
Myelin Thickness:
 $(Dt-Di)/2$
gRatio: Di/Dt

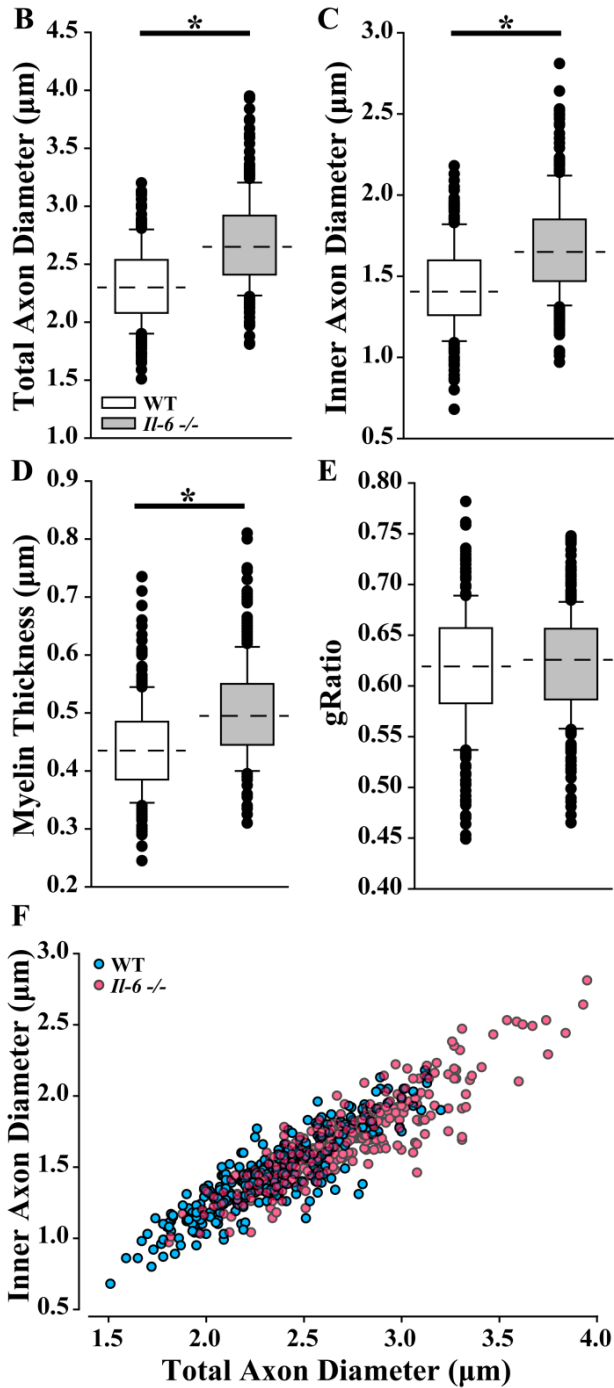
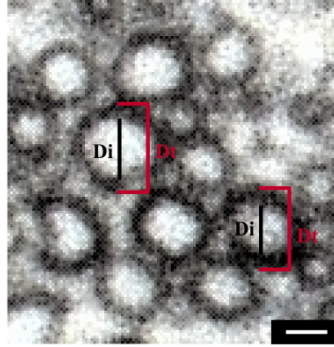


Figure 4.8. *Il-6*^{-/-} mice have larger axons. (A) Diagram describing how total axon diameter and inner axon diameter were measured and how myelin thickness and gRatio were calculated. Scale bar= 1µm. (B) Quantification of total axon diameter shows *Il-6*^{-/-} mice have significantly larger axons than WT mice ($p<0.001$, Mann-Whitney RANK Sum Test, n=300 axons/genotype). (C-D) Increase in axon size is attributed to both a larger inner axon diameter (C; $p<0.001$, Mann-Whitney RANK Sum Test) and a thicker myelin sheath (D; $p<0.001$, Mann-Whitney RANK Sum Test). (E) Despite, the overall increase in axon size, optic nerve axon g-ratio (inner axon thickness/total axon thickness) was similar between WT and *Il-6*^{-/-} mice ($p=0.356$, Mann-Whitney RANK Sum Test). (F) Plots of the total axon diameter (axon + myelin sheath) against inner axon diameter (axon) for WT (blue) and *Il-6*^{-/-} (pink) optic nerves. The slopes of the populations, which represent g-ratio, were similar. $*=p<0.001$. Dashed line in boxplots indicates median value.

IL-6 Deficiency Alters Microtubule Arrangement in RGC Axons

To determine whether enlargement of RGC axons could be related to delayed axon transport, we examined the cytoarchitecture of RGC axons. CTB and WGA are transported in anterograde and retrograde fashions through the microtubule network of axons (Kobbert et al., 2000, Abbott et al., 2013). Microtubules are composed of α - and β - subunits of tubulin along with a variety of microtubule associated proteins (MAPs), such as tau (Desai and Mitchison, 1997). In contrast, actin and neurofilaments contribute to the architecture of the axon, but are not directly related to axon transport. Therefore, we examined the arrangement of microtubules, neurofilaments and actin in the unmyelinated segment of RGC axons in WT and *Il-6*^{-/-} mice. We found that, in WT mice, immunolabeling against neuronal specific β -tubulin III (TUJ1) exhibited a compact, linear pattern parallel with the trajectory of the axon in both peripheral (top panel) and central regions (middle/bottom panels) of the retina (Figure 4.9A). However, in *Il-6*^{-/-} mice, β -Tubulin labeling exhibited a zig-zag appearance with evidence of clump-like aggregations (Figure 4.9B). This observation was corroborated by a similar aggregation pattern of MAP tau, a microtubule-associated protein (Figure 4.9C,D).

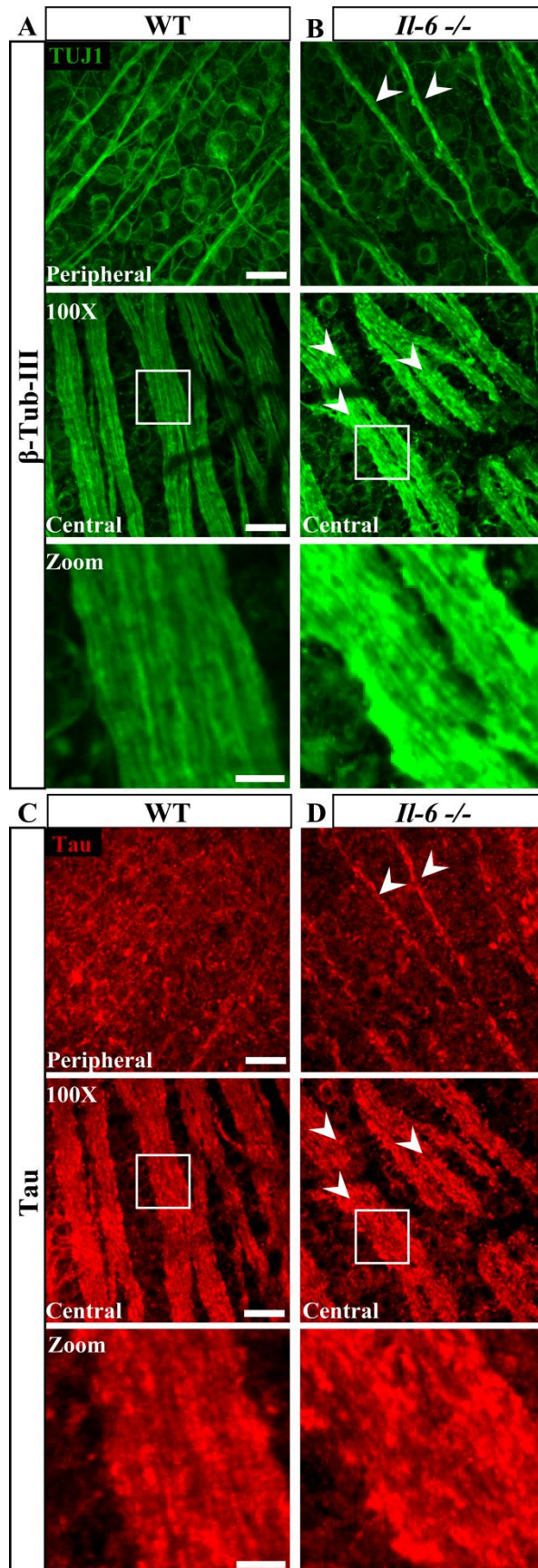


Fig 4.9. *Il-6*^{-/-} mice contain disorganized microtubules in retina. **(A-B)** Representative 100X confocal images of β -Tubulin (TUJ1; green) from WT **(A)** and *Il-6*^{-/-} **(B)** un-myelinated axons in the peripheral (top) and central (middle) retina. β -Tubulin in axons from *Il-6*^{-/-} mice presents with an aggregated appearance (arrowheads), unlike the linear morphology present in axons from WT mice. Scale bars= 20 μ m. **(C-D)** Representative 100X confocal images of microtubule associated protein Tau (red) from WT **(C)** and *Il-6*^{-/-} **(D)** mice. Similar to β -Tubulin, the appearance appears aggregated in axons of *Il-6*^{-/-} mice compared to WT mice (arrowheads). Scale bars= 20 μ m. Boxed regions were zoomed to highlight aggregations.

IL-6-related disorganization of the axon cytoskeleton appeared specific to microtubules as labeling against actin (Figure 4.10A) and phosphorylated heavy neurofilament (pNF-H; (Figure 4.10B) revealed a comparable linear architecture in RGC axons from both WT and *Il-6*^{-/-} mice.

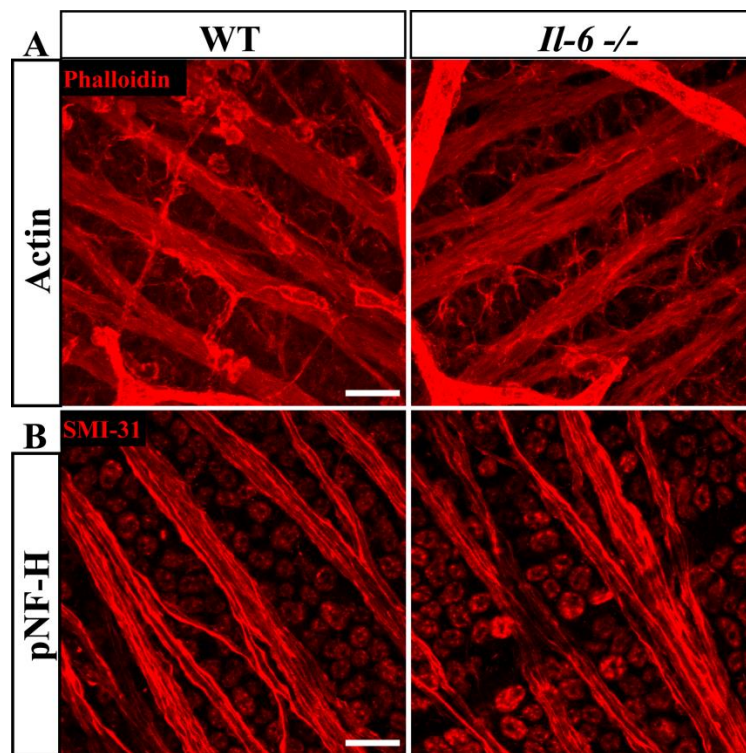


Figure 4.10. Cytoskeletal abnormalities in *Il-6*^{-/-} mice are restricted to microtubules. **(A-B)** Representative 100X confocal images of **(A)** Actin and **(B)** phosphorylated neurofilament heavy (pNF-H) localization in axons from WT and *Il-6*^{-/-} mice. Both WT and *Il-6*^{-/-} mice show a similar linear morphology of both Actin (phalloidin) and pNF-H (SMI-31) in un-myelinated RGC axons. Scale bars= 20 μ m.

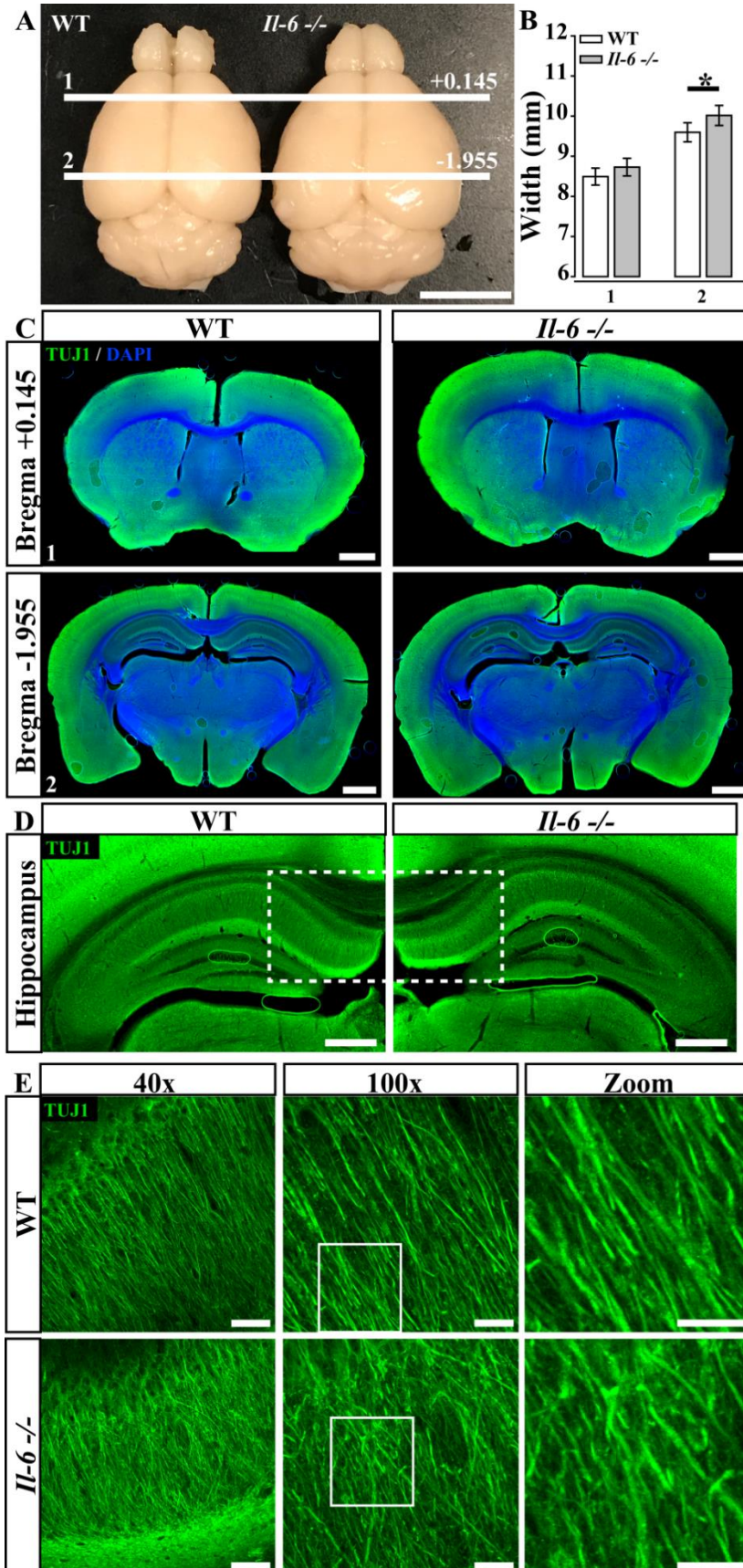


Figure 4.11. Microtubule abnormalities also occur in hippocampus of *Il-6*^{-/-} mice. **(A)** Representative examples of whole brains from WT and *Il-6*^{-/-} mice depict a slight enlargement in brain size. **(B)** Quantification of brain width at two locations (solid lines in A; Line 1: 0.145mm rostral of Bregma, Line 2: 1.955mm caudal of Bregma) show a significant increase in brain width at 1.955mm rostral of Bregma in *Il-6*^{-/-} mice ($p=0.008$, two-tailed t-test, $n=8-9$ /genotype). Scale bar= 5mm. **(C)** Representative 4X montages of WT (left) and *Il-6*^{-/-} (right) brain sections labeled for β -Tubulin (TUJ1; green) at Bregma coordinates mentioned above. Scale bar= 1mm. **(D)** Blow up of hippocampi of WT (left) and *Il-6*^{-/-} (right) mice. Scale bar= 500 μ m. **(E)** Representative 40X (far left) and 100X (middle) confocal images of pyramidal cell axon morphology in the CA1 region (boxed region in D) of the hippocampus shows disorganization of pyramidal cell axons in *Il-6*^{-/-} mice (bottom) compared to WT mice (top). Zoomed in regions from 100X images (far right) highlight disorganization. Scale bars= 50 μ m (40X), 20 μ m (100X and Zoom).

To determine whether microtubule disorganization was specific to the retina, we examined overall morphology and beta-tubulin labeling in coronal sections of brain from *Il-6*^{-/-} and WT mice. We found that the brain of *Il-6*^{-/-} mice generally appeared broader than that of WT mice, particularly towards the center of the brain (Figure 4.11A). Quantification of brain width at a rostral (Bregma +0.196mm) and central (Bregma -1.995mm) location, confirmed this increase in central (2, $p=0.008$; Figure 4.11B), but not rostral areas (1, $p=0.065$; Figure 4.11B). Examination of beta-tubulin labeling at low magnification revealed more robust labeling in *Il-6*^{-/-} mice than WT, with pockets of high intensity labeling scattered through structures (Figure 4.11C). Interestingly, the aggregated appearance of β -tubulin III was specific to the retina. Examination of pyramidal cell axons in the CA1 region of the hippocampus in *Il-6*^{-/-} mice did not reveal aggregations of tubulin, but did show disorganization compared to WT pyramidal cell axons (Figure 4.11D,E).

Acute Exposure to IL-6 Influences Tubulin Arrangement and Fast Axon Transport

The *Il-6*^{-/-} mice utilized in our studies is a germline deficiency and thus, impacts IL-6 activities both in development and maturity. To examine whether the axon transport and microtubule phenotypes noted in *Il-6*^{-/-} mice arise from developmental or mature activities, we provided short-term replacement of recombinant IL-6 in adult *Il-6*^{-/-} mice and examined axon transport and microtubule staining. *Il-6*^{-/-} mice received a single injection of recombinant IL-6 (rIL-6; 500ng) or equal volume of 0.1% BSA in the vitreal cavity 24 hours prior to CTB injection. Similar to naïve experiments, BSA-treated *Il-6*^{-/-} mice exhibited impaired transport of CTB to the SC after 3 days (median= 77.359%) that resolved when the tracing latency was increased to 5 days (median= 95.868%, $p=0.003$, Figure 4.12A). Pre-treatment with rIL-6 in *Il-6*^{-/-} mice significantly increased transport facility with a tracing latency of 3 days (median= 91.875%; $p=0.024$; Figure 4.12A). However, transport facility achieved following 3 days tracing latency and IL-6 treatment did not quite reach that observed with a latency of 5 days in BSA-treated mice ($p=0.039$; Figure 4.12A). Examination of tubulin microstructure revealed that *Il-6*^{-/-} mice receiving either BSA (Figure 4.12B) or rIL-6 (Figure 4.12C) appeared to have an improved tubulin microstructure regardless of the quantity of intact SC transport.

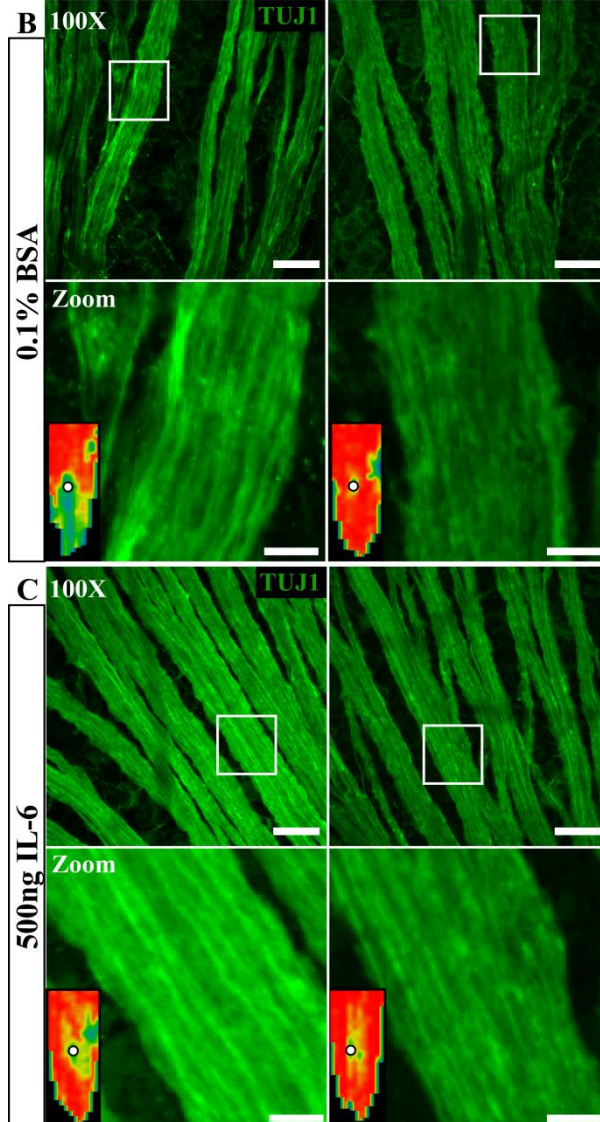
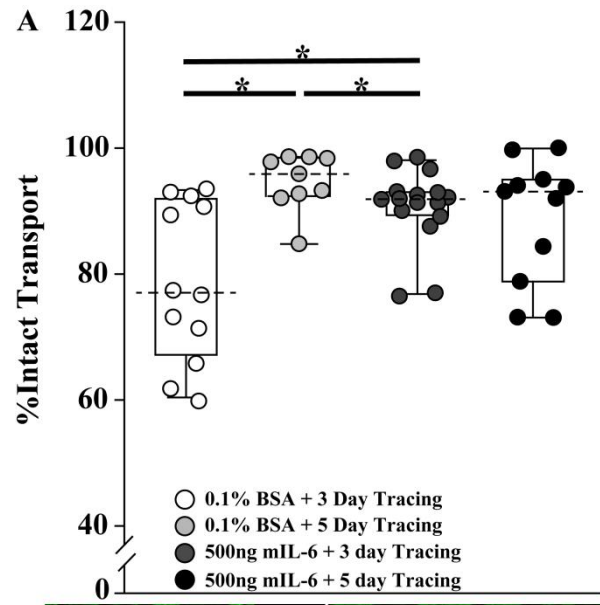


Figure 4.12. Transport latencies in *Il-6*^{-/-} mice improve with recombinant IL-6. **(A)** Boxplots of % intact transport of 3 or 5 day CTB tracing from *Il-6*^{-/-} mice receiving an intravitreal injection of 500ng of recombinant murine IL-6 or equal volume 0.1% BSA 24 hours before CTB injection. Intravitreal injection of IL-6 24 hours before CTB injection significantly improved anterograde transport in *Il-6*^{-/-} mice after 3 days of tracing compared to *Il-6*^{-/-} mice with intravitreal injections of 0.1% BSA ($p=0.024$, Mann-Whitney RANK Sum Test, $n=12-16$ SC/group). Similar to naïve studies, 5 days of CTB tracing led to significantly improved RGC to SC tracing compared to 3 days in *Il-6*^{-/-} mice injected with 0.1% BSA ($p=0.003$, Mann-Whitney RANK Sum Test, $n=11-12$ SC/group). Dashed lines in boxplots indicate median value. **(B-C)** Representative 100X confocal images of β -Tubulin and corresponding contralateral 3 day CTB transport map in *Il-6*^{-/-} retinas following injection of BSA **(B)** or 500ng of IL-6 **(C)**. After BSA or IL-6 injection tubulin abnormalities improve in *Il-6*^{-/-} mice, regardless of intact transport. Zoomed in regions from 100X images (bottom) show tubulin improvement. Dashed line in boxplots indicates median value. Scale bars= 20 μ m. $*=p<0.05$.

Discussion

Cytokine signaling in the CNS, particularly IL-6 signaling, is normally discussed in the context of neuroinflammation and its effect on neurodegeneration. However, there is increasing evidence that IL-6, along with other gp130 cytokines, is instrumental in proper development and maintenance of neurons and glia within the CNS. Here, we show evidence that IL-6 is constitutively expressed by RGCs throughout postnatal development into adulthood, suggesting a potential relevance for IL-6 signaling in the development of the optic projection (Figure 4.1). IL-6 expression from neurons is reported in other neuronal populations. In the healthy CNS expression is thought to be initiated by Ca^{2+} influx caused by membrane depolarization or glutamate activation of NMDA receptors. As RGCs are constantly depolarizing in response to light mediated glutamatergic signaling, it is possible that IL-6 production in RGCs is facilitated in a similar fashion. To follow up on this observation, we utilized *Il-6*^{-/-} mice to ascertain functional and structural consequences of IL-6 deficiency, specifically in RGCs, throughout development. From our data, we found evidence of rather discreet abnormalities that are centered upon RGC function and axon development in response to IL-6 deficiency. Altogether, this data provides the first evidence implicating IL-6 signaling in the development of the optic projection.

In vivo assessment of the retina using SD-OCT suggests that IL-6 deficiency leads to a slight, yet significant decrease in overall retinal thickness (Figure 4.2). However, IL-6 deficiency does not greatly impact overall structure and morphology of the retina, including that of the GCL where RGCs reside. Significant differences in specific retinal layers included decreases in RPE, ONL, OPL and increases in the INL. The significant decrease in the former suggests a reduction in photoreceptors while an increase in the latter suggests a larger population of bipolar, horizontal and amacrine cells. While further studies are needed to confirm this finding, genetic

ablation of fellow gp130 cytokines CNTF and LIF also alters photoreceptor and bipolar development (Rhee and Yang, 2010)

Interestingly, these structural changes in the retina were coupled with abnormalities in the cortical response to light at certain intensities as measured by FVEPs. The FVEP waveform represents a summed potential of cortical response along the early visual pathway (Ridder and Nusinowitz, 2006). Based on studies in multiple sclerosis, the amplitude and latency of the N1/P1 components constitutes the strength and speed of the light response as it travels through the optic projection (You et al., 2011, You et al., 2012). Assessment of the FVEP waveform in *Il-6*^{-/-} mice revealed an increase in the amplitude and latency of the N1 component at light intensities of 1.0 and 5.0 cd.s/m² (Figure 4.3B,C), but not 0.01 cd.s/m² (Figure 4.3A). This suggests that IL-6 deficiency results in a stronger electrophysiological response along the optic projection (increased N1 amplitude) that travels poorly along the optic projection (increased N1 latency) at higher light intensities. While additional experiments are needed to elucidate the mechanisms behind these differences, evidence from the literature and our data can provide a preliminary hypothesis for these observations. For example, the increase in amplitude of the N1 component seen in the higher light intensities is likely attributed to differences in cone photoreceptor mediated activation of RGCs, as they become sensitive to light intensities above 0.01 cd.s/m² (Heiduschka et al., 2010b). Therefore, the increase seen in *Il-6*^{-/-} mice may be due to a higher population of cones within the retina. In regards to the observed increases in latency of the N1 component, insufficient myelination of axons is thought to contribute to delays in N1 latency (You et al., 2011). This, coupled with *in vitro* reports showing that IL-6 signaling is involved with oligodendrocyte differentiation and gene expression involved with myelin production (Valerio et al., 2002, Zhang et al., 2006, Zhang et al., 2007), indicates that loss of IL-

6 may lead to deficiencies in RGC axon myelination. Interestingly, our data actually suggests that myelinated axons in *Il-6*^{-/-} mice have increased myelin thickness (Figure 4.8D). However, we also noted a 20% decrease in the amount of myelinated axons in our *Il-6*^{-/-} mice (Figure 4.7F). While this might be interpreted as a 20% decrease in all axons with the *Il-6*^{-/-} optic nerve, our investigation of optic nerve axons utilized PPD-stained semi-thin sections and light microscopy, which only allows assessment of myelinated axons. Therefore, it is possible that these absent axons in *Il-6*^{-/-} mice are indeed unmyelinated axons, which would account for the N1 latency delays observed in the *Il-6*^{-/-} FVEP waveform.

In addition to the abnormalities seen in the F-VEP, we found that *Il-6*^{-/-} mice exhibited a 15-20% deficit in fast anterograde axonal transport three days after CTB/WGA injection, which is a significant tracing deficit compared to WT mice (Figure 4.4A-D). These deficits were not accompanied with decreases in RGC number (Figure 4.4E-F), deficits in projection terminals (Figure 4.5A) or tracer uptake (Figure 4.5C-G) suggesting capacity of transport was not affected. Instead, our data suggests that IL-6 influences the rate of axon transport as transport deficits of CTB and WGA were resolved following 5 days of tracing. Interestingly, this increase in tracing latency was accompanied by structural abnormalities in the RGC axons. In the myelinated portion, we found fewer, but larger RGC axons (Figure 4.7, Figure 4.8). In glaucoma, enlargement of the axon is an early sign of degeneration, caused by accumulation of cytoskeletal components, specifically phosphorylated neurofilaments (Cooper et. al., 2016). While we did not note any differences in actin or neurofilament cytoskeletal proteins (Figure 4.10), we did note disorganization of microtubule components β -Tubulin and tau (Figure 4.9). Interestingly, these abnormalities associated with microtubules were not restricted to the retina as disorganization was also noted in β -Tubulin positive axons in the hippocampus (Figure 4.11), a region where

previous studies show an important role for IL-6 signaling. Microtubules are composed of α - and β - subunits of tubulin and utilize a variety of microtubule associated proteins (MAPs), such as tau for stabilization (Desai and Mitchison, 1997). Given the association between microtubules and axon transport, it is likely that retardation of fast axon transport and microtubule disorganization in *Il-6*^{-/-} mice are related as the identity and physical characteristics of proteins in the axoplasm are known to influence axoplasm resistance (Sabry et al., 1995).

While IL-6 and BSA treatment both improved microtubule organization in *Il-6*^{-/-} mice (Figure 4.12B,C), only rIL-6 treatment influenced the rate of axon transport (Figure 4.12A). Interestingly, changes in microtubule organization were more consistent than those in the rate of axon transport. While this result suggests that the microtubule abnormalities are not directly responsible for the increase in axon transport latency, the improvement in transport latency following IL-6 treatment argues that these effects are specific to IL-6 deficiency.

Together, our structural and functional analyses in WT and *Il-6*^{-/-} mice depict an axis of IL-6 signaling not involved in an injury response, but revolves around RGCs, particularly the development of RGC axons. While our studies describe novel functions of IL-6 in the early visual pathway and strongly implicate IL-6 as an important mediator of RGC axon function, we utilized global IL-6 deficient mice from homozygous breeding. Thus, our findings are solely in the context of how IL-6 deficiency primarily affects development of the early visual system. This is important as IL-6 shares the signal transduction receptor gp130 with other IL-6 family members and therefore, compensatory mechanisms from other IL-6 family members are possible. To avoid potential confounds from compensatory gp130 signaling during development and to delineate between development and maintenance functions of IL-6 in retina, further studies using temporal and perhaps, cell type-specific control of IL-6 deficiency are needed.

CHAPTER 5

Summary

Purpose of Studies

The objective of these studies was to ascertain how the pleiotropic cytokine interleukin-6 (IL-6) affects RGCs during conditions of homeostasis and glaucoma-related neurodegeneration. Prior experiments conducted by our laboratory and others showed that IL-6 signaling is relevant to glaucomatous pathology and that it influences RGC survival in response to elevated hydrostatic pressure *in vitro*. These studies, coupled with other reports showing IL-6 mediated CNS degeneration and nervous system defects in IL-6 deficient mice led us to our hypothesis that IL-6 has opposing roles in the healthy and compromised optic projection. Specifically, we proposed that in response to a chronic stressor (i.e. elevated IOP) IL-6 promotes RGC degeneration. However, constitutive IL-6 signaling is required for proper development and function of the optic projection. This hypothesis was addressed using these three specific aims:

Aim 1. Establish the expression profile for IL-6 machinery in response to glaucoma-related stressors.

Aim 2. Determine whether IL-6 influences RGC degeneration caused by ocular hypertension.

Aim 3. Identify structural and functional outcomes of constitutive IL-6 signaling in the naïve optic projection.

Aim 1: Outcome and Future Directions

Establishing the expression profile for IL-6 machinery in response to glaucoma-related stressors.

IL-6 signaling is characterized by the isoform of the IL-6R α . Classical signaling utilizes mIL-6R α while trans-signaling utilizes sIL-6R α (Scheller et al., 2011a). Studies in the CNS and other organ systems suggest that trans-signaling is associated with pathogenic IL-6 signaling, while classical signaling is involved in maintaining homeostasis (Scheller et al., 2011a, Rothaug et al., 2016). Examining how glaucoma-related stressors alter the IL-6R α isoform allowed us to better understand the form of IL-6 signaling utilized in response to age and age-dependent increases in IOP. As expected, retina from aging (8mo) DBA/2J mice presented with elevations in sIL-6R α compared to young (4mo) DBA/2J mice. Interestingly, this was also seen in aged-matched C57 controls, suggesting normal aging is sufficient to induce production of the sIL-6R α isoform. Gp130 protein was elevated in aged C57 retina compared to young C57 retina. However, no change was seen between young and aged DBA/2J mice, suggesting IOP elevation affects age-dependent gp130 elevation.

In the retina, histological assessment showed that the mIL-6R α and sIL-6R α isoforms and gp130 localized to RGCs in both young and aging DBA/2J retina. Consistent with the biochemical data in total retina, sIL-6R α was more prevalent in RGCs from aged DBA/2J mice, while no change was observed in gp130. As expected, CTB uptake from RGCs was compromised in aged DBA2/J compared to young DBA/2J, indicative of poor RGC health. Our correlation analysis revealed that sIL-6R α is localized primarily to compromised RGCs in aging DBA/2J mice. Interestingly, no correlation between gp130 intensity and CTB intensity was present, suggesting gp130 expression does not reliably predict RGC integrity and sensitivity to

IL-6 signaling in the DBA/2J model of glaucoma is primarily facilitated by sIL-6R α production. As sIL-6R α is attributed to the pathogenic arm of IL-6 signaling known as trans-signaling, these results provide support to our hypothesis that IL-6 is detrimental to RGC pathology.

Aim 1: Future Directions

Future directions for this aim would involve experiments that elucidate 1) the concentration and localization of sIL-6R α later in DBA/2J glaucoma pathology 2) the mechanism behind sIL-6R α production, and 3) downstream targets of IL-6 trans-signaling. First, it would be interesting to determine whether sIL-6R α concentration continues to be elevated during later stages of the disease. While our aged time-point (7-8 mo) coincides with onset of RGC dysfunction and transport deficits, significant axon pathology doesn't occur until close to 12 months of age, with RGC loss occurring later (Buckingham et al., 2008, Crish et al., 2010). Therefore, it would be of interest to see not only how sIL-6R α expression and localization is affected at these time points, but whether sIL-6R α concentration correlates to the severity of axon degeneration and RGC loss seen at these time points. This would further validate our hypothesis that IL-6 trans-signaling is involved in glaucomatous pathology.

Second, it would be important to determine the source of sIL-6R α and mechanisms behind sIL-6R α production in DBA/2J glaucoma. While these data and others show IL-6R α expression from RGCs, studies also report IL-6R α within microglia and astrocytes elsewhere in the CNS (Erta et al., 2012). Therefore, future experiments would entail using immunohistochemistry or flow cytometry to determine whether glial cells within the retina also express IL-6R α . A follow up experiment using primary cell culture, would be to determine which cell type(s) are responsible for sIL-6R α cleavage. In terms of mechanism, it is currently

accepted that the matrix metalloproteases, ADAM10 and ADAM17, are responsible for facilitating sIL-6R α cleavage from mIL-6R α in the mouse (Scheller et al., 2011a, Rothaug et al., 2016). However, it is unknown whether expression or activation of ADAM10/17 is altered by glaucoma- related stressors. Correlating ADAM10/17 expression/ activation to sIL-6R α concentration would corroborate its role in sIL-6R α production in response to glaucoma specific stressors. Lastly, our data shows that normal aging and aging accompanied by IOP elevation leads to increased sIL-6R α production. However, it is unknown whether IOP elevation alone is sufficient to elevate sIL-6R α . Using the *in vivo* microbead occlusion model or the *in vitro* hydrostatic pressure chamber model, we can determine whether sIL-6R α elevation also occurs in response to age-independent increases in IOP elevation using the biochemical and histological assays utilized in our study.

Finally, it would be beneficial to determine potential differences in the downstream targets for IL-6 classical and trans-signaling, as it would elevate our understanding on whether classical and trans-signaling lead to different survival outcomes. By adding soluble gp130 into the system, which blocks trans-signaling but not classical signaling, we can compare differences in signal transduction cascade activation and subsequent gene expression associated with cellular integrity between the two signaling mechanisms.

Aim 2: Outcome and Future Directions

Determine whether IL-6 influences RGC degeneration caused by ocular hypertension.

Based on our knowledge that glaucoma related stressors lead to increases in IL-6 and that sIL-6R α localizes to compromised RGCs, we wanted to examine whether IL-6 signaling influences measures of RGC axonopathy. To determine the impact of all forms of IL-6 signaling on RGC axonopathy, we induced ocular hypertension for 8 weeks using our microbead occlusion model in WT and IL-6 deficient mice. As expected, ocular hypertension led to transport deficits of CTB in the SC of WT. Interestingly, similar transport deficits were noted in *Il-6*^{-/-} mice. Examination of RGC axons in the distal optic nerve revealed decreases in myelinated axon density in microbead injected WT mice. While *Il-6*^{-/-} mice presented with genotype dependent decreases in myelinated axon density, further analysis by electron microscopy is required to confirm an actual decrease. As our analysis was done using light microscopy, we could only reliably quantify myelinated axons. Therefore, this genotype dependent decrease could be the result of more unmyelinated axons in the *Il-6*^{-/-} optic nerve. Regardless, we saw no microbead dependent decreases in myelinated axon density between saline and microbead injected *Il-6*^{-/-} mice. Similarly, unlike WT mice, *Il-6*^{-/-} mice were spared from microbead induced deficits in visual acuity threshold. While resistant to microbead induced axon degeneration and visual acuity deficits, *Il-6*^{-/-} mice were sensitive to corneal injury caused by the intracameral injection. Overall, these results further support our hypothesis that IL-6 signaling is detrimental to glaucoma mediated RGC pathology. Additionally, it provides evidence that IL-6 signaling specifically influences the progression from functional deficits to structural degeneration in glaucoma.

Aim 2: Future Directions

Future directions for this aim would entail a number of experiments describing the impact of IL-6 deficiency in more chronic models of glaucoma and characterizing the mechanisms behind IL-6 deficiency and its protective effect in RGC axonopathy in glaucoma. The first of these experiments would involve replicating these findings in the more chronic DBA/2J model of glaucoma. However, this would involve a significant amount of time as we would need to 1) backcross the IL-6 mutation onto the DBA/2J genetic background, 2) develop a large enough colony to not only ascertain the effect of IL-6 deficiency at different ages, but overcome that natural variability of the DBA/2J mouse and 3) wait for several cohorts to reach the age where significant axon and RGC pathology is prevalent. However, as the DBA/2J models the progressive nature of glaucoma that is seen in humans, these experiments would be extremely beneficial.

Borrowing on the results we obtained regarding sIL-6R α in the aged DBA/2J mouse, another set of experiments would involve determining whether IL-6 trans-signaling is responsible for the IL-6 mediated effects seen in our WT mice. This would involve inducing ocular hypertension in mice that overexpress soluble gp130. If trans-signaling was responsible, we would see a similar mitigation of axon degeneration and visual acuity deficits in microbead injected sgp130 mice as we did in *Il-6*^{-/-} mice.

Third, I would determine the cellular mechanism behind IL-6 mediated RGC axonopathy. Specifically, I would conduct a microarray from retinal samples from microbead injected WT and *Il-6*^{-/-} mice exposed to various time periods of ocular hypertension to see if any changes in gene expression are apparent. Preliminary results from our lab shows that following 4 weeks of ocular hypertension, genes associated with inflammation (i.e. TNF α) and cell health (BCL-XL)

differentially altered between microbead injected WT and *Il-6*^{-/-} mice. Interestingly, the pattern of these changes suggests a higher level of inflammation as seen by increased TNF α expression (Figure 5.1B) and lower levels of cell survival as seen by decreased anti-apoptotic marker Bcl-XL in microbead injected retina of *Il-6*^{-/-} compared to that of WT (Figure 5.1D). While this result would suggest that IL-6 deficiency is detrimental, gene expression studies done at 8 weeks would provide more accurate results.

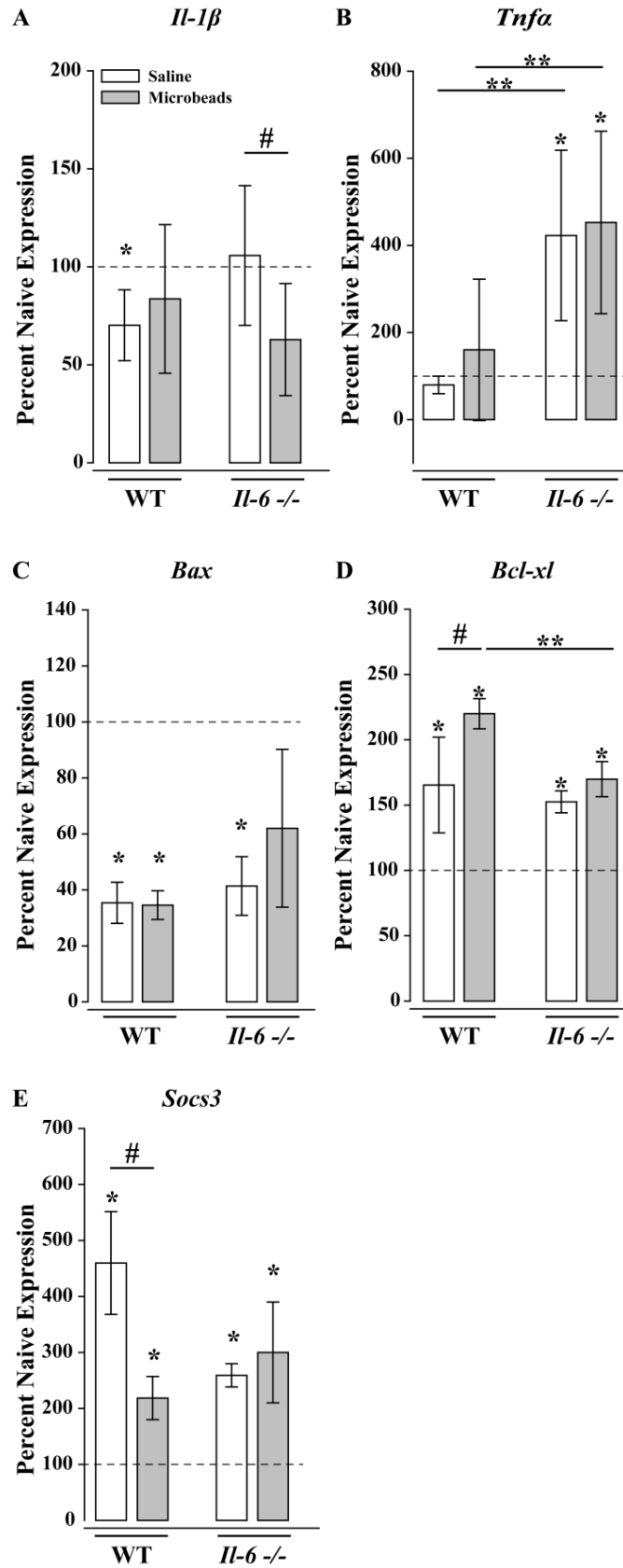


Figure 5.1. IL-6 deficiency influences glaucoma-related changes in gene expression of neuroinflammatory, cell health and gp130 modulators. (A–E) Percent gene expression of *Tnfa* (A), *Il-1 β* (B), *Bcl-xl* (C), *Bax* (D) and *Socs3* (E) in WT or *Il-6*^{-/-} eyes injected with saline (white) or microbeads (gray). mRNA levels of gene targets were normalized to *Gapdh* and compared to respective naïve expression levels (dotted line) via the $\Delta\Delta C_t$ method. Statistical significance ($p < 0.05$) is indicated as follows: * naïve versus experimental, ** between genotype comparison, # within genotype comparison.

Figure from (Echevarria et al., 2016) and used in accordance with the Creative Commons Attribution-Non Commercial 4.0 International License.

Finally, it would be beneficial to determine how the other gp130 cytokines impact RGC degeneration in glaucoma. Indeed, we have shown previously that all other members of the gp130 family are upregulated in response to glaucoma related stressors in the DBA/2J mouse (Figure 5.2). Therefore, it would be interesting to see whether genetic ablation of these cytokines leads to similar outcomes in RGC pathology.

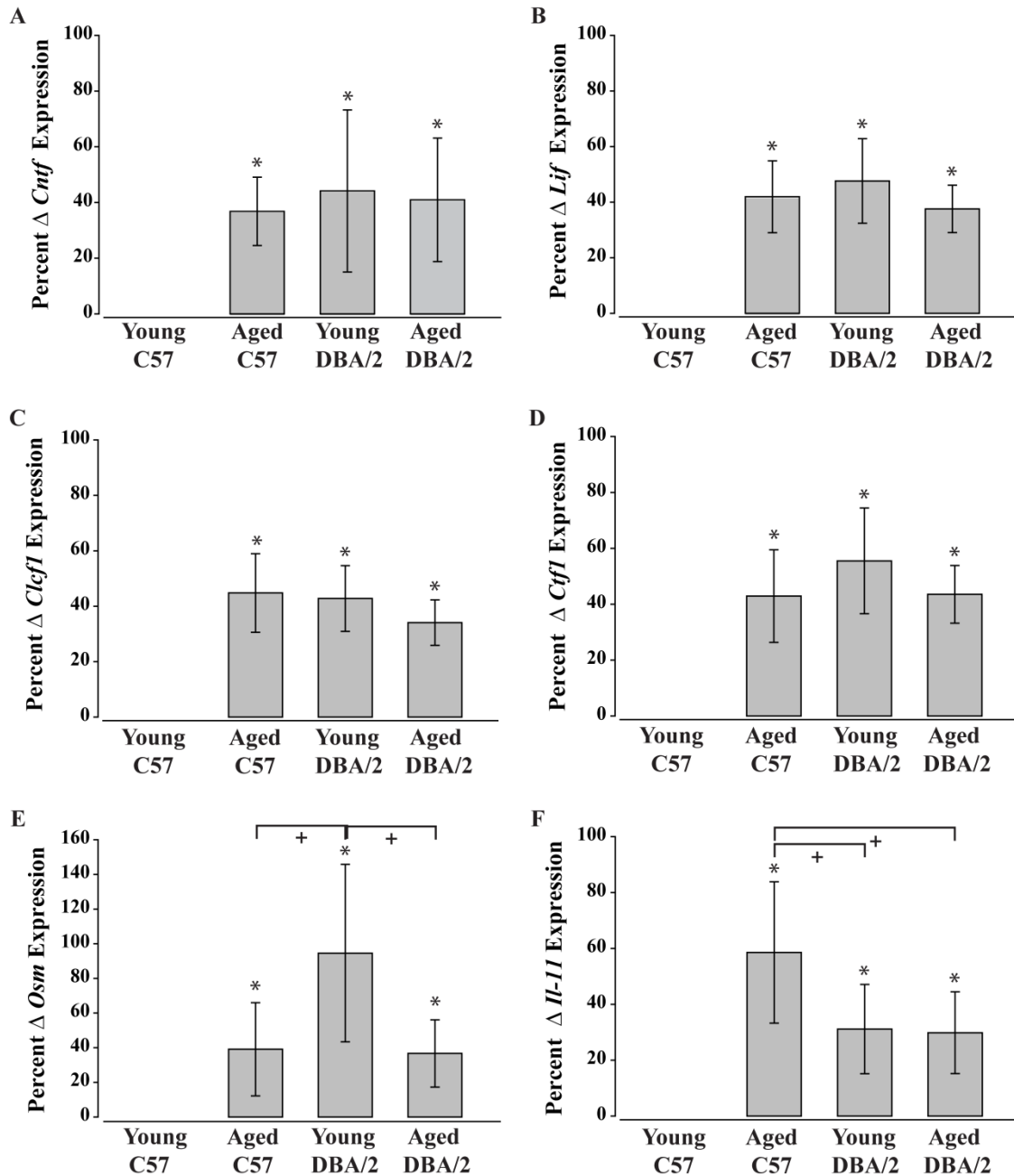


Figure 5.2. Glaucoma-related stressors elevate expression of IL-6 family members in a stressor dependent manner. (A-F) Gene expression of *Cntf* (A), *Lif* (B), *Clcf1* (C), *Ctf1* (D), *Osm* (E) and *Il-11* (F) in whole retina from young (4mo) and aged (8mo) C57 and DBA/2J mice, as determined by quantitative PCR. mRNA levels of gene targets were normalized to *Gapdh*. Data are presented as percent change in gene expression relative to expression in young C57 retina ($\Delta\Delta CT$). Asterisks denote statistical significance ($p < 0.05$), as compared to expression in young C57 retina. $* = p < 0.05$.

Figure from (Echevarria et al., 2013) and used in accordance with the Creative Commons Attribution-Non Commercial 4.0 International License.

Aim 3: Outcome and Future Directions

Identify structural and functional outcomes of constitutive IL-6 signaling in the naïve optic projection.

In vitro, IL-6 facilitates neurite extension in RGCs, while IL-6 promotes axon regeneration following optic nerve crush (Chidlow et al., 2012, Leibinger et al., 2013, Leibinger et al., 2016). Additionally, IL-6 deficiency is attributed to structural and functional deficits in other areas of the nervous system (Zhong et al., 1999, Baier et al., 2009, Bowen et al., 2011, Kong et al., 2015). Therefore, we utilized a number of structural and functional outcomes to determine whether constitutive IL-6 signaling is important in the development and maintenance of the optic projection. Our observation that IL-6 is expressed by RGCs throughout post-natal development and adulthood provided the first set of evidence implicating IL-6 in post-natal development. From there we found that while IL-6 deficiency did not impact overall visual acuity, it perturbed the cortical response to light stimuli (FVEP) and led to decreased retinal thickness. Neural tracing studies revealed that anterograde axonal transport along the retinocollicular projection was slower in *Il-6*^{-/-} mice compared to WT mice. This apparent decrease in the rate of fast axonal transport was not due to gross abnormalities in superior colliculus architecture, retinal ganglion cell number or deficiencies in tracer uptake. Examination of cytoskeletal elements within the un-myelinated portion of RGC axons revealed disorganization of the axon cytoskeleton specific to microtubules, which are responsible for fast axonal transport. Examination of the hippocampus revealed similar disruptions in microtubule arrangement. Investigation into the myelinated segment of optic nerve axons revealed that IL-6 deficiency led to larger axons with thicker myelin sheaths, which was accompanied by a decline in myelinated axon density and total number of axons in the optic nerve. Pharmacological reversal of IL-6

deficiency appeared to improve the rate of axon transport while also improving tubulin arrangement.

Aim 3: Future Directions

Similar to the other aims, future directions for this part would entail a number of experiments focusing on characterizing the cellular mechanism(s) behind our results. Specifically, I would supplement our FVEP data by utilizing other electrophysiological paradigms that collect data specifically from RGCs. While the FVEP signal is dependent on RGCs connecting to the brain, the message could be perturbed as it travels through the RGC axon and into the visual cortex. More accurate RGC signals could be obtained by measuring PERG responses directly from the retina. Additionally, individual recording from RGCs via patch clamp electrophysiology would provide information regarding the activity of individual RGCs.

Another set of experiments would be to delineate whether IL-6 related deficits are truly the result of a developmental defect. To accomplish this, I would conditionally ablate IL-6 signaling in the adult mouse and see if similar structural and functional phenotypes. If not, that would suggest these defects are associated with IL-6 signaling during development. If that were the case, I would ablate IL-6 signaling at different points in development to determine the crucial period in which IL-6 signaling is necessary for development of the optic projection. Finally, in line with Aim 2, I would test the roles of the other gp130 cytokines in the development of the optic projection to see if these abnormalities are IL-6 specific.

Potential mechanism behind outcomes of IL-6 signaling in RGC health and disease.

Our studies utilizing the microbead occlusion model in IL-6 deficient mice suggest that constitutive IL-6 signaling is necessary for proper tubulin cyto-architecture and latency of fast axonal transport, yet in response to glaucoma related IOP elevation, IL-6 signaling promotes axonopathy and vision loss. Based on the literature and our studies in the DBA/2J mouse model of glaucoma, we speculate sIL-6R α may be responsible for transforming IL-6 from a constructive signal to a destructive signal in the optic projection. Prior to forming a hypothesis on the potential mechanism(s) behind this phenomenon, it is important to understand the molecular outcome(s) of IL-6 signaling and how it is affected in neurodegenerative disease. One particular outcome of IL-6 signaling involves influx of Ca²⁺ in the intracellular space (Qiu et al., 1995, Nelson et al., 2002, Orellana et al., 2005) . This is especially interesting as studies show 1) involvement of Ca²⁺ signaling in axon development (Lohmann, 2009, Rosenberg and Spitzer, 2011) and 2) dysregulated Ca²⁺ signaling within RGCs affected by glaucoma (Crish and Calkins, 2011).

Ca²⁺ is an important intracellular signaling ion in the CNS that regulates a variety of necessary functions within neurons including gene transcription, neurotransmitter release, synaptic plasticity and axon development (Berridge et al., 2000, Lohmann, 2009, Rosenberg and Spitzer, 2011) . Interestingly, multiple studies report that incubation of neurons with IL-6 leads to increases in intracellular Ca²⁺ (Qiu et al., 1995, Nelson et al., 2002, Orellana et al., 2005). Our studies in naïve IL-6 deficient mice suggest a positive role for IL-6 in microtubule structure and axon transport. Indeed, previous studies report that application of IL-6 promotes neurite extension *in vitro* and axon regeneration *in vivo* (Chidlow et al., 2012, Leibinger et al., 2013, Leibinger et al., 2016). While there are currently no reports describing an effect of IL-6 on

microtubule integrity directly, neurite extension and alteration of synapses involve changes in microtubule assembly (Conde and Caceres, 2009). As Ca^{2+} signaling is required for proper axonal navigation and establishing proper synaptic connections in the developing CNS, one could suggest that the phenotypes observed in the *Il-6*^{-/-} optic projection is due to altered Ca^{2+} signaling during development and possibly adulthood (Figure 5.3A). An important study would be to utilizing Ca^{2+} imaging or single cell electrophysiology to determine the capacity of Ca^{2+} signaling in *Il-6*^{-/-} mice.

Tight regulation of Ca^{2+} influx is imperative, as surpassing its normal spatial and temporal limits within the cytoplasm can lead to degenerative outcomes, including axon degeneration and production of reactive oxygen species (ROS), both of which contribute to apoptosis of the cell soma. As with most neurodegenerative diseases, aberrant Ca^{2+} signaling is prominent throughout glaucoma pathology (Crish and Calkins, 2011). While the mechanism behind Ca^{2+} dysregulation in glaucoma is not well understood, it is hypothesized that chronic Ca^{2+} influx triggers excessive activation of downstream targets including calpain (Crish and Calkins, 2011). Calpain is a protease that leads to phosphorylation of the microtubule associated protein tau, which can lead to defects in axon transport and subsequent degeneration of the axon. Interestingly, Ca^{2+} mediated phosphorylation of tau in hippocampal neurons is also seen following incubation with IL-6, suggesting a connection between IL-6 and Ca^{2+} mediated effects in glaucomatous axonopathy (Orellana et al., 2005). From these data, we can hypothesize that the reduction in axonopathy seen in our microbead injected *Il-6*^{-/-} mice may be due to a mitigation in aberrant Ca^{2+} signaling (Figure 5.3B).

The dichotomous outcomes of IL-6 signaling have been well described in both the CNS and the periphery, with classical signaling via mIL-6R α and trans-signaling via sIL-6R α

implicated in positive and negative outcomes respectively (Scheller et al., 2011a). Our studies in the DBA/2J model of glaucoma indicate that sIL-6R α elevation coincides with axon transport deficits, a component of glaucoma pathology that precedes axon degeneration. As our microbead studies suggest that IL-6 signaling is involved in glaucoma related axonopathy, it is plausible to suggest that the increase in sIL-6R α changes IL-6 signaling from classical to trans, promoting a shift from axon transport deficits to axon degeneration (Figure 5.3B). While it is not known how signaling through sIL-6R α leads to degeneration directly, it is believed that IL-6 binding to sIL-6R α not only increases the circulating half-life of IL-6, but increases the propensity for IL-6 signaling events to occur in domains where IL-6 is released (Hunter and Jones, 2015). If indeed IL-6 signaling leads to Ca²⁺ influx, a stronger and longer IL-6 signal brought on by sIL-6R α could lead to the aberrant Ca²⁺ influx and subsequent pathology seen in glaucoma (Figure 5.3B).

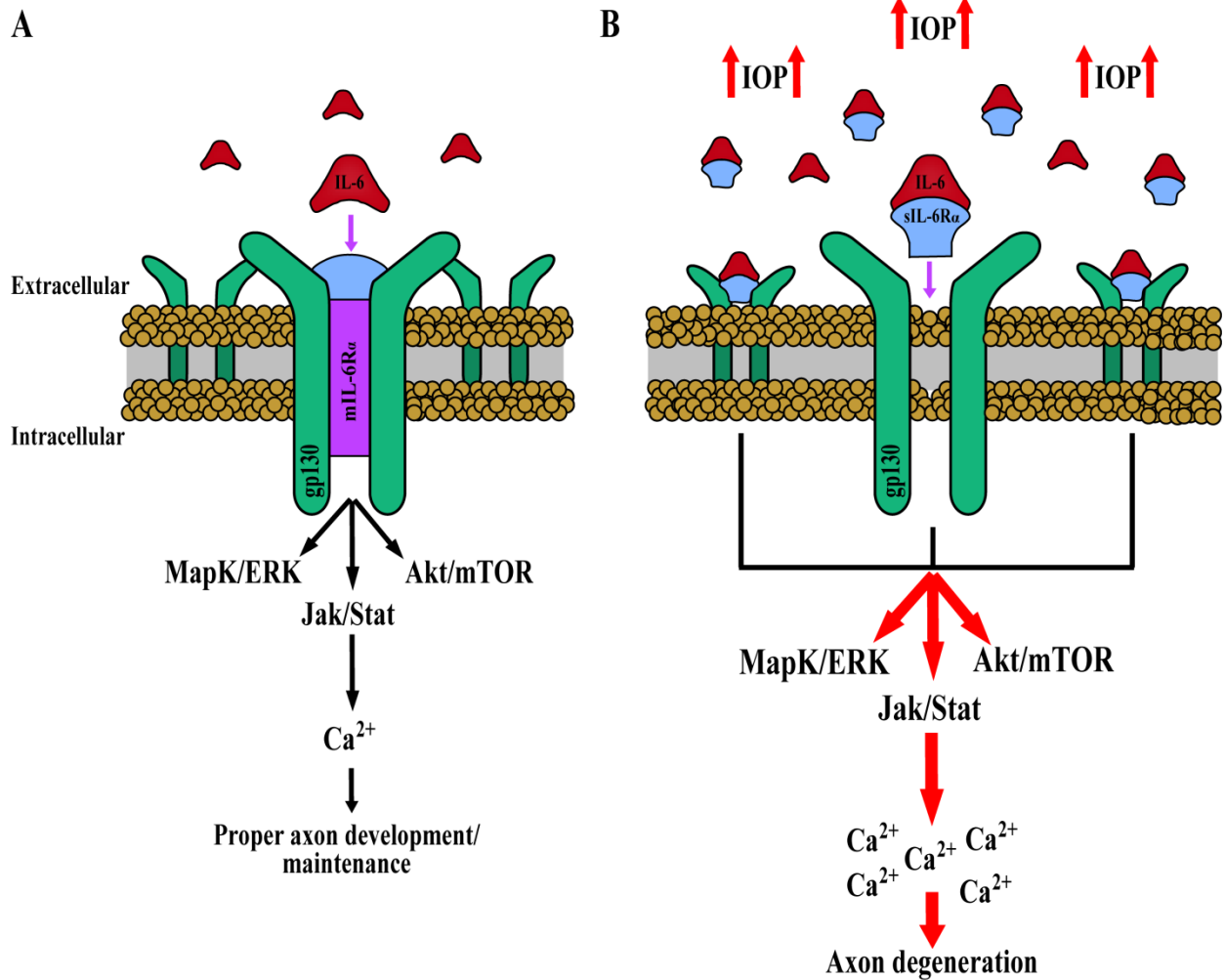


Figure 5.3. Proposed mechanism behind outcomes of IL-6 signaling in RGC health and disease. **(A)** In the naïve optic projection, Ca²⁺ influx via IL-6 mediated STAT3 activation facilitates proper axon development and maintenance, by directly or indirectly acting on microtubules. **(B)** In response to glaucoma related stressors (e.g. elevated IOP), we propose that the upregulation of IL-6 and sIL-6R α leads to an increase in IL-6 signaling events, causing an unhealthy influx of Ca²⁺ and overtime leading to axon degeneration.

Figure adapted from (Echevarria et al., 2016) and used in accordance with the Creative Commons Attribution-Non Commercial 4.0 International License.

Conclusions

Altogether, these data indicate that IL-6 signaling is detrimental to glaucoma mediated RGC pathology, yet necessary for proper development and maintenance of the optic projection. In the DBA/2J mouse, age-related increases in IOP lead to increased production of sIL-6R α that localizes primarily to RGCs with poor CTB transport. Due to the age of these mice and the known progression of CTB transport deficits, this suggests a relationship between the increased prevalence of pathological IL-6 trans-signaling and the time period between axon transport deficits and axon degeneration (Figure 5.4). In examining the impact of IL-6 signaling on RGC degeneration caused by microbead induced ocular hypertension, IL-6 deficient mice were protected against axon degeneration and deficits in visual acuity, yet experienced a similar degree of axon transport deficits. Taken together, these results suggest that 1) IL-6 signaling, specifically trans-signaling, facilitates axon degeneration in glaucoma (Figure 5.4). Finally, we show a role for constitutive IL-6 in optic projection development, particularly in regards to maintaining proper axon transport and tubulin cyto-architecture. As a whole, these results suggest that IL-6 is likely involved in multiple facets of CNS activity including development and degeneration. Furthermore, seemingly disparate outcomes of IL-6 signaling are likely to arise from a complex regulatory system that includes transitions between classical and trans-signaling pathways that are mediated by receptor isoforms. Together, our findings have significant implications for our understanding of IL-6 signaling within the CNS, with particular impact on its role as in CNS development and maintenance as well as a potential therapeutic target for neurodegenerative disease.

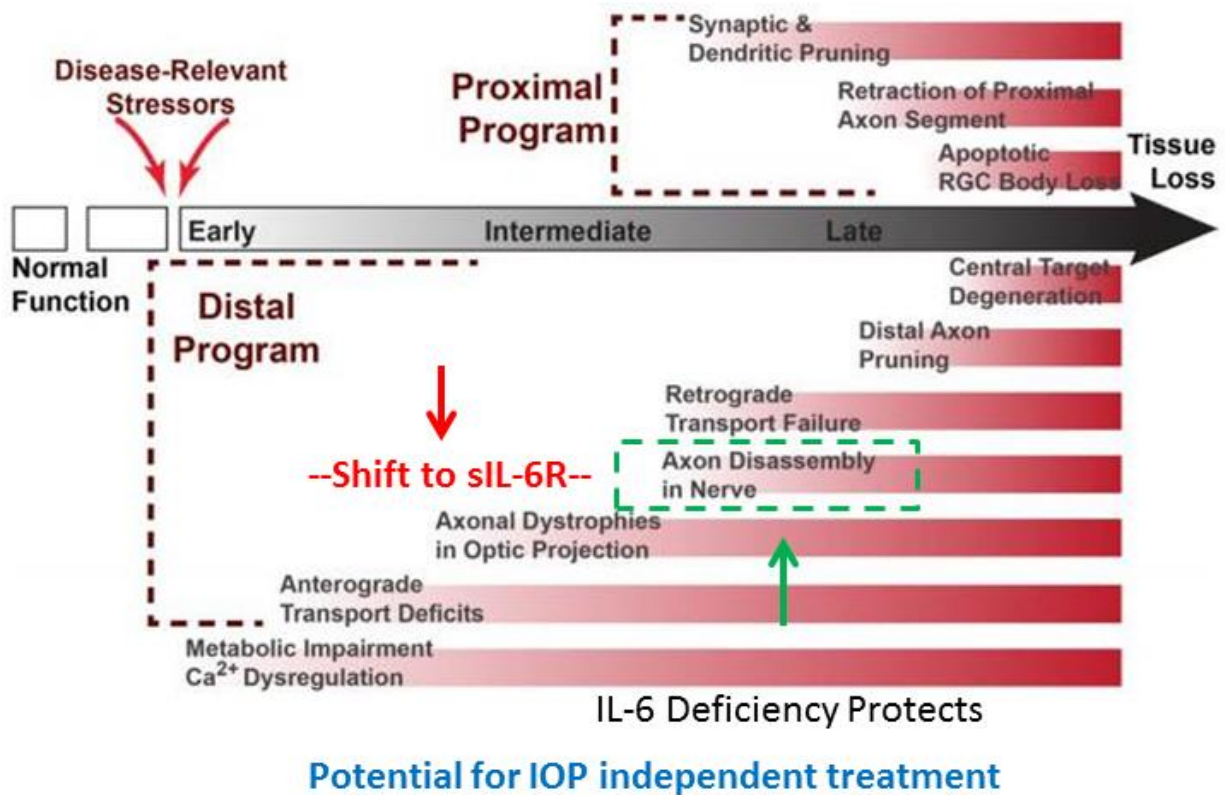


Figure 5.4. Integration of results with proposed timeline of glaucomatous RGC degeneration. Work in animal models suggests a profile that involves loss of function prior to loss of structure and that degeneration occurs in a distal to proximal fashion. For the majority of patients, treatment isn't started until significant disease progression has occurred. Our work in IL-6 suggests a mechanism in which IL-6 trans-signaling is upregulated early in disease (red arrow) and is involved in propagating axon degeneration (green arrow). In these results suggests a potential window in which anti-IL-6 signaling therapy could inhibit axon degeneration and subsequent vision loss in glaucoma.

Figure modified from (Calkins, 2012) with permission from DJ Calkins and used in accordance with Copyright Clearance Center's RightsLink service.

REFERENCES

- Abbott CJ, Choe TE, Lusardi TA, Burgoyne CF, Wang L, Fortune B (2013) Imaging axonal transport in the rat visual pathway. *Biomed Opt Express* 4:364-386.
- Agorastos A, Hauger RL, Barkauskas DA, Moeller-Bertram T, Clopton PL, Haji U, Lohr JB, Geraciotti TD, Jr., Patel PM, Chrousos GP, Baker DG (2014) Circadian rhythmicity, variability and correlation of interleukin-6 levels in plasma and cerebrospinal fluid of healthy men. *Psychoneuroendocrinology* 44:71-82.
- Albon J, Karwatowski WS, Avery N, Easty DL, Duance VC (1995) Changes in the collagenous matrix of the aging human lamina cribrosa. *Br J Ophthalmol* 79:368-375.
- Ali C, Nicole O, Docagne F, Lesne S, MacKenzie ET, Nouvelot A, Buisson A, Vivien D (2000) Ischemia-induced interleukin-6 as a potential endogenous neuroprotective cytokine against NMDA receptor-mediated excitotoxicity in the brain. *J Cereb Blood Flow Metab* 20:956-966.
- Alleva E, Cirulli F, Bianchi M, Bondiolotti GP, Chiarotti F, De Acetis L, Panerai AE (1998) Behavioural characterization of interleukin-6 overexpressing or deficient mice during agonistic encounters. *The European journal of neuroscience* 10:3664-3672.
- Alsarraf O, Fan J, Dahrouj M, Chou CJ, Yates PW, Crosson CE (2014) Acetylation preserves retinal ganglion cell structure and function in a chronic model of ocular hypertension. *Invest Ophthalmol Vis Sci* 55:7486-7493.
- Anderson MG, Smith RS, Hawes NL, Zabaleta A, Chang B, Wiggs JL, John SW (2002) Mutations in genes encoding melanosomal proteins cause pigmentary glaucoma in DBA/2J mice. *Nat Genet* 30:81-85.
- Andratsch M, Mair N, Constantin CE, Scherbakov N, Benetti C, Quarta S, Vogl C, Sailer CA, Uceyler N, Brockhaus J, Martini R, Sommer C, Zeilhofer HU, Muller W, Kuner R, Davis JB, Rose-John S, Kress M (2009) A Key Role for gp130 Expressed on Peripheral Sensory Nerves in Pathological Pain. *Journal of Neuroscience* 29:13473-13483.
- Archibald NK, Clarke MP, Mosimann UP, Burn DJ (2009) The retina in Parkinson's disease. *Brain* 132:1128-1145.
- Armario A, Hernandez J, Bluethmann H, Hidalgo J (1998) IL-6 deficiency leads to increased emotionality in mice: evidence in transgenic mice carrying a null mutation for IL-6. *J Neuroimmunol* 92:160-169.

- Arruda JL, Colburn RW, Rickman AJ, Rutkowski MD, DeLeo JA (1998) Increase of interleukin-6 mRNA in the spinal cord following peripheral nerve injury in the rat: potential role of IL-6 in neuropathic pain. *Brain Res Mol Brain Res* 62:228-235.
- Assali A, Gaspar P, Rebsam A (2014) Activity dependent mechanisms of visual map formation--from retinal waves to molecular regulators. *Semin Cell Dev Biol* 35:136-146.
- Baier PC, May U, Scheller J, Rose-John S, Schiffelholz T (2009) Impaired hippocampus-dependent and -independent learning in IL-6 deficient mice. *Behav Brain Res* 200:192-196.
- Baltan S, Inman DM, Danilov CA, Morrison RS, Calkins DJ, Horner PJ (2010) Metabolic vulnerability disposes retinal ganglion cell axons to dysfunction in a model of glaucomatous degeneration. *J Neurosci* 30:5644-5652.
- Banitt MR, Ventura LM, Feuer WJ, Savatovsky E, Luna G, Shif O, Bosse B, Porciatti V (2013) Progressive loss of retinal ganglion cell function precedes structural loss by several years in glaucoma suspects. *Invest Ophthalmol Vis Sci* 54:2346-2352.
- Bauer S, Kerr BJ, Patterson PH (2007) The neuroipoietic cytokine family in development, plasticity, disease and injury. *Nat Rev Neurosci* 8:221-232.
- Behrens C, Schubert T, Haverkamp S, Euler T, Berens P (2016) Connectivity map of bipolar cells and photoreceptors in the mouse retina. *Elife* 5.
- Beirowski B, Babetto E, Coleman MP, Martin KR (2008) The *WldS* gene delays axonal but not somatic degeneration in a rat glaucoma model. *The European journal of neuroscience* 28:1166-1179.
- Bell MJ, Kochanek PM, Doughty LA, Carcillo JA, Adelson PD, Clark RS, Wisniewski SR, Whalen MJ, DeKosky ST (1997) Interleukin-6 and interleukin-10 in cerebrospinal fluid after severe traumatic brain injury in children. *J Neurotrauma* 14:451-457.
- Berridge MJ, Lipp P, Bootman MD (2000) The versatility and universality of calcium signalling. *Nat Rev Mol Cell Biol* 1:11-21.
- Berry RH, Qu J, John SW, Howell GR, Jakobs TC (2015) Synapse Loss and Dendrite Remodeling in a Mouse Model of Glaucoma. *PLoS One* 10:e0144341.
- Beurel E, Jope RS (2009) Lipopolysaccharide-induced interleukin-6 production is controlled by glycogen synthase kinase-3 and STAT3 in the brain. *J Neuroinflammation* 6:9.
- Birke MT, Birke K, Lutjen-Drecoll E, Schlotzer-Schrehardt U, Hammer CM (2011) Cytokine-dependent ELAM-1 induction and concomitant intraocular pressure regulation in porcine anterior eye perfusion culture. *Invest Ophthalmol Vis Sci* 52:468-475.

- Blindenbacher A, Wang X, Langer I, Savino R, Terracciano L, Heim MH (2003) Interleukin 6 is important for survival after partial hepatectomy in mice. *Hepatology* 38:674-682.
- Blum-Degen D, Muller T, Kuhn W, Gerlach M, Przuntek H, Riederer P (1995) Interleukin-1 beta and interleukin-6 are elevated in the cerebrospinal fluid of Alzheimer's and de novo Parkinson's disease patients. *Neurosci Lett* 202:17-20.
- Blumberg D, Skaat A, Liebmann JM (2015) Emerging risk factors for glaucoma onset and progression. *Prog Brain Res* 221:81-101.
- Bluthe RM, Michaud B, Poli V, Dantzer R (2000) Role of IL-6 in cytokine-induced sickness behavior: a study with IL-6 deficient mice. *Physiol Behav* 70:367-373.
- Boland B, Platt FM (2015) Bridging the age spectrum of neurodegenerative storage diseases. *Best Pract Res Clin Endocrinol Metab* 29:127-143.
- Bond WS, Hines-Beard J, GoldenMerry YP, Davis M, Farooque A, Sappington RM, Calkins DJ, Rex TS (2016) Virus-mediated EpoR76E Therapy Slows Optic Nerve Axonopathy in Experimental Glaucoma. *Mol Ther* 24:230-239.
- Bosco A, Inman DM, Steele MR, Wu G, Soto I, Marsh-Armstrong N, Hubbard WC, Calkins DJ, Horner PJ, Vetter ML (2008) Reduced retina microglial activation and improved optic nerve integrity with minocycline treatment in the DBA/2J mouse model of glaucoma. *Invest Ophthalmol Vis Sci* 49:1437-1446.
- Bouhenni RA, Dunmire J, Sewell A, Edward DP (2012) Animal models of glaucoma. *J Biomed Biotechnol* 2012:692609.
- Bourne RR (2012) The optic nerve head in glaucoma. *Community Eye Health* 25:55-57.
- Bowen KK, Dempsey RJ, Vemuganti R (2011) Adult interleukin-6 knockout mice show compromised neurogenesis. *Neuroreport* 22:126-130.
- Bozkurt B, Mesci L, Irkec M, Ozdag BB, Sanal O, Arslan U, Ersoy F, Tezcan I (2012) Association of tumour necrosis factor-alpha -308 G/A polymorphism with primary open-angle glaucoma. *Clin Exp Ophthalmol* 40:e156-162.
- Broadway DC (2012) Visual field testing for glaucoma - a practical guide. *Comm Eye Health* 25:66-70
- Buckingham BP, Inman DM, Lambert W, Oglesby E, Calkins DJ, Steele MR, Vetter ML, Marsh-Armstrong N, Horner PJ (2008) Progressive ganglion cell degeneration precedes neuronal loss in a mouse model of glaucoma. *J Neurosci* 28:2735-2744.

- Bunt AH, Hendrickson AE, Lund JS, Lund RD, Fuchs AF (1975) Monkey retinal ganglion cells: morphometric analysis and tracing of axonal projections, with a consideration of the peroxidase technique. *J Comp Neurol* 164:265-285.
- Burgoyne CF, Downs JC, Bellezza AJ, Suh JK, Hart RT (2005) The optic nerve head as a biomechanical structure: a new paradigm for understanding the role of IOP-related stress and strain in the pathophysiology of glaucomatous optic nerve head damage. *Prog Retin Eye Res* 24:39-73.
- Burroughs SL, Kaja S, Koulen P (2011) Quantification of deficits in spatial visual function of mouse models for glaucoma. *Invest Ophthalmol Vis Sci* 52:3654-3659.
- Burton MD, Johnson RW (2012) Interleukin-6 trans-signaling in the senescent mouse brain is involved in infection-related deficits in contextual fear conditioning. *Brain Behav Immun* 26:732-738.
- Burton MD, Rytch JL, Freund GG, Johnson RW (2013) Central inhibition of interleukin-6 trans-signaling during peripheral infection reduced neuroinflammation and sickness in aged mice. *Brain Behav Immun* 30:66-72.
- Burton MD, Sparkman NL, Johnson RW (2011) Inhibition of interleukin-6 trans-signaling in the brain facilitates recovery from lipopolysaccharide-induced sickness behavior. *J Neuroinflammation* 8:54.
- Butterweck V, Prinz S, Schwaninger M (2003) The role of interleukin-6 in stress-induced hyperthermia and emotional behaviour in mice. *Behav Brain Res* 144:49-56.
- Cafferty WB, Gardiner NJ, Das P, Qiu J, McMahon SB, Thompson SW (2004) Conditioning injury-induced spinal axon regeneration fails in interleukin-6 knock-out mice. *J Neurosci* 24:4432-4443.
- Calkins DJ (2012) Critical pathogenic events underlying progression of neurodegeneration in glaucoma. *Prog Retin Eye Res* 31:702-719.
- Calkins DJ, Horner PJ (2012) The cell and molecular biology of glaucoma: axonopathy and the brain. *Invest Ophthalmol Vis Sci* 53:2482-2484.
- Campbell IL, Abraham CR, Masliah E, Kemper P, Inglis JD, Oldstone MB, Mucke L (1993) Neurologic disease induced in transgenic mice by cerebral overexpression of interleukin 6. *Proc Natl Acad Sci U S A* 90:10061-10065.
- Campbell IL, Erta M, Lim SL, Frausto R, May U, Rose-John S, Scheller J, Hidalgo J (2014) Trans-signaling is a dominant mechanism for the pathogenic actions of interleukin-6 in the brain. *J Neurosci* 34:2503-2513.
- Cardenas H, Bolin LM (2003) Compromised reactive microgliosis in MPTP-lesioned IL-6 KO mice. *Brain Res* 985:89-97.

- Carson MJ, Doose JM, Melchior B, Schmid CD, Ploix CC (2006) CNS immune privilege: hiding in plain sight. *Immunol Rev* 213:48-65.
- Cesareo M, Martucci A, Ciuffoletti E, Mancino R, Cerulli A, Sorge RP, Martorana A, Sancesario G, Nucci C (2015) Association Between Alzheimer's Disease and Glaucoma: A Study Based on Heidelberg Retinal Tomography and Frequency Doubling Technology Perimetry. *Front Neurosci* 9:479.
- Chalaris A, Rabe B, Paliga K, Lange H, Laskay T, Fielding CA, Jones SA, Rose-John S, Scheller J (2007) Apoptosis is a natural stimulus of IL6R shedding and contributes to the proinflammatory trans-signaling function of neutrophils. *Blood* 110:1748-1755.
- Chang B, Smith RS, Hawes NL, Anderson MG, Zabaleta A, Savinova O, Roderick TH, Heckenlively JR, Davisson MT, John SW (1999) Interacting loci cause severe iris atrophy and glaucoma in DBA/2J mice. *Nat Genet* 21:405-409.
- Chen HH, Wei X, Cho KS, Chen GC, Sappington R, Calkins DJ, Chen DF (2011a) Optic Neuropathy Due to Microbead-Induced Elevated Intraocular Pressure in the Mouse. *Invest Ophth Vis Sci* 52:36-44.
- Chen KH, Wu CC, Roy S, Lee SM, Liu JH (1999) Increased interleukin-6 in aqueous humor of neovascular glaucoma. *Invest Ophthalmol Vis Sci* 40:2627-2632.
- Chen SK, Badea TC, Hattar S (2011b) Photoentrainment and pupillary light reflex are mediated by distinct populations of ipRGCs. *Nature* 476:92-95.
- Chen YP, Chiao CC (2014) Spatial distribution of excitatory synapses on the dendrites of ganglion cells in the mouse retina. *PLoS One* 9:e86159.
- Chevalier-Larsen E, Holzbaur EL (2006) Axonal transport and neurodegenerative disease. *Biochim Biophys Acta* 1762:1094-1108.
- Chidlow G, Ebnetter A, Wood JPM, Casson RJ (2011) The optic nerve head is the site of axonal transport disruption, axonal cytoskeleton damage and putative axonal regeneration failure in a rat model of glaucoma. *Acta Neuropathol* 121:737-751.
- Chidlow G, Wood JP, Ebnetter A, Casson RJ (2012) Interleukin-6 is an efficacious marker of axonal transport disruption during experimental glaucoma and stimulates neuritogenesis in cultured retinal ganglion cells. *Neurobiol Dis* 48:568-581.
- Chiu K, Chan TF, Wu A, Leung IY, So KF, Chang RC (2012) Neurodegeneration of the retina in mouse models of Alzheimer's disease: what can we learn from the retina? *Age (Dordr)* 34:633-649.

- Chourbaji S, Urani A, Inta I, Sanchis-Segura C, Brandwein C, Zink M, Schwaninger M, Gass P (2006) IL-6 knockout mice exhibit resistance to stress-induced development of depression-like behaviors. *Neurobiol Dis* 23:587-594.
- Chucair-Elliott AJ, Conrady C, Zheng M, Kroll CM, Lane TE, Carr DJ (2014) Microglia-induced IL-6 protects against neuronal loss following HSV-1 infection of neural progenitor cells. *Glia* 62:1418-1434.
- Clark WM, Rinker LG, Lessov NS, Hazel K, Eckenstein F (1999) Time course of IL-6 expression in experimental CNS ischemia. *Neurol Res* 21:287-292.
- Clark WM, Rinker LG, Lessov NS, Hazel K, Hill JK, Stenzel-Poore M, Eckenstein F (2000) Lack of interleukin-6 expression is not protective against focal central nervous system ischemia. *Stroke* 31:1715-1720.
- Conde C, Caceres A (2009) Microtubule assembly, organization and dynamics in axons and dendrites. *Nat Rev Neurosci* 10:319-332.
- Cooper ML, Crish SD, Inman DM, Horner PJ, Calkins DJ (2016) Early Astrocyte redistribution in the optic nerve precedes axonopathy in the DBA/2J mouse model of glaucoma. *Exp Eye Res* 150:22-23.
- Crish SD, Calkins DJ (2011) Neurodegeneration in glaucoma: progression and calcium-dependent intracellular mechanisms. *Neuroscience* 176:1-11.
- Crish SD, Dapper JD, MacNamee SE, Balaram P, Sidorova TN, Lambert WS, Calkins DJ (2013) Failure of axonal transport induces a spatially coincident increase in astrocyte BDNF prior to synapse loss in a central target. *Neuroscience* 229:55-70.
- Crish SD, Sappington RM, Inman DM, Horner PJ, Calkins DJ (2010) Distal axonopathy with structural persistence in glaucomatous neurodegeneration. *Proc Natl Acad Sci U S A* 107:5196-5201.
- Cueva Vargas JL, Osswald IK, Unsain N, Aurousseau MR, Barker PA, Bowie D, Di Polo A (2015) Soluble Tumor Necrosis Factor Alpha Promotes Retinal Ganglion Cell Death in Glaucoma via Calcium-Permeable AMPA Receptor Activation. *J Neurosci* 35:12088-12102.
- Cvenkel B, Kopitar AN, Ihan A (2010) Inflammatory molecules in aqueous humour and on ocular surface and glaucoma surgery outcome. *Mediators Inflamm* 2010:939602.
- Dalrymple A, Wild EJ, Joubert R, Sathasivam K, Bjorkqvist M, Petersen A, Jackson GS, Isaacs JD, Kristiansen M, Bates GP, Leavitt BR, Keir G, Ward M, Tabrizi SJ (2007) Proteomic profiling of plasma in Huntington's disease reveals neuroinflammatory activation and biomarker candidates. *J Proteome Res* 6:2833-2840.

- de Vos AF, Klaren VN, Kijlstra A (1994) Expression of multiple cytokines and IL-1RA in the uvea and retina during endotoxin-induced uveitis in the rat. *Invest Ophthalmol Vis Sci* 35:3873-3883.
- Deleidi M, Jaggle M, Rubino G (2015) Immune aging, dysmetabolism, and inflammation in neurological diseases. *Front Neurosci* 9:172.
- Della Santina L, Inman DM, Lupien CB, Horner PJ, Wong RO (2013) Differential progression of structural and functional alterations in distinct retinal ganglion cell types in a mouse model of glaucoma. *J Neurosci* 33:17444-17457.
- Dengler-Crish CM, Smith MA, Inman DM, Wilson GN, Young JW, Crish SD (2014) Anterograde transport blockade precedes deficits in retrograde transport in the visual projection of the DBA/2J mouse model of glaucoma. *Front Neurosci* 8:290.
- Desai A, Mitchison TJ (1997) Microtubule polymerization dynamics. *Annu Rev Cell Dev Biol* 13:83-117.
- Deverman BE, Patterson PH (2009) Cytokines and CNS development. *Neuron* 64:61-78.
- DiStefano PS, Friedman B, Radziejewski C, Alexander C, Boland P, Schick CM, Lindsay RM, Wiegand SJ (1992) The neurotrophins BDNF, NT-3, and NGF display distinct patterns of retrograde axonal transport in peripheral and central neurons. *Neuron* 8:983-993.
- Domenici L, Origlia N, Falsini B, Cerri E, Barloscio D, Fabiani C, Sanso M, Giovannini L (2014) Rescue of retinal function by BDNF in a mouse model of glaucoma. *PLoS One* 9:e115579.
- Dong HW (2008) *Allen Reference Mouse Atlas*. Hoboken, New Jersey: John Wiley & Sons, Inc.
- Douglas RM, Alam NM, Silver BD, McGill TJ, Tschetter WW, Prusky GT (2005) Independent visual threshold measurements in the two eyes of freely moving rats and mice using a virtual-reality optokinetic system. *Vis Neurosci* 22:677-684.
- Downs JC (2015a) IOP telemetry in the nonhuman primate. *Exp Eye Res* 141:91-98.
- Downs JC (2015b) Optic nerve head biomechanics in aging and disease. *Exp Eye Res* 133:19-29.
- Downs JC, Burgoyne CF, Seigfreid WP, Reynaud JF, Strouthidis NG, Sallee V (2011) 24-hour IOP telemetry in the nonhuman primate: implant system performance and initial characterization of IOP at multiple timescales. *Invest Ophthalmol Vis Sci* 52:7365-7375.
- Dreher B, Sefton AJ, Ni SY, Nisbett G (1985) The morphology, number, distribution and central projections of Class I retinal ganglion cells in albino and hooded rats. *Brain Behav Evol* 26:10-48.

- Du S, Huang W, Zhang X, Wang J, Wang W, Lam DS (2016) Multiplex cytokine levels of aqueous humor in acute primary angle-closure patients: fellow eye comparison. *BMC Ophthalmol* 16:6.
- Dugan LL, Ali SS, Shekhtman G, Roberts AJ, Lucero J, Quick KL, Behrens MM (2009) IL-6 mediated degeneration of forebrain GABAergic interneurons and cognitive impairment in aged mice through activation of neuronal NADPH oxidase. *PLoS One* 4:e5518.
- Dvorianchikova G, Barakat DJ, Hernandez E, Shestopalov VI, Ivanov D (2010) Toll-like receptor 4 contributes to retinal ischemia/reperfusion injury. *Mol Vis* 16:1907-1912.
- Echevarria F, Walker C, Abella S, Won M, Sappington R (2013) Stressor-dependent Alterations in Glycoprotein 130: Implications for Glial Cell Reactivity, Cytokine Signaling and Ganglion Cell Health in Glaucoma. *J Clin Exp Ophthalmol* 4.
- Echevarria FD (2014) Interleukin-6 Signaling in the Central Nervous System: Pointing the Finger at Trans-signaling in Neuroinflammatory-mediated Neurodegeneration. *VRN* 6.
- Echevarria FD, Rickman AE, Sappington RM (2016) Interleukin-6: A Constitutive Modulator of Glycoprotein 130, Neuroinflammatory and Cell Survival Signaling in Retina. *J Clin Cell Immunol* 7.
- Echevarria FD, Formichella CR, Sappington RM (2017) Interleukin-6 Deficiency Attenuates Retinal Ganglion Cell Axonopathy and Glaucoma-related Vision Loss. *Front. Neuro* 11:318
- El-Danaf RN, Huberman AD (2015) Characteristic patterns of dendritic remodeling in early-stage glaucoma: evidence from genetically identified retinal ganglion cell types. *J Neurosci* 35:2329-2343.
- Ellis EM, Gauvain G, Sivyer B, Murphy GJ (2016) Shared and distinct retinal input to the mouse superior colliculus and dorsal lateral geniculate nucleus. *Journal of Neurophysiology* 116:602-610.
- Engel LA, Muether PS, Fauser S, Hueber A (2014) The effect of previous surgery and topical eye drops for primary open-angle glaucoma on cytokine expression in aqueous humor. *Graefes Arch Clin Exp Ophthalmol* 252:791-799.
- Erta M, Quintana A, Hidalgo J (2012) Interleukin-6, a major cytokine in the central nervous system. *Int J Biol Sci* 8:1254-1266.
- Eugster HP, Frei K, Kopf M, Lassmann H, Fontana A (1998) IL-6-deficient mice resist myelin oligodendrocyte glycoprotein-induced autoimmune encephalomyelitis. *Eur J Immunol* 28:2178-2187.

- Fang XX, Jiang XL, Han XH, Peng YP, Qiu YH (2013) Neuroprotection of interleukin-6 against NMDA-induced neurotoxicity is mediated by JAK/STAT3, MAPK/ERK, and PI3K/AKT signaling pathways. *Cell Mol Neurobiol* 33:241-251.
- Feng L, Chen H, Yi J, Troy JB, Zhang HF, Liu X (2016) Long-Term Protection of Retinal Ganglion Cells and Visual Function by Brain-Derived Neurotrophic Factor in Mice With Ocular Hypertension. *Invest Ophthalmol Vis Sci* 57:3793-3802.
- Feng L, Zhao Y, Yoshida M, Chen H, Yang JF, Kim TS, Cang JH, Troy JB, Liu XR (2013) Sustained Ocular Hypertension Induces Dendritic Degeneration of Mouse Retinal Ganglion Cells That Depends on Cell Type and Location. *Invest Ophthalmol Vis Sci* 54:1106-1117.
- Ferguson LR, Grover S, Dominguez JM, 2nd, Balaiya S, Chalam KV (2014) Retinal thickness measurement obtained with spectral domain optical coherence tomography assisted optical biopsy accurately correlates with ex vivo histology. *PLoS One* 9:e111203.
- Fernandez DC, Pasquini LA, Dorfman D, Aldana Marcos HJ, Rosenstein RE (2012) Early distal axonopathy of the visual pathway in experimental diabetes. *Am J Pathol* 180:303-313.
- Fischer AJ, Zelinka C, Milani-Nejad N (2015) Reactive retinal microglia, neuronal survival, and the formation of retinal folds and detachments. *Glia* 63:313-327.
- Fisher J, Mizrahi T, Schori H, Yoles E, Levkovitch-Verbin H, Haggia S, Revel M, Schwartz M (2001) Increased post-traumatic survival of neurons in IL-6-knockout mice on a background of EAE susceptibility. *J Neuroimmunol* 119:1-9.
- Formichella C, Abella, SK, Sims, SM, Cathcart, HM, Sappington, RM (2014) Astrocyte Reactivity: A Biomarker for Ganglion Cell Health in Retinal Neurodegeneration. *Journal of Clinical and Cellular Immunology* 5:15.
- Franceschi C, Bonafe M, Valensin S, Olivieri F, De Luca M, Ottaviani E, De Benedictis G (2000) Inflamm-aging. An evolutionary perspective on immunosenescence. *Ann N Y Acad Sci* 908:244-254.
- Franchimont N, Wertz S, Malaise M (2005) Interleukin-6: An osteotropic factor influencing bone formation? *Bone* 37:601-606.
- Frank-Cannon TC, Alto LT, McAlpine FE, Tansey MG (2009) Does neuroinflammation fan the flame in neurodegenerative diseases? *Mol Neurodegener* 4:47.
- Freddo TF, Gong H (2009) Etiology of Iop Elevation in Primary Open Angle Glaucoma. *Optom Glaucoma Soc E J* 4.
- Gadient RA, Otten U (1993) Differential expression of interleukin-6 (IL-6) and interleukin-6 receptor (IL-6R) mRNAs in rat hypothalamus. *Neurosci Lett* 153:13-16.

- Gadient RA, Otten U (1994a) Expression of interleukin-6 (IL-6) and interleukin-6 receptor (IL-6R) mRNAs in rat brain during postnatal development. *Brain Res* 637:10-14.
- Gadient RA, Otten U (1994b) Identification of interleukin-6 (IL-6)-expressing neurons in the cerebellum and hippocampus of normal adult rats. *Neurosci Lett* 182:243-246.
- Gadient RA, Otten U (1995) Interleukin-6 and interleukin-6 receptor mRNA expression in rat central nervous system. *Ann N Y Acad Sci* 762:403-406.
- Gallego BI, Salazar JJ, de Hoz R, Rojas B, Ramirez AI, Salinas-Navarro M, Ortin-Martinez A, Valiente-Soriano FJ, Aviles-Trigueros M, Villegas-Perez MP, Vidal-Sanz M, Trivino A, Ramirez JM (2012) IOP induces upregulation of GFAP and MHC-II and microglia reactivity in mice retina contralateral to experimental glaucoma. *J Neuroinflammation* 9:92.
- Garbers C, Jänner N, Chalaris A, Moss ML, Floss DM, Meyer D, Koch-Nolte F, Rose-John S, Scheller J (2011) Species specificity of ADAM10 and ADAM17 proteins in interleukin-6 (IL-6) trans-signaling and novel role of ADAM10 in inducible IL-6 receptor shedding. *Journal of Biological Chemistry* 286:14804-14811.
- Garcia-Valenzuela E, Shareef S, Walsh J, Sharma SC (1995) Programmed cell death of retinal ganglion cells during experimental glaucoma. *Exp Eye Res* 61:33-44.
- Ghanem A, Arafa L, Elewa A (2011) Tumor Necrosis Factor- α and Interleukin-6 Levels in patients with primary open-angle Glaucoma. *J Clinic Experiment Ophthalmol* 2:2.
- Goldblum D, Mittag T (2002) Prospects for relevant glaucoma models with retinal ganglion cell damage in the rodent eye. *Vision Res* 42:471-478.
- Grotzinger J, Kernebeck T, Kallen KJ, Rose-John S (1999) IL-6 type cytokine receptor complexes: hexamer, tetramer or both? *Biol Chem* 380:803-813.
- Gruol DL, Vo K, Bray JG (2014) Increased astrocyte expression of IL-6 or CCL2 in transgenic mice alters levels of hippocampal and cerebellar proteins. *Front Cell Neurosci* 8:234.
- Guo L, Duggan J, Cordeiro MF (2010a) Alzheimer's disease and retinal neurodegeneration. *Curr Alzheimer Res* 7:3-14.
- Guo Y, Cepurna WO, Dyck JA, Doser TA, Johnson EC, Morrison JC (2010b) Retinal cell responses to elevated intraocular pressure: a gene array comparison between the whole retina and retinal ganglion cell layer. *Invest Ophthalmol Vis Sci* 51:3003-3018.
- Guo Y, Johnson E, Cepurna W, Jia L, Dyck J, Morrison JC (2009) Does elevated intraocular pressure reduce retinal TRKB-mediated survival signaling in experimental glaucoma? *Exp Eye Res* 89:921-933.

- Hagberg H, Gilland E, Bona E, Hanson LA, Hahin-Zoric M, Blennow M, Holst M, McRae A, Soder O (1996) Enhanced expression of interleukin (IL)-1 and IL-6 messenger RNA and bioactive protein after hypoxia-ischemia in neonatal rats. *Pediatr Res* 40:603-609.
- Hama T, Miyamoto M, Tsukui H, Nishio C, Hatanaka H (1989) Interleukin-6 as a neurotrophic factor for promoting the survival of cultured basal forebrain cholinergic neurons from postnatal rats. *Neurosci Lett* 104:340-344.
- Hans VH, Kossmann T, Joller H, Otto V, Morganti-Kossmann MC (1999a) Interleukin-6 and its soluble receptor in serum and cerebrospinal fluid after cerebral trauma. *Neuroreport* 10:409-412.
- Hans VH, Kossmann T, Lenzlinger PM, Probstmeier R, Imhof HG, Trentz O, Morganti-Kossmann MC (1999b) Experimental axonal injury triggers interleukin-6 mRNA, protein synthesis and release into cerebrospinal fluid. *J Cereb Blood Flow Metab* 19:184-194.
- Harwerth RS, Quigley HA (2006) Visual field defects and retinal ganglion cell losses in patients with glaucoma. *Archives of ophthalmology* 124:853-859.
- Health Quality O (2006) Routine eye examinations for persons 20-64 years of age: an evidence-based analysis. *Ont Health Technol Assess Ser* 6:1-81.
- Heavner W, Pevny L (2012) Eye development and retinogenesis. *Cold Spring Harb Perspect Biol* 4.
- Heiduschka P, Julien S, Schuettauf F, Schnichels S (2010a) Loss of retinal function in aged DBA/2J mice - New insights into retinal neurodegeneration. *Exp Eye Res* 91:779-783.
- Heiduschka P, Schnichels S, Fuhrmann N, Hofmeister S, Schraermeyer U, Wissinger B, Alavi MV (2010b) Electrophysiological and histologic assessment of retinal ganglion cell fate in a mouse model for OPA1-associated autosomal dominant optic atrophy. *Invest Ophthalmol Vis Sci* 51:1424-1431.
- Heijl A, Leske MC, Bengtsson B, Hyman L, Bengtsson B, Hussein M, Early Manifest Glaucoma Trial G (2002) Reduction of intraocular pressure and glaucoma progression: results from the Early Manifest Glaucoma Trial. *Archives of ophthalmology* 120:1268-1279.
- Heinrich PC, Behrmann I, Muller-Newen G, Schaper F, Graeve L (1998) Interleukin-6-type cytokine signalling through the gp130/Jak/STAT pathway. *Biochem J* 334 (Pt 2):297-314.
- Hendriks JJ, Teunissen CE, de Vries HE, Dijkstra CD (2005) Macrophages and neurodegeneration. *Brain Res Brain Res Rev* 48:185-195.

- Hines-Beard J, Bond WS, Backstrom JR, Rex TS (2016) Virus-mediated EpoR76E gene therapy preserves vision in a glaucoma model by modulating neuroinflammation and decreasing oxidative stress. *J Neuroinflammation* 13:39.
- Hodes GE, Menard C, Russo SJ (2016) Integrating Interleukin-6 into depression diagnosis and treatment. *Neurobiol Stress* 4:15-22.
- Hoene M, Runge H, Haring HU, Schleicher ED, Weigert C (2013) Interleukin-6 promotes myogenic differentiation of mouse skeletal muscle cells: role of the STAT3 pathway. *Am J Physiol Cell Physiol* 304:C128-136.
- Hogan D, Morrow JD, Smith EM, Opp MR (2003) Interleukin-6 alters sleep of rats. *J Neuroimmunol* 137:59-66.
- Holcombe DJ, Lengefeld N, Gole GA, Barnett NL (2008) Selective inner retinal dysfunction precedes ganglion cell loss in a mouse glaucoma model. *Br J Ophthalmol* 92:683-688.
- Hollands H, Johnson D, Hollands S, Simel DL, Jinapriya D, Sharma S (2013) Do findings on routine examination identify patients at risk for primary open-angle glaucoma? The rational clinical examination systematic review. *JAMA* 309:2035-2042.
- Hood DC, Kardon RH (2007) A framework for comparing structural and functional measures of glaucomatous damage. *Prog Retin Eye Res* 26:688-710.
- Hoon M, Okawa H, Della Santina L, Wong RO (2014) Functional architecture of the retina: development and disease. *Prog Retin Eye Res* 42:44-84.
- Horstmann L, Schmid H, Heinen AP, Kurschus FC, Dick HB, Joachim SC (2013) Inflammatory demyelination induces glia alterations and ganglion cell loss in the retina of an experimental autoimmune encephalomyelitis model. *J Neuroinflammation* 10:120.
- Howell GR, Libby RT, Jakobs TC, Smith RS, Phalan FC, Barter JW, Barbay JM, Marchant JK, Mahesh N, Porciatti V, Whitmore AV, Masland RH, John SW (2007a) Axons of retinal ganglion cells are insulted in the optic nerve early in DBA/2J glaucoma. *J Cell Biol* 179:1523-1537.
- Howell GR, Libby RT, Marchant JK, Wilson LA, Cosma IM, Smith RS, Anderson MG, John SW (2007b) Absence of glaucoma in DBA/2J mice homozygous for wild-type versions of Gpnmb and Tyrp1. *BMC Genet* 8:45.
- Howell GR, Macalinao DG, Sousa GL, Walden M, Soto I, Kneeland SC, Barbay JM, King BL, Marchant JK, Hibbs M, Stevens B, Barres BA, Clark AF, Libby RT, John SW (2011) Molecular clustering identifies complement and endothelin induction as early events in a mouse model of glaucoma. *Journal of Clinical Investigation* 121:1429-1444.

- Howell GR, Soto I, Ryan M, Graham LC, Smith RS, John SW (2013) Deficiency of complement component 5 ameliorates glaucoma in DBA/2J mice. *J Neuroinflammation* 10:76.
- Hsu MP, Frausto R, Rose-John S, Campbell IL (2015) Analysis of IL-6/gp130 family receptor expression reveals that in contrast to astroglia, microglia lack the oncostatin M receptor and functional responses to oncostatin M. *Glia* 63:132-141.
- Huang W, Chen S, Gao X, Yang M, Zhang J, Li X, Wang W, Zhou M, Zhang X, Zhang X (2014) Inflammation-related cytokines of aqueous humor in acute primary angle-closure eyes. *Invest Ophthalmol Vis Sci* 55:1088-1094.
- Huang W, Dobberfuhl A, Filippopoulos T, Ingelsson M, Fileta JB, Poulin NR, Grosskreutz CL (2005) Transcriptional up-regulation and activation of initiating caspases in experimental glaucoma. *Am J Pathol* 167:673-681.
- Hunter CA, Jones SA (2015) IL-6 as a keystone cytokine in health and disease. *Nat Immunol* 16:448-457.
- Iester M, De Feo F, Douglas GR (2012) Visual field loss morphology in high- and normal-tension glaucoma. *J Ophthalmol* 2012:327326.
- Inman DM, Horner PJ (2007) Reactive nonproliferative gliosis predominates in a chronic mouse model of glaucoma. *Glia* 55:942-953.
- Inman DM, Sappington RM, Horner PJ, Calkins DJ (2006) Quantitative correlation of optic nerve pathology with ocular pressure and corneal thickness in the DBA/2 mouse model of glaucoma. *Invest Ophthalmol Vis Sci* 47:986-996.
- Inomata Y, Hirata A, Yonemura N, Koga T, Kido N, Tanihara H (2003) Neuroprotective effects of interleukin-6 on NMDA-induced rat retinal damage. *Biochem Biophys Res Commun* 302:226-232.
- Inzelberg R, Ramirez JA, Nisipeanu P, Ophir A (2004) Retinal nerve fiber layer thinning in Parkinson disease. *Vision Res* 44:2793-2797.
- Ito YA, Belforte N, Cueva Vargas JL, Di Polo A (2016) A Magnetic Microbead Occlusion Model to Induce Ocular Hypertension-Dependent Glaucoma in Mice. *J Vis Exp* e53731.
- Jafarzadehpour E, Radinmehr F, Pakravan M, Mirzajani A, Yazdani S (2013) Pattern electroretinography in glaucoma suspects and early primary open angle glaucoma. *J Ophthalmic Vis Res* 8:199-206.
- Jakobs TC, Libby RT, Ben Y, John SW, Masland RH (2005) Retinal ganglion cell degeneration is topological but not cell type specific in DBA/2J mice. *J Cell Biol* 171:313-325.

- John SW, Smith RS, Savinova OV, Hawes NL, Chang B, Turnbull D, Davisson M, Roderick TH, Heckenlively JR (1998) Essential iris atrophy, pigment dispersion, and glaucoma in DBA/2J mice. *Invest Ophthalmol Vis Sci* 39:951-962.
- Johnson EC, Doser TA, Cepurna WO, Dyck JA, Jia L, Guo Y, Lambert WS, Morrison JC (2011) Cell proliferation and interleukin-6-type cytokine signaling are implicated by gene expression responses in early optic nerve head injury in rat glaucoma. *Invest Ophthalmol Vis Sci* 52:504-518.
- Johnson EC, Morrison JC (2009) Friend or foe? Resolving the impact of glial responses in glaucoma. *J Glaucoma* 18:341-353.
- Johnson TV, Tomarev SI (2010) Rodent models of glaucoma. *Brain Res Bull* 81:349-358.
- Joos KM, Li C, Sappington RM (2010) Morphometric changes in the rat optic nerve following short-term intermittent elevations in intraocular pressure. *Invest Ophthalmol Vis Sci* 51:6431-6440.
- Ju KR, Kim HS, Kim JH, Lee NY, Park CK (2006) Retinal glial cell responses and Fas/FasL activation in rats with chronic ocular hypertension. *Brain Res* 1122:209-221.
- Kalesnykas RP, Sparks DL (1996) The primate superior colliculus and the control of saccadic eye movements. *Neuroscientist* 2:284-292.
- Keeley PW, Whitney IE, Madsen NR, St John AJ, Borhanian S, Leong SA, Williams RW, Reese BE (2014) Independent Genomic Control of Neuronal Number across Retinal Cell Types. *Dev Cell* 30:103-109.
- Khan D, Fernando P, Cicvaric A, Berger A, Pollak A, Monje FJ, Pollak DD (2014) Long-term effects of maternal immune activation on depression-like behavior in the mouse. *Transl Psychiatry* 4:e363.
- Kim HS, Park CK (2005) Retinal ganglion cell death is delayed by activation of retinal intrinsic cell survival program. *Brain Res* 1057:17-28.
- Kitaoka Y, Munemasa Y, Kojima K, Hirano A, Ueno S, Takagi H (2013) Axonal protection by Nmnat3 overexpression with involvement of autophagy in optic nerve degeneration. *Cell Death Dis* 4:e860.
- Kobbert C, Apps R, Bechmann I, Lanciego JL, Mey J, Thanos S (2000) Current concepts in neuroanatomical tracing. *Prog Neurobiol* 62:327-351.
- Kompass KS, Agapova OA, Li W, Kaufman PL, Rasmussen CA, Hernandez MR (2008) Bioinformatic and statistical analysis of the optic nerve head in a primate model of ocular hypertension. *BMC Neurosci* 9:93.

- Kong E, Sucic S, Monje FJ, Savalli G, Diao W, Khan D, Ronovsky M, Cabatic M, Koban F, Freissmuth M, Pollak DD (2015) STAT3 controls IL6-dependent regulation of serotonin transporter function and depression-like behavior. *Sci Rep* 5:9009.
- Kopf M, Baumann H, Freer G, Freudenberg M, Lamers M, Kishimoto T, Zinkernagel R, Bluethmann H, Kohler G (1994) Impaired immune and acute-phase responses in interleukin-6-deficient mice. *Nature* 368:339-342.
- Kossmann T, Hans V, Imhof HG, Trentz O, Morganti-Kossmann MC (1996) Interleukin-6 released in human cerebrospinal fluid following traumatic brain injury may trigger nerve growth factor production in astrocytes. *Brain Res* 713:143-152.
- Kossmann T, Hans VH, Imhof HG, Stocker R, Grob P, Trentz O, Morganti-Kossmann C (1995) Intrathecal and serum interleukin-6 and the acute-phase response in patients with severe traumatic brain injuries. *Shock* 4:311-317.
- Lambert WS, Ruiz L, Crish SD, Wheeler LA, Calkins DJ (2011) Brimonidine prevents axonal and somatic degeneration of retinal ganglion cell neurons. *Mol Neurodegener* 6:4.
- Lee SC, Liu W, Dickson DW, Brosnan CF, Berman JW (1993) Cytokine production by human fetal microglia and astrocytes. Differential induction by lipopolysaccharide and IL-1 beta. *J Immunol* 150:2659-2667.
- Lee YB, Nagai A, Kim SU (2002) Cytokines, chemokines, and cytokine receptors in human microglia. *J Neurosci Res* 69:94-103.
- Lehtimäki KA, Peltola J, Koskikallio E, Keränen T, Honkaniemi J (2003) Expression of cytokines and cytokine receptors in the rat brain after kainic acid-induced seizures. *Brain Res Mol Brain Res* 110:253-260.
- Leibinger M, Andreadaki A, Gobrecht P, Levin E, Fischer D (2016) Boosting CNS axon regeneration by circumventing limitations of natural cytokine signaling. *Mol Ther*.
- Leibinger M, Müller A, Gobrecht P, Diekmann H, Andreadaki A, Fischer D (2013) Interleukin-6 contributes to CNS axon regeneration upon inflammatory stimulation. *Cell Death Dis* 4:e609.
- Levin LA (2001) Relevance of the site of injury of glaucoma to neuroprotective strategies. *Surv Ophthalmol* 45 Suppl 3:S243-249; discussion S273-246.
- Levkovitch-Verbin H, Harizman N, Dardik R, Nisgav Y, Vander S, Melamed S (2007) Regulation of cell death and survival pathways in experimental glaucoma. *Exp Eye Res* 85:250-258.

- Levkovitch-Verbin H, Quigley HA, Martin KR, Valenta D, Baumrind LA, Pease ME (2002) Translimbal laser photocoagulation to the trabecular meshwork as a model of glaucoma in rats. *Invest Ophthalmol Vis Sci* 43:402-410.
- Libby RT, Anderson MG, Pang IH, Robinson ZH, Savinova OV, Cosma IM, Snow A, Wilson LA, Smith RS, Clark AF, John SW (2005a) Inherited glaucoma in DBA/2J mice: pertinent disease features for studying the neurodegeneration. *Vis Neurosci* 22:637-648.
- Libby RT, Li Y, Savinova OV, Barter J, Smith RS, Nickells RW, John SW (2005b) Susceptibility to neurodegeneration in a glaucoma is modified by Bax gene dosage. *PLoS Genet* 1:17-26.
- Licastro F, Candore G, Lio D, Porcellini E, Colonna-Romano G, Franceschi C, Caruso C (2005) Innate immunity and inflammation in ageing: a key for understanding age-related diseases. *Immun Ageing* 2:8.
- Lin HJ, Tsai FJ, Chen WC, Shi YR, Hsu Y, Tsai SW (2003a) Association of tumour necrosis factor alpha -308 gene polymorphism with primary open-angle glaucoma in Chinese. *Eye (Lond)* 17:31-34.
- Lin ZQ, Kondo T, Ishida Y, Takayasu T, Mukaida N (2003b) Essential involvement of IL-6 in the skin wound-healing process as evidenced by delayed wound healing in IL-6-deficient mice. *J Leukoc Biol* 73:713-721.
- Livingstone M, Hubel D (1988) Segregation of form, color, movement, and depth: anatomy, physiology, and perception. *Science* 240:740-749.
- Loddick SA, Turnbull AV, Rothwell NJ (1998) Cerebral interleukin-6 is neuroprotective during permanent focal cerebral ischemia in the rat. *J Cereb Blood Flow Metab* 18:176-179.
- Lohmann C (2009) Calcium signaling and the development of specific neuronal connections. *Prog Brain Res* 175:443-452.
- London A, Benhar I, Schwartz M (2013) The retina as a window to the brain-from eye research to CNS disorders. *Nat Rev Neurol* 9:44-53.
- Lucas SM, Rothwell NJ, Gibson RM (2006) The role of inflammation in CNS injury and disease. *Brit J Pharmacol* 147:S232-S240.
- Luo C, Yang X, Kain AD, Powell DW, Kuehn MH, Tezel G (2010) Glaucomatous tissue stress and the regulation of immune response through glial Toll-like receptor signaling. *Invest Ophthalmol Vis Sci* 51:5697-5707.
- Lye-Barthel M, Sun D, Jakobs TC (2013) Morphology of astrocytes in a glaucomatous optic nerve. *Invest Ophthalmol Vis Sci* 54:909-917.

- Maday S, Twelvetrees AE, Moughamian AJ, Holzbaur EL (2014) Axonal transport: cargo-specific mechanisms of motility and regulation. *Neuron* 84:292-309.
- Maimone D, Guazzi GC, Annunziata P (1997) IL-6 detection in multiple sclerosis brain. *J Neurol Sci* 146:59-65.
- Makinodan M, Ikawa D, Miyamoto Y, Yamauchi J, Yamamuro K, Yamashita Y, Toritsuka M, Kimoto S, Okumura K, Yamauchi T, Fukami SI, Yoshino H, Wanaka A, Kishimoto T (2016) Social isolation impairs remyelination in mice through modulation of IL-6. *FASEB J* 30:4267-4274.
- Malsch P, Andratsch M, Vogl C, Link AS, Alzheimer C, Brierley SM, Hughes PA, Kress M (2014) Deletion of interleukin-6 signal transducer gp130 in small sensory neurons attenuates mechanonociception and down-regulates TRPA1 expression. *J Neurosci* 34:9845-9856.
- Martin A, Hofmann HD, Kirsch M (2003) Glial reactivity in ciliary neurotrophic factor-deficient mice after optic nerve lesion. *J Neurosci* 23:5416-5424.
- Marx MS, Podos SM, Bodis-Wollner I, Lee PY, Wang RF, Severin C (1988) Signs of early damage in glaucomatous monkey eyes: low spatial frequency losses in the pattern ERG and VEP. *Exp Eye Res* 46:173-184.
- Marz P, Cheng JG, Gadiant RA, Patterson PH, Stoyan T, Otten U, Rose-John S (1998) Sympathetic neurons can produce and respond to interleukin 6. *Proc Natl Acad Sci U S A* 95:3251-3256.
- McFarland-Mancini MM, Funk HM, Paluch AM, Zhou M, Giridhar PV, Mercer CA, Kozma SC, Drew AF (2010) Differences in wound healing in mice with deficiency of IL-6 versus IL-6 receptor. *J Immunol* 184:7219-7228.
- McKinnon SJ, Lehman DM, Kerrigan-Baumrind LA, Merges CA, Pease ME, Kerrigan DF, Ransom NL, Tahzib NG, Reitsamer HA, Levkovitch-Verbin H, Quigley HA, Zack DJ (2002) Caspase activation and amyloid precursor protein cleavage in rat ocular hypertension. *Invest Ophthalmol Vis Sci* 43:1077-1087.
- Medawar PB (1948) Immunity to homologous grafted skin; the fate of skin homografts transplanted to the brain, to subcutaneous tissue, and to the anterior chamber of the eye. *Br J Exp Pathol* 29:58-69.
- Medeiros FA, Lisboa R, Weinreb RN, Liebmann JM, Girkin C, Zangwill LM (2013) Retinal Ganglion Cell Count Estimates Associated with Early Development of Visual Field Defects in Glaucoma. *Ophthalmology* 120:736-744.
- Medzhitov R (2008) Origin and physiological roles of inflammation. *Nature* 454:428-435.

- Mendel I, Katz A, Kozak N, Ben-Nun A, Revel M (1998) Interleukin-6 functions in autoimmune encephalomyelitis: a study in gene-targeted mice. *Eur J Immunol* 28:1727-1737.
- Mendonca Torres PM, de Araujo EG (2001) Interleukin-6 increases the survival of retinal ganglion cells in vitro. *J Neuroimmunol* 117:43-50.
- Minckler DS, Bunt AH, Johanson GW (1977) Orthograde and retrograde axoplasmic transport during acute ocular hypertension in the monkey. *Invest Ophthalmol Vis Sci* 16:426-441.
- Mo JS, Streilein JW (2001) Immune privilege persists in eyes with extreme inflammation induced by intravitreal LPS. *Eur J Immunol* 31:3806-3815.
- Mogi M, Harada M, Narabayashi H, Inagaki H, Minami M, Nagatsu T (1996) Interleukin (IL)-1 beta, IL-2, IL-4, IL-6 and transforming growth factor-alpha levels are elevated in ventricular cerebrospinal fluid in juvenile parkinsonism and Parkinson's disease. *Neurosci Lett* 211:13-16.
- Morikawa Y, Tamura S, Minehata K, Donovan PJ, Miyajima A, Senba E (2004) Essential function of oncostatin m in nociceptive neurons of dorsal root ganglia. *J Neurosci* 24:1941-1947.
- Morrison JC, Moore CG, Deppmeier LM, Gold BG, Meshul CK, Johnson EC (1997) A rat model of chronic pressure-induced optic nerve damage. *Exp Eye Res* 64:85-96.
- Morrow JD, Opp MR (2005) Sleep-wake behavior and responses of interleukin-6-deficient mice to sleep deprivation. *Brain Behav Immun* 19:28-39.
- Morzaev D, Nicholson JD, Caspi T, Weiss S, Hochhauser E, Goldenberg-Cohen N (2015) Toll-like receptor-4 knockout mice are more resistant to optic nerve crush damage than wild-type mice. *Clin Exp Ophthalmol* 43:655-665.
- Moschos MM, Tagaris G, Markopoulos I, Margetis I, Tsapakis S, Kanakis M, Koutsandrea C (2011) Morphologic changes and functional retinal impairment in patients with Parkinson disease without visual loss. *European journal of ophthalmology* 21:24-29.
- Moschovakis AK (1996) The superior colliculus and eye movement control. *Current opinion in neurobiology* 6:811-816.
- Mossbock G, Weger M, Moray M, Renner W, Haller-Schober EM, Mattes D, Schmut O, Wegscheider B, El-Shabrawi Y (2006) TNF-alpha promoter polymorphisms and primary open-angle glaucoma. *Eye (Lond)* 20:1040-1043.
- Mousa A, Bakhiet M (2013) Role of cytokine signaling during nervous system development. *Int J Mol Sci* 14:13931-13957.

- Mukaino M, Nakamura M, Yamada O, Okada S, Morikawa S, Renault-Mihara F, Iwanami A, Ikegami T, Ohsugi Y, Tsuji O, Katoh H, Matsuzaki Y, Toyama Y, Liu M, Okano H (2010) Anti-IL-6-receptor antibody promotes repair of spinal cord injury by inducing microglia-dominant inflammation. *Exp Neurol* 224:403-414.
- Murphy PG, Ramer MS, Borthwick L, Gauldie J, Richardson PM, Bisby MA (1999) Endogenous interleukin-6 contributes to hypersensitivity to cutaneous stimuli and changes in neuropeptides associated with chronic nerve constriction in mice. *European Journal of Neuroscience* 11:2243-2253.
- Nakano Y, Shimazawa M, Ojino K, Izawa H, Takeuchi H, Inoue Y, Tsuruma K, Hara H (2017) Toll-like receptor 4 inhibitor protects against retinal ganglion cell damage induced by optic nerve crush in mice. *J Pharmacol Sci*.
- Nakazawa T, Nakazawa C, Matsubara A, Noda K, Hisatomi T, She H, Michaud N, Hafezi-Moghadam A, Miller JW, Benowitz LI (2006) Tumor necrosis factor- α mediates oligodendrocyte death and delayed retinal ganglion cell loss in a mouse model of glaucoma. *J Neurosci* 26:12633-12641.
- Navarro-Partida J, Martinez-Rizo AB, Ramirez-Barrera P, Velazquez-Fernandez JB, Mondragon-Jaimes VA, Santos-Garcia A, Benites-Godinez V (2017) Association of Toll-like receptor 4 single-nucleotide polymorphisms Asp299Gly and Thr399Ile with the risk of primary open angle glaucoma. *Graefes Arch Clin Exp Ophthalmol*.
- Nelson TE, Ur CL, Gruol DL (2002) Chronic interleukin-6 exposure alters electrophysiological properties and calcium signaling in developing cerebellar purkinje neurons in culture. *J Neurophysiol* 88:475-486.
- Nickells RW (2012) The cell and molecular biology of glaucoma: mechanisms of retinal ganglion cell death. *Invest Ophthalmol Vis Sci* 53:2476-2481.
- Nongpiur ME, Ku JY, Aung T (2011) Angle closure glaucoma: a mechanistic review. *Curr Opin Ophthalmol* 22:96-101.
- Ogai K, Kuwana A, Hisano S, Nagashima M, Koriyama Y, Sugitani K, Mawatari K, Nakashima H, Kato S (2014) Upregulation of leukemia inhibitory factor (LIF) during the early stage of optic nerve regeneration in zebrafish. *PLoS One* 9:e106010.
- Okuda Y, Sakoda S, Bernard CC, Fujimura H, Saeki Y, Kishimoto T, Yanagihara T (1998) IL-6-deficient mice are resistant to the induction of experimental autoimmune encephalomyelitis provoked by myelin oligodendrocyte glycoprotein. *Int Immunol* 10:703-708.
- Oppenheim RW, Wiese S, Prevette D, Armanini M, Wang S, Houenou LJ, Holtmann B, Gotz R, Pennica D, Sendtner M (2001) Cardiotrophin-1, a muscle-derived cytokine, is required for the survival of subpopulations of developing motoneurons. *J Neurosci* 21:1283-1291.

- Orellana DI, Quintanilla RA, Gonzalez-Billault C, Maccioni RB (2005) Role of the JAKs/STATs pathway in the intracellular calcium changes induced by interleukin-6 in hippocampal neurons. *Neurotox Res* 8:295-304.
- Panagis L, Zhao X, Ge Y, Ren L, Mittag TW, Danias J (2011) Retinal gene expression changes related to IOP exposure and axonal loss in DBA/2J mice. *Invest Ophthalmol Vis Sci* 52:7807-7816.
- Pang IH, Clark AF (2007) Rodent models for glaucoma retinopathy and optic neuropathy. *J Glaucoma* 16:483-505.
- Parisi V, Miglior S, Manni G, Centofanti M, Bucci MG (2006) Clinical ability of pattern electroretinograms and visual evoked potentials in detecting visual dysfunction in ocular hypertension and glaucoma. *Ophthalmology* 113:216-228.
- Pavelko KD, Howe CL, Drescher KM, Gamez JD, Johnson AJ, Wei T, Ransohoff RM, Rodriguez M (2003) Interleukin-6 protects anterior horn neurons from lethal virus-induced injury. *J Neurosci* 23:481-492.
- Peng YP, Qiu YH, Lu JH, Wang JJ (2005) Interleukin-6 protects cultured cerebellar granule neurons against glutamate-induced neurotoxicity. *Neurosci Lett* 374:192-196.
- Penkowa M, Giralt M, Carrasco J, Hadberg H, Hidalgo J (2000) Impaired inflammatory response and increased oxidative stress and neurodegeneration after brain injury in interleukin-6-deficient mice. *Glia* 32:271-285.
- Penkowa M, Giralt M, Lago N, Camats J, Carrasco J, Hernandez J, Molinero A, Campbell IL, Hidalgo J (2003) Astrocyte-targeted expression of IL-6 protects the CNS against a focal brain injury. *Exp Neurol* 181:130-148.
- Penkowa M, Molinero A, Carrasco J, Hidalgo J (2001) Interleukin-6 deficiency reduces the brain inflammatory response and increases oxidative stress and neurodegeneration after kainic acid-induced seizures. *Neuroscience* 102:805-818.
- Penkowa M, Moos T, Carrasco J, Hadberg H, Molinero A, Bluethmann H, Hidalgo J (1999) Strongly compromised inflammatory response to brain injury in interleukin-6-deficient mice. *Glia* 25:343-357.
- Perigolo-Vicente R, Ritt K, Goncalves-de-Albuquerque CF, Castro-Faria-Neto HC, Paes-de-Carvalho R, Giestal-de-Araujo E (2014) IL-6, A1 and A2aR: a crosstalk that modulates BDNF and induces neuroprotection. *Biochem Biophys Res Commun* 449:477-482.
- Perigolo-Vicente R, Ritt K, Pereira MR, Torres PM, Paes-de-Carvalho R, Giestal-de-Araujo E (2013) IL-6 treatment increases the survival of retinal ganglion cells in vitro: the role of adenosine A1 receptor. *Biochem Biophys Res Commun* 430:512-518.

- Pernet V, Joly S, Dalkara D, Jordi N, Schwarz O, Christ F, Schaffer DV, Flannery JG, Schwab ME (2013) Long-distance axonal regeneration induced by CNTF gene transfer is impaired by axonal misguidance in the injured adult optic nerve. *Neurobiol Dis* 51:202-213.
- Perry VH, Anthony DC, Bolton SJ, Brown HC (1997) The blood-brain barrier and the inflammatory response. *Mol Med Today* 3:335-341.
- Perry VH, Oehler R, Cowey A (1984) Retinal ganglion cells that project to the dorsal lateral geniculate nucleus in the macaque monkey. *Neuroscience* 12:1101-1123.
- Porciatti V (2015) Electrophysiological assessment of retinal ganglion cell function. *Exp Eye Res* 141:164-170.
- Qiu Z, Parsons KL, Gruol DL (1995) Interleukin-6 selectively enhances the intracellular calcium response to NMDA in developing CNS neurons. *J Neurosci* 15:6688-6699.
- Qu J, Wang D, Grosskreutz CL (2010) Mechanisms of retinal ganglion cell injury and defense in glaucoma. *Exp Eye Res* 91:48-53.
- Quigley H, Anderson DR (1976) The dynamics and location of axonal transport blockade by acute intraocular pressure elevation in primate optic nerve. *Invest Ophthalmol* 15:606-616.
- Quigley HA (1985) Early detection of glaucomatous damage. II. Changes in the appearance of the optic disk. *Surv Ophthalmol* 30:111, 117-126.
- Quigley HA (1993) Open-angle glaucoma. *N Engl J Med* 328:1097-1106.
- Quigley HA, Broman AT (2006) The number of people with glaucoma worldwide in 2010 and 2020. *Br J Ophthalmol* 90:262-267.
- Rangarajan KV, Lawhn-Heath C, Feng L, Kim TS, Cang J, Liu X (2011) Detection of visual deficits in aging DBA/2J mice by two behavioral assays. *Curr Eye Res* 36:481-491.
- Ransohoff RM, Brown MA (2012) Innate immunity in the central nervous system. *J Clin Invest* 122:1164-1171.
- Reyes TM, Fabry Z, Coe CL (1999) Brain endothelial cell production of a neuroprotective cytokine, interleukin-6, in response to noxious stimuli. *Brain Res* 851:215-220.
- Rhee KD, Yang XJ (2010) Function and mechanism of CNTF/LIF signaling in retinogenesis. *Adv Exp Med Biol* 664:647-654.
- Ridder WH, 3rd, Nusinowitz S (2006) The visual evoked potential in the mouse--origins and response characteristics. *Vision Res* 46:902-913.

- Ritch R (2002) Exfoliation syndrome: More than meets the eye. *Acta Ophthalmol Scand* 80:465-467.
- Rojas B, Gallego BI, Ramirez AI, Salazar JJ, de Hoz R, Valiente-Soriano FJ, Aviles-Trigueros M, Villegas-Perez MP, Vidal-Sanz M, Trivino A, Ramirez JM (2014) Microglia in mouse retina contralateral to experimental glaucoma exhibit multiple signs of activation in all retinal layers. *J Neuroinflammation* 11:133.
- Rose-John S (2013) 216: The pro-inflammatory activities of interleukin-6 are mediated by the soluble interleukin-6 receptor via trans-signaling. *Cytokine* 63:294.
- Rosenbaum JT, Woods A, Kezic J, Planck SR, Rosenzweig HL (2011) Contrasting ocular effects of local versus systemic endotoxin. *Invest Ophthalmol Vis Sci* 52:6472-6477.
- Rosenberg SS, Spitzer NC (2011) Calcium signaling in neuronal development. *Cold Spring Harb Perspect Biol* 3:a004259.
- Rothaug M, Becker-Pauly C, Rose-John S (2016) The role of interleukin-6 signaling in nervous tissue. *Biochim Biophys Acta* 1863:1218-1227.
- Rubin DC, Shaker A, Levin MS (2012) Chronic intestinal inflammation: inflammatory bowel disease and colitis-associated colon cancer. *Front Immunol* 3:107.
- Sabry J, O'Connor TP, Kirschner MW (1995) Axonal transport of tubulin in Ti1 pioneer neurons in situ. *Neuron* 14:1247-1256.
- Sakai M, Sakai H, Nakamura Y, Fukuchi T, Sawaguchi S (2003) Immunolocalization of heat shock proteins in the retina of normal monkey eyes and monkey eyes with laser-induced glaucoma. *Jpn J Ophthalmol* 47:42-52.
- Saleh M, Nagaraju M, Porciatti V (2007) Longitudinal evaluation of retinal ganglion cell function and IOP in the DBA/2J mouse model of glaucoma. *Invest Ophthalmol Vis Sci* 48:4564-4572.
- Salinas-Navarro M, Alarcon-Martinez L, Valiente-Soriano FJ, Ortin-Martinez A, Jimenez-Lopez M, Aviles-Trigueros M, Villegas-Perez MP, de la Villa P, Vidal-Sanz M (2009) Functional and morphological effects of laser-induced ocular hypertension in retinas of adult albino Swiss mice. *Mol Vis* 15:2578-2598.
- Sallmann S, Juttler E, Prinz S, Petersen N, Knopf U, Weiser T, Schwaninger M (2000) Induction of interleukin-6 by depolarization of neurons. *J Neurosci* 20:8637-8642.
- Salmon JF (1999) Predisposing factors for chronic angle-closure glaucoma. *Prog Retin Eye Res* 18:121-132.

- Samoilova EB, Horton JL, Hilliard B, Liu TS, Chen Y (1998) IL-6-deficient mice are resistant to experimental autoimmune encephalomyelitis: roles of IL-6 in the activation and differentiation of autoreactive T cells. *J Immunol* 161:6480-6486.
- Sanchez RN, Chan CK, Garg S, Kwong JM, Wong MJ, Sadun AA, Lam TT (2003) Interleukin-6 in retinal ischemia reperfusion injury in rats. *Invest Ophthalmol Vis Sci* 44:4006-4011.
- Sappington RM, Calkins DJ (2006) Pressure-induced regulation of IL-6 in retinal glial cells: involvement of the ubiquitin/proteasome pathway and NFkappaB. *Invest Ophthalmol Vis Sci* 47:3860-3869.
- Sappington RM, Calkins DJ (2008) Contribution of TRPV1 to microglia-derived IL-6 and NFkappaB translocation with elevated hydrostatic pressure. *Invest Ophthalmol Vis Sci* 49:3004-3017.
- Sappington RM, Carlson BJ, Crish SD, Calkins DJ (2010) The microbead occlusion model: a paradigm for induced ocular hypertension in rats and mice. *Invest Ophthalmol Vis Sci* 51:207-216.
- Sappington RM, Chan M, Calkins DJ (2006) Interleukin-6 protects retinal ganglion cells from pressure-induced death. *Invest Ophthalmol Vis Sci* 47:2932-2942.
- Sappington RM, Sidorova T, Long DJ, Calkins DJ (2009) TRPV1: contribution to retinal ganglion cell apoptosis and increased intracellular Ca²⁺ with exposure to hydrostatic pressure. *Invest Ophthalmol Vis Sci* 50:717-728.
- Satoh T, Nakamura S, Taga T, Matsuda T, Hirano T, Kishimoto T, Kaziro Y (1988) Induction of neuronal differentiation in PC12 cells by B-cell stimulatory factor 2/interleukin 6. *Mol Cell Biol* 8:3546-3549.
- Sawada M, Suzumura A, Marunouchi T (1992) TNF alpha induces IL-6 production by astrocytes but not by microglia. *Brain Res* 583:296-299.
- Saxton WM, Hollenbeck PJ (2012) The axonal transport of mitochondria. *J Cell Sci* 125:2095-2104.
- Scheller J, Chalaris A, Schmidt-Arras D, Rose-John S (2011a) The pro- and anti-inflammatory properties of the cytokine interleukin-6. *Biochim Biophys Acta* 1813:878-888.
- Scheller J, Chalaris A, Schmidt-Arras D, Rose-John S (2011b) The pro-and anti-inflammatory properties of the cytokine interleukin-6. *Biochimica et Biophysica Acta (BBA)-Molecular Cell Research* 1813:878-888.
- Schlamp CL, Li Y, Dietz JA, Janssen KT, Nickells RW (2006) Progressive ganglion cell loss and optic nerve degeneration in DBA/2J mice is variable and asymmetric. *BMC Neurosci* 7:66.

- Schobitz B, de Kloet ER, Sutanto W, Holsboer F (1993) Cellular localization of interleukin 6 mRNA and interleukin 6 receptor mRNA in rat brain. *The European journal of neuroscience* 5:1426-1435.
- Schobitz B, Voorhuis DA, De Kloet ER (1992) Localization of interleukin 6 mRNA and interleukin 6 receptor mRNA in rat brain. *Neurosci Lett* 136:189-192.
- Schuettauf F, Zurakowski D, Quinto K, Varde MA, Besch D, Laties A, Anderson R, Wen R (2005) Neuroprotective effects of cardiotrophin-like cytokine on retinal ganglion cells. *Graefes Arch Clin Exp Ophthalmol* 243:1036-1042.
- Sebire G, Emilie D, Wallon C, Hery C, Devergne O, Delfraissy JF, Galanaud P, Tardieu M (1993) In vitro production of IL-6, IL-1 beta, and tumor necrosis factor-alpha by human embryonic microglial and neural cells. *J Immunol* 150:1517-1523.
- Sehi M, Grewal DS, Goodkin ML, Greenfield DS (2010) Reversal of retinal ganglion cell dysfunction after surgical reduction of intraocular pressure. *Ophthalmology* 117:2329-2336.
- Shibuya E, Meguro A, Ota M, Kashiwagi K, Mabuchi F, Iijima H, Kawase K, Yamamoto T, Nakamura M, Negi A, Sagara T, Nishida T, Inatani M, Tanihara H, Aihara M, Araie M, Fukuchi T, Abe H, Higashide T, Sugiyama K, Kanamoto T, Kiuchi Y, Iwase A, Ohno S, Inoko H, Mizuki N (2008) Association of Toll-like receptor 4 gene polymorphisms with normal tension glaucoma. *Invest Ophthalmol Vis Sci* 49:4453-4457.
- Shields MB (2008) Normal-tension glaucoma: is it different from primary open-angle glaucoma? *Curr Opin Ophthalmol* 19:85-88.
- Shohami E, Novikov M, Bass R, Yamin A, Gallily R (1994) Closed head injury triggers early production of TNF alpha and IL-6 by brain tissue. *J Cereb Blood Flow Metab* 14:615-619.
- Shou T, Liu J, Wang W, Zhou Y, Zhao K (2003) Differential dendritic shrinkage of alpha and beta retinal ganglion cells in cats with chronic glaucoma. *Invest Ophthalmol Vis Sci* 44:3005-3010.
- Sims SM, Holmgren L, Cathcart HM, Sappington RM (2012) Spatial regulation of interleukin-6 signaling in response to neurodegenerative stressors in the retina. *Am J Neurodegener Dis* 1:168-179.
- Sivak JM (2013) The aging eye: common degenerative mechanisms between the Alzheimer's brain and retinal disease. *Invest Ophthalmol Vis Sci* 54:871-880.
- Smith SE, Li J, Garbett K, Mirnics K, Patterson PH (2007) Maternal immune activation alters fetal brain development through interleukin-6. *J Neurosci* 27:10695-10702.

- Soto I, Howell GR (2014) The complex role of neuroinflammation in glaucoma. *Cold Spring Harb Perspect Med* 4.
- Soto I, Oglesby E, Buckingham BP, Son JL, Roberson ED, Steele MR, Inman DM, Vetter ML, Horner PJ, Marsh-Armstrong N (2008) Retinal ganglion cells downregulate gene expression and lose their axons within the optic nerve head in a mouse glaucoma model. *J Neurosci* 28:548-561.
- Soto I, Pease ME, Son JL, Shi X, Quigley HA, Marsh-Armstrong N (2011) Retinal ganglion cell loss in a rat ocular hypertension model is sectorial and involves early optic nerve axon loss. *Invest Ophthalmol Vis Sci* 52:434-441.
- Sparkman NL, Buchanan JB, Heyen JR, Chen J, Beverly JL, Johnson RW (2006) Interleukin-6 facilitates lipopolysaccharide-induced disruption in working memory and expression of other proinflammatory cytokines in hippocampal neuronal cell layers. *J Neurosci* 26:10709-10716.
- Spath-Schwalbe E, Hansen K, Schmidt F, Schrezenmeier H, Marshall L, Burger K, Fehm HL, Born J (1998) Acute effects of recombinant human interleukin-6 on endocrine and central nervous sleep functions in healthy men. *J Clin Endocrinol Metab* 83:1573-1579.
- Spittau B, Zhou X, Ming M, Kriegstein K (2012) IL6 protects MN9D cells and midbrain dopaminergic neurons from MPP⁺-induced neurodegeneration. *Neuromolecular Med* 14:317-327.
- Stasi K, Nagel D, Yang X, Wang RF, Ren L, Podos SM, Mittag T, Danias J (2006) Complement component 1Q (C1Q) upregulation in retina of murine, primate, and human glaucomatous eyes. *Invest Ophthalmol Vis Sci* 47:1024-1029.
- Steele MR, Inman DM, Calkins DJ, Horner PJ, Vetter ML (2006) Microarray analysis of retinal gene expression in the DBA/2J model of glaucoma. *Invest Ophthalmol Vis Sci* 47:977-985.
- Stevens B, Allen NJ, Vazquez LE, Howell GR, Christopherson KS, Nouri N, Micheva KD, Mehalow AK, Huberman AD, Stafford B, Sher A, Litke AM, Lambris JD, Smith SJ, John SW, Barres BA (2007) The classical complement cascade mediates CNS synapse elimination. *Cell* 131:1164-1178.
- Straub RH, Schradin C (2016) Chronic inflammatory systemic diseases: An evolutionary trade-off between acutely beneficial but chronically harmful programs. *Evol Med Public Health* 2016:37-51.
- Sullivan TA, Geisert EE, Hines-Beard J, Rex TS (2011) Systemic adeno-associated virus-mediated gene therapy preserves retinal ganglion cells and visual function in DBA/2J glaucomatous mice. *Hum Gene Ther* 22:1191-1200.

- Sun D, Lye-Barthel M, Masland RH, Jakobs TC (2009) The morphology and spatial arrangement of astrocytes in the optic nerve head of the mouse. *J Comp Neurol* 516:1-19.
- Tada M, Diserens AC, Desbaillets I, de Tribolet N (1994) Analysis of cytokine receptor messenger RNA expression in human glioblastoma cells and normal astrocytes by reverse-transcription polymerase chain reaction. *J Neurosurg* 80:1063-1073.
- Takai Y, Tanito M, Ohira A (2012) Multiplex cytokine analysis of aqueous humor in eyes with primary open-angle glaucoma, exfoliation glaucoma, and cataract. *Invest Ophthalmol Vis Sci* 53:241-247.
- Takano Y, Shi D, Shimizu A, Funayama T, Mashima Y, Yasuda N, Fukuchi T, Abe H, Ideta H, Zheng X, Shiraishi A, Ohashi Y, Nishida K, Nakazawa T, Fuse N (2012) Association of Toll-like receptor 4 gene polymorphisms in Japanese subjects with primary open-angle, normal-tension, and exfoliation glaucoma. *Am J Ophthalmol* 154:825-832 e821.
- Tezel G (2008) TNF-alpha signaling in glaucomatous neurodegeneration. *Prog Brain Res* 173:409-421.
- Thomas BB, Seiler MJ, Sada SR, Coffey PJ, Aramant RB (2004) Optokinetic test to evaluate visual acuity of each eye independently. *J Neurosci Methods* 138:7-13.
- Tiberio GA, Tiberio L, Benetti A, Cervi E, Montani N, Dreano M, Garotta G, Cerea K, Steimberg N, Pandolfo G, Ferrari-Bravo A, Mazzoleni G, Giulini SM, Schiaffonati L (2008) IL-6 Promotes compensatory liver regeneration in cirrhotic rat after partial hepatectomy. *Cytokine* 42:372-378.
- Tong J, Wang J, Sun F (2002) Dual-directional optokinetic nystagmus elicited by the intermittent display of gratings in primary open-angle glaucoma and normal eyes. *Curr Eye Res* 25:355-362.
- Toulmond S, Vige X, Fage D, Benavides J (1992) Local infusion of interleukin-6 attenuates the neurotoxic effects of NMDA on rat striatal cholinergic neurons. *Neurosci Lett* 144:49-52.
- Umegaki H, Yamada K, Naito M, Kameyama T, Iguchi A, Nabeshima T (1996) Protective effect of interleukin-6 against the death of PC12 cells caused by serum deprivation or by the addition of a calcium ionophore. *Biochem Pharmacol* 52:911-916.
- Valerio A, Ferrario M, Dreano M, Garotta G, Spano P, Pizzi M (2002) Soluble interleukin-6 (IL-6) receptor/IL-6 fusion protein enhances in vitro differentiation of purified rat oligodendroglial lineage cells. *Mol Cell Neurosci* 21:602-615.
- Vallieres L, Rivest S (1997) Regulation of the genes encoding interleukin-6, its receptor, and gp130 in the rat brain in response to the immune activator lipopolysaccharide and the proinflammatory cytokine interleukin-1beta. *J Neurochem* 69:1668-1683.

- Vecino E, Rodriguez FD, Ruzafa N, Pereiro X, Sharma SC (2016) Glia-neuron interactions in the mammalian retina. *Prog Retin Eye Res* 51:1-40.
- Wang H, Wu M, Zhan C, Ma E, Yang M, Yang X, Li Y (2012) Neurofilament proteins in axonal regeneration and neurodegenerative diseases. *Neural Regen Res* 7:620-626.
- Wang X, Tay SSW, Ng YK (2000) An immunohistochemical study of neuronal and glial cell reactions in retinæ of rats with experimental glaucoma. *Experimental Brain Research* 132:476-484.
- Ward NJ, Ho KW, Lambert WS, Weitlauf C, Calkins DJ (2014) Absence of transient receptor potential vanilloid-1 accelerates stress-induced axonopathy in the optic projection. *J Neurosci* 34:3161-3170.
- Wassle H (2004) Parallel processing in the mammalian retina. *Nature Reviews Neuroscience* 5:747-757.
- Weber AJ, Kaufman PL, Hubbard WC (1998) Morphology of single ganglion cells in the glaucomatous primate retina. *Invest Ophthalmol Vis Sci* 39:2304-2320.
- Wei H, Chadman KK, McCloskey DP, Sheikh AM, Malik M, Brown WT, Li X (2012) Brain IL-6 elevation causes neuronal circuitry imbalances and mediates autism-like behaviors. *Biochim Biophys Acta* 1822:831-842.
- Weinreb RN, Aung T, Medeiros FA (2014) The pathophysiology and treatment of glaucoma: a review. *JAMA* 311:1901-1911.
- Weinreb RN, Leung CKS, Crowston JG, Medeiros FA, Friedman DS, Wiggs JL, Martin KR (2016) Primary open-angle glaucoma. *Nat Rev Dis Primers* 16067.
- Wenk GL (2003) Neuropathologic changes in Alzheimer's disease. *J Clin Psychiat* 64:7-10.
- Williams PA, Marsh-Armstrong N, Howell GR, Lasker HoA, Glaucomatous Neurodegeneration P (2017) Neuroinflammation in glaucoma: A new opportunity. *Exp Eye Res*.
- Williams PA, Tribble JR, Pepper KW, Cross SD, Morgan BP, Morgan JE, John SW, Howell GR (2016) Inhibition of the classical pathway of the complement cascade prevents early dendritic and synaptic degeneration in glaucoma. *Mol Neurodegener* 11:26.
- Williams RW, Moody SA (2003) Developmental and genetic control of cell number in the retina. *The visual neurosciences* (Chalupa LM, Werner JS, eds) pp 65-78.
- Williams RW, Strom RC, Rice DS, Goldowitz D (1996) Genetic and environmental control of variation in retinal ganglion cell number in mice. *J Neurosci* 16:7193-7205.

- Wilson GN, Inman DM, Dengler Crish CM, Smith MA, Crish SD (2015) Early pro-inflammatory cytokine elevations in the DBA/2J mouse model of glaucoma. *J Neuroinflammation* 12:176.
- Wilson GN, Smith MA, Inman DM, Dengler-Crish CM, Crish SD (2016) Early Cytoskeletal Protein Modifications Precede Overt Structural Degeneration in the DBA/2J Mouse Model of Glaucoma. *Front Neurosci* 10:494.
- Winter CD, Pringle AK, Clough GF, Church MK (2004) Raised parenchymal interleukin-6 levels correlate with improved outcome after traumatic brain injury. *Brain* 127:315-320.
- Woiciechowsky C, Schoning B, Cobanov J, Lanksch WR, Volk HD, Docke WD (2002) Early IL-6 plasma concentrations correlate with severity of brain injury and pneumonia in brain-injured patients. *J Trauma* 52:339-345.
- WoldeMussie E, Ruiz G, Wijono M, Wheeler LA (2001) Neuro-protection of retinal ganglion cells by brimonidine in rats with laser-induced chronic ocular hypertension. *Invest Ophthalmol Vis Sci* 42:2849-2855.
- Wong AA, Brown RE (2012) A neurobehavioral analysis of the prevention of visual impairment in the DBA/2J mouse model of glaucoma. *Invest Ophthalmol Vis Sci* 53:5956-5966.
- Xanthos DN, Sandkuhler J (2014) Neurogenic neuroinflammation: inflammatory CNS reactions in response to neuronal activity. *Nature Reviews Neuroscience* 15:43-53.
- Xia X, Wen R, Chou TH, Li Y, Wang Z, Porciatti V (2014) Protection of pattern electroretinogram and retinal ganglion cells by oncostatin M after optic nerve injury. *PLoS One* 9:e108524.
- Xin X, Gao L, Wu T, Sun F (2013) Roles of tumor necrosis factor alpha gene polymorphisms, tumor necrosis factor alpha level in aqueous humor, and the risks of open angle glaucoma: a meta-analysis. *Mol Vis* 19:526-535.
- Xu WQ, Wang YS (2016) The role of Toll-like receptors in retinal ischemic diseases. *Int J Ophthalmol* 9:1343-1351.
- Xu XJ, Hao JX, Andell-Jonsson S, Poli V, Bartfai T, Wiesenfeld-Hallin Z (1997) Nociceptive responses in interleukin-6-deficient mice to peripheral inflammation and peripheral nerve section. *Cytokine* 9:1028-1033.
- Yamada M, Hatanaka H (1994) Interleukin-6 protects cultured rat hippocampal neurons against glutamate-induced cell death. *Brain Res* 643:173-180.
- Yan HQ, Banos MA, Herregodts P, Hooghe R, Hooghe-Peters EL (1992) Expression of interleukin (IL)-1 beta, IL-6 and their respective receptors in the normal rat brain and after injury. *Eur J Immunol* 22:2963-2971.

- Yang X, Luo C, Cai J, Powell DW, Yu D, Kuehn MH, Tezel G (2011) Neurodegenerative and inflammatory pathway components linked to TNF-alpha/TNFR1 signaling in the glaucomatous human retina. *Invest Ophthalmol Vis Sci* 52:8442-8454.
- Yaqub M (2012) Visual fields interpretation in glaucoma: a focus on static automated perimetry. *Community Eye Health* 25:1.
- You Y, Klistorner A, Thie J, Graham SL (2011) Latency delay of visual evoked potential is a real measurement of demyelination in a rat model of optic neuritis. *Invest Ophthalmol Vis Sci* 52:6911-6918.
- You Y, Klistorner A, Thie J, Gupta VK, Graham SL (2012) Axonal loss in a rat model of optic neuritis is closely correlated with visual evoked potential amplitudes using electroencephalogram-based scaling. *Invest Ophthalmol Vis Sci* 53:3662.
- Yu L, Wang L, Chen S (2010) Endogenous toll-like receptor ligands and their biological significance. *J Cell Mol Med* 14:2592-2603.
- Yuan L, Neufeld AH (2000) Tumor necrosis factor-alpha: a potentially neurodestructive cytokine produced by glia in the human glaucomatous optic nerve head. *Glia* 32:42-50.
- Zhang PL, Izrael M, Ainbinder E, Ben-Simchon L, Chebath J, Revel M (2006) Increased myelinating capacity of embryonic stem cell derived oligodendrocyte precursors after treatment by interleukin-6/soluble interleukin-6 receptor fusion protein. *Mol Cell Neurosci* 31:387-398.
- Zhang PL, Levy AM, Ben-Simchon L, Haggiag S, Chebath J, Revel M (2007) Induction of neuronal and myelin-related gene expression by IL-6-receptor/IL-6: a study on embryonic dorsal root ganglia cells and isolated Schwann cells. *Exp Neurol* 208:285-296.
- Zhao S, Gu Y, Dong Q, Fan R, Wang Y (2008) Altered interleukin-6 receptor, IL-6R and gp130, production and expression and decreased SOCS-3 expression in placentas from women with pre-eclampsia. *Placenta* 29:1024-1028.
- Zhong J, Dietzel ID, Wahle P, Kopf M, Heumann R (1999) Sensory impairments and delayed regeneration of sensory axons in interleukin-6-deficient mice. *J Neurosci* 19:4305-4313.
- Zhou X, Li F, Kong L, Tomita H, Li C, Cao W (2005) Involvement of inflammation, degradation, and apoptosis in a mouse model of glaucoma. *J Biol Chem* 280:31240-31248.